

“Development of a Model to Predict the Performance & Estimate the Life of Low Voltage Induction Motor Driven by Pulse Width Modulation Converter”

A thesis submitted for the award of the Degree of

DOCTOR OF PHILOSOPHY

in

Electrical Engineering

By

Mr. Suresh J. Patel



**ELECTRICAL ENGINEERING DEPARTMENT
FACULTY OF TECHNOLOGY & ENGINEERING**

THE MAHARAJA SAYAJIRAO UNIVERSITY OF BARODA

VADODARA – 390 001

**GUJARAT, INDIA
December 2012**

ABSTRACT

In industrial drives market, requirements related to control quality and price of drives are important. In any drive, aims are achieving of good performance and longer life.

The motor parameters are required to estimate the performance of motors and working environment for estimating the life of insulation and hence motor.

Hence it is necessary to determine the exact value of these parameters. Various methods are available in literatures to estimate the parameters from motor label or by simple measurements. However these parameters vary due to variation in atmospheric conditions, saturation level or due to measurement. In this work the parameters are calculated from simple no load and blocked rotor test and presented to algorithm based on NR method to modify it. Results obtained are very encouraging and matches with the experimental results.

For the investigation purpose four motors were designed and manufactured. Two motors were manufactured to investigate the distribution of voltage in winding whereas two more motors were manufactured for the purpose of performance evaluation.

Ten Programs MATLAB are developed to evaluate the motor Output, Input, Efficiency, PF, Torque and Speed of the motor. These performance parameters are compared with the actual test parameters. The results are in good agreement. Hence these programs can be used to predict the performance of the other motors.

CRO of Yokogawa, Japan, Model No. DL 750 was used for the measurement purpose. Investigation was made for three different source of voltages [1] Sinusoidal utility 50 Hz supply [2] Filtered inverter supply taken from drive No. VDF007B43A of Delta [3] Unfiltered inverter supply taken from drive no. VFD004S43A of Delta. Around 600 wave forms are being

recorded and investigated. Investigated wave forms are of coil voltages with respect to phase voltage and voltage of one coil with respect to voltage of second coil. When motor is operated on sinusoidal supply, then during switching period voltage across motor phase becomes equal to supply line voltage and the maximum voltage across any of the coil obtained is 80 V. Unexpected behaviour was observed in variation of coil voltage (harmonic voltage after few cycle from starting) with sinusoidal supply during starting, however this is not producing over voltages or high dv/dt . Voltage rise time when motor is supplied with converter is very small and is of the order of micro second. In some cases the peak voltage at motor terminals reaches to value which more than twice the value of dc link voltage and rated line to line voltage of the motor. However for low voltage motor as peak is not reaches to large value coil manufactured with medium covering enamel wire and due care is taken to maintain the thickness around the conductor can with stand this voltages even though the variation of supply voltage is very peculiar particularly at low frequency.

The distribution of voltage during switching condition is not even among the coils of a winding and hence turns. The voltage drop in coils near terminal is more than that of in other coils. The measured voltage drop across first coil from terminal of winding of four coils in series is varying 30 to 56% of the phase voltage against 25% of the phase voltage. During the transition period voltage across first coil may be 70% of the total voltage. Comparison of wave forms for sinusoidal supply and inverter supply shows that distortions were very large with inverter supply which increases the losses and produces more stresses on the insulations.

Certificate

This is to certify that the thesis entitled, “Development of a Model to Predict the Performance & Estimate the Life of Low Voltage Induction Motor Driven by Pulse Width Modulation Converter” submitted by **Mr. Suresh J. Patel** in fulfillment of the degree of **DOCTOR OF PHILOSOPHY** in Electrical Engineering Department, Faculty of Technology & Engineering, The M. S. University of Baroda, Vadodara is a bona-fide record of investigations carried out by him in the Department of Electrical Engineering, Faculty of Technology & Engineering, M. S. University of Baroda, Vadodara under my guidance and supervision. In my opinion the standards fulfilling the requirements of the Ph.D. Degree as prescribed in the regulations of the University has been attained

December-2012

Prof. S. K. Joshi

Guide

Department of Electrical Engineering,
Faculty of Technology & Engineering,
The Maharaja Sayajirao University,
Vadodara-390 001

Certificate

This is to certify that the thesis entitled, “Development of a Model to Predict the Performance & Estimate the Life of Low Voltage Induction Motor Driven by Pulse Width Modulation Converter” submitted by **Mr. Suresh J. Patel** in fulfillment of the degree of **DOCTOR OF PHILOSOPHY** in Electrical Engineering Department, Faculty of Technology & Engineering, The M. S. University of Baroda, Vadodara is a bonafide record of investigations carried out by him in the Department of Electrical Engineering, Faculty of Technology & Engineering, M. S. University of Baroda, Vadodara.

December-2012

Head

Department of Electrical Engineering,
Faculty of Technology & Engineering,
The Maharaja Sayajirao University,
Vadodara-390 001

Dean

Faculty of Technology & Engineering,
The Maharaja Sayajirao University,
Vadodara-390 001

Declaration

I, **Mr. Suresh J. Patel**, hereby declare that the work reported in this thesis entitled **“Development of a Model to Predict the Performance & Estimate the Life of Low Voltage Induction Motor Driven by Pulse Width Modulation Converter”** submitted for the award of the degree of **DOCTOR OF PHILOSOPHY** in Electrical Engineering Department, Faculty of Technology & Engineering, The M. S. University of Baroda, Vadodara is original and has been carried out in the Department of Electrical Engineering, Faculty of Technology & Engineering, M. S. University of Baroda, Vadodara. I further declare that this thesis is not substantially the same as one, which has already been submitted in part or in full for the award of any degree or academic qualification of this University or any other Institution or examining body in India or abroad.

December-2012

Suresh J. Patel

ACKNOWLEDGEMENTS

I express sincere appreciation to Prof. Dr. S. K. Joshi for his valuable advices and guidance throughout all stages of this project.

I offer sincere thanks to Prof. S.K. Shah, Head Electrical Engineering Department, who encouraged me for all the time for this project work.

I would like to thank Dr. Chetwani, (Sr. Manager, Motor and Pump testing division, Electrical Research and development Association, Vadodara) and testing engineer Mr. R.P. Singh for the help and suggestions during the experimentations.

Finally I would like to thank my family for their precious support during all stages of my life.

Suresh J. Patel

Index

Chapter	Description	Page
1	Introduction and Contents of the Thesis	1-5
1.1	Introduction	1
1.2	Speed control	2
2	Identification of Equivalent Circuit Parameters, Life of the motor and Methods of Prediction	6-17
2.1	Introduction	6
2.2	Basic Theory of Induction Motor	7
2.3	Steady State Performance of Induction Motor	8
2.4	Life of the Motor	10
2.5	Prediction Techniques	11
2.5.1	Introduction	11
2.5.2	Moving Average Technique	12
2.5.3	Exponential Smoothing	13
2.5.4	Regression	15
3	Speed control of an Induction motor	18-53
3.1	Introduction	18
3.2	Stator Voltage Control for Speed Control of Induction Motor	20
3.2.1	Variation of Stator Current and Efficiency in Stator Voltage Control	21
3.2.2	Thyristor Based Stator Voltage Controller	23
3.2.3	Starting/Stopping Control By Stator Voltage Control	24
3.2.4	Stator Voltage Control for Optimum Efficiency Operation of Motor	25
3.2.5	Basic Principles of Voltage Control	26
3.3	Changing Frequency of Supply Voltage	29
3.4	Control Techniques	34
3.5	Scalar Control	34
3.6	Six-Step PWM	35
3.7	Voltage Source Inverter (VSI) Control	35
3.8	Voltage Control of Inverters	39
3.9	Sinusoidal PWM	41
3.10	Cycloconverter	43
3.11	Constant Volts/Hertz Induction Motor Drives	46
3.12	Compensation for Supply Voltage Variations	48
3.13	I_r Compensation	48
3.14	Slip Compensation	49
3.15	Volt-Second Compensation	50

3.16	Space Vector Modulation PWM (SVMPWM)	51
3.17	SVMPWM With Over modulation	51
3.18	Vector Control	51
3.19	Direct Torque Control (DTC)	53
4	Motor Insulation System and Transient Produced by Variable Speed Drives	54-81
4.1	Introduction	54
4.2	Motor Windings	56
4.3	Rise Time and Peak Voltage Concerns	57
4.4	Surges	62
4.5	The Surge Environment	63
4.6	Factors Affecting Surge Amplitude and Rise Times	64
4.7	Steep Fronted Switching Surges	65
4.7.1	Breaker Types	65
4.7.2	Surge Generation	65
4.7.3	Cables	67
4.8	Motor Design Effects	67
4.9	Surge Distribution in the Winding	68
4.10	Standards	68
4.11	Causes of Turn Insulation Failures	69
5	Development of a Model to Estimate the Parameters of Equivalent Circuit and Prediction of Performance	82-101
5.1	Introduction	82
5.2	Accuracy of Estimation	84
5.3.1	Measurement of Winding Resistance	84
5.3.2	No Load Test	86
5.3.3	Blocked Rotor Test	86
5.4	Mathematical Modeling of Induction Motor Based On Equivalent Circuit Method	87
5.4.1	Machine Model for Inverter Fed Induction Motor	91
5.5	Numerical Algorithm For Parameter Estimation	92
5.5.1	Initial Values of Parameter and Stopping Criteria	94
5.6	Flow Chart for Calculation of Parameters.	97
5.7	Sensitivity Analysis	98
5.8	Steady State Performance Of Induction Motor	99
5.9	Matlab programs for predicting performance of induction motor and transient over voltage	101
6	Details of motors, Experimental setup and Voltage waveforms	102-155
6.1	Introduction	102
6.2	Stamping	103

6.3	Winding Detail	104
6.4	Slot Insulation	105
6.5	Terminal Insulation Sleeve	105
6.6	Varnishing	106
6.7	Testing of Motors	106
7	Discussion and Analysis of Experiment Results	156-164
7.1	Comparison of Performance	156
7.2	Maximum Voltage to Winding	158
7.3	Variation Of Phase Voltage And Variation Of Voltage In Coil Near Terminals	159
7.4	Avoiding Life Reduction Due To Partial Discharges	162
7.4.1	Use A Low Voltage System	162
7.4.2	Using a Longer Rise Time ASD	162
7.4.3	Keeping Cable Lengths Short	163
7.4.4	Using Filters	163
7.4.5	Using Form Coil Motors	164
7.4.6	Using Motors with a Random Wound System	164
8	Conclusion	165-167
8.1	Performance of the Motor	165
8.2	Turn Insulation	165
8.3	Extension of Work	167
	Annexure	168 – 184
	References	185 – 191
	Certificate from Delmer Product Ltd.	192

List of Figures		
Figure No.	Description	Page No.
1.1	Major drive type categories	4
2.1	Equivalent circuit of an Induction motor	8
3.1	T-S Curves for various voltages for high slip Induction motor	20
3.2	Variation of ratio of maximum copper loss to rated copper loss with rated slip for Induction motor with fan load	23
3.3	Thyristor voltage controller	24
3.4	Wave form of Voltage and Current with Thyristor control	24
3.5	Approximate Equivalent Circuit of an Induction motor	26
3.6	Torque speed curves for standard and high slip Induction Motor	27
3.7	Torque speed curves for changes in hold off angel	29
3.8	Variation of torque and voltage with speed for V/F control method	31
3.9	Speed torque curves for constant V/F control	32
3.10	Block diagram for variable frequency control	33
3.11	Three phase bridge Inverter	36
3.12	Voltage waveforms of an inverter shown in fig. 3.11	37
3.13	Voltage waveforms of an inverter shown in fig. 3.11 for star connected load	38
3.14	VSI controlled IM drives	40
3.15	Single phase bridge Inverter and its output voltage waveforms	41
3.16	Multi pulse modulation scheme	42
3.17	Sinusoidal pulse width modulated inverter	43
3.18	Three phase to single phase cycloconverter.	44
3.19	Output voltage waveforms of cycloconverter.	45
3.20	Three phase to three phase cycloconverter.	46
4.1	Impact of number of cable's equivalent networks on investigated characteristic at the motor terminals, Cable length = 50 m, V_{dc} is dc bus voltage.	60
4.2	Details of line to line voltage wave form at motor terminals. $f_c = 2 \text{ Khz}$, $f_{out} = 60 \text{ Hz}$	61
4.3	Lightning and step-fronted surges.	63
4.4	Typical Motor cable system.	66
4.5	Flux distribution in the slot obtained with eddy current analysis.	72
4.6	Variation of self-inductance of individual turns with distance along the width of the slot.	73
4.7	Variation of turn-to-ground capacitance of individual turns with distance along the width of the slot.	74
4.8	Partially distributed equivalent circuit of the line-end coil.	75
4.9	Simulated inverter output voltage and motor terminal voltage with 100 foot long cable.	76

4.10	Experimental results of a PWM Induction motor drive with 100 foot long cable between the inverter and the motor.	77
4.11	Simulated inverter output voltage and motor terminal voltage with 50 foot long cable.	78
4.12	Simulated inverter output voltage and motor terminal voltage with 10 foot long cable.	78
4.13	Experimental results of a PWM Induction motor drive with 10 foot long cable between the inverter and the motor.	79
4.14	Line-end coil voltage with 10 foot cable.	80
4.15	Line-end coil voltage with 100 foot cable and 0.2 μ s rise-time.	80
5.1	Equivalent circuit of an Induction motor	87
5.2	Harmonic equivalent circuit of an Induction motor	92
5.3	Blocked rotor simplified Induction motor equivalent circuit	95
5.4	No load simplified Induction motor equivalent circuit	96
W.3	Three phase 24-slots, 2-pole winding.	104
W.4	Three phase 24-slots, 4-pole winding.	105
6.1	Measurement of voltage waveforms.	106
6.2	Experimental setup for loading the motor	109
6.3	Experimental setup for loading the motor	110
6.4	Measuring Instruments	111
6.5	Dynamometer for loading the motor.	112
6.6	Dynamometer for loading the motor.	113
6.7	Waveform recording at ERDA.	121
6.8	Waveform recording at ERDA.	122
7.1	Critical cable length vs rise time	163

List of Tables		
Table No.	Description	Page No.
1.1	Industrial applications where motion control is require.	4
5.1	Stray load losses	83
5.2	Motor Efficiency as per different standards	83
5.3	Values of Performance Characteristic of 2 Pole Energy Efficient Induction Motors.	83
5.4	Values of Performance Characteristic of 4 Pole Energy Efficient Induction Motors.	84
5.5	List of MATLAB Program	101
6.1	Resistance of I.M., Frame 63, 3-phase, 415 V, 250 W, 50 Hz, 2-Pole.	106
6.2	No load test results of I.M., Frame 63, 3-phase, 415 V, 250 W, 50 Hz, 2-Pole.	107
6.3	Blocked Rotor test, Frame 63, 3-phase, 415 V, 470 W, 1.3 A, 50 Hz, 2-Pole, I.M.	107
6.4	Table 6.4 Equivalent Circuit Parameters Frame 63, 3-phase, 415 V, 470 W, 1.3 A 50 Hz, 2-Pole, I.M.	107
6.5	Table 6.5 Performance of Frame 63, 3-phase, 415 V, 470 W, 1.3 A, 50 Hz, 2-Pole, I.M. obtained using MATLAB program B9.	108
6.6	The weight requires to be coupled with gear box shaft of ratio 30 for producing necessary torque at motor shaft.	108
6.7	Observations Table of Load Test of Frame 63, 3-phase, 415 V, 470 W, 1.3 A 50 Hz, 2-Pole, I.M.	114
6.8	Performance of Frame 63, 3-phase, 415 V, 470 W, 1.3 A 50 Hz, 2-Pole, I.M. from Load test.	114
6.9	Equivalent Circuit Modified Parameters Frame 63, 3-phase, 415 V, 470 W, 1.3 A 50 Hz, 2-Pole, I.M.	115
6.10	Performance of Frame 63, 3-phase, 415 V, 470 W, 1.3 A 50 Hz, 2-Pole, I.M. based on modified Parameters.	115
6.11	Resistance of Frame 63, 3-phase, 380 V, 470 W, 1.4 A, 50 Hz, 2-Pole, I.M.	115
6.12	No Load test, Frame 63, 3-phase, 380 V, 470 W, 1.4 A, 50 Hz, 2-Pole, I.M.	116
6.13	Blocked Rotor test, Frame 63, 3-phase, 380 V, 470 W, 1.4 A 50 Hz, 2-Pole, I.M.	116
6.14	Observations Table of Load Test of Frame 63, 3-phase, 380 V, 470 W, 1.4 A 50 Hz, 2-Pole, I.M.	116
6.15	Performance of Frame 63, 3-phase, 380 V, 470 W, 1.4 A 50 Hz, 2-Pole, I.M. from Load test.	117
6.16	Equivalent Circuit Parameters Frame 63, 3-phase, 380 V, 470 W, 1.4 A 50 Hz, 2-Pole, I.M.	117
6.17	Performance of Frame 63, 3-phase, 380 V, 470 W, 1.4 A, 50 Hz, 2-Pole, I.M. obtained using MATLAB program B9.	117

6.18	Equivalent Circuit Modified Parameters Frame 63, 3-phase, 380 V, 470 W, 1.4 A 50 Hz, 2-Pole, I.M.	117
6.19	Performance of Frame 63, 3-phase, 380 V, 470 W, 1.4 A 50 Hz, 2-Pole, I.M. based on modified Parameters.	118
6.20	Resistance of Motor No.3.	118
6.21	Resistance of Motor No.4.	119
6.22	No Load test of 380 V, 50 Hz, 1.2 KW, 4-Pole IM.	119
6.23	Blocked rotor Test 380 V, 50 Hz, 1.2 KW, 4-Pole IM.	120
6.24	List of waveforms for 2 P windings.	123
6.25	List of waveforms for 4 P windings.	125
7.1	Comparison of performance of Frame 63, 3-phase, 415 V, 470 W, 1.3 A, 50 Hz, 2-Pole, I.M.	156
7.2	Comparison of performance of Frame 63, 3-phase, 380 V, 470 W, 1.4 A, 50 Hz, 2-Pole, I.M.	157
7.3	Voltage of R-Phase-30 Hz Wave form No. KRK0107	160
7.4	Voltage of Y-Phase-30 Hz Wave form No. KRK0122	160
7.5	Voltage of B-Phase, 30 Hz Wave form No. KRK0127	160
7.6	Voltage of R-Phase-40 Hz Wave form No. KRK0108	160
7.7	Voltage of Y-Phase-40 Hz Wave form No. KRK0123	160
7.8	Voltage of B-Phase, 40 Hz Wave form No. KRK0128	161
7.9	Voltage of R-Phase-50 Hz Wave form No. KRK0109	161
7.10	Voltage of Y-Phase-50 Hz Wave form No. KRK0124	161
7.11	Voltage of B-Phase, 50 Hz Wave form No. KRK0129	161
7.12	Voltage of R-Phase-60 Hz Wave form No. KRK0110	161
7.13	Voltage of Y-Phase-60 Hz Wave form No. KRK0125	161
7.14	Voltage of B-Phase, 60 Hz Wave form No. KRK0130	162

List of Abbreviation

ASD =Adjustable speed drive,
ATP = Alternative Transient Program,
CRNGO = Cold rolled non-grain oriented,
GPC = Generalized predictive control,
GTO = Gate turn off thyristor,
GTOs = Gate turn-off Thyristor,
IEC = International Electro-technical Commission,
IGBT = Insulated gate bipolar transistor,
IGCT = Insulated gate commutated thyristor,
VSI = Voltage Source Inverter,
CSI = Current Source Inverter,
MCTs = MOS-Controlled Thyristor,
MOS = Metal-Oxide-Semiconductors,
MOSFET = Metal Oxide Field Effect Transistor,
NEMA = National Electrical Manufacturers Association,
PI = Proportional and Integral,
PILC = Paper Insulated Lead Covered cable
PVC = Polyvinyl Chloride
SLL = Stray Load Losses,
SVM = Space Vector Modulation,
THD = Total Harmonic Distortion,
VPI = Vacuum Pressure Impregnation,
XLPE = Cross-linked Polyethylene.

List of symbols

\widehat{R}_1 = Estimated value of resistance,

c = Speed of light,

$\cos \phi$ = Power factor,

f_e^* = External command frequency,

f_R = Rated Value of line frequency,

f_R and f_e are the rated and line frequency in Hertz,

I_0 = No load current,

I_1 = Stator current (A),

I_{1Re} = real component of rms stator current,

I_2 = Rotor current (A),

I_2' = Rotor current referred to stator (A),

I_m = Magnetizing branch current (A),

$\text{Im}\{Z\}$ = Imagery part of Z,

I_p = peak value o current in ampere,

I_R = Rated Value of stator current,

I_s = rms current,

L_2' = Rotor leakage inductance referred to stator (H),

l_c = Crucial length of cable,

L_s = Stator leakage inductance (H),

N = Rotor speed in rps

P = Ohmic loss in watts,

P_0 = No load input power, P_0 and I_0 is no load input and current.

P_{in} = Power input to the motor (W),

P_{out} = Power output of the motor (W),

P_R = Rated Value of power input,

$\text{Re}\{Z\}$ = Real part of Z,

R_{FE} = Magnetizing resistance (Ω),

R_{FE} = Resistance corresponds to core loss,

R_L = Load resistance,

R_r = Rotor resistance,

R_r, R_2 = Rotor resistance (Ω),

R_s = Stator resistance (Ω),

R_s = Stator winding resistance per phase,

s = Slip,

S_R = Rated Value of slip,

t = Temperature,

T_g = Gross torque developed by the motor.

T_g = Gross torque,

T_R = Rated Value of torque.

t_{rise} = Rise time of inverter's voltage pulses,

U_{AV} = Energy stored in magnetic field in Joules,

v = Wave velocity,

V_0 = No load voltage,

V_{1R} = Base (rated) rms phase voltage at base frequency,

V_s = Supply voltage (V),

X_m = Magnetising branch reactance,

X_m = Magnetizing reactance (Ω),

X_r = Rotor leakage reactance (Ω),

X_r = Rotor reactance,

X_s = Stator leakage reactance (Ω),

X_s = Stator winding leakage reactance per phase,

Y_t = Actual (or observed) value of the random variable in period t ,

Y_t^* = Estimated value of the random variable in period t ,

Z = Total impedance of motor circuit under blocked rotor condition,

Z_0 = Magnetizing Impedance (Ω),

Z_{eq} = Equivalent Impedance of the motor (Ω),

Z_r = Rotor Impedance (Ω),

ϵ_0 = Permittivity of free space,

ϵ_r = Relative permittivity of cable insulation material,

ϵ_t = Random component (or noise) in period t ,

η_R = Rated Value of efficiency,

ω = Speed (radian per second),

ρ = Charge density,

Chapter 1

Introduction and Contents of the Thesis

1.1 INTRODUCTION

Energy conservation continues to get higher and higher attention at National & International levels. Various government and private agencies along with Green activists are propagating higher and higher acceptance norms on efficiency of various products. All these have resulted in the need of test procedures for efficiency measurement which are more precise, reproducible and have better co-relation with actual energy consumption.

Normally performance determinations mean the determination of efficiency, power factor, speed, current etc. The determination of efficiency of the motor on line involves measurement of torque developed by the motor and speed of the motor. For this purpose of measuring torque it is require to connect, the torque transducer mechanically with motor shaft. There is a practical difficulty in the insertion of transducers for the torque measuring on electro-pumping groups related with the mechanical disconnection of coupled machines. This is sometimes not fast or even not feasible.

A number of induction machines modeling methods are available for different types of application, namely machine dynamics and control [1] steady state starting performance analysis [2],[3], steady state efficiency and torque evaluation at or under rated conditions [4], [5], [6], [7] as well as for different rotor types (single-, double cage-, wound-rotor) and power supply waveforms [3],[7]. Besides model structures, parameter identification and test procedures are of special concern when specific studies require especially accurate modeling.

Standard test procedures have been established for a variety of situations following a long and valuable experience in the field [8]. The efficiency estimation of induction motors is treated in the most important international standards in the field, namely IEEE Std. 112 and IEC 60034-2. The key issue in efficiency evaluation is the determination of all losses in the machine. Besides copper losses, Iron losses, friction and windage losses, the STRAY LOAD LOSSES (SLL) represent a non negligible part in the summation.

These last are difficult to evaluate accurately and some studies [4], [6] have been devoted to the comparison of standard methods for that purpose, especially those in IEEE Std. 112 and IEC 60034-2: the simplest approach uses assumed values according to machine rating, that may be still corrected by the square of rotor current, or even using more complex solutions as in IEEE 112-method B.

As the direct torque measurement is not feasible in some cases the efficiency evaluation based on equivalent circuit is presented in chapter 2 and 5. A numerical procedure using a Newton-Raphson method for the calculation of Induction motor model parameters is presented.

1.2 SPEED CONTROL

Human and animal powers are the traditional modes of power utilized by mankind to drive different types of machines required by the people during various stages of development. Water-wheels are believed to have been used in China around 3000 BC. This was the first crude means of mechanization. Later it was the wind power and after the industrial revolution, steam power and IC engines were developed for driving machines. However, by the end of the nineteenth century, three-phase ac power becomes available which completely transformed the nature of industrial drives. The electric motors have now become the main source of driving equipment. An electric drive has so many advantages over other forms of drives that it has replaced almost all of them in industrial applications.

The electric drive makes use of electric motors as prime movers. The electric motors have the advantage that they can be brought very close to the working machine (thus eliminating the transmission links), can be operated at any desired speed and can be started and reversed in very short periods of time. The electric motors are available in a wide range of power ratings, from one watt to few thousand of kilowatts capacity. These motor are now electronically controlled using solid state circuit for starting, reversing and speed control. The electric drives are therefore very efficient, less expensive, and reliable. With the availability of such a wide range of motor capacities with simple control circuit, it is possible to develop efficient drives to meet any requirement of modern industries.

An important factor in industrial progress during the past five decades has been the increasing sophistication of factory automation which has improved productivity manifold. Control motion or speed of electrical motors

in general plays very important role in modern industries, commercial buildings and house hold appliances.

In number of applications motor must satisfy the speed requirement. For example speed of electric fan. As per the requirement of comfort of the persons it must throw an air and that is possible only by adjusting fan speed. However, there are certain industrial applications where motor must have wide speed range and speed should vary smoothly or should have step-less variation as economically as possible. Consider an example of train driven by electric motor. In this case motor has to accelerate very heavy weight consist on number of bogies along with passengers. Here motor is required to perform very stringent duty as speed should increase smoothly and jerk-less so that it will not create any discomfort to passengers and at the same time speed should increase very fast so that acceleration time can be reduced. This may not possible for all motors and all the time. From the speed control point of view induction motors are inferior to the dc motors. The speed of dc motor can be adjusted in wide range with good efficiency and speed regulation with relatively low cost equipments which is not possible for an induction motor.

Manufacturing lines typically involve a variety of variable speed motor drives which serve to power conveyor belts, robot arms, overhead cranes, steel process lines, paper mills, and plastic and fiber processing lines to name only a few. Prior to the 1950s all such applications required the use of a DC motor drive since AC motors were not capable of smoothly varying speed since they inherently operated synchronously or nearly synchronously with the frequency of electrical input. To a large extent, these applications are now serviced by what can be called general purpose AC drives. In general, such AC drives often feature a cost advantage over their DC counterparts and, in addition, offer lower maintenance, smaller motor size, and improved reliability. However, the control flexibility available with these drives is limited and their application is, in the main, restricted to fan, pump, and compressor types of applications where the speed need be regulated only roughly and where transient response and low-speed performance are not critical.

More demanding drives used in machine tools, spindles, high speed elevators, dynamometers, mine winders, rolling mills, glass float lines, and the like have much more sophisticated requirements and must afford the flexibility to allow for regulation of a number of variables, such as speed, position, acceleration, and torque. Such high-performance applications typically require a high speed holding accuracy better than 0.25%, a wide speed range of at least 20:1, and fast transient response, typically better than 50 rad/s, for the speed loop. Until recently, such drives were almost exclusively the domain of DC motors combined with various configurations of

AC-to-DC converters depending upon the application. With suitable control, however, induction motor drives have been shown to be more than a match for DC drives in high-performance applications. While control of the induction machine is considerably more complicated than its DC motor counterpart, with continual advancement of microelectronics, these control complexities have essentially been overcome. Although induction motor drives have already overtaken DC drives during the next decade it is still too early to determine if DC drives will eventually be relegated to the history book. However, the future decade will surely witness a continued increase in the use of AC motor drives for all variable speed applications.

AC motor drives can be broadly categorized into two types, thyristor based and transistor based drives. Thyristors possess the capability of self turn-on by means of an associated gate signal but must rely upon circuit conditions to turn off whereas transistor devices are capable of both turn-on and turn-off. Because of their turn-off limitations, thyristor based drives must utilize an alternating EMF to provide switching of the devices (commutation) which requires reactive volt-amperes from the EMF source to accomplish.

A brief list of the available drive types is given in Figure 1.1. The drives are categorized according to switching nature (natural or force commutated), converter type and motor type. Naturally commutated devices require external voltage across the power terminals (anode-cathode) to accomplish turn-off of the switch whereas a force commutated device uses a low power gate or base voltage signal which initiates a turn-off mechanism in the switch itself. In this figure the category of transistor based drives is intended to also include other hard switched turn-off devices such as GTOs, MCTs and IGCTs which are, in reality, avalanche turn-on (four-layer) devices.

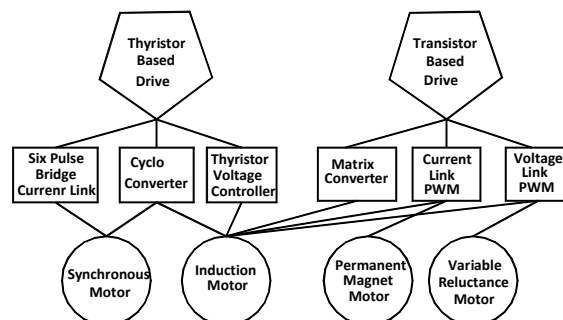


Figure 1.1 Major Drives type categories

The motion control used in various industries is shown in table 1.1

Table 1.1 Industrial Applications where motion control is require		
Sr. No.	INDUSTRY	APPLICATION
1	Automotive and transport equipment	Conveyer, marine, pumps
2	Chemicals and pharmaceuticals	Centrifugal pumps, fans, filling machine, labeling machine
3	Electronics ,electric and cables	Conveyors ,vacuum pump, winders
4	Food and beverage	Centrifugals ,agitators, pumps

Cont.

5	Metal working	Saws ,lathes, drills ,grinders presses, flying tools ,indexers, punchers, cranes
6	Material handling, lifts and cranes	Conveyors, hoists, screw feeder, cranes and lips
7	Metals ,minerals and mining	Dregs ,conveyors ,crusher ,ovens, smelters, and rolling mills
8	Oil ,gas and energy	Separators, conveyor and fans and pump
9	Packing machinery	Pelletizes high rise store, foil wrappers
10	Paper and printing	Pumps, wood chippers, washers, winders, printers, paper and cardboards lines,
11	Stone ,clay and glass	Conveyors, grinders, crushers, ovens, palletizers,
12	Textile and fiber	Man-made lines, cards, spinning frames, winders, weaving and knitting machine, cutting machine
13	Wood working	Sawmills, lathes, plywood lines, conveyor, indexers

In chapter 3 various methods used for controlling the speed of an induction motor is discussed also the problems associated with them are discussed.

As depicted in figure 1.1 current source inverter and voltage source inverter are being used for controlling speed of an induction motor. In this method motor winding is subjected to number of pulses per second. The effect of these pulses on motor winding is discussed in chapter 4. In chapter 5

MATLAB/SIMULINK program is presented for conducting No Load and Locked Rotor test on an induction motor.

Chapter 6 describe the detail of motors manufactured for the study purpose, experimental setup and voltage wave forms recorded during experiments for sinusoidal 50 Hz utility supply and with IGBT base PWM inverter supply with different frequency.

Discussion on wave forms obtained during experimentation is presented in chapter 7. How to improve the motor insulation performance is also discussed in this chapter.

Conclusion derived from the work and suggestions for possible direction for extension and scope for the enhancement are discussed in chapter 8.

Chapter 2

Identification of Equivalent Circuit Parameters, Life of the Motor and Methods of Prediction

2.1 INTRODUCTION

Advances in technology have made it possible to use AC drive in applications where high dynamic response, high speed accuracy is required. AC drives are light weight, less expensive and have low maintenance compared to DC drives.

AC motors require power converters and voltage controllers in order to control frequency, voltage and current. The three phase induction motor is work-horse of modern industry. Three phase induction motors are commonly used in constant speed application and adjustable-speed applications. Computer based Modeling and simulation of induction machine has opened new horizons for performance analysis. The realization of that analysis requires elaboration of mathematical models of motors under consideration. It requires solution of two basic problems:

- Formulation of a system of differential equations,
- Calculation of the values of coefficients (parameters), which are used in these equations.

A good mathematical model can help in predicting the behavior of induction machine under different operating conditions and in selecting the appropriate machine for specific operation.

In this chapter, the work proposes a method for estimation of parameter and prediction of steady state performance for induction motor based on equivalent circuit. The equivalent circuit parameters are found out by different tests of induction motor i.e. no load test, block rotor test, dc test etc, to evaluate the parameters of the IM equivalent circuit and draw the circle diagram, making it possible to deduce the IM characteristics, these tests are done in simulink and to facilitate the transition from tests to drawing the circle, the procedure was automated via a user friendly program written in

the matlab environment for conventional and converter fed induction motor. This saves time and gives better accuracy.

Equivalent circuit parameters are modified or estimated using numerically optimization method (Newton-Raphson method-discussed in chapter 5), which is a fast local convergence method used to solve nonlinear equations. Programming is done matlab M-file, because differential equations are easily solved with jacobian in matlab.

Once the exact parameters are determined performance can be calculated algebraically as well as graphically and performance can be predicated using any one of the three methods given on page 12, 13, and 15.

2.2 BASIC THEORY OF INDUCTION MOTOR

Like any conventional electric machine, the induction motor has two active elements, a stator and a rotor, which interact via an air gap where the energy exchange take place. In normal operation, the stator is excited by alternating voltage. This creates a rotating magnetic field inducing currents in the rotor winding. These currents, in turn, interact with rotating field to produce torque. Under some assumptions regarding the operation (balanced currents, unsaturated circuits), the stator and rotor fluxes can be calculated. Because of symmetry of balanced three phase IM stator and rotor windings, it is sufficient to take only one phase into account. Each phase has a resistance R in series with a linkage inductance L , and windings are magnetically coupled through a mutual inductance L_m . Since the frequency of stator currents is f_1 , the frequency of current induced in the rotor winding is equal to $f_2 = s*f_1$. Accordingly, the voltage and current equations for the stator (primary) and rotor (secondary) are expressed as follows:

$$V_s = R_s I_1 + j\omega L_s I_1 + j\omega L_m I_2 \quad (2.1)$$

$$\frac{V_2}{s} = \frac{R_2}{s} I_2 + j\omega L_2 I_2 + j\omega L_m I_1 \quad (2.2)$$

$$I_1 = I_m + I_2' \quad (2.3)$$

Where I_1 , I_2 , I_2' and I_m are respectively the stator, the rotor, the rotor referred to the stator, and magnetizing currents and $X_l = \omega L$, where $\omega = 2\pi f$.

R_s : stator resistance, X_s : stator leakage reactance, R_{FE} : magnetizing resistance, X_m : magnetizing reactance, R_r : rotor resistance, X_r : rotor reactance, s : slip, V_s : supply voltage (V)

To take into account the iron losses, a resistance R_{FE} can be added in parallel with magnetizing reactance X_m . As there is an analogy between the IM and transformer, the per phase equivalent circuit T-diagram referred to the stator of the IM is depicted in fig.2.1. With this equivalent circuit, the operational performances of an IM can be completely described. In normal operation, this diagram is used with constant voltage and frequency, therefore with a constant flux linkage.

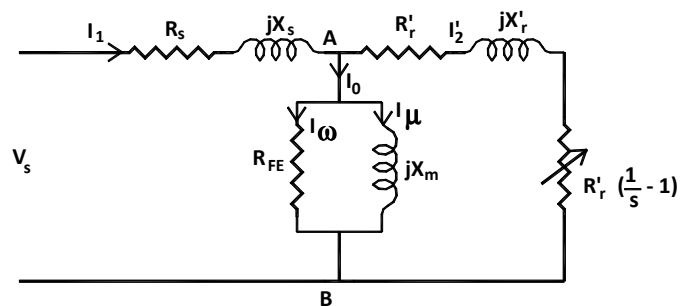
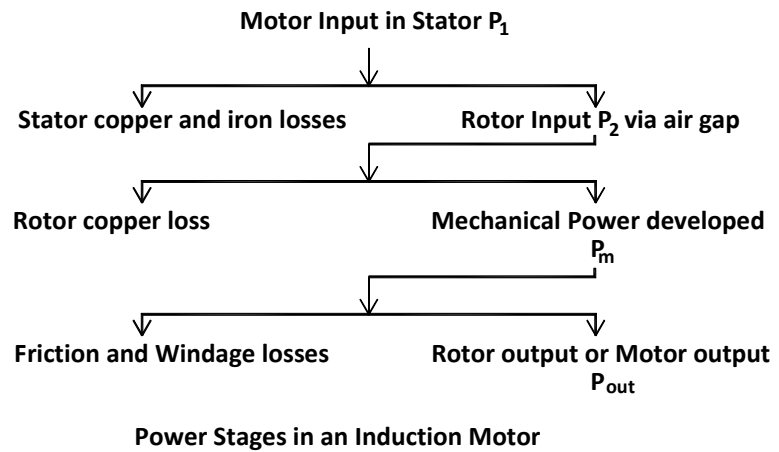


Figure 2.1 Equivalent circuit of an Induction Motor

2.3 STEADY STATE PERFORMANCE OF INDUCTION MOTOR

Steady state performances of induction motor are found out algebraically as well as graphically.

Power stages in an induction motor are as below



Performances are determined from following equations from equivalent circuit (Figure 2.1):

Stator input = Stator output + Stator losses

The stator output is transferred entirely inductively to the rotor circuit.

Obviously, Rotor input = Stator output

Rotor gross output = Rotor input – Rotor Cu losses

This Rotor output is converted into mechanical energy and gives rise to gross torque T_g .

Let N r.p.s. be the actual speed of the rotor and if T_g is an N-m, Then

$2\pi N * T_g =$ Rotor gross output in watts

$$R_L = R_r \left(\frac{1}{s} - 1 \right) \text{---(2.4)}$$

$$Z_r = \frac{R_r}{s} + jX_r \text{---(2.5)}$$

$$\frac{1}{Z_0} = \frac{1}{R_{FE}} + \frac{1}{jX_r} \text{---(2.6)}$$

$$\frac{1}{Z_{co}} = \frac{1}{Z_2} + \frac{1}{Z_0} \text{---(2.7)}$$

$$Z_{eq} = Z_{co} + Z_s \text{---}(2.8)$$

$$I_1 = V/Z_{eq} = I_0 + I_2 \text{---}(2.9)$$

$$I_2 = I_1 * \frac{Z_0}{Z_0 + Z_r} \text{---}(2.10)$$

$$P_{out} = 3I_2^2 R_L \text{---}(2.11)$$

$$T_g = P_{out}/\omega_m \text{---}(2.12)$$

$$\text{Rotor input} = T_g * 2\pi N_s \text{---}(2.13)$$

$$\text{Rotor cu loss} = T_g * 2\pi(N_s - N) \text{---}(2.14)$$

$$\phi = \left[\tan^{-1} \left\{ \frac{\text{Im}(Z_{eq})}{\text{Re}(Z_{eq})} \right\} \right] \text{---}(2.15)$$

$$\text{Power factor} = \cos \phi \text{---}(2.16)$$

$$\text{Power Input } P_{in} = 3VI_{eq} \cos \phi \text{---}(2.17)$$

$$\text{Efficiency} = \frac{P_{out}}{P_{in}} * 100 \text{---}(2.18)$$

2.4 LIFE OF THE MOTOR:

Life of the motor means the period of time for which motor is available for doing specified work or is able to deliver the rated power starting from the time from which motor is put in to the service. Normally the life of the motor is decided by the healthiness of insulation system and bearing.

Induction motors are widely used in industry, and usually have a long life. To predict the life and reliability of the motors within a reasonable time, a simple and available accelerated degradation testing method is presented by Deqiang Zheng [9]. To simulate the unbalanced load on the motor, the lamina with circular holes is mounted on the shaft of the motor eccentrically, and different unbalanced loads are obtained by changing the mounted places of the lamina. A motor accelerated test with three kinds of stress is applied, and the Orbit Areas are used to reveal the performance degradation index of motor. The life and reliability of the motor is finally predicted and evaluated with a balanced lamina mounted on the shaft as its normal working condition. The accelerated degradation testing approach has been proven to be practical to predict the life of the motors.

The development of high-frequency pulse width-modulation-based adjustable-speed drives (ASDs) has increased the efficiency, performance, and controllability in induction motor applications [10]. However, the high switching frequencies and the faster switching times of insulated gate bipolar transistors (the device of choice in these ASDs) introduce disadvantages like over voltages at the motor terminals when long cables are used between the drive and the motor. Another industry-wide concern is the generation of rotor shaft voltage and the resulting bearing current. The grease film in a bearing act as a capacitor that charges due to the transitions in the common-mode voltage imposed at the motor terminals by the drive. The breakdown of the film causes a spike of current to flow that can damage the bearing and reduce life. A significant amount of effort has been directed at understanding the shaft voltage phenomenon and the associated bearing current. This paper attempts to develop circuit models to predict the level of the shaft voltage. The circuit models can then be used to predict the shaft voltage levels at different installations, using simulation software like PSpice. Circuit models for two specific motors are developed. The predicted shaft voltage is very close to the actual voltage levels seen on the shaft when the motors are operated by ASDs.

Researchers have presented a various methods for determining the effect of bearing currents on life of the bearings [11 to 17].

2.5 PREDICTION TECHNIQUES:

2.5.1 INTRODUCTION

In decision making, one deal with devising future plans. The data describing the decision situation must thus be representative of what occurs in the future. For example, in inventory control, we base our decisions on the nature of demand for the controlled item during specified planning horizon. Also, in financial planning, we need to predict the pattern of cash flow over time.

In electrical drive system sometimes one comes across a situation where he/she is require to predict the behaviour of the motor or predict the performance of the motor ahead of the time. For example we are interested

Where b is an unknown constant parameter estimated from the historical data. The random error ϵ_t is assumed to have a zero expected value and a constant variance. Additionally, the data for the different periods are not correlated.

The moving average technique assumes that the most recent n observations are equally important in estimating the parameter b . Thus, at a current period t , if the data for the most recent n periods are

$$Y_{t-n+1}, Y_{t-n+2}, Y_{t-n+3}, \dots, Y_n \quad (2.20)$$

then the estimated value for period $t+1$ is computed as

$$Y_{t+1}^* = \frac{Y_{t-n+1} + Y_{t-n+2} + \dots + Y_n}{n} \quad (2.21)$$

There is no exact rule for selecting the moving average base, n . If the variations in the variable remain reasonably constant over time, a large n is recommended. Otherwise, a small value of n is advisable if the variable exhibits changing patterns. In practice, the value of n ranges between 2 and 10.

If we use $n=3$, the estimated demand for next time ($t=6$) will equal the average of the demands for time 3 to 5- that is,

$$Y_6^* = \frac{Y_3 + Y_4 + Y_5}{3} \quad (2.22)$$

2.5.3 EXPONENTIAL SMOOTHING

The exponential smoothing technique assumes that the process is constant, the same assumption used in the development of the moving average method. However it is designed to alleviate a drawback in the moving average method, where the same weight on all the data is used in computing the average. Specifically, exponential smoothing places a larger weight on the most recent observation.

Define α ($0 < \alpha < 1$) as the smoothing constant, and assume that the time series points for the past t periods are $y_1, y_2, y_3, \dots, y_n$. Then y_{t+1}^* , the estimate for period $t + 1$ is computed as

$$y_{t+1}^* = \alpha y_t + \alpha(1 - \alpha)y_{t-1} + \alpha(1 - \alpha)^2 y_{t-2} \dots \dots \dots (2.23)$$

Because the respective coefficients of $y_t, y_{t-1}, y_{t-2} \dots$ are progressively smaller, the new procedure puts more weight on the more recent data points.

The formula for computing y_{t+1}^* can be simplified as follows:

$$y_{t+1}^* = \alpha y_t + \alpha(1 - \alpha)y_{t-1} + \alpha(1 - \alpha)^2 y_{t-2} \dots \dots \dots (2.24)$$

$$y_{t+1}^* = \alpha y_t + (1 - \alpha)[\alpha y_{t-1} + \alpha(1 - \alpha)y_{t-2} \dots \dots \dots] (2.25)$$

$$y_{t+1}^* = \alpha y_t + (1 - \alpha)y_t^* (2.26)$$

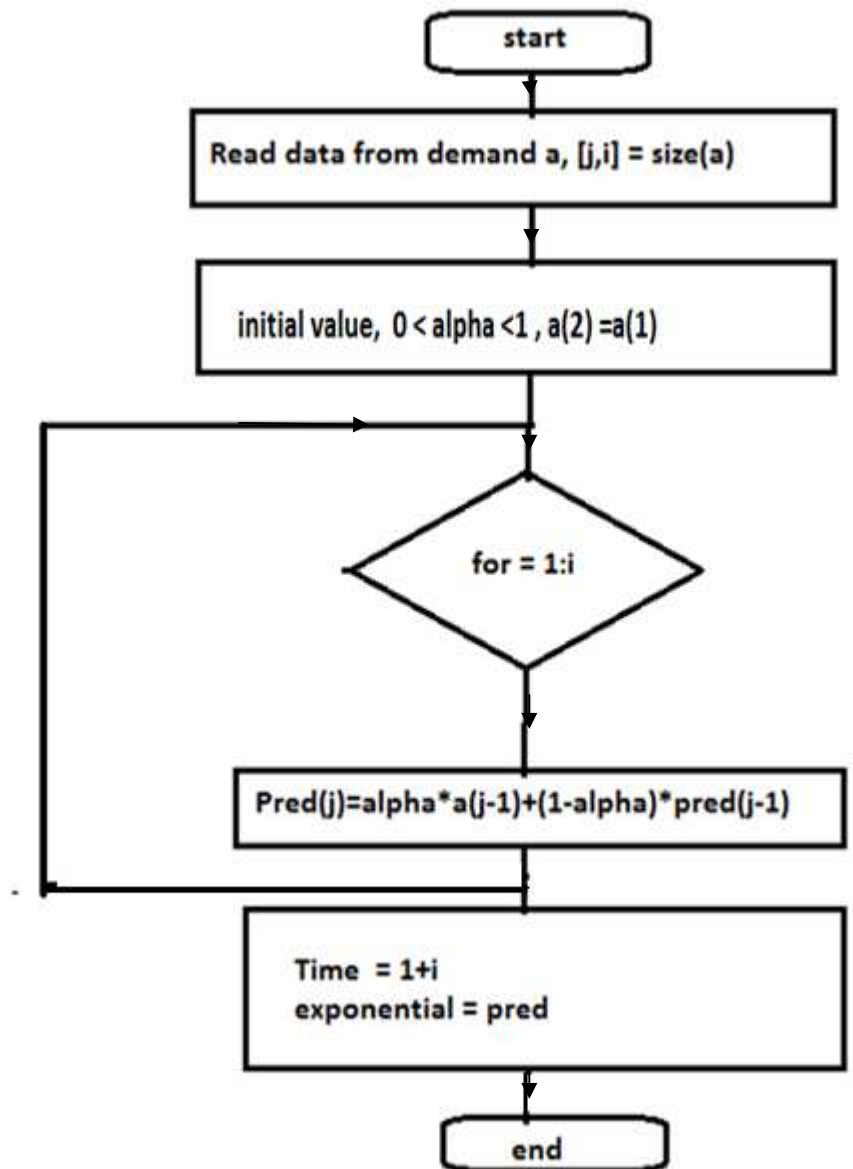
In this manner, y_{t+1}^* can be computed recursively from y_t^* . The recursive equation is started by skipping the estimate y_1^* at $t = 1$ and assuming that the estimate for $t = 2$ is taken equal to the actual data value for $t = 1$, that is $y_2^* = y_1$. Actually, any reasonable procedure can be used to start the computations. For example, some suggest estimating y_0^* as the average of a “reasonable” number of periods at the start of the time series.

The selection of the smoothing constant α is crucial in estimating future forecasts. A large value of α implies that recent observations carry heavier weights.

For the given computations, the estimate for $t = 6$ is computed as

$$y_6^* = \alpha y_5 + (1 - \alpha) y_4^* (2.27)$$

Flow chart for exponential smoothing method



2.5.4 REGRESSION

Regression analysis determines the relationship between a dependent variable (e.g., performance for a drive) and an independent variable (e.g., load/situation/time). The general regression formula between the dependent variable Y and the independent variable X is given as

$$y = b_0 + b_1X_1 + b_2X_2 + \dots + b_nX_n + \epsilon \text{ (2.28)}$$

Where b_0, b_1, \dots, b_n are unknown parameters. The random error ϵ has a zero mean and a constant standard deviation.

The simplest form of the regression model assumes that the dependent variable varies linearly with time—that is,

$$Y^* = a + bX \text{ (2.28)}$$

The constants a and b are determined from the time series data based on the least square criterion that seeks to minimize the sum of the square of the differences between the observed and the estimated values. Let (Y_i, X_i) represent the i^{th} point of the raw data representing the time series, $i = 1, 2, \dots, n$, and define

$$S = \sum_{i=1}^n (Y_i - a - bX_i)^2 \text{ (2.29)}$$

as the sum of the square of the deviations between the observed and estimated values. The values of a and b are determined by solving the following necessary conditions for the minimizations of S – that is,

$$\frac{\partial S}{\partial a} = -2 \sum_{i=1}^n (Y_i - a - bX_i) = 0 \text{ (2.30)}$$

$$\frac{\partial S}{\partial b} = -2 \sum_{i=1}^n (Y_i - a - bX_i)X_i = 0 \text{ (2.31)}$$

After some algebraic manipulations, we obtain the following solution:

$$b = \frac{\sum_{i=1}^n y_i x_i - n \bar{y} \bar{x}}{\sum_{i=1}^n x_i^2 - n \bar{x}^2} \quad (2.32)$$

$$a = \bar{y} - b \bar{x} \quad (2.33)$$

$$\bar{x} = \frac{\sum_{i=1}^n x_i}{n} \quad (2.34)$$

$$\bar{y} = \frac{\sum_{i=1}^n y_i}{n} \quad (2.35)$$

The equations show that we need to compute b first, from which the value of a can be computed.

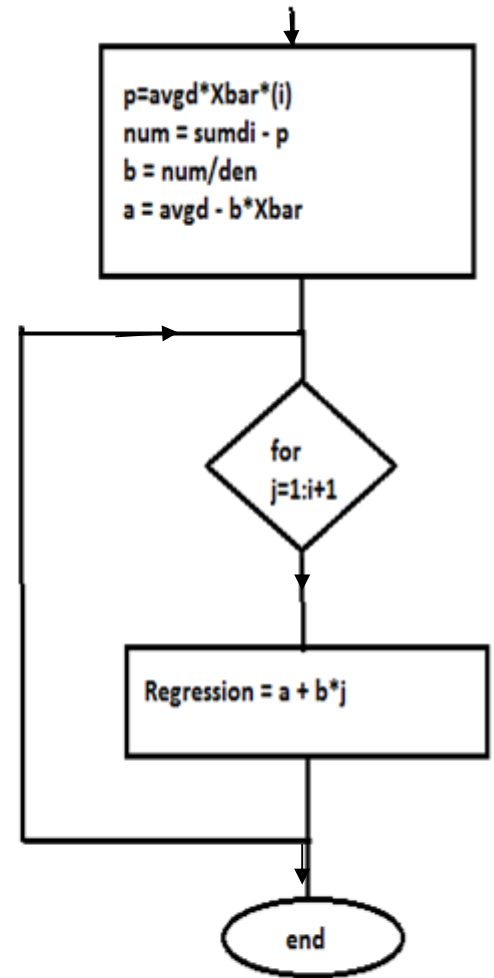
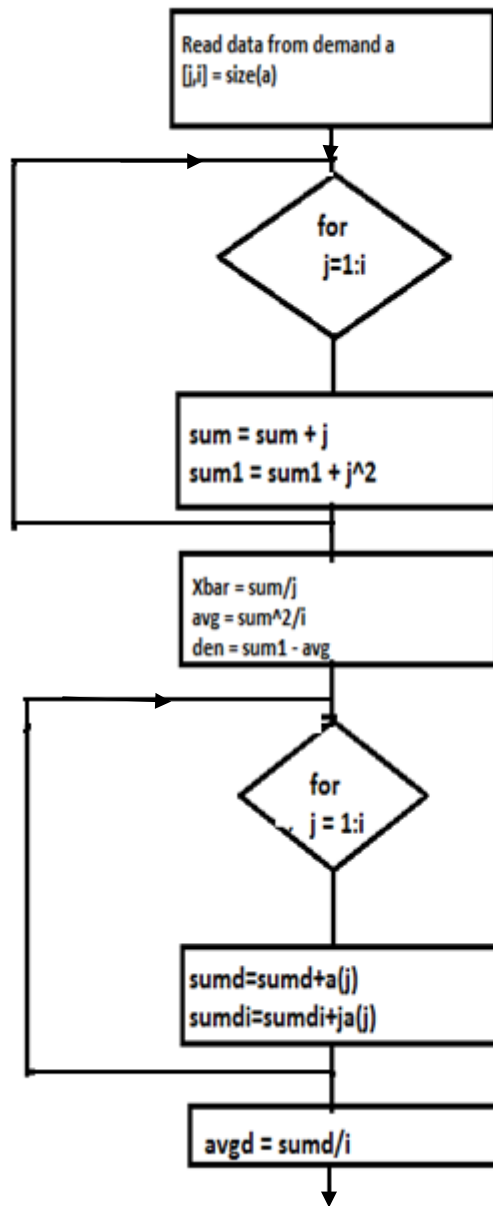
The estimates of a and b are valid for any probabilistic distribution of Y_i . However, if Y_i is normally distributed with a constant standard deviation, a confidence interval can be established on the mean value of the estimator at $X = X_0$ (i.e, $Y_0 = a + bX_0$) as

$$(a + bx) \pm t_{\frac{\alpha}{2}, n-2} \sqrt{\frac{\sum_{i=1}^n (y_i - y_i^*)^2}{n-2}} * \sqrt{\frac{1}{n} + \frac{(x - \bar{x})^2}{\sum_{i=1}^n (x_i^2 - n \bar{x}^2)}} \quad (2.36)$$

The expression $(Y_i - Y_i^*)$ represents the deviation between the i^{th} observed and estimated values of the dependent variable.

For future predicted values of the dependent variable, Y, we are interested in determining its prediction interval (rather than the confidence interval on its mean value). As would be expected, the prediction interval of a future value is wider than the confidence interval on the mean value. Indeed, the formula for the prediction interval is the same as that of the confidence interval except that the term $\frac{1}{n}$ under the second square root is replaced with $\frac{(n+1)}{n}$.

Flow chart for regression method



Chapter 3

Speed control of an Induction motor

3.1 INTRODUCTION

Apart from the nonlinear characteristics of the induction motor, there are various issues attached to the driving of the motor. Let us look at them one by one. Earlier motors tended to be over designed to drive a specific load over its entire range. This resulted in a highly inefficient driving system, as a significant part of the input power was not doing any useful work. Most of the time, the generated motor torque was more than the required load torque.

For the induction motor, the steady state motoring region is restricted from 80% of the rated speed to 100% of the rated speed due to the fixed supply frequency and the number of poles. When an induction motor starts, it will draw very high inrush current due to the absence of the back EMF at start. This results in higher power loss in the transmission line and also in the rotor, which will eventually heat up and may fail due to insulation failure. The high inrush current may cause the voltage to dip in the supply line, which may affect the performance of other utility equipment connected on the same supply line. When the motor is operated at a minimum load (i.e., open shaft), the current drawn by the motor is primarily the magnetizing current and is almost purely inductive. As a result, the PF is very low, typically as low as 0.1. When the load is increased, the working current begins to rise. The magnetizing current remains almost constant over the entire operating range, from no load to full load. Hence, with the increase in the load, the PF will improve. When the motor operates at a PF less than unity, the current drawn by the motor is not sinusoidal in nature. This condition degrades the power quality of the supply line and may affect performances of other utility equipment connected on the same line. The PF is very important as many distribution companies have started imposing penalties on the customer drawing power at a value less than the set limit of the PF. This means the customer is forced to maintain the full-load condition for the entire operating time or else pay penalties for the light load condition. While operating, it is often necessary to stop the motor quickly and also reverse it. In applications like cranes or hoists, the torque of the drive motor may have to be controlled so that the load does not have any undesirable acceleration (e.g., in the case of lowering of loads under the influence of gravity). The speed and accuracy of stopping or reversing operations improve the productivity of the system and the quality of the product. For the previously mentioned applications, braking is required. Earlier, mechanical brakes were in use. The frictional force between the rotating parts and the brake drums provided the required

braking. However, this type of braking is highly inefficient. The heat generated while braking represents loss of energy. Also, mechanical brakes require regular maintenance.

In many applications, the input power is a function of the speed like fan, blower, pump and so on. In these types of loads, the torque is proportional to the square of the speed and the power is proportional to the cube of speed. Variable speed, depending upon the load requirement, provides significant energy saving. A reduction of 20% in the operating speed of the motor from its rated speed will result in an almost 50% reduction in the input power to the motor. This is not possible in a system where the motor is directly connected to the supply line. In many flow control applications, a mechanical throttling device is used to limit the flow. Although this is an effective means of control, it wastes energy because of the high losses and reduces the life of the motor valve due to generated heat.

When the supply line is delivering the power at a PF less than unity, the motor draws current rich in harmonics. This results in higher rotor loss affecting the motor life. The torque generated by the motor will be pulsating in nature due to harmonics. At high, speed, the pulsating torque frequency is large enough to be filtered out by motor impedance. But at low speed, the pulsating torque results in the motor speed pulsation. This results in jerky motion and affects the bearings life. The supply line may experience a surge or sag due to the operation of other equipment on the same line. If the motor is not protected from such conditions, it will be subjected to higher stress than designed for, which ultimately may lead to its premature failure.

All of the previously mentioned problems, faced by both consumers and the industry, strongly advocated the need for an intelligent motor control. With the advancement of solid state device technology (BJT, MOSFET, IGBT, SCR, etc.) and IC fabrication technology, which gave rise to high-speed microcontrollers capable of executing real-time complex algorithm to give excellent dynamic performance of the AC induction motor, the electrical Variable Frequency Drive became popular.

The speed of an induction motor is given by

$$N = \frac{120 f}{P} (1 - s) \text{_____} (3.1)$$

From above equation, it is clear that we can change the speed of the motor by either changing frequency of the supply voltage, number of poles of the winding, or slip of the motor.

The methods of changing the speed of an induction motor can be divided in to two parts. (1) Control from stator side (1-a) Changing supply voltage, (1-b) changing frequency of supply voltage (1-c) changing number of poles of the stator winding (2) control from rotor sides (2-a) changing resistance in rotor winding, (2-b) injecting emf in rotor circuit.

The methods of controlling speed from stator sides are applicable to both the motors viz. slip ring motor and squirrel cage motor, whereas methods of controlling speed from rotor side are applicable to only slip ring motor.

Stator Voltage Control of an Induction Motor is used generally for three purposes (a) to control the speed of the motor (b) to control the starting and braking behaviour of the motor (c) to maintain optimum efficiency in the motor when the motor load varies over a large range. It is simple in hardware and reliable compared to the more complex Variable Frequency Drives as far as speed control application is concerned. However, it turns out to be a somewhat dissipative method of speed control and results in lowered efficiency and rotor overheating. Fundamental aspects of Stator Voltage Control aimed at the above three objectives is covered in this lecture.

3.2 STATOR VOLTAGE CONTROL FOR SPEED CONTROL OF INDUCTION MOTOR:

With fixed frequency and variable magnitude pure sine wave source the torque at any particular slip is proportional to square of Voltage in an Induction Motor. Fig. 3.1 below shows the Torque-Speed curves of 3-phase, 5 HP, 4-pole, 415 V, 50 Hz Induction Motor at various sinusoidal voltages. Also included is the torque-speed curve of a typical fan load. Note that the torque-speed curves of the Induction Motor clearly indicate that it is a motor designed for a large running slip. Otherwise the curves would have been steeper than this around full load rated speed. It can be clearly seen that the speed of the fan can be varied more or less uniformly in the range of 90% to 40% of synchronous speed of the motor by varying the voltage between 100% and 40%.

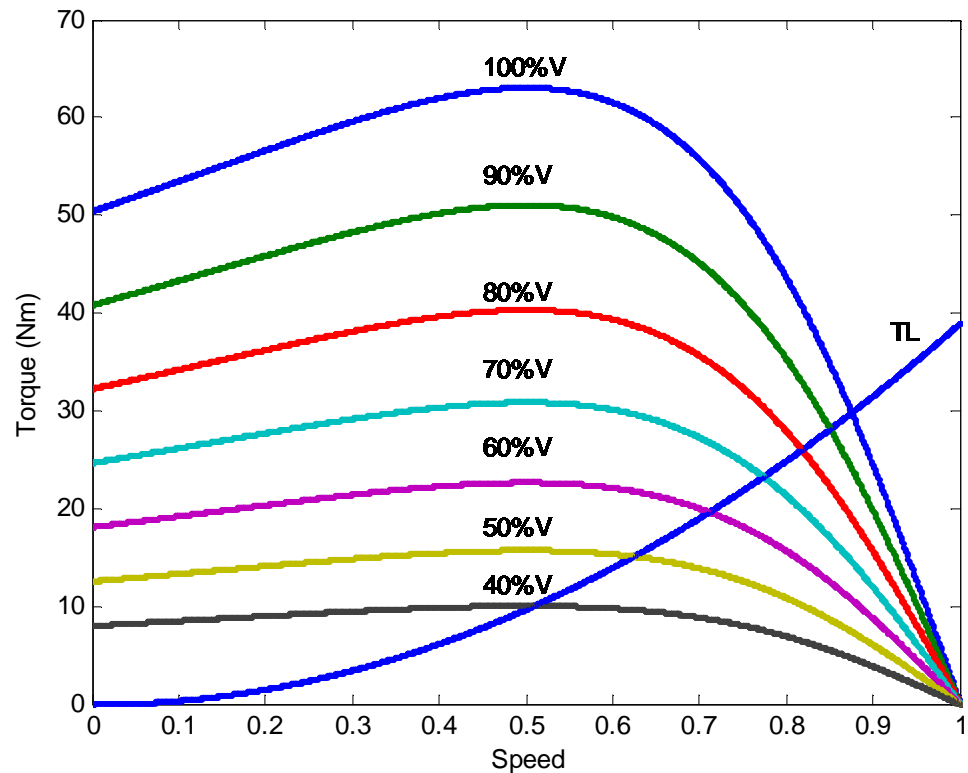


Fig. 3.1 Torque speed curve of fan motor for various voltages.

Had the torque-speed curves of the Induction Motor been steep around synchronous speed (as it is in the case of a well designed Squirrel cage Motor with a running slip in the range of 2% to 5%) the possible speed range in the case of a fan load with voltage control would have been lower than this. The motor will pull out at around 55% voltage or so. Moreover, even the available speed variation will be highly non-uniform with the voltage variation. Hence it is necessary that an Induction Motor intended for speed control applications using stator voltage control has to be designed with a higher running slip and hence lower full load efficiency. (Because higher full-load slip implies higher rotor resistance). Such motors are usually designed with a full load slip value of 12%. Obviously their rotor must be of special design in order to withstand the higher rotor losses developed in the rotor.

The range of speed control available by voltage control is a strong function of nature of load torque variation with load. With a constant torque load, the available speed range is more limited than in the case of a fan load and the motor pulls out at voltage levels closer to 100%. Thus fan loads which have low starting torque demand, pump loads with little or no static head component in the system curve, blower loads with small starting torque demand etc. are the loads suitable for speed control by voltage variation.

3.2.1 VARIATION OF STATOR CURRENT AND EFFICIENCY IN

STATOR VOLTAGE CONTROL

For simplicity the analysis to follow will neglect the magnetising current of the machine. Though the magnetising current can be as much as 50% of full load current at rated voltage, it comes down rapidly with voltage and hence the above assumption is reasonable.

Assuming sinusoidal quantities, the average torque produced by the stator field reacting with rotor current is given by the following proportionality:

$$T_m \propto \frac{I_2^2 * R_2}{s} \text{ (3.2)}$$

where T_m is the motor torque, R_2 the rotor resistance, I_2 the rotor current and s is the slip.

Neglecting the magnetising current and core loss current the stator current is proportional to rotor current. If the load torque is related to the square of motor speed as is approximately true for a fan load, then

$$T_L \propto (1 - s)^2 \text{ (3.3)}$$

where T_L is the load torque.

At steady state the motor torque and load torque will be equal. This results in the following proportionality for stator current.

$$I_1 \propto \frac{(1 - s)\sqrt{s}}{\sqrt{R_2}} \text{ (3.4)}$$

This function has a maximum at $s = 1/3$ (for fix value of rotor resistance differentiate numerator and equate to zero).

Thus for a true fan type load stator voltage control will result in a maximum current at 66.7% of synchronous speed.

The ratio of this maximum current at $s = 0.33$ to the rated full load current of the motor will vary sharply with the rated full load slip. The ratio is 1.75 if full load slip is 0.05 and it is 1.25 if the full load slip is 0.12. This implies that the maximum rotor copper loss (and stator Copper loss) in the machine will take place when the voltage applied is such that the fan load runs with a slip of 0.33 and that this maximum loss will be closer (but higher) to the rated full load copper loss if the rated slip of the machine is higher than normal (i.e. around 5%). Usually the motors for this service are designed with a full load slip of 0.12 and hence their current can go up to 25% higher than rated value as the speed of a fan load is varied by varying voltage.

Similarly their copper losses can go to 50% more than the full load copper loss under a variable voltage-fan load context. Thus we need an inherently inefficient machine to start with and the machine operation gets more and more inefficient at lower speeds. Hence this kind of speed control is used only on fan type loads and when only about 60% to 100% speed range is needed. Even then a motor with high rotor resistance (i.e. with a running slip of about 12%) should be used. Ordinary Squirrel Cage motors will suffer from rotor over heating on stator voltage control and should not be used for such service. Substituting $s = 1/3$ in equation (3.4) we have maximum current equation as

$$I_m \propto \frac{(1 - 1/3)\sqrt{1/3}}{\sqrt{R_2}} \text{-----} (3.4)$$

And rated current as

$$I_R \propto \frac{(1 - s_R)\sqrt{s_R}}{\sqrt{R_2}} \text{-----} (3.5)$$

Taking ration of maximum rotor copper loss to rated copper loss, we have

$$\frac{\text{Maximum rotor copper loss}}{\text{Rated copper loss}} = \frac{4}{s_R(1 - s_R)^2} \text{-----} (3.6)$$

Variation of maximum rotor copper loss with rated slip is shown in fig. 3.2

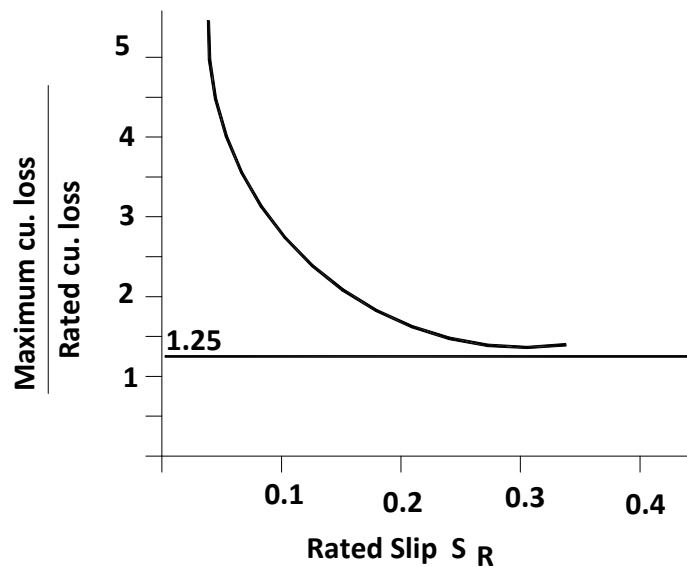


Fig. 3.2 Variation of ratio of maximum cu losses to rated cu loss for Induction motor fan type load

3.2.2 THYRISTOR BASED STATOR VOLTAGE CONTROLLER

The stator voltage is controlled in these speed control systems by means of a power electronic controller. Normally thyristors in phase control mode are used. Various connection schemes exist. However detailed investigations into various connections had established in early eighties that the six thyristor-unconnected neutral scheme is the best in terms of minimum r.m.s current requirement and harmonic injection. Here two thyristors in anti parallel are connected between the line and motor in a phase as shown in fig. 3.3. Typical wave form of voltage and current for this method is shown in fig. 3.4. If the motor is star connected the neutral is left unconnected. This scheme was proved to take only 8% more r.m.s current (due to harmonics and converter induced reactive power requirement) than a pure sine wave source at the maximum current slip value of $s = 0.33$. All other possible thyristor connections take more than this. Hence this 6-thyristor scheme is almost invariably used to control the applied voltage to Induction Motors in speed control schemes. The control is exercised by changing the firing angle α of thyristors.

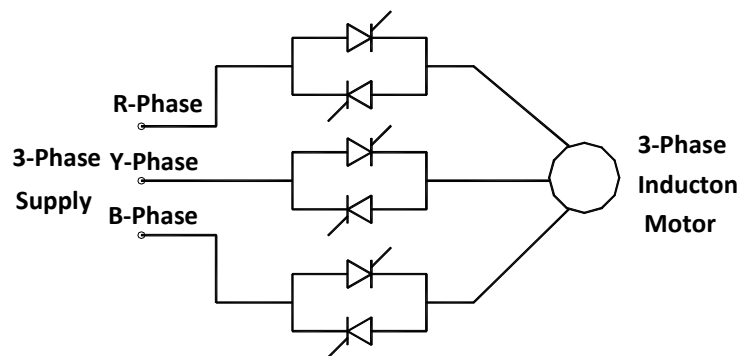


Fig. 3.3 Thyristor Voltage controller for Induction Motor

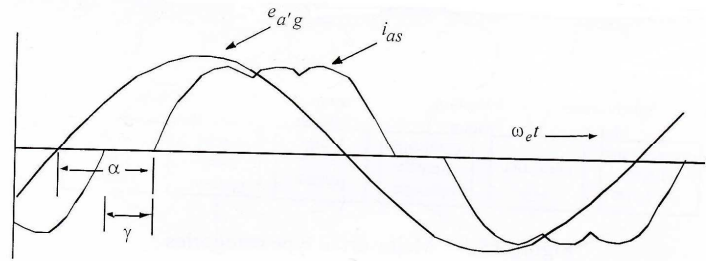


Fig.3.4 Wave form of voltage and current with thyristor voltage control.

The thyristor controller brings in two more sources of power loss. Power loss takes place in the power devices in the controller. In addition, harmonic losses take place in the motor due to harmonic currents flowing in the winding due to phase control. These two additional loss components will make this speed controller further inefficient. Also over heating of the motor on harmonic losses is another possibility. Harmonic currents can result in cogging/crawling etc. especially when attempts are made to run the motor at very low speeds. In spite of all these problems these speed controllers are popular; especially for fan loads with limited speed variation, due to their simplicity and reliability.

3.2.3 STARTING/STOPPING CONTROL BY STATOR VOLTAGE CONTROL

The commercially available Starting Torque Controllers (STC), Soft Starters etc. make use of stator voltage control using the 6-thyristor scheme to control the starting/stopping behaviour of the motors. They behave like a continuously variable autotransformer during starting. After starting, the thyristors are shorted by contactors to avoid device losses and full voltage is directly applied to the motor.

3.2.4 STATOR VOLTAGE CONTROL FOR OPTIMUM EFFICIENCY OPERATION OF MOTOR

Induction Motors are highly efficient at rated load and have efficiencies in the range 85%-95%. Motor losses consist of three main components: (1) Friction and Windage Losses (2) Iron Losses (3) Copper Losses. Friction and Windage Losses are insensitive to load changes, as speed is essentially constant.

Iron losses consist of hysteresis losses and eddy current losses. At constant frequency, hysteresis loss is proportional to $B^{1.6}$ and the eddy current loss is proportional to B^2 , where B is the maximum flux density in the air gap. The maximum flux density remains constant if the applied voltage is kept constant. Thus, as load is decreased, voltage remaining constant, the

iron loss constitutes a greater percentage of the output. This results in poor efficiency at part loads.

Part load efficiency can be improved by reducing the applied voltage to the motor. The motor has to be a standard squirrel cage motor optimised for full load running. In the case of such a motor the running slip will be around 0.04 and hence its torque-slip curve will be steep around zero slip. When the applied voltage is reduced, the load torque intersects the motor curve at a new point on the new torque-slip curve. However due to the steepness of T-s curves, the speed of machine will not vary much though it will decrease a little. Hence as a first approximation it may be assumed that the motor speed does not change when voltage across an under loaded motor is varied. If the speed does not change the load torque and mechanical power output will not change. And since voltage has come down the motor will draw an increased active current component to supply the same output. The reactive current component is predominantly magnetising in nature and it will come down since applied voltage has come down. The total stator current which is constituted by active and reactive components can increase or decrease depending on the amount of voltage reduction. Thus when the voltage across an under loaded motor is gradually reduced its stator current decreases first, reaches a minimum at a particular voltage and increases with further reduction in voltage. The value of minimum current will depend on the exact load on the motor.

Coming to the loss variations, with reduction in voltage the iron loss comes down. And initially the currents and hence copper losses also come down. When the voltage is reduced to sufficiently low level, the consequent increase in copper losses will at some point turn the total losses away from its decreasing trend i.e. there will be one particular voltage at which the total losses in the motor will be a minimum. This voltage value will not coincide with the voltage value at which the current is a minimum at the same loading level; but they will be close.

With the assumption that the speed of the motor does not vary with reduction in voltage the minimum current point will coincide with maximum power factor (or minimum phase angle) condition. Similarly the minimum loss point (i.e. maximum efficiency point) will coincide with minimum power input point. Minimum current point does not correspond to maximum efficiency point as already mentioned; but they are close. But if the small variation in motor speed and consequent changes in output power are also considered, the optimum voltage point for a particular load condition in the four cases i.e. the minimum current point, the minimum power factor angle point, the minimum power input point and the minimum loss (maximum efficiency) point, will be different. The minimum loss point is difficult to monitor electronically; though that is what we want to do. However, the other three conditions can be monitored electronically by sensing motor voltage and current and using some form of a minimum search algorithm implemented either digitally or in analog circuits. Of course, the loss reduction achieved will be less than optimal. Minimum power condition is the closest to maximum efficiency condition followed closely by current

minimum condition. It is easier to process the current minimum search and hence it is current minimum search that is employed in most of the Smart Motor Controllers available in the market.

The six-thyristor scheme is used in all these SMCs. The SMCs also take care of the control of starting and stopping of the motor also. Essentially, they start up the motor and apply full voltage first. Then, the current is sampled. A search routine is initiated. The voltage is decreased slightly and the change in current is noted. If the current decreases the voltage is further reduced in steps till the current shows a tendency to turn back i.e. to increase. If, in the first voltage reduction step the current increased, then the voltage is taken up in steps till the current reaches a minimum. This procedure is repeated in a periodic manner to fine-tune the applied voltage against load variations.

3.2.5 BASIC PRINCIPLES OF VOLTAGE CONTROL

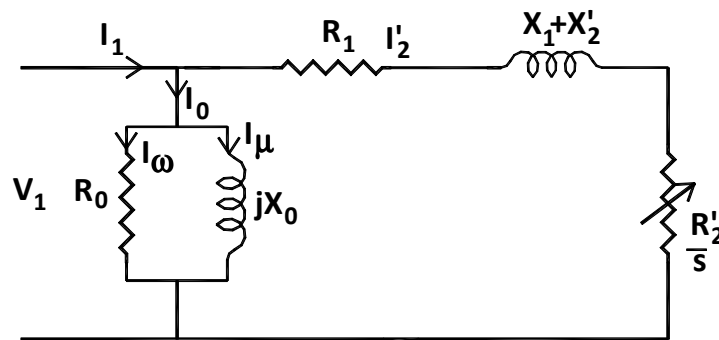


Fig. 3.5 Simplified Approximate equivalent circuit of an Induction Motor referred to stator

The basic principles of voltage control can be obtained readily from the conventional induction motor equivalent circuit shown in Figure 3.5 and the associated constant voltage speed-torque curves illustrated in Figure 3.6. The torque produced by the machine is equal to the power transferred across the air gap divided by synchronous speed,

$$T = \frac{3}{2} * P \left(\frac{I_2^2 * R_2}{s * f} \right) \text{-----} (3.7)$$

where P = number of poles, s is the per unit slip, f is line frequency and I_2, R_2 are the rotor rms current and rotor resistance respectively. Approximately this equation can be written as

$$T = \frac{3}{\omega_s * s} \left(\frac{V_1^2 * R_2'}{\left(R_1 + \frac{R_2'}{s}\right)^2 + (X_1 + X_2')^2} \right) \text{-----(3.8)}$$

The peak torque points on the curves in Figure 3.7 occur when maximum power is transferred across the air gap and are easily shown to take place at a

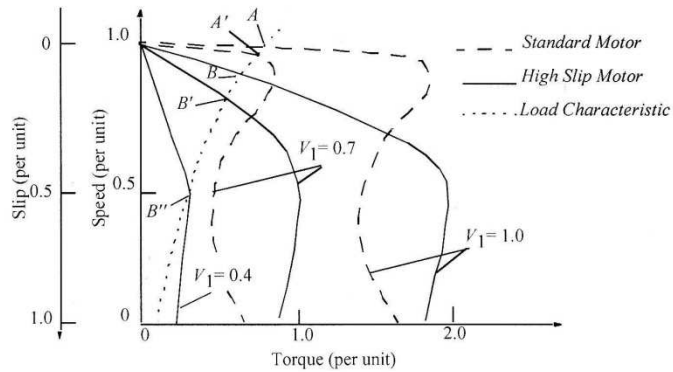


Fig.3.6 Torque slips Curves for standard and high slip Induction Motor.

Slip

$$s_m = \pm \frac{R_2'}{R_1 \pm \sqrt{(R_1^2 + (X_1 + X_2')^2)}} \text{-----(3.9)}$$

Substituting equation (3.9) into equation (3.8) gives the equation of maximum torque as

$$T_m = \frac{3}{2 * \omega_s} \left(\frac{V_1^2}{R_1 \pm \sqrt{(R_1^2 + (X_1 + X_2')^2)}} \right) \text{-----(3.10)}$$

where X_1 and X_2' are the stator and rotor leakage reactance. From these results and the equivalent circuit, the following principles of voltage control are evident.

(1) For any fixed slip or speed, the current varies directly with voltage and the torque and power with voltage squared.

(2) As a result of (1) the torque-speed curve for a reduced voltage maintains its shape exactly but has reduced torque at all speeds, see Figure 3.6.

(3) For a given load characteristic, a reduction in voltage will produce an increase in slip (from A to A' for the conventional machine in Figure 3.6,

(4) A high-slip machine has relatively higher rotor resistance and results in a larger speed change for a given voltage reduction and load characteristic.

(compare A to A' with B to B' in Figure 3.6).

(5) At small values of torque, the slip is small and the major power loss is the core loss in R_0 . Reducing the voltage will reduce the core loss at the expense of higher slip and increased rotor and stator loss. Thus there is an optimal slip which maximizes the efficiency and varying the voltage can maintain high efficiency even at low torque loads.

It has been shown that a very accurate fundamental component model for a voltage converter comprised of inverse parallel thyristors (or Triacs) is a series reactance given by [19]:

$$x_{eq} = x_s' * f(\gamma) \quad (3.11)$$

where

$$x_s' = x_1 + \frac{x_0 * x_2'}{x_0 + x_2'} \text{ and } x_1, x_2', x_0 \quad (3.12)$$

are the induction motor stator leakage, rotor leakage and magnetizing reactance respectively and γ is the thyristor *hold-off angle* identified in Figure 3.4 and

$$f(\gamma) = \left(\frac{3}{\pi}\right) \frac{(\gamma + \sin \gamma)}{1 - \frac{3}{\pi}(\gamma + \sin \gamma)} \quad (3.13)$$

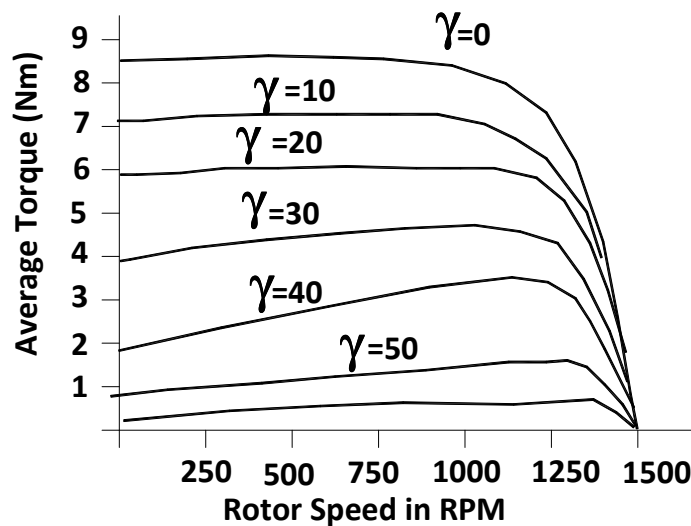


Fig. 3.7 Torque Slip Curves for changing in hold off angle γ

This reactance can be added in series with the motor equivalent circuit to model a voltage-controlled system. For typical machines the accuracy is well within acceptable limits although the approximation is better in larger machines and for smaller values of (γ) . In most cases of interest, the error is quite small. However, the harmonic power losses and torque ripple produced by the current harmonics implied in Figure 3.4 are entirely neglected. A plot of typical torque versus speed characteristics as a function of (γ) is shown in Figure 3.7 for a squirrel cage induction machine [20].

3.3 CHANGING FREQUENCY OF SUPPLY VOLTAGE

Synchronous speed and, therefore, the motor speed can be controlled by varying supply frequency. The supply voltage to motor is sinusoidal then its RMS value is given by equation

$$V = 4.44 \phi f T_{ph} \quad (3.14)$$

Where

$$\begin{aligned} \phi &= \text{Flux per pole wb, } f = \text{frequency of supply voltage, } T_{ph} \\ &= \text{No. of turns phase} \end{aligned}$$

Hence if magnitude of supply voltage is constant product of flux and frequency is constant. For the purpose of changing speed if we decrease the frequency, without a change in the magnitude of voltage, causes an increase in the air-gap flux. Induction motors are designed to operate at the knee point of the magnetization characteristic to make full use of the magnetic material. Therefore, the increase in flux will saturate the magnetic circuit of the motor. This will increase the magnetizing current, distort the line current and voltage, increase the core loss and the stator copper loss, and produce a undesirable noise. Similarly increase in supply frequency will decrease the magnitude of flux and hence reduces the torque capability of the motor. Therefore, the variable frequency control below the rated frequency is generally carried out at rated air gap flux by varying terminal voltage with frequency so as to maintain (V/f) ratio constant at the rated value.

Now substituting value of stator and rotor leakage reactance in terms of inductances in equation (3.10) we have

or

$$T_m = \left(\frac{K \left(\frac{V}{f} \right)^2}{\frac{R_s}{f} \pm \sqrt{\left(\frac{R_s}{f} \right)^2 + 4\pi^2 (L_s + L'_r)^2}} \right) \text{---(3.15)}$$

$$\text{Where } K \text{ is a constant} = \frac{3P}{8\pi} \text{---(3.16)}$$

and L_s and L'_r are, respectively, the stator and stator referred rotor inductances. Positive sign is for motoring operation where as negative sign is for braking operation.

When frequency is large such that

$$\frac{R_s}{f} \ll 2\pi(L_s + L'_r) \text{---(3.17)}$$

Then from equation (3.1)

$$T_m = \pm \left(\frac{K \left(\frac{V}{f} \right)^2}{2\pi(L_s + L'_r)} \right) \text{---(3.18)}$$

Equation (3.4) suggests that with a constant (V/f) ratio, motor develops a constant maximum torque, except at low speeds (or frequencies). Motor therefore operates in constant torque mode. According to Equation (3.1), for low frequencies (or low speeds) due to stator resistance voltage drop [i.e. when (R_s/f) is not negligible compared to $2\pi(L_s + L'_r)$] the maximum torque will have lower value in motoring (+ve sign) and large value in braking operation (-ve sign). This behaviour is due to reduction in flux during motoring operation and increase in flux during braking operation. When it is require to maintain the same maximum torque at low speeds during motoring operation it is necessary to increase (V/f) at low frequencies. This causes further increase in maximum braking torque and considerable saturation of the machine in braking operation.

When voltage reaches rated value corresponding to base speed, it cannot be increased with frequency. Therefore, above base speed, frequency is changed with voltage maintained constant. According to equation (3.18), with voltage maintained constant, maximum torque decreases with increase in frequency.

The variation of voltage and torque with speed is shown in fig. 3.8 and Torque speed curve for (V/f) is shown in fig. 3.9

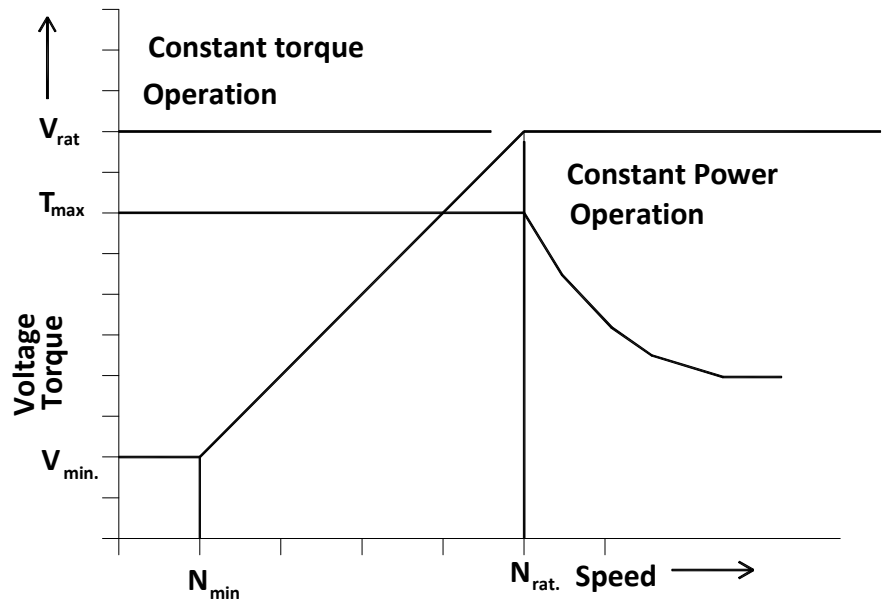


Fig. 3.8 Variation of torque and voltage with speed for V/F control method

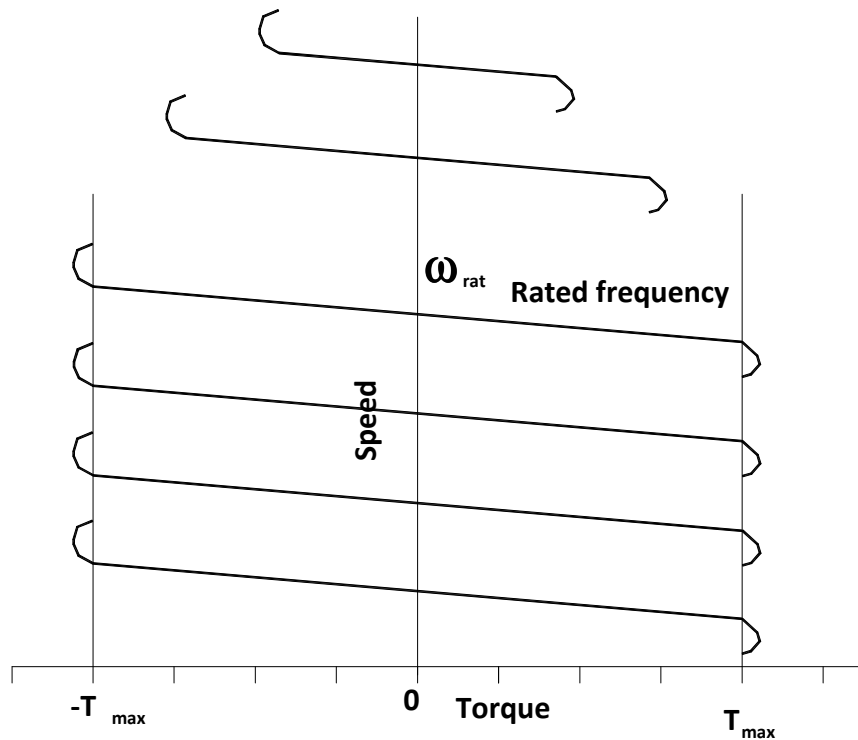


Fig. 3.9 Speed torque curve for V/f control

A given torque is obtained with a lower current when the operation at any frequency is restricted between the synchronous speed and the maximum torque point, both for motoring and braking operations. Therefore, the motor operation for each frequency is restricted between the synchronous speed and the maximum torque point as shown by solid lines in fig. 3.9

The variable frequency control provides good running and transient performance because of the following features:

- (i) Speed control and braking operation are available from zero speed to above base speed.
- (ii) During transients (starting, braking and speed reversal) the operation can be carried out at the maximum torque with reduced current giving good dynamic response.
- (iii) Copper losses are low, and efficiency and power factor are high as the operation is restricted between synchronous speed and maximum torque point at all frequencies.
- (iv) Drop in speed from no load to full load is small.

The most important advantage of variable frequency control is this that it allows a variable speed drive with above mentioned good running and

transient performance to be obtained from a squirrel cage induction motor. The squirrel cage induction motor has a number of advantages over a dc motor. It is cheap, rugged, reliable and long listing. Because of the absence of commutator and brushes, it requires practically no maintenance, it can be operated in an explosive and contaminated environment, and it can be designed for higher speeds, voltage and power ratings. It also has lower inertia, volume and weight. Though the cost of a squirrel cage motor is much lower compared to that of a dc motor of the same rating, the overall cost of variable frequency induction motor drive, in general are higher. But because of the advantages listed above, variable frequency induction motor drives are preferred over dc motor drives for most applications.

In special applications requiring maintenance free operation, such as underground or underwater installation, and also in applications involving explosive and contaminated environments, such as in mines and chemical industry, variable frequency induction motor drives are natural choice. They have several other applications such as traction, mill run out tables, steel mills, fans, pumps, blowers, compressors, spindle drives, conveyers, machine tools, and so on.

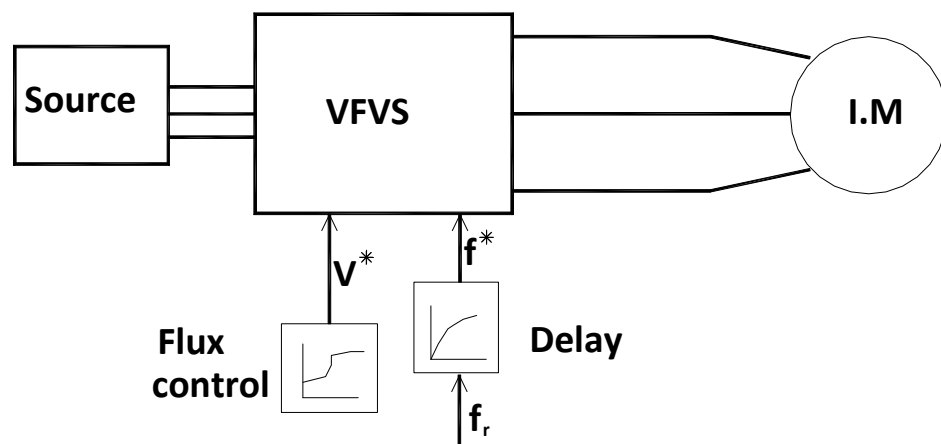


Fig.3.10 Block diagram for variable frequency control

Block diagram of variable frequency speed control scheme is shown in fig. 3.10. The motor is fed from a variable frequency voltage source (VFVS).

V^* and f^* are voltage and frequency commands for VFVS. Flux control box produces a voltage command V^* for VFVS in order to maintain the relationship of fig. 3.9 between V^* and f^* . Reference frequency f_r is changed to control the speed. A delay circuit is introduced between f_r and f^* , so that even when f_r is changed by large amount, f^* will change only slowly so that motor speed can track changes in f^* , thus restricting the motor operation for each frequency between synchronous speed and the maximum torque point. VFVS can be a voltage source inverter or a Cycloconverter.

VFDs eliminate the need for mechanical or hydraulic drives (clutches, gears, pulley, valves, and vanes). The term adjustable speed drive (ASD) is often used interchangeably with VFDs, though this is not quite accurate. ASDs include VFDs, but also methods to control the speed of dc motors, technology that has been around since the early 1960s. During the 1980s, VFDs become the preferred method of driving many types of load at continuously variable speeds. VFDs are used with ordinary types of ac induction motors or synchronous motors.

Working of variable frequency drives:-

The three main parts of a VFD are as follows:

1. Regulator-controls the rectifier and inverter to produce the desired ac frequency and voltage.
2. Rectifier-converts the fixed frequency ac voltage to dc.
3. Inverter-switches the rectified dc voltage to ac, creating variable ac frequency (and controlling current flow, if desired).

VFDs are totally electronic devices that convert alternating current to direct current by a rectifier. The direct current is converted back to alternating current by an inverter, at a frequency that will drive the motor at the desired speed. VFDs change the speed of the motor by using high-power semiconductor switching devices (silicon controlled rectifiers, thyristors, or power transistors). These devices change the frequency of the current that is supplied to the motor, but do so only in an on/off manner. As a result, the alternating current that is provided to the motor is not a smooth sine wave. Although this makes the motor itself less efficient, the ability of the motor to respond to load variations increases the overall energy efficiency. Without a VFD a motor might run efficiently at a single speed, but it may likely be the wrong speed as the motor's load varies.

3.4 CONTROL TECHNIQUES

Various speed control techniques implemented by modern age VFD

are mainly classified in the following three categories:

[A] Scalar Control (V/f Control)

[B] Vector Control (Indirect Torque Control)

[C] Direct Torque Control (DTC)

3.5 SCALAR CONTROL

In this type of control, the motor is fed with variable frequency signals generated by the PWM control from an inverter. Here, the V/F ratio is maintained constant in order to get constant torque over entire operating range. Since only magnitudes of the input variables- frequency and voltage- are controlled, this is known as scalar control. Generally, drives with such a control are without any feedback devices (open loop control). Hence, a control of this type offers low cost and an easy to implement solution.

In such controls, very little knowledge of the motor is required for frequency control. Thus, this control is widely used. A disadvantage of such a control is that the torque developed is load dependent as it is not controlled directly. Also, the transient response of such a control is not fast due to the predefined switching pattern of the inverter. However, if there is a continuous block to the rotor rotation, it will lead to heating of the motor regardless of implementation of the over current control loop. By adding a speed/position sensor, the problem relating to the blocked rotor and the load dependent speed can be overcome. However, this will add to the system cost, size and complexity. There are a number of ways to implement scalar control. The popular schemes are described in the following sections.

3.6 SIX-STEP PWM

The inverter of the VFD has six distinct switching states. When it is switched in a specific order, the three- phase AC induction motor can be rotated. The advantage of this method is that there is no intermediate calculation required and thus, is easiest to implement. Also, the magnitude of the fundamental voltage is more than the DC bus. The disadvantage is higher low-order harmonics which cannot be filtered by the motor inductance. This means higher losses in the motor, higher torque ripple and jerky operation at low speed.

3.7 VOLTAGE SOURCE INVERTER (VSI) CONTROL

The inverter used for the control of as drives can be a voltage source inverter or a current source inverter. An inverter circuit can be a voltage source inverter if, viewed from the load side, the ac terminals of the inverter

function as a voltage source. Similarly, a current source inverter is that inverter function as a current source.

Voltage source inverter has low internal impedance and thus its terminal voltage remains substantially constant with variation in load. Therefore VSI is suitable for multi-motor drives, although it is equally good for a single motor drive.

The current source inverter (CSI) because of its large internal impedance is not suitable for multi-motor drives, because any change in load on one of the motor will affect the voltage supplied to other motors also.

Since the inverter current of CSI is independent of the load impedance, it has inherent protection against short circuit across its terminals. Any short circuit in VSI may give rise to high currents and therefore a fast over current protection device is essential.

Variable frequency and variable voltage supply for induction motor control can be obtained either from voltage source inverter (VSI) or a cycloconverter.

Voltage source inverter allows a variable frequency to be obtained from a dc supply. Fig. 3.11 shows a VSI employing thyristors. Any other self-commutated device can be used instead of transistor.

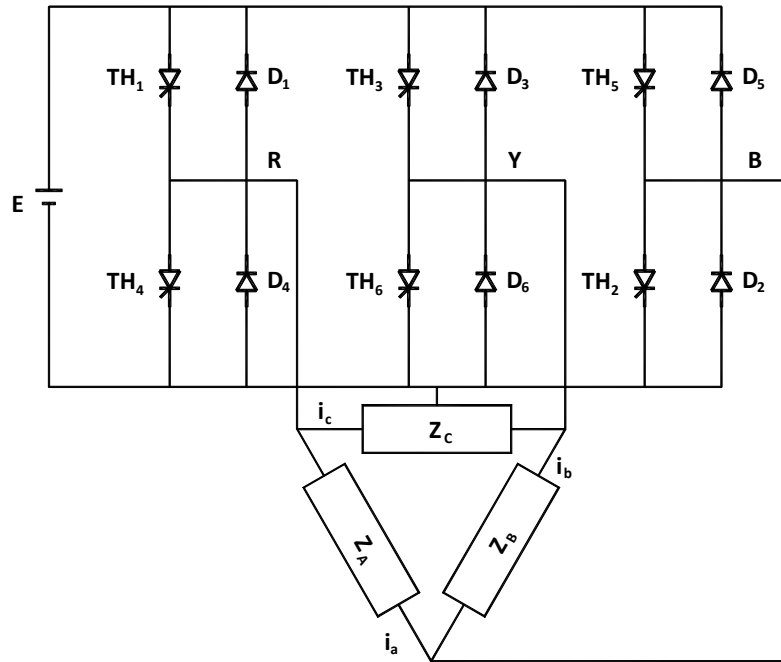


Fig. 3.11 Three Phase Bridge Inverter

Generally MOSFET is used in low voltage and low power inverter, IGBT (Insulated gate bipolar transistor) and power transistors are used up to medium power levels and GTO (gate turn off thyristor) and IGCT (Insulated gate commutated thyristor) are used for high power levels.

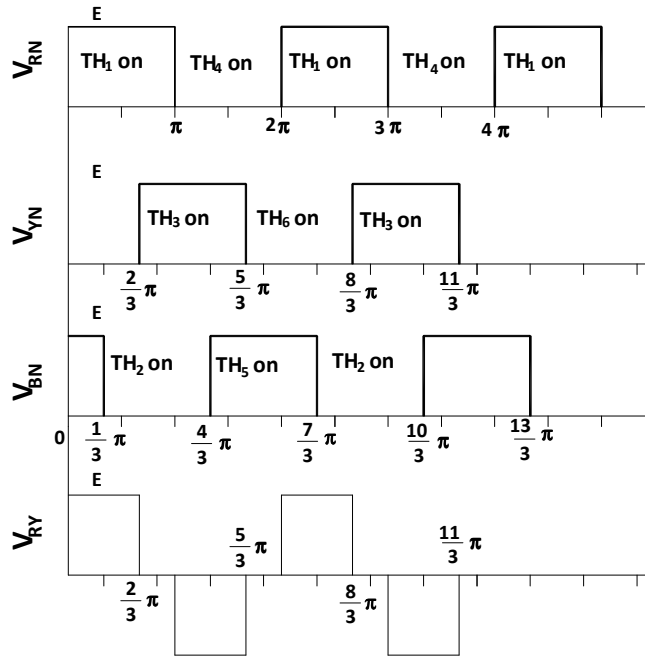


Fig. 3.12 Voltage Waveforms of the Inverter shown in fig. 3.11

VSI can be operated as a stepped wave inverter or a pulse-width modulated (PWM) inverter. When operated as a stepped wave inverter, thyristors are switched in the sequence of their numbers with a time difference of $T/6$ and each transistor is kept on for the duration $T/2$, where T is the time period for one cycle. Resultant line voltage wave form is shown in fig. 3.12. Frequency of inverter operation is varied by varying T and the output voltage of the inverter is varied by varying dc input voltage.

Inverter output phase voltage and line voltage is given by following Fourier series.

$$V_{RN} = \frac{2}{\pi} E \left[\sin \omega t + \frac{1}{5} \sin 5\omega t + \frac{1}{7} \sin 7\omega t \right] \text{---(3.19)}$$

The rms value of the fundamental phase voltage is given by

$$V_P = \frac{\sqrt{2}}{\pi} E \text{---(3.20)}$$

$$V_{RY} = \frac{2\sqrt{3}}{\pi} E \left[\sin \omega t - \frac{1}{5} \sin 5\omega t - \frac{1}{7} \sin 7\omega t + \frac{1}{11} \sin 11\omega t + \frac{1}{13} \sin 13\omega t \dots \dots \right] \text{---(3.21)}$$

The rms value of the fundamental line voltage is given by

$$V_L = \frac{\sqrt{6}}{\pi} E = 0.78E \text{---(3.22)}$$

The rms value of the line voltage given by eq. (3.21) is

$$V_{TL} = \sqrt{\frac{2}{3}} E = 0.816E \text{---(3.22)}$$

Therefore, the total harmonic component is not more than 31.08 percent of the fundamental. By using more complex circuits having more number of thyristors, the number of steps in the voltage waveform can be increased which makes the wave forms more ideal.

If the load is star connected instead of delta, the voltage waveform with respect to neutral point is as shown in fig. 3.13. The Fourier analysis of this waveform yields the following expression:

$$V_{RO} = \frac{3}{\pi} E \left[\sin \omega t - \frac{1}{5} \sin 5\omega t - \frac{1}{7} \sin 7\omega t + \frac{1}{11} \sin 11\omega t + \frac{1}{13} \sin 13\omega t \dots \dots \right] \text{---(3.23)}$$

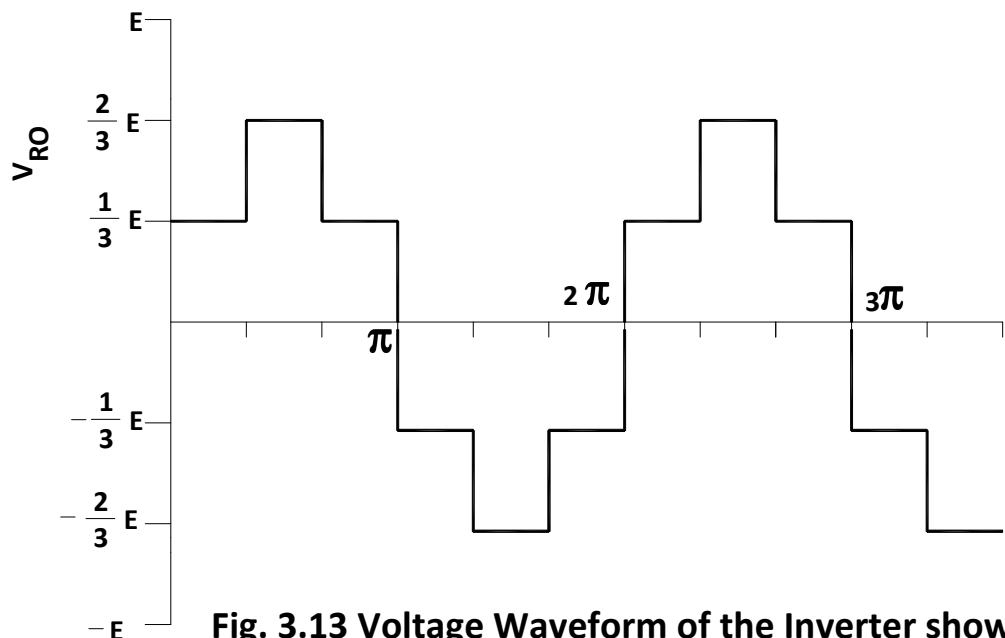


Fig. 3.13 Voltage Waveform of the Inverter shown in fig. 3.11 for star connected load

The current waveforms consist of series of exponentially rising or decreasing components depending on the switching of the thyristors.

3.8 VOLTAGE CONTROL OF INVERTERS

To maintain a constant flux density in the induction motor, the inverter must maintain constant ratio of voltage to frequency. This voltage variation can be obtained by one of the following possible methods:

[1] By varying direct voltage input of the inverter.

[2] By varying output voltage of the inverter.

[3] By using switching techniques within the inverter.

In a dc link inverter, the magnitude of its output ac voltage depends on the magnitude of its input dc voltage. Therefore by having a variable dc supply obtained from the converter, the output voltage of the inverter can be varied.

When supply is dc, variable dc input voltage is obtained by connecting a chopper between dc supply and inverter (fig.3.14(a)). When supply is ac, variable dc input voltage is obtained by connecting a controlled rectifier between ac supply and inverter (3.14(b)). A Large electrolytic filter capacitor **C** is connected in dc link to make inverter operation independent of rectifier or chopper and to filter out harmonic in dc link voltage.

For controlling the output voltage of the inverter from its outside, a variable ratio output transformer may be used. The output of the inverter is connected to input terminals of the transformer. The voltages tapping of the transformer are controlled automatically using closed loop control.

The third method of voltage control requires control of switching in the thyristors to modify the output wave form. The most common method used for this type of control is by having pulse width modulated inverter.

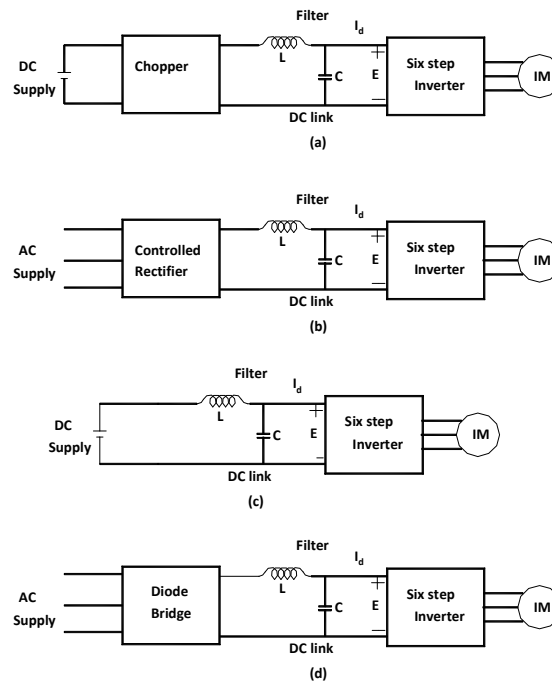


Fig. 3.14 VSI controlled IM drives

The main drawback of stepped wave inverter is the large harmonics of low frequency in the output voltage. Consequently, an induction motor drive fed from a stepped wave inverter suffers from the following drawbacks:

- [1] Because of low frequency harmonics, the motor losses are increased at all speeds causing derating of the motor.
- [2] Motor develops pulsating torques due to fifth, seventh, eleventh and thirteenth harmonics which cause jerky motion of the rotor at low speeds.
- [3] Harmonic content in motor current increases at low speeds. The machine saturates at light loads at low speeds due to high (V/f) ratio. These two effects overheat the machine at low speeds, thus limiting lowest speed to around 40% of the base speed.

Harmonics are reduced, low frequency harmonics are eliminated, associated losses are reduced and smooth motion is obtained at low speed also when inverter is operated as a pulse-width modulated inverter.

The method of voltage control using the pulse width modulation scheme can be explain with the help of single phase bridge inverter of fig. 3.15. The output voltage waveform of this inverter is shown in fig. 3.15(b). It is a square wave having $+E$ magnitude for $0 < \omega t < \pi$ and $-E$ for $\pi < \omega t < 2\pi$. If the voltage control is desired the output pulse may be controlled as shown in fig 3.15(c).

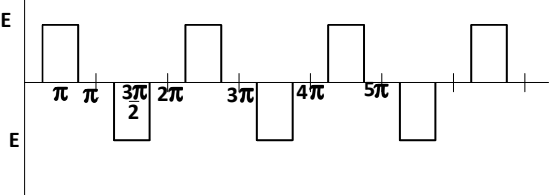
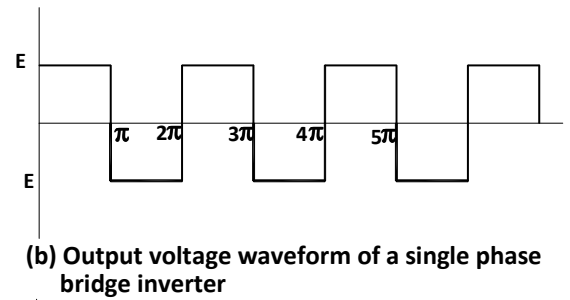
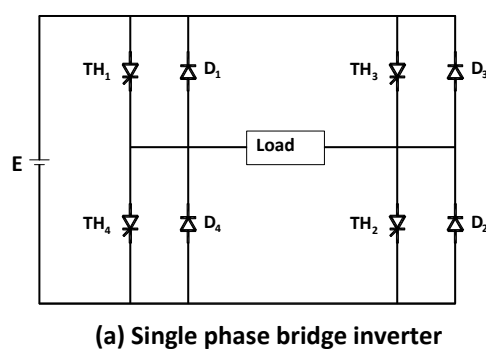


Fig. 3.15 Single phase bridge inverter and its output voltage waveforms

The thyristors connecting the load to the supply are not always 'ON' but there is some period for which no supply is connected to the load. In a single pulse modulation, a pulse width is created around $\pi/2$ and $3\pi/2$; the variation in voltage is obtained by varying the width of these pulses. As can be seen from fig.3.15, the harmonic contents are increases for low voltage output of the inverter. Therefore, multiple pulse modulation schemes are preferred. In a multiple pulse scheme, instead of one pulse in each half cycle, there are several equidistant pulses as shown in fig. 7.16 are generated. As shown in figure, there are M pulses, each of height E , and the variation in voltage magnitude is obtained by varying the pulse width. This type of modulation is achieved by comparing a dc level with triangular wave. By varying the dc voltage level, the pulse width can be varied.

The advantage of multi pulse modulation is that the voltage control is achieved with simultaneous reduction of lower order harmonics. However at very low frequency, and for constant V/F the out voltage wave form deteriorates, since the interval between pulses increases.

3.9 SINUSOIDAL PWM

A still better method of pulse width modulation scheme is possible in which the pulse width is varied throughout the half cycle. In this method, the sinusoidal weighted values are used. Here the pulse width is made the sinusoidal function of the angular position of the pulse in the cycle. The advantage of this technique is that very little calculation is required. Only on look-up table of sine wave is required, as all the motor phases are 120° (electrical) displaced. The disadvantage of this method is that the magnitude of the fundamental voltage is less than 90%. Also, the harmonics at PWM switching frequency have significant magnitude

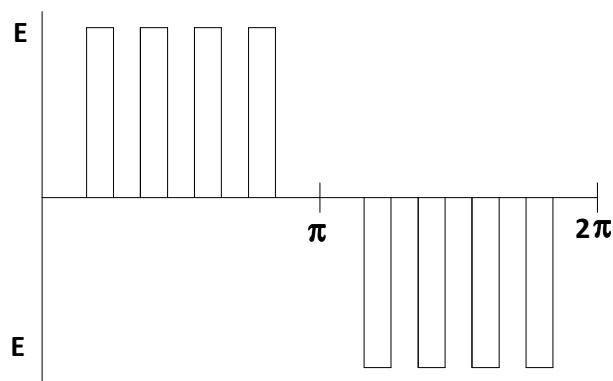


Fig. 3.16 Multipulse modulation scheme

Thus the pulse width increases as the angle increases from 0 to 90° then the width decreases from 90° to 180° again the pulse width increases in negative direction from 180° to 270° then the width decreases from 270° to 360° . The output voltage waveform of sinusoidal pulse width modulated inverter is shown in fig.3.17. The waveforms can be generated by means of a control circuit in which a high frequency triangular wave form is compared with a rectified sinusoidal wave.

Since output voltage can now be controlled by pulse width modulation, no arrangement is required for the variation of input dc voltage, hence inverter can be directly connected when the supply is dc [fig. 3.14(c)] and through a diode rectifier when supply is ac [fig. 3.14(d)].

The fundamental component in the output phase voltage of a PWM inverter operating with sinusoidal PWM is given by

$$V = m \frac{E}{2\sqrt{2}} \quad (3.24)$$

Where m is the modulation index.

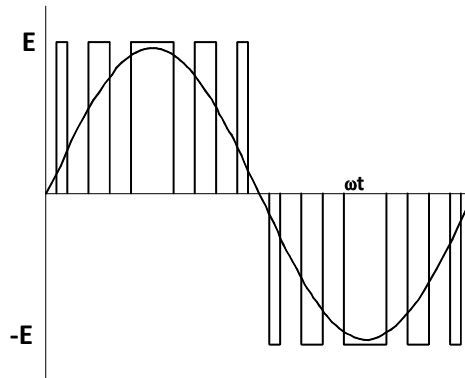


Fig. 3.17 Sinusoidal Pulse width modulated inverter

The harmonics in the motor current produce torque pulsation and derate the motor. For a given harmonic content in motor terminal voltage, the current harmonics are reduced when the motor has higher leakage inductance; this reduces derating and torque pulsations. Therefore, when fed from VSI, induction motors with large (compared to when fed from sinusoidal supply) leakage inductance is used.

3.10 CYCLOCONVERTER

In cycloconverter the ac voltage at supply frequency is directly converted to a voltage source of lower frequency. Normally cycloconverters are used to get a single phase or a three phase supply output from a three phase input. Basically it consists of two group of phase controlled rectifier circuit for each phase of the output, one group for the positive portion and the other group for the negative portion. By delaying the firing angle of the controlled rectifier the mean output voltage of the rectifier can be controlled. If the rectifier firing angle is slowly varied from **90** degree to **0** degree and **0** degree to **90** degree, the mean output voltage will vary from zero to maximum value, then from maximum to zero. Therefore, it is possible to have low frequency sinusoidal variations superimposed on the output voltage

of the rectifier. A second group of the rectifiers is used to produce negative half cycle of the waveform. The frequency of the superimposed voltage is totally dependent on the firing angle control and is independent of the supply frequency. A three-phase to single phase cycloconverter is shown in fig. 3.18.

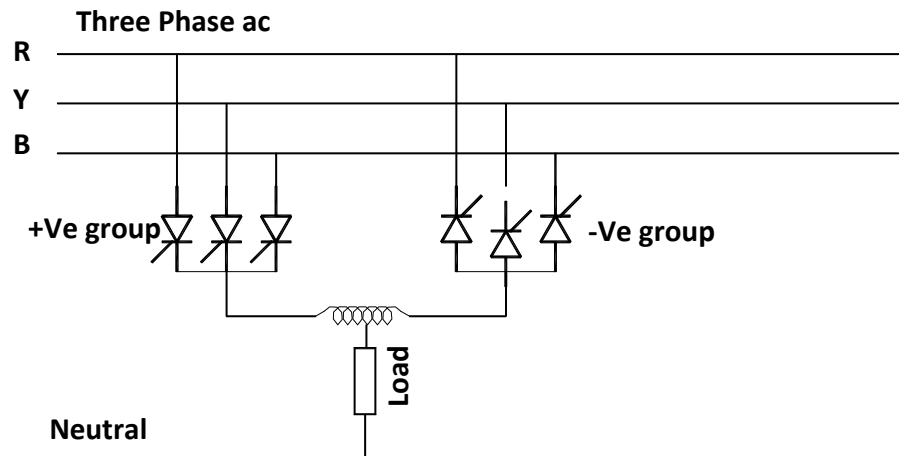


Fig 3.18 Three Phase to Single Phase cycloconverter

The variation of firing angle for the positive group rectifier and for the negative group rectifier is shown in fig. 3.19(a) and 3.19 (b) respectively. As can be seen from fig. 3.19(a), the firing angle at **H** is $\pi/2$ and average value of output voltage is zero. The firing angle is decreased at **J, K**, and it is zero at **L**. The firing angle is again increased at **M, N, O** and it $\pi/2$ at **P**. The average value of the voltage is shown as broken line. Similarly, for the negative group of the rectifier bridge, by controlling the firing angle from 0 to $\pi/2$, the mean output voltage can be obtained which has lower frequency as shown in fig. 3.19(b).

The average back emf of the inverter may also be controlled in a sinusoidal form by varying the firing angle from $\pi/2$ to π and the power flow can be reversed. Thus it is possible to have regenerative operation of the induction motor fed from a cycloconverter.

Since the positive and negative group of rectifiers are connected in inverse parallel, their average output voltage must be equal. This is achieved by making the firing angle for the negative group $\alpha_n = \pi - \alpha_p$ where α_p is

firing angle for the positive group. However, instantaneous output voltages of the two groups are not equal and a centre-tapped reactor is used to limit the circulating current.

For three phases to three cycloconverter circuits, three single phase cycloconverters with a phase displacement of 120° between their outputs are used as shown in fig. 3.20. The cycloconverter has certain advantages as well as disadvantages over dc link inverter. It has the following advantages.

[1] the cycloconverter is more efficient as there is only one stage of conversion compared to two stages of conversion required in dc link inverters. Also the cycloconverter does not require forced commutation and nearly 90 % efficiency can be obtained.

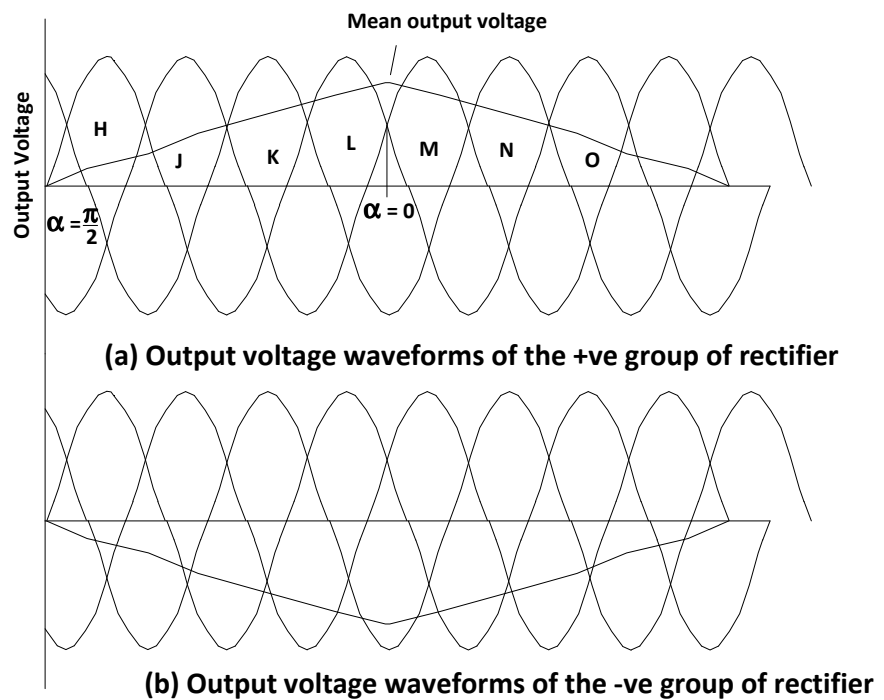


Fig 3.19 Output voltage waveforms of cycloconverter

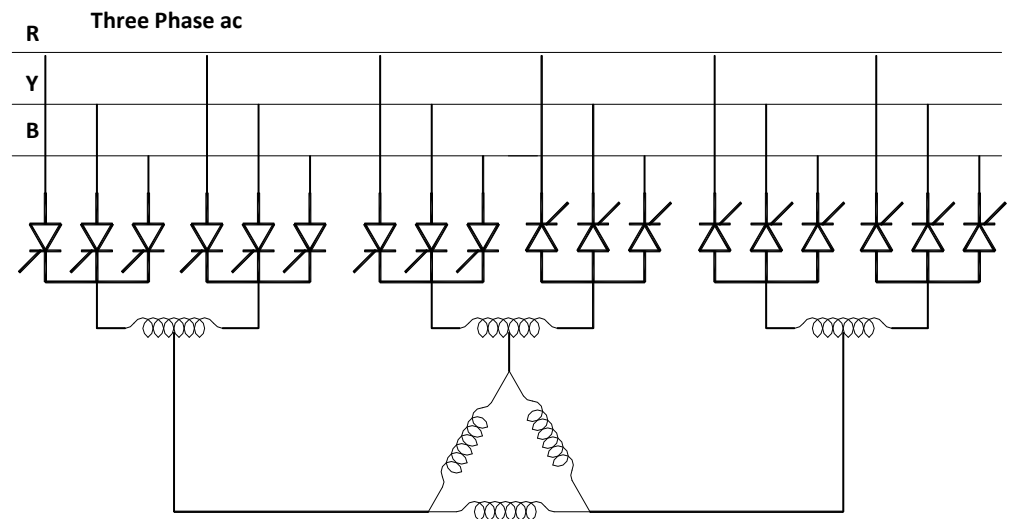


Fig 3.20 Three Phase to Three Phase cycloconverter

[2] The output waveform of cycloconverter voltage is almost pure sinusoidal whereas most dc link inverters produce stepped voltage waveform.

[3] The cycloconverter is capable of power transfer in both directions, therefore regenerative braking is possible.

The main disadvantage of the cycloconverter is that the maximum output frequency must be less than one third of the input frequency and, therefore, the minimum speed of the drive motor is limited to 1/3 of the speed corresponds to input frequency. The cycloconverter also requires more thyristors than the dc link inverter and, therefore, is not economical for low power motors.

Thus cycloconverter is more useful for high power low speed reversible drives whereas the dc link inverter is more suitable for high speed operations.

3.11 CONSTANT VOLTS/HERTZ INDUCTION MOTOR DRIVES

The operation of induction machines in a constant volt per hertz mode back to the late fifties and early sixties but were limited in their low

speed range [21]. Today constant volt per hertz drives are built using PWM-IGBT-based inverters of the types discussed earlier and the speed range has widened to include very low speeds [22] although operation very near zero speed (less than 1 Hz) remains as a challenge mainly due to inverter non-linearities at low output voltages.

Ideally, by keeping a constant V/f ratio for all frequencies the nominal torque-speed curve of the induction motor can be reproduced at any frequency as discussed in Section 3.2. Specifically if stator resistance is neglected and keeping a constant slip frequency the steady state behaviour of the induction machine can be characterized as impedance proportional to frequency. Therefore, if the V/f ratio is kept constant the stator flux, stator current, and torque will be constant at any frequency. This feature suggests that to control the torque one needs to simply apply the correct amount of V/Hz to stator windings. This simple, straight forward approach, however, does not work well in reality due to several factors, the most important ones being

- 1) Effect of supply voltage variations
- 2) Influence of stator resistance
- 3) Non-ideal torque/speed characteristic (effects of slip)
- 4) Non-linearities introduced by the PWM inverter.

Low frequency operation is the particularly difficult to achieve since these effects are most important at low voltages. Also, the non-linearities within the inverter, if not adequately compensated, yield highly distorted output voltages which, in turn, produces pulsating torques that lead to vibrations and increased acoustic noise.

In addition to these considerations, a general purpose inverter must accommodate a variety of motors from different manufacturers. Hence it must compensate for the above mentioned effects regardless of machine parameters. The control strategy must also be capable of handling parameter variations due to temperature and/or saturation effects. This fact indicates that in a true general purpose inverter it is necessary to include some means to estimate and/or measure some of the machine parameters. Another aspect that must be considered in any practical implementation deals with the DC bus voltage regulation, which, if not taken into account, may lead to large errors in the output voltage.

Because general purpose drives are cost sensitive it is also desired to reduce the number of sensing devices within the inverter. Generally speaking only the do link inverter voltage and current are measured; hence the stator current and voltage must be estimated based only on these measurements. Speed encoders or tachometers are not used because they add cost as well as reduce system reliability.

Other aspects that must be considered in the implementation of an ideal constant V/f drive relate to:

- a) Current measurement and regulation,

- b) Changes in gain due to pulse dropping in the PWM inverter,
- c) Instabilities due to poor volt-second compensation that result in lower damping. This problem is more important in high efficiency motors, and
- d) Quantization effects in the measured variables.

Another aspect that must be carefully taken into account is the quantization effect introduced by the A/D converters used for signal acquisition. A good cost to resolution compromise seems to be the use of 10 bit converters. However, a high performance drive is likely to require 12 bit accuracy.

3.12 COMPENSATION FOR SUPPLY VOLTAGE VARIATIONS

In an industrial environment, a motor drive is frequently subjected to supply voltage fluctuations which, in turn, imposed voltage fluctuations on the DC link of the inverter. If these variations are not compensated for, the motor will be impressed with either an under or an overvoltage which produces excessive I^2R loss or excessive iron loss respectively. The problem can be avoided if the DC link voltage is measured and the voltage command V^* adjusted to produce a modified command V^{**} such that

$$V^* = \left(\frac{V_{busR}}{V_{bus}} \right) V^{**} \quad (3.25)$$

Where V_{busR} = Rated value of bus voltage.

3.13 IR COMPENSATION

A simple means to compensate for the resistive drop is to boost the stator voltage by $I_1 R_1$ (voltage proportional to the current magnitude) and neglect the effect of the current phase angle. To avoid the direct measurement of the stator current this quantity can be estimated from the magnitude of the dc-link current [23]. In this paper a good ac current estimate was demonstrated at frequencies as low as 2 Hz but the system requires high accuracy in the dc-link current measurement making it impractical for low cost applications. A robust **IR** boost method must include both magnitude and phase angle compensation. Typically currents of two phases must be measured with the third current inferred since the currents sum to zero. In either case the value of the stator resistance must be known.

The value of the stator resistance can be estimated by using any one of several known techniques [24]-[26]. Unfortunately these parameter estimation techniques require knowing the rotor position or velocity and the stator current. An alternate method of 'boosting' the stator voltage at low frequencies is presented in [27]. Here the V/f ratio is adjusted by using the change in the sine of the phase angle of motor impedance. This approach also requires knowing the rotor speed and it is also dependent on the variation of the other machine parameters. Its practical usefulness is

questionable because of the technical difficulty of measuring phase angles at frequencies below 2 Hz.

Constant Volts/Hz control strategy is typically based on keeping the stator flux linkage magnitude constant and equal to its rated value. Using the steady state equivalent circuit of the induction motor, shown in Figure 3.5, an expression for stator voltage compensation for resistive drop can be shown to be

$$V_1 = \frac{\sqrt{2}}{3} I_{1Re} \widehat{R}_1 + \sqrt{\frac{V_{1R} f_e}{f_R} + \frac{2}{9} (I_{1Re} \widehat{R}_1)^2 - (I_1 \widehat{R}_1)^2} \quad (3.26)$$

Where V_{1R} is the base (rated) rms phase voltage at base frequency, f_R and f_e are the rated and line frequency in Hertz, \widehat{R}_1 is the estimated value of resistance, I_s is the rms current obtained on a instantaneous basis by,

$$I_s = \sqrt{\frac{2}{3} \sqrt{i_a(i_a + i_c) + i_c^2}} \quad (3.27)$$

And I_{1Re} is the real component of rms stator current obtained from

$$I_{1Re} = i_a \left[\cos \theta_e - \cos \left(\theta_e - \frac{2\pi}{3} \right) \right] + i_c \left[\cos \left(\theta_e + \frac{2\pi}{3} \right) - \cos \left(\theta_e - \frac{2\pi}{3} \right) \right] \quad (3.28)$$

where i_a and i_c are two of the instantaneous three phase stator currents, $\theta_e = \omega_e t$ and the cosine terms are obtained from the voltage command signals. The estimated value of resistance can be obtained either by a simple dc current measurement corrected for temperature rise or by a variety of known methods [24]-[26]. Derivation details of these equations are found in [28]. Given the inherently positive feedback characteristic of an Ir boost algorithm it is necessary to stabilize the system by introducing a first order lag in the feedback loop (low-pass filter).

3.14 SLIP COMPENSATION

By its nature, the induction motor develops its torque as a rotor speed slightly lower than synchronous speed (effects of slip). In order to achieve a desired speed, the applied frequency must therefore be increased by an amount equal to the slip frequency. The usual method of correction is to assume a linear relationship exists between torque and speed in the range of interest, Hence, the slip can be compensated by knowing this relationship. This approximation gives good results as long as the breakdown torque is not approached. However, for high loads the relationship becomes non-linear. Ref. [28] describes a correction which can be used for high slip,

$$f_{slip} = \frac{1}{2 - A * P_{gap}} \left\{ \sqrt{f_e^{*2} + \frac{\frac{S_m}{S_R} S_{linear}}{2 * \frac{T_{bd}}{T_R}} P_{gap} - B * P_{gap}^2 - f_e^*} \right\} \quad (3.29)$$

where f_e^* is the external command frequency and,

$$A = \frac{P}{4\pi S_{bd} T_{bd} f_R} \quad (3.30)$$

and

$$B = \left(\frac{P}{4\pi T_{bd}} \right)^2 \quad (3.31)$$

and P is the number of poles. The slope of linear portion of the torque speed curve is given by

$$s_{linear} = \frac{P S_R f_R}{\pi T_R} \quad (3.32)$$

Finally the air gap power is

$$P_{gap} = 3V_1 I_1 (pf) - 3I_1^2 \widehat{R}_1 - P_{core} \quad (3.33)$$

where P_{core} at rated frequency can be obtained from

$$P_{coreR} = P_{inR} \left(1 - \frac{\eta_R}{1 - S_R} \right) - 3I_1^2 \widehat{R}_1 \quad (3.34)$$

Where the quantities $S_R, f_R, \eta_R, I_1, P_{inR}$ and T_R are the rated values of slip, line frequency, efficiency, stator current, input power and torque respectively. All of these quantities can be inferred from the name plate data.

3.15 VOLT-SECOND COMPENSATION

One of the main problems in open-loop controlled PWM-VSI drives is the non-linearity caused by the non-ideal characteristics of the power switches. The most important non-linearity is introduced by the necessary blanking time to avoid short circuiting the DC link during the commutations. To guarantee that both switches are never on simultaneously a small time delay is added to the gate signal of the turning-on device. This delay, added to the device's inherent turn-on and turn-off delay times, introduces a magnitude and phase error in the output voltage [29]. Since the delay is added in every PWM carrier cycle the magnitude of the error grows in proportion to the switching frequency, introducing large errors when the

switching frequency is high and the total output voltage is small.

The second main non-linear effect is due to the finite voltage drop across the switch during the on-state [30]. This introduces an additional error in the magnitude of the output voltage, although somewhat smaller, which needs to be compensated.

To compensate for the dead-time in the inverter it is necessary to know the direction of the current and then change the reference voltage by adding or subtracting the required volt-seconds. Although in principle this is simple, the dead time also depends on the magnitude and phase of the current and the type of device used in the inverter. The dead-time introduced by the inverter causes serious waveform distortion and fundamental voltage drop when the switching frequency is high compared to the fundamental output frequency. Several papers have been written on techniques to compensate for the dead time [29],[31]-[33].

Regardless of the method used, all dead time compensation techniques are based on the polarity of the current, hence current detection becomes an important issue. This is specially true around the zero-crossings where an accurate measurement is needed to correctly compensate for the dead time. Current detection becomes more difficult due to the PWM noise and because the use of filters introduces phase delays that needed to be taken into account.

The name “dead-time compensation” often misleads since the actual dead time, which is intentionally introduced, is only one of the elements accounting for the error in the output voltage, for this reason here it is referred as volt-second compensation.

3.16 SPACE VECTOR MODULATION PWM (SVMPWM)

This control technique is based on the fact that three-phase voltage vectors of the induction motor can be converted into a single rotating vector. Rotation of this space vector can be implemented by VFD to generate three-phase sine waves. The advantages are less harmonic magnitude at the PWM switching frequency due to averaging, less memory requirement compared to sinusoidal PWM, etc. The disadvantages are not full utilization of the DC bus voltage, more calculation required, etc.

3.17 SVMPWM WITH OVERMODULATION

Implementation of SVMPWM with over modulation can generate a fundamental sine wave of amplitude greater than the DC bus level. The disadvantage is complicated calculation, line-to-line waveforms are not clean and the THD increases, but still less than the THD of the six-step PWM method.

3.18 VECTOR CONTROL

The various techniques for producing a variable frequency supply source for controlling speed-torque characteristic for an induction motor have provided good steady state response. The constant V/F control technique provides constant flux and hence constant torque for the entire range of operation. However at low speed i.e. at low frequencies the steady state response is not as good as at higher frequencies.

The dynamic response of the drive is poor. This poor dynamic response is because of the deviation of air gap flux linkage from their set values. This deviation is not only in magnitude but also in phase. The variation in the flux linkages have to control by the magnitude and frequency of the stator and rotor phase current and their instantaneous phases. So far, the control techniques have utilized the stator phase current magnitude and frequency and not their phases. This resulted in the deviation of the phase and magnitudes of the air gap flux linkages from their set values.

The oscillations in the air gap flux linkages result in oscillations in electromagnetic torque oscillations. If phenomenon is neglected (i.e. not attended) then it results in speed oscillations. This is undesirable in many high-performance applications, such as in robotic actuators, centrifuges, servos, process drives and metal rolling mills, where high precision, fast positioning, or speed control are required. Such requirement will not be met with the sluggishness of control due to the flux oscillations. Further, air gap flux variations result in large variation of stator currents, requiring large peak converter and inverter ratings to meet the dynamics. An enhancement of peak inverter rating increases cost and reduces the competitive edge of ac drives in the marketplace, in spite of excellent advantages of the ac drives over dc drives.

Vector control is also known as the field oriented control or flux oriented control or indirect torque control. Using field orientation (Clarke-Park transformation), three phase current vectors are converted to a two dimensional rotating reference frame (d-q) from a three-dimensional stationary reference frame.

The **d** component represents the flux producing component of the stator current and the **q** component represents the torque producing component. These two decoupled components can be independently controlled by passing through separate **PI** controllers. The outputs of the **PI** controllers are transformed back to the three-dimensional stationary reference plane using the inverse of the Clarke-Park transformation. The corresponding switching pattern is pulse width modulated and implemented using the SVM.

This control simulates a separately excited DC motor model, which provides an excellent torque-speed curve. The transformation from the stationary reference frame to the rotating reference frame is done and controlled with reference to a specific flux linkage space vector (stator flux linkage, rotor flux linkage or magnetizing flux linkage). In general, there exists three possibilities for such selection and hence, three different vector controls. They are:

- [1] Stator flux oriented control
- [2] Rotor flux oriented control

[3] Magnetizing flux oriented control

As the torque producing component in this type of control is controlled only after transformation is done and is not the main input reference, such control is known as indirect torque control. The most challenging and ultimately, the limiting feature of the field orientation, is the method whereby the flux angle is measured or estimated. If the field angle is calculated by using terminal voltages and currents or Hall sensors or flux sensing windings, then it is known as **direct vector control**. The field angle can also be obtained by using rotor position measurement and partial estimation with only machine parameters but not any other variables, such as voltages or currents; using this field angle leads to a class of control schemes known as **indirect vector control**.

In *direct vector control*, the flux measurement is done by using the flux sensing coils or the Hall devices. This adds to additional hardware cost and in addition, measurement is not highly accurate. Therefore, this method is not a very good control technique. The more common method is *indirect vector control*. In this method, the flux angle is not measured directly, but is estimated from the equivalent circuit model and from measurements of the rotor speed, the stator current and the voltage.

One common technique for estimating the rotor flux is based on the slip relation. This requires the measurement of the rotor position and the stator current. With current and position sensors, this method performs reasonably well over the entire speed range. The most high-performance VFDs in operation today employ indirect field orientation based on the slip relation. The main disadvantage of this method is the need of the rotor position information using the shaft mounted encoder. This means additional wiring and component cost. This increases the size of the motor. When the drive and the motor are far apart, the additional wiring poses a challenge.

To overcome the sensor/encoder problem, today's main research focus is in the area of a sensor less approach. The advantages of the vector control are better torque response compared to the scalar control, full-load torque close to zero speed, accurate speed control and performance approaching DC drive, among others. But this requires a complex algorithm for speed calculation in real-time. Due to feedback devices, this control becomes costly compared to the scalar control.

3.19 DIRECT TORQUE CONTROL (DTC)

The difference between the traditional vector control and the DTC is that the DTC has no fixed switching pattern. The DTC switches the inverter according to the load needs. Due to elimination of the fixed switching pattern (characteristic of the vector and the scalar control), the DTC response is extremely fast during the instant load changes. Although the speed accuracy up to 0.5% is ensured with this complex technology, it eliminates the requirement of any feedback device. The block diagram of the DTC implementation is shown in Figure 24. The heart of this technology is its

adaptive motor model. This model is based on the mathematical expressions of basic motor theory. This model requires information about the various motor parameters, like stator resistance, mutual inductance, saturation coefficient, etc. The algorithm captures all these details at the start from the motor without rotating the motor. But rotating the motor for a few seconds helps in the tuning of the model. The better tuning gives higher accuracy of speed and torque control. With the DC bus voltage, the line currents and the present switch position as inputs, the model calculates actual flux and torque of the motor. These values are fed to two-level comparators of the torque and flux, respectively. The output of these comparators is the torque and flux reference signals for the optimal switch selection table. Selected switch position is given to the inverter without any modulation, which means faster response time. The external speed set reference signal is decoded to generate the torque and flux reference. Thus, in the DTC, the motor torque and flux become direct controlled variables and hence, the name Direct Torque Control.

The advantage of this technology is the fastest response time, elimination of feedback devices, reduced mechanical failure, performance nearly the same as the DC machine without feedback, etc. The disadvantage is due to the inherent hysteresis of the comparator, higher torque and flux ripple exist. Since switching is not done at a very high frequency, the low-order harmonics increases. It is believed that the DTC can be implemented using an Artificial Intelligence model instead of the model based on mathematical equations. This will help in better tuning of the model and less dependence on the motor parameters.

CHAPTER 4

MOTOR INSULATION SYSTEM AND TRANSIENT PRODUCED BY VARIABLE SPEED DRIVES

4.1 INTRODUCTION

Worldwide, various standards exist which specify various operating and constructional parameters of a motor. The two most widely used parameters are the National Electrical Manufacturers Association (NEMA) and the International Electro-technical Commission (IEC). Standards followed for manufacturing electric motors are from INDIAN STANDARD INSTITUTION.

NEMA

NEMA sets standards for a wide range of electrical products, including motors. NEMA is primarily associated with motors used in North America. The standards developed represent the general industry practices and are supported by manufacturers of electrical equipment. These standards can be found in the NEMA Standard Publication No. MG 1. Some large AC motors may not fall under NEMA standards. They are built to meet the requirements of a specific application. They are referred to as above NEMA motors.

IEC

IEC is a European-based organization that publishes and promotes worldwide, the mechanical and electrical standards for motors, among other things. In simple terms, it can be said that the IEC is the international counterpart of the NEMA. The IEC standards are associated with motors used in many countries. These standards can be found in the IEC 34-1-16. The motors which meet or exceed these standards are referred to as IEC motors.

The NEMA standards mainly specify four design types for AC induction motors – Design A, B, C and D. Their typical torque-speed curves are shown in Figure 18.

Design A has normal starting torque (typically 150-170% of rated) and relatively high starting current. The breakdown torque is the highest of all the NEMA types. It can handle heavy overloads for a short duration. The slip is $\leq 5\%$. A typical application is the powering of injection molding machines.

Design B is the most common type of AC induction motor sold. It has a normal starting torque, similar to Design A, but offers low starting current. The locked rotor torque is good enough to start many loads encountered in the industrial applications. The slip is $\leq 5\%$. The motor efficiency and full-load PF are comparatively high, contributing to the popularity of the design. The typical applications include pumps, fans and machine tools.

Design C has high starting torque (greater than the previous two designs, say 200%), useful for driving heavy breakaway loads like conveyors, crushers, stirring machines, agitators, reciprocating pumps, compressors, etc. These motors are intended for operation near full speed without great overloads. The starting current is low. The slip is $\leq 5\%$.

Design D has high starting torque (higher than all the NEMA motor types). The starting current and full-load speed are low. The high slip values (5-13%) make this motor suitable for applications with changing loads and subsequent sharp changes in the motor speed, such as in machinery with energy storage flywheels, punch presses, shears, elevators, extractors, winches, hoists, oil-well pumping, wire-drawing machines, etc. The speed regulation is poor, making the design suitable only for punch presses, cranes, elevators and oil well pumps. This motor type is usually considered a “special order” item.

Recently, **NEMA** has added one more design – **Design E** – in its standard for the induction motor. Design E is similar to Design B, but has a higher efficiency, high starting currents and lower full-load running currents. The torque characteristics of Design E are similar to IEC metric motors of similar power parameters.

The IEC Torque-Speed Design Ratings practically mirror those of NEMA. The IEC Design N motors are similar to NEMA Design B motors, the most common motors for industrial applications. The IEC Design H motors are nearly identical to NEMA Design C motors.

There is no specific IEC equivalent to the NEMA Design D motor. The IEC Duty Cycle Ratings are different from those of NEMA's. Where NEMA usually specifies continuous, intermittent or special duty (typically expressed in minutes), the IEC uses nine different duty cycle designations (IEC 34 -1).

Normally motor design as per different standards is meant for operation on sinusoidal supply

Prior to the introduction of insulated gate bipolar transistor (IGBT) switching devices, the main issue motor designers were concerned with in mating a motor to an adjustable speed drive (ASD) was the increase in temperature rise from the harmonic losses the ASD introduced [34].

With the introduction of the IGBT ASD, a second issue has become as important as the thermal issue-insulation integrity. When long cable lengths

are used between the motor and the ASD, transmission line theory explains that when the motor surge impedance is high compared to the cable characteristic impedance, the effect is voltage doubling (test show even higher than doubling) on leading edge of the voltage pulse at the motor [35]. On pulse width modulation (PWM) ASDs, thousands of pulses per second are applied to the motor. The National Electrical Manufacturers Association (NEMA) recognized that these pulses could damage the motor insulation and has written into their standard NEMA MG1-31 that motor designed for use on ASDs must be capable of operation in the presence of 1600 V peak amplitude pulses with a rise time of 0.1 microsecond or greater [36]. NEMA standard MG1-30 also defines the insulation capability of the standard motors used on drives to a much lower number- 1000 V peak with a 2 microsecond rise time [37].

Voltage rise time is a very important parameter in determining motor insulation system integrity. It determines voltage amplitude at the motor (in conjunction with the cable length between the motor and the ASD) and voltage distribution in the individual motor coils.

It should be noted that voltage doubling did occur on ASDs prior to the introduction of IGBT switches. However, the previous technology switches (GTOS and bipolar junction transistors) had longer rise times resulting in voltage doubling occurring with longer cable lengths and more even voltage distribution in the motor windings. The net effect of these is that ASDs with IGBT switches have more severely stressed motor insulation.

4.2 MOTOR WINDINGS

To understand the various ways motors are built to handle the higher voltage amplitude and voltage distribution differences an ASD introduces, it is necessary to understand the type of the coils of the winding. There are two type of coils used in motor winding; (1) Form Coil and (2) random wound coil.

Motor built for medium voltage applications are rated for the system voltages to which they are applied. At medium voltages, motors are typically built with form coil windings. Form coil windings have insulated rectangular wire, and are carefully taped or wrapped and varnished to eliminate the presence of air so that partial discharge between wires is avoided. (Partial discharge is defined as the ionization of air leading to an electrical breakdown in a void of any geometry within insulation subjected to an electric field). The nature of the construction assures that the turns are in sequential order. Therefore, Turn 1 would only touch Turn 2, Turn 2 would only touch Turns 1

and 3, etc. with this careful turn placement, the voltage between adjacent wires is limited to the turn to turn voltage.

Conversely, on low voltage systems - 600 V and below – motors are usually built with what is known in the industry as random windings. Random wound motors are wound with multiple strands of round magnet wire and are often wound on tooling to specific shape, then inserted into the stator slots. During this wind/insert process, the adjacent wires could in the worst case have the first and the last turn touching (hence the term random winding). If the first and last turns are in contact within a coil, adjacent turn voltage can be full coil voltage, not sequential turn voltage. Additionally, on some types of random coil windings, the end turns of adjacent coils are not separated, so in the end turns, turns in adjacent coils can touch, resulting in adjacent wire voltage exceeding coil voltage.

Random windings are often vacuum pressure impregnated (VPI), dip, or flood varnished. This is done in an attempt to eliminate all air pockets between wires, replacing them with varnish. The numerous crossovers and wire interfaces combined with the round wire geometry make it virtually impossible to eliminate all the air pockets. As stated above, these little air pockets make partial discharges possible if an adequate voltage to start the partial discharge is presented.

As can be seen, the two big differences between the forms coil and random windings are:

- Adjacent wire voltage can be higher in the random winding, and
- Random windings are more likely to have air pockets between wires. (Air is a necessary ingredient for partial discharges.)

4.3 RISE TIME AND PEAK VOLTAGE CONCERNS

The voltage is evenly distributed across all the windings in slowly changing voltage signals like 50 Hz sine wave power. But with short rise times a disproportionate portion of the voltage is distributed across the first coil – sometimes reaching in excess of 75% of the total line to line voltage across the coil [38].

Since a large part of the total line to line voltage can be across the first coil, since the line to line voltage at the motor can be as much as twice the voltage at the ASD terminals (as explain by transmission line theory), and since the first and last turns of a coil can in worst case be touching (the first turn of the first coil can even be touching a turn in the second coil in the end

turn- as explained above), it will be noted that the presence of the IGBT PWM ASD can greatly increase the voltage between adjacent wires in a random wound motor.

These higher voltages present between adjacent wires in a random-wound motor can be high enough that partial discharge occurs. Standard random wound machines were not designed for operation in partial discharge environment.

Reiterating, the factors that bring adjacent turn voltages high enough so that partial discharge may occur include:

- The short rise time of an IGBT drives causes uneven voltage distribution putting high voltages on the first coil.
- With the long cable lengths, the voltage may exceed twice what it would be if the ASD were next to the motor terminals, and
- The use of random winding on low voltage motors creates a possibility of full coil voltage between adjacent wires.

L. Manz [39] has reported that average life for the insulation is 10^8 cycle when voltage level is 600 V. The life of the insulation decreases with increase in voltage level and becomes 10^7 cycles when voltage increases to 4500 V. the sharp decrease in life with present magnet wire operating in partial discharge; it is a requirement that motors be operated below the starting voltage for partial discharge for the long life expected from today's motors. Some of the premature failures seen when operating standard motors with IGBT PWM ASDs are due to partial discharge. These motor can fail within months (even weeks) of installation.

Adjustable speed drives fed from modern frequency converters with voltage source inverters (VSI) are operated in a wide range of traction and industrial applications. The converters that employ modern power electronic devices provide more flexible motor operation, low torque ripple, improved system efficiency and many other benefits. Unfortunately some unintended disturbances accompany operation of these drives. Well-known transient over voltages stress insulation system of fed motor and dramatically decrease motor lifetime. Recently, it is recorded in practice tremendous over voltages with peaks that significantly exceed twice dc bus voltage level. Such surges cause very fast motor insulation breakdown. Familiarity with motor overvoltage theory, understanding of generation causes and knowledge of factors that influence these surges are necessary for design of whole drive system and for development of diagnostic methods. Investigation of high frequency transient effects requires exact model of the drive system. A lot of very interesting papers have reported on motor over voltages [40] - [48], however, this effect is still not sufficiently described. Literature is especially

lacking on general theory of surges that lead to overshoots significantly exceeding twice dc bus voltage.

Zdenek Peroutka [49] has presented simulation and experiments results which have been performed for both laboratory set-ups (4kW/400V/50Hz). As an illustrative example, tests were performed on main drive of light rail vehicle recently developed in `koda Electric. His experimental set-up was consisting of frequency converter with PWM voltage source inverter and induction motor that is connected by power cable to the converter. Output transformer was placed at inverter output. The application of step-up transformer is typical for example for drives used in oil exploitation or in mining industry. Protective devices could be connected on either converter or motor terminals. A lot of very sophisticated models of frequency converter with voltage source inverter have been published in literature [50]. For investigation of motor transient over voltages, frequency converter's model can often be simplified with sufficient accuracy. Voltage source inverter can be replaced by controlled voltage sources that generate trapezoidal pulses. The model may be completed by resistance and stray inductance in order to get better accuracy of dc link output impedance. However, such simplified model is not useful in all cases. More complex analysis (e.g. design of some filters) requires considering properties of dc bus circuit and input rectifier.

Power cable models can be divided into two basic groups:

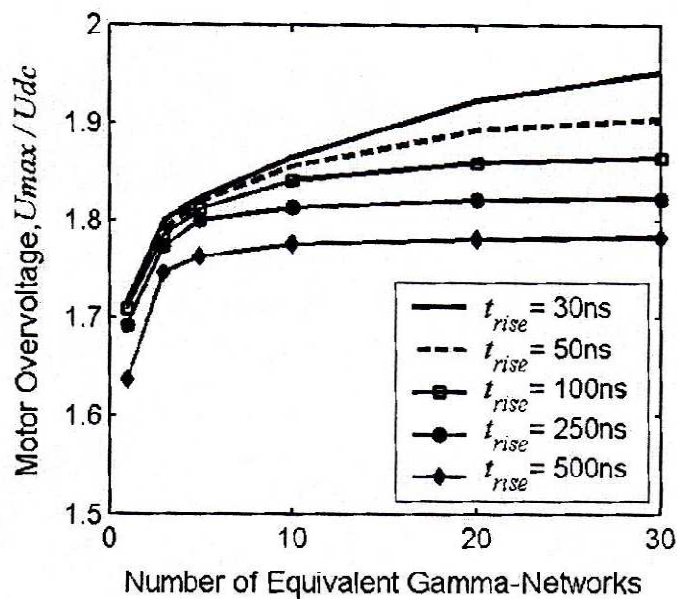
1) Models with lumped parameters and 2) models with distributed parameters.

In first case, the cable is replaced by finite number of equivalent networks with lumped parameters in cascade connection. The problem is how to choose the number of networks? It is suggested to estimate the number of networks (n) based on crucial cable length (l_c). Crucial cable length legibly define border between system with lumped and distributed parameters. This border is of course not an exact line between these systems. Crucial length is expressed as:

$$l_c = \frac{v * t_{rise}}{2} = \frac{c * t_{rise}}{2 * \sqrt{\epsilon_r}} \quad (4.1)$$

Where t_{rise} is rise time of inverter's voltage pulses, v is wave velocity, c is speed of light t_{rise} and ϵ_r is relative permittivity of cable insulation material. It is well-known that v is closed to half of speed of light, because ϵ_r of common cables is approximately 4 ÷ 5. The number of equivalent networks for cable of length l is given by:

$$n = \frac{l}{l_c} = \frac{2l}{v * t_{rise}} = \frac{2l\sqrt{\epsilon_r}}{c * t_{rise}} \quad (4.2)$$



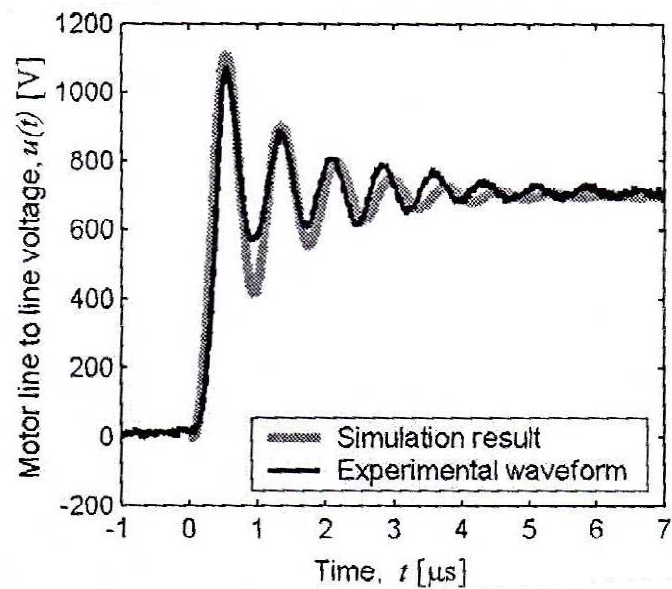
Impact of number of cable's equivalent networks on investigated characteristics at the motor terminals; cable length $l = 50$ m, U_{dc} is dc bus voltage

Figure 4.1

From Fig. 4.1 is evident, how peak voltage at the motor terminals (and of course other important characteristics as oscillation frequency, rise time of the voltage at the motor terminals) is approaching exact value with increasing number of equivalent networks. From a number of performed simulations, it is possible to conclude that 10 gamma networks get sufficient accuracy in range of typical cable lengths (up to 100m) and rise times

(down to tens nanoseconds).

Number of distributed models have already been published- distortion less line model [51]; multi-node model [47] and especially very interesting model [52]. In his research Zdene k Peroutka [49] has proposed general transmission line model. [53, 54]. This model is directly based on continue mathematical model of transmission line – telegraph equations that represents system of partial differential equations. The results are shown in figure 4.2.



Detail of line to line voltage waveform at motor terminals, $f_c = 2 \text{ KHz}$, $f_{out} = 60 \text{ Hz}$

Figure 4.2

The design of the ac stator winding insulation must take into consideration both the steady-state operating voltages and the voltage transients (surges) caused by the factors such as lightning strikes and switching phenomena. Both types of over voltages stress the ground insulation and, if the surge is steep enough, also over-stress the turn insulation. Steep-fronted surges with magnitudes as high as 4.5 per unit (pu) and rise times of 0.1- 0.2 microsecond are possible during normal breaker operation, where one pu is the crest of the rated line-to-ground voltage or

$$1 \text{ pu} = \sqrt{\frac{2}{3}} * \text{rated line voltage}$$

Surge voltages of 6 pu and higher are not unknown.

Next to bearing failure, turn insulation failure is probably the most common failure mode in ac motors. Since this type of failure also usually leads to ground wall insulation failure, a turn insulation failure has been mistaken as a ground wall insulation failure by motor users in the past. Because of the wide uses of vacuum switching devices, and a large numbers of studies undertaken, awareness of turn insulation performance and potential problems has, in recent years, been heightened in the minds of motor users.

Turn insulation failures typically occur in the stator end-winding and usually at the first bend from the straight portion where the coil exit the slot, or at the nose of the coil. This is so because bending and pulling operations during coil manufacturing place additional strain on insulation at these locations causing it to lose some dielectric strength.

Turn insulation failures can be due to crack in the insulating materials, deficiencies in insulation design, irregularities in manufacturing, or inadequate quality control. In operation, they can also be caused by voltage surges that are higher or more frequent than the specified capability, poor preventive maintenance practices, normal deterioration of insulation dielectric strength with time , or mechanical rubbing of one insulated part

with another due to coil movements as might be the case during motor starting, speed switching, and motor vibration.

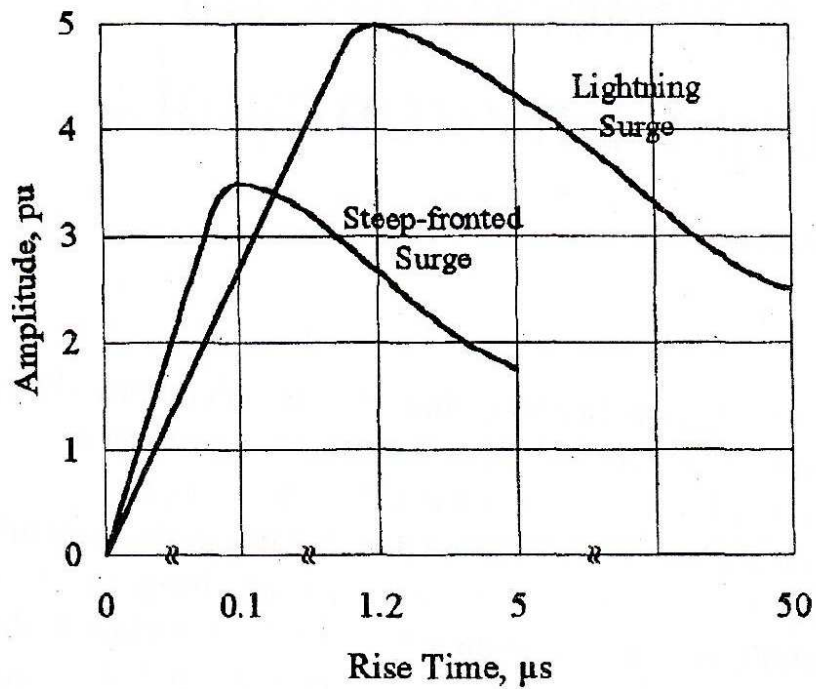
4.4 SURGES

The standards make a distinction between impulses and surges. An impulse[34] is an intentionally applied a periodic transient voltage which usually rises rapidly to a peak value and then falls more slowly to zero, whereas a surge refers to transients occurring in electrical equipment of networks in service.

There are two kinds of surges or transient over voltages; those originated by lightning strikes and those caused by switching phenomena. The standards again makes a distinction [55] between switching and lightning surges on the bases of the duration of the front or the rise time from zero to peak value. Surges, with fronts of up to 20 μs are defined as lightning surges, and those with longer fronts are defined as switching surges.

The actual shape- the rise and decay times and the amplitude-can vary enormously. Therefore, it is necessary to define these surges by relatively simple means for simulation and testing purposes. A standard lightening surges is defined as one having a virtual front time of 1.2 μs and a virtual time to half value of 50 μs . A steep-fronted surge is one with a rise time of 0.1-0.5 μs and a virtual time to half value of around 5 μs (Figure 4.3).

A steep-fronted surge with a rise of 0.2 μs appears entirely across the first or line end coil of the winding. Further, its distribution in the coil is not quite linear. This results in voltage stresses across the turn insulation that is much higher than the steady-state values. It is for this reason that most turn insulation failures occur in the line coils.



Lighting and steep-fronted surges
Figure 4.3

4.5 THE SURGE ENVIRONMENT

The availability and use of new and improved materials and devices and the desire to produce cost-effective competitive products has resulted in greater exposure of the motor to high amplitude, steeper-fronted surges. Because of their reliability, compact size, low maintenance needs, and longer life IGBT drives are most widely used. However they produce repetitive, high amplitude, steep-fronted surges. The use of low loss a cable between the drive and the motor does not increase the surge front or lower its amplitude.

IGBT drives are used to achieve operational economies. The increase in motor power densities due to improved technology, economic and competitive considerations, and the need to reduced losses and improve efficiencies has resulted in motors that are less conservatively designed than they used to be. They do not use dedicated turn insulation when not required by the design. The strand insulation is now designed to function as h turn insulation also.

Thus, it has become increasingly important to understand the surge phenomena, its causes, the system parameters that affect their amplitudes

and rise time, and the manner in which these surges distribute themselves in the windings so as to permit adequate design of the turn insulation and/or of motor surge protection.

4.6 FACTORS AFFECTING SURGE AMPLITUDE AND RISE TIMES

The amplitude and rise time of the surge appearing at the motor terminals depends on the operating voltage, the system design, characteristics of the devices in the system, and indeed the design of motor itself. The following factors are important in this regards:

1) Transient event taking place:

- a) Rate of normal pulses:
- b) Motor starting:
- c) Aborted starts:
- d) Switching locked rotor insures current;
- e) Winding being switched:
- f) Bus transfer.

2) Motor:

- a) Capacitance and surge impedance (and hence motor size);
- b) Parallel circuits.

3) Cable connecting the motor to the breaker and its characteristics:

- a) Type single phase, triplexed or, belted);
- b) Cable insulation;
 - i) XLPE, EPR (low loss);
 - ii) PVC, PILC (HIGHER LOSS);
- C) Cable length;
- d) Whether shielded or unshielded;
- e) Whether the shield is grounded, and if so, where.

4) Power devices

- a) IGBT
 - b) MOSFETs
 - c) Power Transistor
 - d) GTO
- 5) Other loads connected to the bus.
- 6) The device between drive and motor which is making connection:
- a) Air-magnetic break;
 - b) Vacuum breaker;
 - c) Maximum chopping current, contactor material and design.

4.7 STEEP FRONTED SWITCHING SURGES

4.7.1 BREAKER TYPES

Circuit breakers can be classified as vacuum, SF₆, air-magnetic, and minimum oil. Air-magnetic breakers have been popular in the US. Vacuum breakers are used universally and because of economic considerations are now used in a large number of installations.

Voltage transients are produced by circuit breakers during contact opening as well as contact closing. Air-magnetic breakers produce a fast rise time surge during closing only, whereas the vacuum breaker produces steep-fronted surges during opening as well as closing. Also, switching in vacuum produces multiple surges during closing (prestrike) and opening (reignitions). Thus, for a single event of opening or closing, the vacuum breaker produces multiple surges and, therefore, stresses turn insulation more than other switching devices. Further, multiple reignition causes each successive surge to be at a level higher than the previous one. Larger numbers of prestrike are possible at 13.2 KV than 4 KV

4.7.2 SURGE GENERATION

All three contacts in a circuit breaker do not close or open simultaneously due to minor differences in the contact travel times. Some times more than one load is feed from a single bus. Figure 2 is such a motor cable breaker bus system. If Z_c is the motor cable surge impedance and all cables are connected to the bus are identical, V_i is the instantaneous value of the surge launched into the motor cable when the first contact closes or

prestrike, V is the instantaneous line to ground system voltage, n is the number of cables connected to the same bus, then it can be shown [56, 57] that approximately

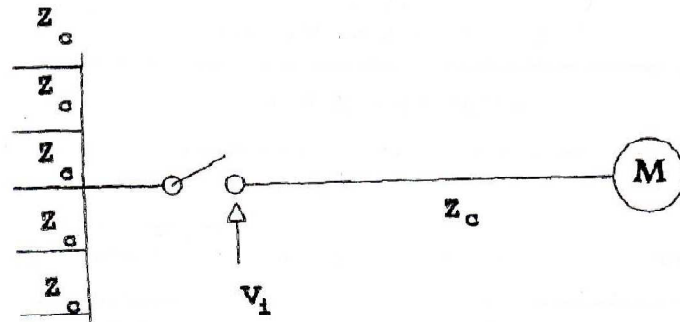


Figure 4.4 Typical cable-motor system

$$V_i = V \left[\frac{Z_c}{Z_c + \frac{Z_c}{n}} \right] = V \left[\frac{n}{n+1} \right] \text{---[4.3]}$$

When this surge arrives at the motor terminals (a point of discontinuity since the surge impedance undergoes a change here), wave reflection back into the cable, and refraction into the motor winding takes place. If Z_m is the motor surge impedance, the amplitude V_m of the surge at the junction that propagates into the motor winding is

$$V_m = V_i \left[\frac{2Z_m}{Z_m + Z_c} \right] \text{---[4.4]}$$

If

$$Z_m \gg Z_c \text{ then}$$

$$V_m \gg 2V_i$$

i.e. under some extreme system conditions, the surge amplitude at the motor terminals can be almost twice the level of the surge injected into the cable at the circuit breaker. This surge will cause the motor cable system to oscillate at its natural frequency and the magnitude of the peak voltage across the second and third contacts of the breaker can be as high as $2.5V_i$. If at this

time a prestrike occurs, a $2.5V_i$ surge will be applied to the motor cable and the doubling effect could result in a surge of almost $5V_i$ at the motor terminals [56]

$$V_m = 2.5 * V \left[\frac{n}{n+1} \right] \left[\frac{2Z_m}{Z_m + Z_c} \right] \text{---[4.5]}$$

The wave front duration of this surge is

$$\frac{3 \left[\frac{n}{n+1} \right] L_b}{Z_c} \text{---[4.6]}$$

Where Z_c is the equivalent inductance of the bus to which the motor is connected [57].

4.7.3 CABLES

The type of motor-to-breaker cable used and the manner in which it is grounded has an effect on the amplitude and rise time of the surge arriving at the motor terminals [58]. The lower the loss in the cable, the lower is the attenuation of the surge; the higher the loss, the higher will be the attenuation. Typically, if the cable is long, the attenuation is larger. However, with modern low loss cables (for example, EPR) practically no attenuation of the surge takes place, irrespective of the length of the cable.

The surge impedance of the cables is different for shielded and unshielded cables. Unshielded cables have relatively high surge impedance. The use of such cables will reduce the magnitude of the surge arriving at the motor terminals, whereas shielded cables will tend to increase the magnitude.

Even in shielded cables, the location of the ground affects the surge profile at the motor. If ground at the motor end, shielded cables reduce the amplitude of the surge. On the other hand, the rise time increases if it is ground at the drive end.

The propagation velocity of surges through an insulated feeder cable is about $150 \text{ m}/\mu\text{s}$. If the motor surge impedance is larger than cable surge impedance, the cable is longer than 15 m and the surge wave front is $0.1 \mu\text{s}$, voltage doubling is possible. The minimum cable length for this phenomenon is 30 m. for a surge wave front of $0.2 \mu\text{s}$.

4.8 MOTOR DESIGN EFFECTS

The inter-turn voltage is a function of the number of series turns per coil and phase. It can thus be reduced by decreasing the number of parallel circuits and correspondingly increasing the number of series turns in the winding.

If the stator winding is not an all-series winding but has more than one parallel circuit in each phase, then, depending on the size and design, the terminations of all parallel circuits may either be brought out into the lead box, or paralleling bars or rings used inside the machine and only two leads per phase brought out. The latter design introduces an inductance between the motor terminal and the lead end coils. This has an effect of increasing the rise time of the surge and limiting the inter-turn voltage.

4.9 SURGE DISTRIBUTION IN THE WINDING

When the steep-fronted surge arrives at the motor terminals, its propagation through the winding and the dielectric stresses it imposes on the turn insulation are a function of its rise time. Many studies have been made [59, 60], and models developed to study the surge distribution in the winding. In general, these studies are based on the treatment of the winding as a single conductor or multi-conductor transmission line and represent it as a set of series and parallel lumped or distributed parameters consisting of capacitances, inductances, and conductances for each conductor (half turn), turn or coil. These studies indicate that for steep-fronted surges:

- 1) The distribution of the surge across the winding is non-uniform and almost the entire surge appears across the line end coil;
- 2) The surge distribution in the coil is not uniform, especially when the rise time is $0.3 \mu s$ or less.
- 3) The distribution depends on the thickness of the ground wall and turn insulation, and the shape, size, and length of the slot and end-winding portions of the coils.

Sensitivity studies [59], [61] and [63] also indicate that:

- 1) The steepness of the surge front (i.e. the rise time of the surge) and the number of turns per coil are the major factors in determining the severity of the dielectric stress on the insulation;
- 2) Inter-turn surge voltage could be as high as 130% of the average value for a surge with a rise of $0.1 \mu s$ and 125% of the average value for a surge with a

rise of $0.2 \mu s$ this ratios are essentially independent of the machine voltage (and, hence, insulation design) and of the coil size;

3) Insulation thickness, shape of the coil, size of the coil (its width and length), and relative length of stator core and overhang portion of the coil have a minor impact on the turn insulation dielectric stress severity.

4.10 STANDARDS

The standards that deal with surges are the following.

1) IEEE Standard 522-1992: IEEE guide for testing turn-to turn insulation on form-wound stator coils for alternating current rotating machines [63]

2) IEEE Standard 792-1987: IEEE Trial-Use Recommended Practice for the Evaluation of the Impulse voltage Capability of the Insulation Systems for AC Electrical Machinery Employing Form wound Stator coils [64].

3) NEMA MG1-1993: Motors and generators [65].

4) IEC 34-15, 1990: Rotating Electrical machines, Part 15: Impulse Voltage withstand Levels of Rotating ac Machines with form-wound coils [66].

5) Draft International Standard 2 (co) 557: Revision of IEC 34-15: 1990 [67].

All of these standards apply to form wound ac windings only, there are no standards for performance or test for motors with random winding, such as the NEMA medium motors in size 500 HP and less at voltages 600 V and below.

NEMA MG1 specifies surge capabilities as well as test methods. It establishes 2 pu at a rise time of $0.1- 0.2 \mu s$ and 4.5 pu at a rise time of $1.2 \mu s$ or longer as the standard surge withstand capability. A capability of 3.5 pu at a rise time of $0.1- 0.2 \mu s$ and 5 pu at a rise time of $1.2 \mu s$ or longer are offered as options when agreed upon between the vendor and user. The methods and instrumentation are as per IEEE Standard 522.

4.11 CAUSES OF TURN INSULATION FAILURES

Turn insulation can fail for a number of reasons, not all of them within control. These could be design, quality, and site condition related:

1) The dielectric stress due to the surge exceeding the capacity of the turn insulation;

- 2) A much larger number of surges per unit time than was foreseen when the motor was specified and designed;
- 3) Insulation degradation over a time under the influence of normal dielectric and thermal stresses, moisture, vibration, and contaminations;
- 4) Turn insulation erosion due to corona if voids exist in locations next to the turn insulation, resulting in partial discharge; this is likely to happen at voltage greater than 6000 V and with voids larger than 0.05 mm in diameter;
- 5) Turn insulation erosion over time if due to high vibration, repeated start, and speed switching, the insulation work loose and relative movement becomes possible between individual turns in a coil;
- 6) Inadequate or absent routine and preventive maintenance of the motor;
- 7) A much more hostile surge environment than was originally envisioned.

Therefore, following points are to be considered while designing the inter-turn insulation.

1. Knowledge of the surge environment in which the motor is to operate is necessary in determining the surge capability requirements of the motor.
2. Although system studies can be made to determine the worst case surge that might impinge on the motor winding, the monitoring of surges at a number of sites on an industry-wide basis over a period of time is desirable to develop a better feel for surge requirements.
3. The surge capability specified for a motor should be based on application requirements, not simply on any particular standard. This is so because actual requirements might be the same, less, or greater than what the standards require.
4. Higher than necessary level of surge capability and specified dedicated turn insulation are not quite "free". Both the size (first cost) and the efficiency (operating expenses) are adversely affected. Dedicated surge protection equipment for the motor should be considered as a factor in the economic analysis for motor selection.
5. The application of dedicated turn insulation is no guarantee of freedom from failure. If the surge amplitude, rise time, and frequency of surges per unit time are higher than those specified, dedicated turn insulation can also fail.
6. In critical applications, irrespective of the level and type of turn insulation specified, the use of dedicated surge protection should be considered.

7. A large number of motors are functioning satisfactorily with a surge capability of 2 pu. It is not necessary to make a global switch to higher surge capability windings, since in many applications the surge environment is not very hostile.
8. A need exists for a standard definition for surges withstand capability of stator winding turn insulation. This definition should address not only the amplitude and rise times, but also the number of such surges that the insulation must be capable of withstanding.

H.A. Toliyat [68] has presented a method of estimating the voltage distribution among the windings of an inverter fed random wound induction motor supplied through feeder cable. For investigation he has used inverter-cable-motor model and the transient analysis is performed using ATP (Alternative Transient Program) package to estimate the voltage distribution among the motor winding. In his work he has shown the method of (1) estimating the high frequency parameters of the feeder cable and the motor, (2) estimating the voltage distribution among the turns and coils of the motor windings with and without feeder cable and (3) developing a comprehensive high frequency model for the cable and the motor in ATP which can be used for analyzing the various phenomena like terminal voltage doubling, effect of filters at the motor terminals, evaluating the voltage transients with different types and configurations of the cables, etc.

In order to form an equivalent circuit for the system, the distributed parameters of the cable and the motor need to be used because of the high frequency content of the sharp rising wave fronts. For example, if the rise-time of the wave front is $0.2 \mu\text{s}$, then the parameters should be evaluated at 5 MHz and so on. The high frequency parameters to be used in the distributed equivalent circuit for the motor include the resistance of each turn, self-inductance of each turn, mutual inductances between the turns, turn-to-ground capacitance and turn-to-turn capacitances. Since the magnetic behavior of the steel at MHz range frequencies will be entirely different from that at power frequencies. He reported that the characteristic impedance of commonly used cable is around 75 ohm [69] while the characteristic impedance of the motor will be much higher and varies over a wide range of values depending on the power rating of the motor.

For computing the turn resistances and inductances, the eddy current solver available in the package is used. A single slot model is used to obtain the parameters in which one stator slot with the along with their insulation are modeled. In the present case, there are 54 turns within a slot. In order to simplify the model, only a two dimensional model for the slot is used for computing the field. This assumes a fixed relative positioning of the conductors with in the slot. For obtaining the impedance of all the turns in the slot, the eddy current solver was used. Setting up the eddy current analysis includes defining material properties, setting up excitation, defining

boundary conditions, etc. when eddy current analysis is used; the package automatically defines each conductor as a current source. The only boundary condition used is balloon boundary condition in which a surface far away from the slot model is set to zero magnetic vector potential. The eddy current field solver calculates the eddy currents by solving for A and ϕ in the field equation:

$$\nabla_x \frac{1}{\mu_r} (\nabla_x * A) = (\sigma + j\omega\epsilon_r)(-Aj\omega - \nabla\phi)$$

Where, A is the magnetic vector potential, ϕ is the electric scalar potential, μ_r is the relative magnetic permeability, ω is the angular frequency at which all quantities are oscillating, σ is the conductivity, ϵ_r is the relative permittivity.

The Maxwell 2D simulator computes the impedance matrix in two steps. First, it solves for the inductances matrix associated with the model. Second, it solves for the matrix resistance and then forms the impedance matrix. The frequency for which the analysis has to be done can be defined while formulating the problem. The simulator generates an eddy-current field solution for each conductor in the model. The first turn is set to 1 A current in the first solution with all other turns current set to zero current. In the second solution, only the second turn is set to 1 A with the other turns set to zero current. After each solution, the inductance and resistance are computed from the magnetic energy stored and the associated ohmic loss respectively. After each field solution, the solver calculates the self inductance of the conductor which was assigned 1 A current during the analysis. Also, the mutual inductances of the conductor with all the other conductors are computed. Similarly, the resistance terms are also computed after each field solution. The final output of the eddy current analysis is a 54 x 54 impedance matrix. After each solution, the inductances and resistances are computed using the following relations:

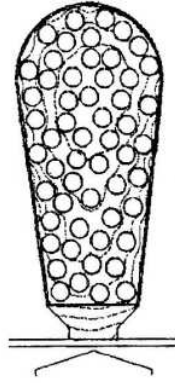
$$L = \frac{4U_{AV}}{I_p^2} \text{ and } R = \frac{2P}{I_p^2}$$

Where,

U_{AV} = the energy stored in magnetic field in Joules,

P = ohmic loss in watts,

I_p = peak value of current in ampere



Flux distribution in the slot obtained with eddy current analysis

Figure 4.5

The flux plot obtained from the eddy current analysis shows an interesting influence of the high frequency behavior of the machine. The flux plot obtained from the eddy current analysis is shown in figure 4.5. The flux plot shows that the flux lines are confined to the slot portion itself and the flux lines do not penetrate the steel laminations because of high frequency effects. Also, there is no flux passing through the air gap to the rotor. The impedance matrix also shows that the different turns have different impedances depending on their relative positioning within the slot.

The capacitance matrix is also obtained in a similar way. For computing the capacitance matrix, electrostatic field analysis is performed with the same geometry. During electrostatic analysis, each conductor is defined as a voltage source and assigned 1 V potential with all the other conductors set to 0V. The electrostatic field simulator computes the static field arising from potential differences and charge distributions. After each field simulation, the capacitance values associated with the conductor which was assigned 1V are computed, which includes turn-to-ground and the turn-to-turn capacitances between the turn being excited and all the other turns. Unlike the impedance calculation procedure, the capacitance calculation need not be carried out at high frequency since the capacitance values are not influenced much by the frequency of excitation. The electrostatic field simulator basically computes static fields arising from potential differences and charge distributions. The field simulator solves for the electric potential, $\phi(x, y)$, in the field equation derived from Gauss's law and is given by

$$\nabla \cdot (\epsilon_r \epsilon_0 \nabla \phi(x, y)) = -\rho$$

ϵ_0 = permittivity of free space.

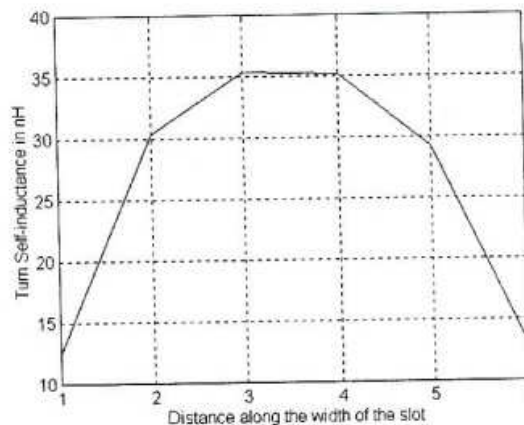
ρ = charge density

To compute the capacitance matrix, the Maxwell 2D field simulator performs a sequence of electrostatic field simulations. For an n-conductor system, n-field simulations are performed. The capacitance between conductor's j and k is therefore:

$$c = 2U_{jk}$$

U_{jk} = energy in the electric field associated with flux lines that connect charges on conductor k to those on conductor k.

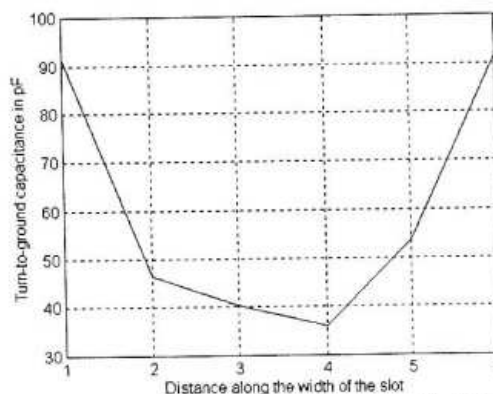
The equivalent circuit parameters of the turns depend highly on the relative positioning within the slot. For example, turns which are adjacent to each other will have higher mutual coupling (both turn-to-turn mutual inductance and capacitance) compared to turns which are far apart. Similarly turns which are adjacent to the slot wall have higher capacitance-to-ground compared to the ones interior to the slot. Figure 4.6 show the variation of self-inductance of individual turns with distance along the width of a slot and figure 4.7 shows the corresponding turn-to-ground capacitance values.



Variation of self-inductance of individual turns with distance along the width of the slot (scale: X-axis 1 div. = 1 mm)

Figure 4.6

Figure 4.6 show that the turns which are adjacent to the slot wall have lower self-inductance values compared to the ones which are interior to the slot because of the vicinity of ground.



Variation of turns to ground capacitance of individual turns with distance along the width of the slot (scale: X-axis 1 div. = 1 mm)

Figure 4.7

The relative positioning of the turns affects their mutual inductance and capacitance values also. For example, two turns which are adjacent to each other have typical mutual inductance values of 20 nH and turns which are far apart have negligible mutual coupling. Similarly, turns which are adjacent to each other have typical capacitance values around 22 pF and turns which are far apart have negligible mutual capacitance. Another observation is that the turns which are located around the periphery of the slot wall have almost identical self-inductance values and so are the turns which are interior to the slot.

The parameters of the feeder cable at frequencies will also be significantly different from its power frequency values. In the present work, the cable constant routine available in ATP package is used for obtaining the high frequency parameters. ATP is the personal computer version of the Electro Magnetic Transient Program (EMTP). First, the geometry and material data of the three phase cable is defined in an input file in a format specified by the ATP users' manual [70]. The type of cable used for connecting the inverter and the motor in the present case is type A as designated in the ATP user manual, viz, a system of coaxial cable without any enclosing pipe. After defining the geometry and physical data, the frequency for which parameters need to be computed is specified. With this input data file, the "Cable Constants" routine is used to compute the parameters at the frequency specified. The parameters of the cable are also computed for a frequency of 5 MHz corresponding to a rise-time of $0.2 \mu S$.

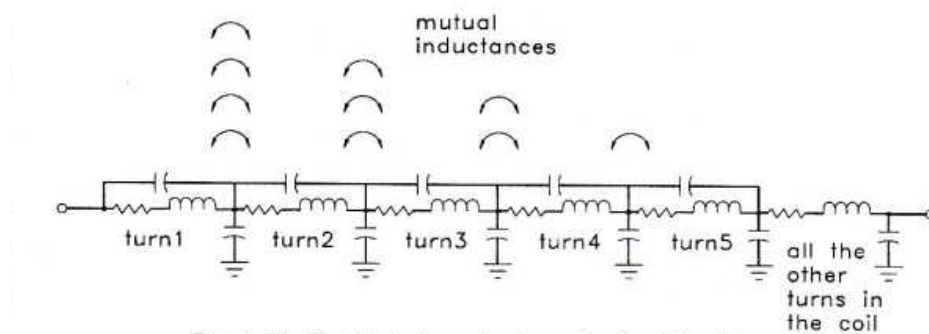
To obtain the voltage distribution among the motor windings, an equivalent circuit model for the inverter-cable-motor system is created in ATPDRAW. The details of the equivalent circuits used are explained in the following subsections.

The output of the voltage source PWM inverter will have a train of wave fronts with very sharp rise-times. The transient voltage pattern among the winding during each PM wave front remains the same throughout the cycle (unless the width of any pulse is so small that before the transients due to rising edge dies down, the falling edge arrives and vice versa. [38]. There will also be several wave fronts occurring in each fundamental cycle. Hence in order to understand the transients during a wave front, it is sufficient to model only one front applied across any two lines of the motor [68]. This simplifies the complexity of the model. In order to model a typical wave front, a RAMP type source is used in ATPDRAW. In ATPDRAW the amplitude, rise-time, starting and duration of the pulse can all be defined. In the present model, only one ramp source is used and applied across phases A & B with phase C open.

Cable can be modeled either as a lumped parameter pi-circuit or as distributed parameter circuit components. A third alternative is to approximate the distributed nature of the parameters by using several cascaded lumped parameter pi-sections. There is also a more advanced

model which can account for changes in the parameters with frequency, however this not considered here due to the rather limited range of frequencies of interest. The main disadvantage of using the lumped pi-section model is that large numbers of sections need to be modeled since the wave lengths corresponding to MHz range frequencies will be very small. To avoid this problem, a distributed parameter model is used in ATP.

From the high frequency parameters obtained from the finite element analysis, a distributed equivalent circuit for the motor is formed. The motor being analyzed in the present case has 54 turns per coil; there are 6 coils per phase pole, two groups of 3 coils being connected in parallel. Ideally, it would be desirable to model each turn within a slot with its distributed parameters and also its mutual impedances with other turn within the slot. However, considering the number of turns per slot, it is not practical to model all the turns with their distributed parameters. However, it is a well known fact that the first few turns of the line end coil get subjected to maximum voltage stress during each wave front [71]. Hence , in the present work, only the first few turns of the line end coil are represented by their distributed parameters with all the other turns in the line-end coil and also the other coils modeled by their lumped parameters; phases A and B are modeled the way explained, phase C is modeled by its lumped parameters.

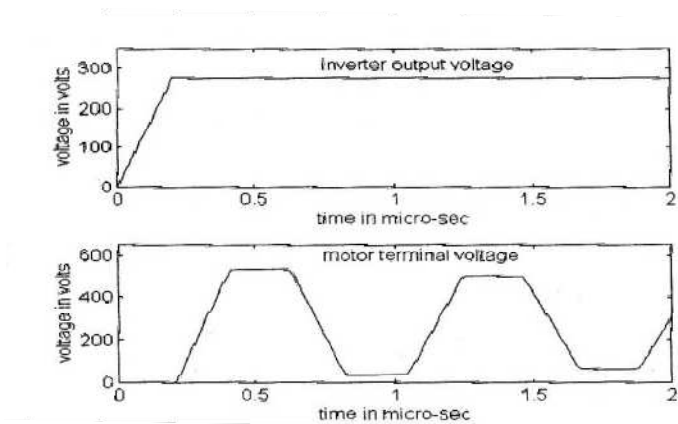


Partially distributed equivalent circuit of the line-end coil

Figure 4.8

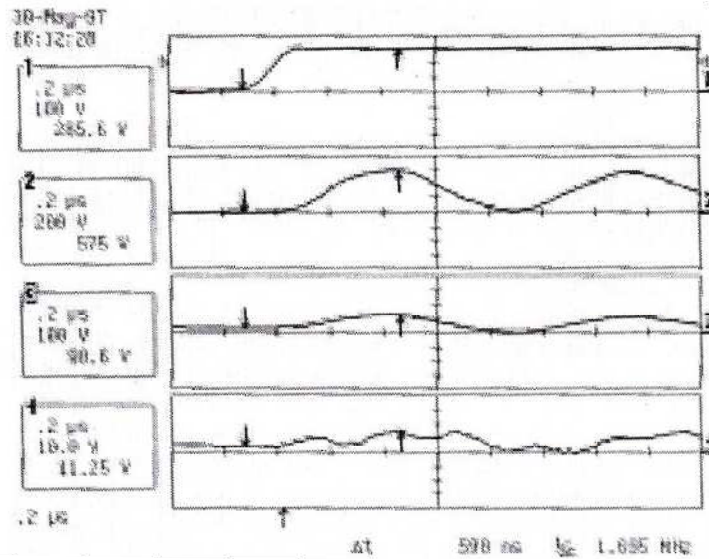
Finite element analysis gives the per unit length values of the parameters of the turns modeled in the slot. Hence while forming the equivalent circuit; these values are multiplied by the mean length of turns which takes care of the end-turn portions of the turns. The equivalent circuit of the line-end coil described in this section is shown in figure 4.8.

To form the equivalent circuit for the whole system, first the ramp type source is inserted. One end of the source is grounded and the other end of the source is connected to one of the three phases in the cable distributed parameters. The output of the cable is connected to the motor equivalent circuit described earlier. This completes the generation of the equivalent circuit for the system. Once the equivalent circuit of the inverter-cable-motor system is developed in ATPDRAW, the type of analysis to be done, duration of analysis, and the time step for simulation are all defined after which ATP simulation performed.



Simulated inverter output voltage and motor terminal voltage
with 100 foot long cable
Figure 4.9

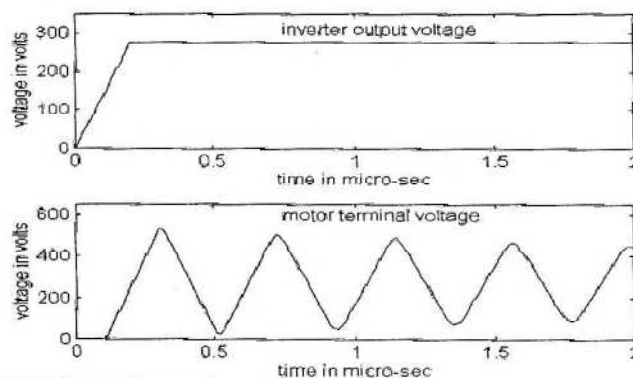
For studying the terminal voltage transients only the feeder cable is modeled with distributed parameters as described earlier. The motor is represented by its lumped parameter model with impedance equal to its characteristic impedance. The characteristic impedance of the motors depends on their power rating and typical values are listed in [69]. In a present case, a resistance value of 1500 ohm is used to represent the motor. The main idea of this simulation is to study the terminal voltage transients in detail. As described earlier, the ATP file for the entire system model is created only once. When different cable lengths are to be simulated, the corresponding entry in the ATP file is changed. Figure 4.9 shows the simulated terminal voltage transient along with the input PWM wave front of a cable length of 100 feet.



Experimental results of a PWM Induction motor drive with 100 foot long cable between the inverter and the motor. Trace 1: Inverter output voltage, Trace 2: Motor terminal voltage, Trace 3: Line end voltage, Trace 4: Turn 1 Voltage.

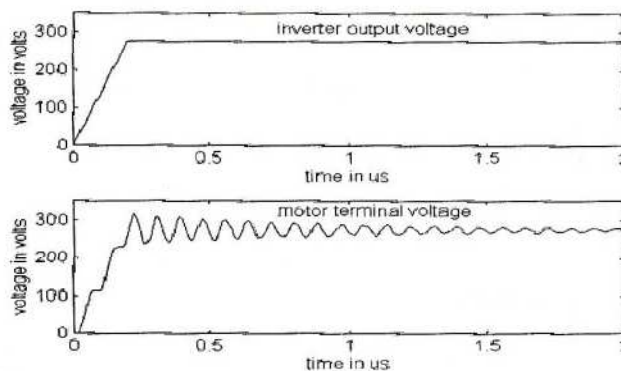
Figure 4.10

Figure 4.10 shows the measured waveforms of the inverter output voltage, motor terminal voltage, line-end coil voltage and turn 1 voltage when the motor is connected to the inverter through 100 feet cable. From the simulated and experimental results, it can be seen that the voltage takes some time to travel from the inverter output to the motor terminals which depends on the cable length. Comparing the amplitude and the frequency of oscillation of the motor terminal voltage, it can be seen that the simulated and experimental results match well.



Simulated inverter output voltage and motor terminal voltage with 50 foot
long cable
Figure 4.11

Figure 4.11 shows the simulated voltage wave forms with 50 feet long cable, comparing figures 4.9 and 4.11, it can be seen that the frequency of oscillation of the motor terminal voltage increases with reduction in cable length. This is because of the fact that voltage wave has to travel longer with increase in cable length while the velocity of propagation remains the same. Figure 4.12 and 4.13 show the simulated and measured inverter output voltage along with the motor terminal voltage when a 10 feet long cable is used. Though the cable length is not very long, some amount of oscillation and over voltage can be seen at the motor terminals. In this case also, good agreement between simulation and experimental results can be seen by comparing figures 4.12 and 4.13.

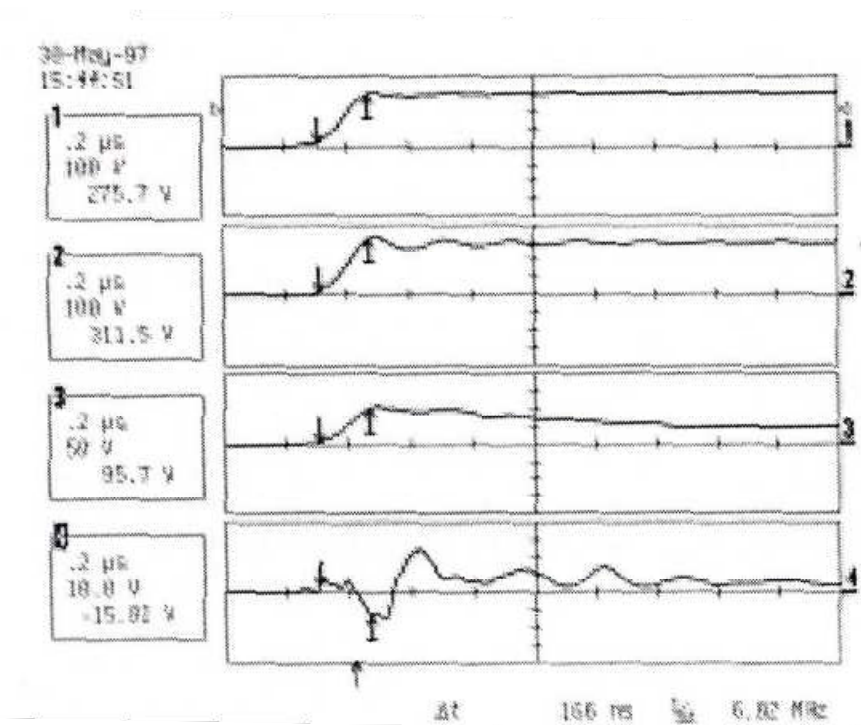


Simulated inverter output voltage and motor terminal voltage with 10 foot
long cable
Figure 4.12

In the second simulation, the motor winding is modeled along with 10 feet cable and the wave front. The main idea is to study the voltage distribution among the windings when the motor is connected to the inverter through a 10 feet long cable. Figure 4.14 shows the line-end coil voltage when rise-time of the wave front is $0.2 \mu S$.

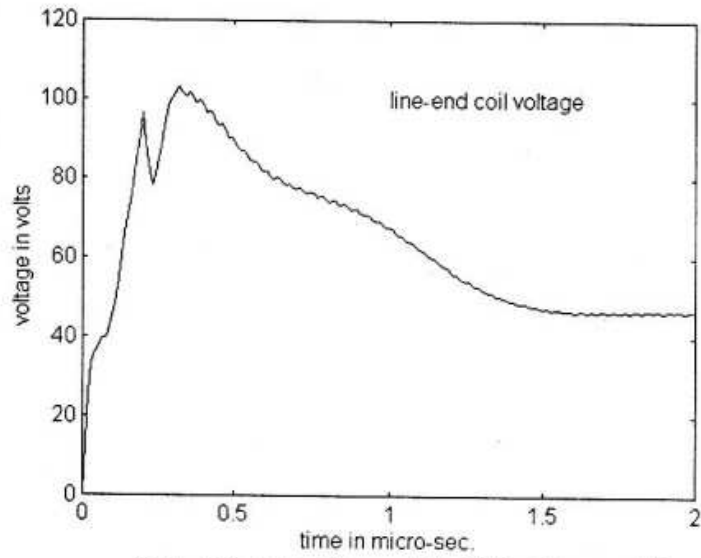
In this simulation, both the feeder cable and the motor are represented by their distributed parameters. This simulation is performed to study the effect of voltage doubling on the voltage distribution among the

windings. Figure 4.15 shows the voltage drop across the line end coil with 100 foot cable used to connect the motor and the inverter. The rise-time of the wave front is $0.2 \mu\text{s}$. The measured line-end coil voltage with 100 foot cable is also shown in Figure 6. While the amplitude of the simulated and measured line-end coil voltages match well, the frequency of oscillations do not quite match well. This is mainly due to the approximate equivalent circuit model used for the motor windings which basically may not represent the actual time constants involved in the transients. As mentioned earlier, it would be desirable to represent all the turns within a given slot by its distributed parameters which would truly represent the high frequency circuit.

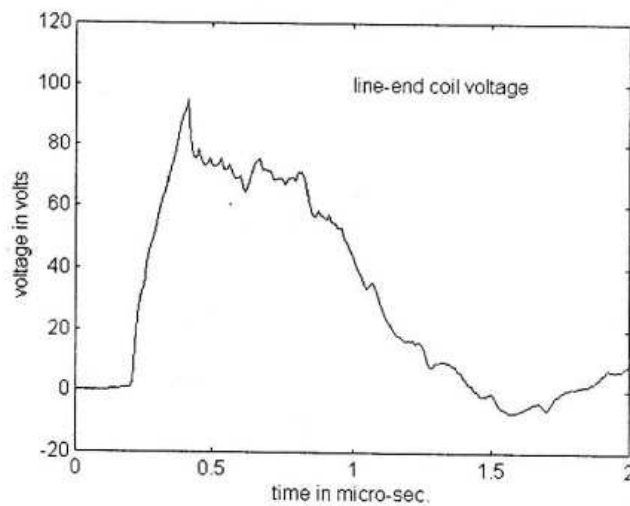


Experimental results of a PWM Induction motor drive with 10 foot long cable between the inverter and the motor. Trace 1: Inverter output voltage, Trace 2: Motor terminal voltage, Trace 3: Line end voltage, Trace 4: Turn 1 Voltage.

Figure 4.13



Line end coil voltage with 10 foot long cable
Figure 4.14



Line end coil voltage with 100 foot long cable and 0.2 μ s rise time
Figure 4.15

One important observation made based on simulation and experimental results is that the peak value of the transient voltage across the line-end coil does not vary appreciably when the feeder cable is introduced, through there is voltage doubling at the motor terminals. In fact, the peak value of the line-end coil voltage slightly reduces when the feeder cable is

used. It is an interesting result because, the insulation of the motor winding has to be designed based on this.

In random wound machines, the placement of the individual turns within a slot will be quite random in nature and there is a possibility that the first and the last turns of the same coil be placed adjacent to each other. In this case, the two turns are separated only by the thin insulation layers of the two turns. During a wave front, it is shown that a considerable portion of the line voltage is dropped across the line end coil and hence this might result in insulation break down. The main concern while using a long feeder cable is that the voltage stress on the line-end coil might be worse because of the terminal voltage doubling. However, the simulation and experimental results obtained in the present work do not show any such additional stress.

Chapter 5

Development of a Model to Estimate the Parameters of Equivalent Circuit and Prediction of Performance

5.1 Introduction

The efficiency calculation of poly phase induction motor by summation of losses method includes the following losses.

[1] Constant losses:

This includes the [a] Losses in active iron and additional losses in other metal parts. [b] Losses due to friction (bearings and brushes, if not lifted during operation) not including any losses in a separate lubricating system. [c] The total windage losses in the machine, includes power absorbed in integral fans, and in auxiliary machines, if any, forming an integral part of the machine.

[2] Load losses:

This includes the [a] Resistance losses in primary winding. [b] Resistance losses in secondary winding. [c] Resistance losses in brushes if any.

[3] Additional load losses:

This includes [a] Losses introduced by the load in active iron and other metal parts other than the conductors. [b] Eddy current losses in primary or secondary winding conductors caused by current dependent flux pulsation.

The above [1] and [2] losses are normally calculated using the parameters of equivalent circuit and the third losses are vary as the square of the primary current assumed that their total value at full load is equal to 0.5 % of the rated input for motor. The calculation of parameters of equivalent circuit is requires the no load test readings at rated voltage and blocked rotor test readings at rated current. These third losses are known as stray load losses. In IEEE-112 method B it is suggested that these losses are assumed as follows.

KW		RPM	A	Percent	Percent	Percent	Percent	Percent
(1)	(2)	(3)	(4)	(5)	(6)	(7)	(8)	(9)
0.37	71	2790	1.2	170	600	650	66.0	70.2
0.55	71	2760	1.6	170	600	650	70.0	74.0
0.75	80	2780	2.0	170	600	650	73.0	77.0

Table 5.4: Values of Performance Characteristic of 4 Pole Energy Efficient Induction Motors.								
Rated Output	Frame Designation	Full Load Speed Min	Full Load Current Max	Break-away Torque In Terms Of full Load torque Min	Breakaway Current in Terms of full Load current Equal or below		Nominal Efficiency	
					Eff 2	Eff 1	Eff 2	Eff 1
KW		RPM	A	Percent	Percent	Percent	Percent	Percent
(1)	(2)	(3)	(4)	(5)	(6)	(7)	(8)	(9)
0.37	71	1330	1.4	170	550	600	66.0	73.0
0.55	80	1340	1.7	170	550	600	70.0	78.0
0.75	80	1360	2.2	170	550	600	73.0	82.5

However, above specifications are not available for smaller motors. In this work investigation is carried out for 470 W motor in frame 63.

5.2 ACCURACY OF ESTIMATION

The accuracy of estimation of efficiency using these parameters depends upon the value of parameters. If the parameters are exact one then accuracy of calculation of efficiency is more and vice-versa. Normally when we are taking observations for one test (say blocked rotor test) at different time then we may not have the observed value second time same as we have observed it at first time. So if we calculate the parameters using these two observations the answer will be different. Same thing will be repeated when instruments will change or recording person will change. To avoid this error in calculated parameters value, I am suggesting the following procedures for determining the parameters of equivalent circuit. The stator resistance is

obtained from dc volt-amp method as given below, and rotor resistance, reactance, magnetizing branch resistance and reactance are calculated from no load test and blocked test and then presented to algorithm to modify it.

5.3.1 MEASUREMENT OF WINDING RESISTANCE

It can be measured by following methods

a) THE DROP OF POTENTIAL OR VOLTMETER-AMMETER METHOD

∴

For this method d.c. voltmeter & d.c. ammeter is used. The d.c. voltmeter is connected at the motor terminal and current is measured from d.c. ammeter when its value being steady. From this value the resistance can be calculated as follows:

$$R_{dc} = \frac{V}{I} \text{---(5.1)}$$

b) THE BRIDGE METHOD :

- If the resistance value above 1 ohm then Wheatstone bridge can be employed.
- If the resistance value below 1 ohm then Kelvin Bridge is being used.

In case of bridge method the unknown resistance is compared with the known resistance by suitable bridge. With Wheatstone bridge, the resistance measured includes resistance of connecting leads which is to be subtracted from the total measured resistance.

In addition to these methods the advent of digital electronics has made possible a direct display of resistance of winding. Digital micro ohm meters are very fast and accurate for measurement of winding resistance.

In case of three phase motors, the winding resistance is measured between all three phases and calculates winding resistance per phase.

Stator winding resistance per phase for star connection

$$R_s = \left(\frac{R_{ry} + R_{yb} + R_{br}}{6} \right) \text{---(5.2)}$$

Stator winding resistance per phase for delta connection

$$R_s = \left(\frac{R_{ry-yb} + R_{yb-br} + R_{br-ry}}{2} \right) \text{---(5.3)}$$

If the winding resistance R_1 is known for any temperature t_1 , it can be calculated at any temperature t_2 as below:

Winding resistance R_2 at temperature t_2

$$R_2 = \left(\frac{235 + t_2}{235 + t_1} \right) * R_1 \text{---(5.4)}$$

5.3.2 NO LOAD TEST

This test is performed to finding out no load current, core loss and friction & windage losses. For this test an induction motor is run in no load condition at rated voltage & frequency. When the readings are being stable the readings of voltage, current, frequency, speed and power input are to be taken. Preferably this test should be conducted after temperature rise test. For finding out constant loss the I^2R Loss should be subtracted from no load input power.

$$\text{Constant loss} = P_0 - 3I_0^2 * R_s \text{ for star connection---(5.5)}$$

$$\text{Constant loss} = P_0 - I_0^2 * R_s \text{ for delta connection---(5.6)}$$

Where P_0 and I_0 is no load input and current.

The constant loss comprises core loss, friction and windage losses. For separating core loss and friction & windage loss, take the readings of current, no load input power at different voltage varying from 15 to 125% of rated voltage. Then plot the graph between V_s and input power in watts and extend the curve to zero voltage axis which gives value of friction and windage losses. These losses are subtracted from constant losses which gives core losses.

Magnetizing branch parameter of equivalent circuit can be determined by following equations:

$$P_o = \sqrt{3}V_0I_0 \cos \phi \text{---(5.7)}$$

$$R_{FE} = \frac{V_s}{I_0 * \cos \phi} \text{---(5.8)}$$

$$X_m = \frac{V_s}{I_0 * \sin \phi} \text{---(5.9)}$$

5.3.3 BLOCKED ROTOR TEST

In this case rotor is blocked (slip is unity) and a reduced voltage is applied to stator terminals to avoid exceeding of the rated current. This test performed for determining starting current, starting torque and the parameters of the equivalent circuit. It also gives information regarding power factor, impedance and circle diagram.

The test under locked rotor condition involves very high mechanical stresses and high rates of heating. Hence following precautions should be taken while doing the test:

- The direction of rotation should be checked prior to locking the rotor
- The mechanical means of locking the rotor is of adequate strength to prevent possible injury to personnel or damage equipment.
- As the winding get heated rapidly during this test, the test should be carried as rapidly as possible.

This test allows the resistance R_r and X_r to be found. Since the rotor current is much larger than the magnetizing current, the excitation branch can be neglected.

$$R_r = (V_2/I_2) * \cos \phi - R_s \text{---} (5.10)$$

$$X_r = X_s = \frac{(V_2/I_2) * \sin \phi}{2} \text{---} (5.11)$$

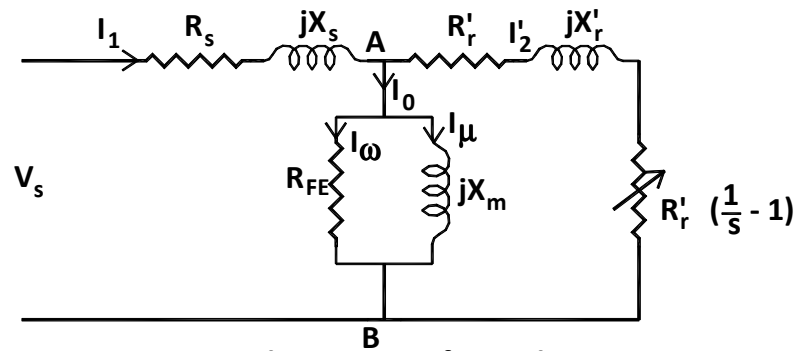


Fig. 5.1 Equivalent circuit of an Induction Motor

5.4 MATHEMATICAL MODELING OF INDUCTION MOTOR BASED ON EQUIVALENT CIRCUIT METHOD

For any closed circuit we can write that

$$Z - \frac{V_s}{I_s} (\cos \phi + j \sin \phi) = 0 \text{---(5.12)}$$

The equivalent impedance of circuit diagram shown figure 5.1 is

$$Z_{eq} = (R_s + jX_s) + \left(\frac{jR_{FE} * X_m}{R_{FE} + jX_m} \right) \parallel \left(\frac{R_r}{s} + jX_r \right) \text{---(5.13)}$$

$$\text{or } Z_{eq} = (R_s + jX_s) + \frac{\left(\frac{jR_{FE} * X_m}{R_{FE} + jX_m} \right) * \left(\frac{R_r}{s} + jX_r \right)}{\left(\frac{jR_{FE} * X_m}{R_{FE} + jX_m} \right) + \left(\frac{R_r}{s} + jX_r \right)} \text{---(5.14)}$$

$$\begin{aligned}
& \text{or } Z_{eq} \\
& = (R_s + jX_s) \\
& + \frac{jR_{FE} * X_m * \frac{R_r}{S} - R_{FE} * X_m * X_r}{jR_{FE} * X_m + (R_{FE} + jX_m) \left(\frac{R_r}{S}\right) + (R_{FE} + jX_m)(jX_r)} \text{---(5.15)}
\end{aligned}$$

$$\begin{aligned}
& \text{or } Z_{eq} \\
& = (R_s + jX_s) \\
& + \frac{-R_{FE} * X_m * X_r + j\frac{R_r}{S} * R_{FE} * X_m}{R_{FE} * \frac{R_r}{S} - X_m * X_r + j \left(R_{FE} * X_m + R_{FE} * X_r + X_m \frac{R_r}{S} \right)} \text{---(5.16)}
\end{aligned}$$

Multiplying and dividing second term by

$$R_{FE} * \frac{R_r}{S} - X_m * X_r - j \left(R_{FE} * X_m + R_{FE} * X_r + X_m \frac{R_r}{S} \right) \text{---(5.17)}$$

$$\begin{aligned}
& \text{or } Z_{eq} = (R_s + jX_s) \\
& + \frac{\left(-R_{FE} * X_m * X_r + j\frac{R_r}{S} * R_{FE} * X_m \right)}{\left[R_{FE} * \frac{R_r}{S} - X_m * X_r + j \left(R_{FE} * X_m + R_{FE} * X_r + X_m \frac{R_r}{S} \right) \right]} \\
& * \frac{\left(R_{FE} * \frac{R_r}{S} - X_m * X_r - j \left(R_{FE} * X_m + R_{FE} * X_r + X_m \frac{R_r}{S} \right) \right)}{\left(R_{FE} * \frac{R_r}{S} - X_m * X_r - j \left(R_{FE} * X_m + R_{FE} * X_r + X_m \frac{R_r}{S} \right) \right)} \text{---(5.18)}
\end{aligned}$$

$$\begin{aligned}
& \text{or } Z_{eq} \\
& = (R_s + jX_s) \\
& + \frac{\left(-R_{FE} * X_m * X_r + j\frac{R_r}{S} * R_{FE} * X_m \right) \left(R_{FE} * \frac{R_r}{S} - X_m * X_r - j \left(R_{FE} * X_m + R_{FE} * X_r + X_m \frac{R_r}{S} \right) \right)}{\left[\left(R_{FE} * \frac{R_r}{S} - X_m * X_r \right)^2 + \left(R_{FE} * X_m + R_{FE} * X_r + X_m \frac{R_r}{S} \right)^2 \right]} \\
& \text{---(5.19)}
\end{aligned}$$

Now for simplification not considering stator impedance we have

$$\begin{aligned}
& \frac{\left(-R_{FE} * X_m * X_r + j\frac{R_r}{S} * R_{FE} * X_m \right) \left(R_{FE} * \frac{R_r}{S} - X_m * X_r - j \left(R_{FE} * X_m + R_{FE} * X_r + X_m \frac{R_r}{S} \right) \right)}{\left[\left(R_{FE} * \frac{R_r}{S} - X_m * X_r \right)^2 + \left(R_{FE} * X_m + R_{FE} * X_r + X_m \frac{R_r}{S} \right)^2 \right]} \\
& \text{---(2.20)}
\end{aligned}$$

Taking product of numerator's first term of first bracket and second bracket

$$\begin{aligned}
& (-R_{FE} * X_m * X_r) \left(R_{FE} * \frac{R_r}{S} - X_m * X_r - j \left(R_{FE} * X_m + R_{FE} * X_r + X_m \frac{R_r}{S} \right) \right) \\
&= (-R_{FE} * X_m * X_r) \left(R_{FE} * \frac{R_r}{S} - X_m * X_r \right) \\
&\quad - (-R_{FE} * X_m * X_r) j \left(R_{FE} * X_m + R_{FE} * X_r + X_m \frac{R_r}{S} \right) \\
&= (-R_{FE} * X_m * X_r) \left(R_{FE} * \frac{R_r}{S} - X_m * X_r \right) \\
&\quad + (R_{FE} * X_m * X_r) j \left(R_{FE} * X_m + R_{FE} * X_r + X_m \frac{R_r}{S} \right)
\end{aligned}$$

Writing real part with green letter and imaginary part with blue letter we have

$$\begin{aligned}
& -R_{FE} * X_m * X_r * R_{FE} * \frac{R_r}{S} + R_{FE} * X_m * X_r * X_m * X_r + j R_{FE} * X_m * X_r \\
&\quad * R_{FE} * X_m + j R_{FE} * X_m * X_r * R_{FE} * X_r + j R_{FE} * X_m * X_r \\
&\quad * X_m \frac{R_r}{S} \text{---(5.21)}
\end{aligned}$$

Similarly taking product of numerator's second term of first bracket and second bracket

$$\begin{aligned}
& \left(j \frac{R_r}{S} * R_{FE} * X_m \right) \left(R_{FE} * \frac{R_r}{S} - X_m * X_r - j \left(R_{FE} * X_m + R_{FE} * X_r + X_m \frac{R_r}{S} \right) \right) \\
& j \frac{R_r}{S} * R_{FE} * X_m * R_{FE} * \frac{R_r}{S} - j \frac{R_r}{S} * R_{FE} * X_m * X_m * X_r + \frac{R_r}{S} * R_{FE} * X_m \\
&\quad * R_{FE} * X_m + \frac{R_r}{S} * R_{FE} * X_m * R_{FE} * X_r + \frac{R_r}{S} * R_{FE} * X_m \\
&\quad * X_m \frac{R_r}{S} \text{---(5.22)}
\end{aligned}$$

Combining real part of equation (5.21) and (5.22) we have

$$\begin{aligned}
&= \frac{R_r}{S} * R_{FE} * X_m * R_{FE} * X_m + \frac{R_r}{S} * R_{FE} * X_m * R_{FE} * X_r + \frac{R_r}{S} * R_{FE} * X_m \\
&\quad * X_m * \frac{R_r}{S} - R_{FE} * X_m * X_r * R_{FE} * \frac{R_r}{S} + R_{FE} * X_m * X_r * X_m \\
&\quad * X_r \\
&= \frac{R_r}{S} * R_{FE} * X_m * R_{FE} * X_m + \frac{R_r}{S} * R_{FE} * X_m * X_m \\
&\quad * \frac{R_r}{S} + R_{FE} * X_m * X_r * X_m * X_r
\end{aligned}$$

Or real part is

$$= (R_{FE} * X_m^2) \left(\frac{R_r}{S} * R_{FE} + \left(\frac{R_r}{S} \right)^2 + X_r^2 \right) \text{---(5.23)}$$

Combining imaginary part of equation (5.21) and (5.22) we have

$$\begin{aligned} & j \frac{R_r}{S} * R_{FE} * X_m * R_{FE} * \frac{R_r}{S} - j \frac{R_r}{S} * R_{FE} * X_m * X_m * X_r + j R_{FE} * X_m * X_r \\ & \quad * R_{FE} * X_m + j R_{FE} * X_m * X_r * R_{FE} * X_r + j R_{FE} * X_m * X_r \\ & \quad * X_m * \frac{R_r}{S} \\ & = j \left(\frac{R_r}{S} * R_{FE} * X_m * R_{FE} * \frac{R_r}{S} R_{FE} * X_m * X_r * R_{FE} * X_m + R_{FE} * X_m * X_r \right. \\ & \quad \left. * R_{FE} * X_r \right) \end{aligned}$$

Or imaginary part is

$$= j \left(R_{FE}^2 * X_m \left(X_m * X_r + \left(\frac{R_r}{S} \right)^2 + X_r^2 \right) \right) \text{---(5.24)}$$

Hence real part of equation (2.20)

$$\begin{aligned} & Re\{Z\} \\ & = R_s \\ & + \frac{R_{FE} X_m^2 \left(\frac{R_r}{S} R_{FE} + \left(\frac{R_r}{S} \right)^2 + X_r^2 \right)}{\left[\left(R_{FE} * \frac{R_r}{S} - X_m * X_r \right)^2 + \left(R_{FE} * X_m + R_{FE} * X_r + X_m \frac{R_r}{S} \right)^2 \right]} \text{---(5.25)} \end{aligned}$$

And imaginary part of equation (5.20)

$$\begin{aligned} & Im\{Z\} \\ & = X_s \\ & + \frac{\left(R_{FE}^2 * X_m \left(X_m * X_r + \left(\frac{R_r}{S} \right)^2 + X_r^2 \right) \right)}{\left[\left(R_{FE} * \frac{R_r}{S} - X_m * X_r \right)^2 + \left(R_{FE} * X_m + R_{FE} * X_r + X_m \frac{R_r}{S} \right)^2 \right]} \text{---(5.26)} \end{aligned}$$

The equations for current, Power factor, output power, torque, input power, Efficiency from the equivalent circuit,

$$I_{eq} = \frac{V_s}{Z_{eq}}, \quad PF = \cos \left[\tan^{-1} \frac{Im\{Z\}}{Re\{Z\}} \right] \text{---(5.27)}$$

$$P_{out} = 3I_r^2 R_L \text{ where } R_L = R_r \left(\frac{1}{S} - 1 \right) \text{---(5.28)}$$

$$T_g = \frac{P_g}{\omega_m}, \quad P_{in} = 3 * V * I_{eq} * \cos \phi,$$

$$Efficiency = \frac{P_{out}}{P_{in}} * 100 \text{---(5.29)}$$

Once R_s is obtained from direct measurement and the stator and rotor reactance are assumed proportional as in IEEE Std 112,

$$x_s = k_{12} * x_r \text{---(5.30)}$$

the no load and block rotor tests yield a system of four non linear equations (subscript B stands for 'Block-rotor' and subscript V for 'No load')

$$F_1 = Re\{Z_B\} - \frac{V_{sB}}{I_{sB}} \cos \phi_B, \quad F_2 = Im\{Z_B\} - \frac{V_{sB}}{I_{sB}} \sin \phi_B \text{---(5.31)}$$

$$F_3 = Re\{Z_V\} - \frac{V_{sV}}{I_{sV}} \cos \phi_V, \quad F_4 = Im\{Z_V\} - \frac{V_{sV}}{I_{sV}} \sin \phi_V \text{---(5.32)}$$

5.4.1 MACHINE MODEL FOR INVERTER FED INDUCTION MOTOR

r_{1k} and L_{1k} : Stator resistance and leakage reactance inductance for K^{th} harmonic

r_{2k} and L_{2k} : rotor resistance and leakage reactance inductance for K^{th} harmonic

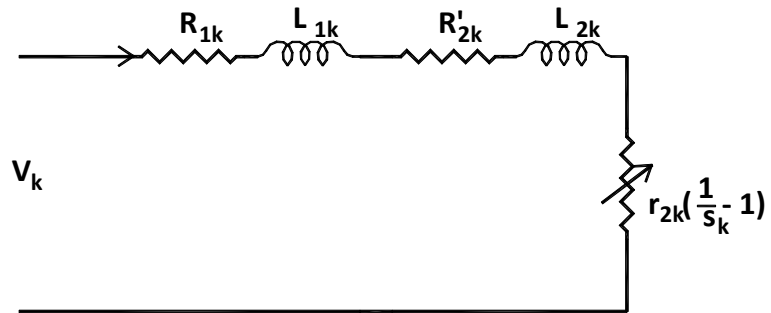


Fig. 5.2 Harmonic equivalent circuit of an Induction Motor

It is important to note that the rotor parameters r_{2k} and l_{2k} are frequency dependent due to skin effect in the rotor bars. Since an inverter fed induction motor is usually started at low frequency. The values of r_{2k} and l_{2k} should be those corresponding to the harmonic frequency K_f , where f is the starting frequency and k is the order of harmonic. The iron loss resistance R_{FE} is also frequency dependent, and should be the value corresponding to the starting frequency. As for the exciting inductance L_m , it does not depend on frequency, but is influenced by magnetic saturation. Since the magnetic saturation tends to occur when the starting frequency is low, it should be considered in the value of L_m . The stator parameters r_{1k} and l_{1k} are assumed, for simplicity, to be independent of frequency.

5.5 NUMERICAL ALGORITHM FOR PARAMETER ESTIMATION

The parameters obtained from no load test and blocked tests are liable to give incorrect performance values. This is because of the possible errors in parameter value due to instrument error, measurement error, human error, deviation of voltage magnitude, deviation of voltage frequency. When evaluated parameters are not exact then they will not satisfy the equation of closed circuit given by equation (5.12). The simplification of closed loop equation for blocked rotor condition and no load condition is given by equations (5.31) and (5.32) respectively. These two equation are non

linear and hence are to be evaluated by numerical method. Here below *Newton-Raphson* method is suggested for solution of above equations.

The performance calculated [1] using the parameters obtained from blocked rotor test and no load test [2]] using the parameters obtained from blocked rotor test and no load test and then modifying it using *Newton-Raphson* are compared with the actual load test performance. The resulted are presented at the end.

The *Newton-Raphson* method is a fast local convergence procedure used to solve nonlinear equations given by equation

$$f(x) = 0 \text{---(5.33)}$$

Using the recurrence formula of equation (5.33) and starting the iterative process with a value $x^{(0)}$ as first guess, the solution of equation (5.32) is obtained. The parameters values which are obtained in this way are very much closer to the exact value of parameter.

$$x^{(j+1)} = x^{(j)} - \frac{f(x)^j}{f'(x)^j} \text{---(5.34)}$$

As in our case there are more number of simultaneous nonlinear equations, the equation (2.36) can be written in the form of matrix as below

$$X^{(j+1)} = X^{(j)} - \frac{F(x)^j}{F'(x)^j}$$

$$X^{(j+1)} = X^{(j)} - J'(x)^{j-1} F(x)^j \text{---(5.35)}$$

Where

$$X^{(j+1)}, \quad X^{(j)},$$

$F(x)^j$ are $n - \text{dimensional}$ coulumn vector and $J'(x)^{j-1}$ is $n*n$ dimensional Jacobian matrix.

$$J^{(j)} = \begin{bmatrix} \left(\frac{\partial f_1}{\partial x_1}\right)^{(j)} & \left(\frac{\partial f_1}{\partial x_2}\right)^{(j)} & \left(\frac{\partial f_1}{\partial x_3}\right)^{(j)} & \text{---} \left(\frac{\partial f_1}{\partial x_n}\right)^{(j)} \\ \left(\frac{\partial f_2}{\partial x_1}\right)^{(j)} & \left(\frac{\partial f_2}{\partial x_2}\right)^{(j)} & \left(\frac{\partial f_2}{\partial x_3}\right)^{(j)} & \text{---} \left(\frac{\partial f_2}{\partial x_n}\right)^{(j)} \\ \left(\frac{\partial f_3}{\partial x_1}\right)^{(j)} & \left(\frac{\partial f_3}{\partial x_2}\right)^{(j)} & \left(\frac{\partial f_3}{\partial x_3}\right)^{(j)} & \text{---} \left(\frac{\partial f_3}{\partial x_n}\right)^{(j)} \\ \left(\frac{\partial f_n}{\partial x_1}\right)^{(j)} & \left(\frac{\partial f_n}{\partial x_2}\right)^{(j)} & \left(\frac{\partial f_n}{\partial x_3}\right)^{(j)} & \text{---} \left(\frac{\partial f_n}{\partial x_n}\right)^{(j)} \end{bmatrix} \text{---(5.36)}$$

$$X^{(0)} = \begin{bmatrix} X_1^{(0)} \\ X_2^{(0)} \\ X_3^{(0)} \\ \vdots \\ X_n^{(0)} \end{bmatrix}, \quad X^{(j)} = \begin{bmatrix} X_1^{(j)} \\ X_2^{(j)} \\ X_3^{(j)} \\ \vdots \\ X_n^{(j)} \end{bmatrix} \quad (5.37)$$

Its application to the circuit non linear equations yields the following numerical algorithm:

$$\begin{bmatrix} R_r^{(j+1)} \\ X_r^{(j+1)} \\ R_{FE}^{(j+1)} \\ X_m^{(j+1)} \end{bmatrix} = \begin{bmatrix} R_r^{(j)} \\ X_r^{(j)} \\ R_{FE}^{(j)} \\ X_m^{(j)} \end{bmatrix} - \begin{bmatrix} \left(\frac{\partial F_1}{\partial R_r}\right)^{(j)} & \left(\frac{\partial F_1}{\partial X_r}\right)^{(j)} & \left(\frac{\partial F_1}{\partial R_{FE}}\right)^{(j)} & \left(\frac{\partial F_1}{\partial X_m}\right)^{(j)} \\ \left(\frac{\partial F_2}{\partial R_r}\right)^{(j)} & \left(\frac{\partial F_2}{\partial X_r}\right)^{(j)} & \left(\frac{\partial F_2}{\partial R_{FE}}\right)^{(j)} & \left(\frac{\partial F_2}{\partial X_m}\right)^{(j)} \\ \left(\frac{\partial F_3}{\partial R_r}\right)^{(j)} & \left(\frac{\partial F_3}{\partial X_r}\right)^{(j)} & \left(\frac{\partial F_3}{\partial R_{FE}}\right)^{(j)} & \left(\frac{\partial F_3}{\partial X_m}\right)^{(j)} \\ \left(\frac{\partial F_4}{\partial R_r}\right)^{(j)} & \left(\frac{\partial F_4}{\partial X_r}\right)^{(j)} & \left(\frac{\partial F_4}{\partial R_{FE}}\right)^{(j)} & \left(\frac{\partial F_4}{\partial X_m}\right)^{(j)} \end{bmatrix}^{-1} \begin{bmatrix} F_1 \\ F_2 \\ F_3 \\ F_4 \end{bmatrix} \quad (5.38)$$

Where F_1 to F_4 are given by equations (5.31) and (5.32)

5.5.1 INITIAL VALUES OF PARAMETER AND STOPPING CRITERIA

5.5.1.1 INITIAL PARAMETER VALUE

The values for the first guess vector will be obtained from no-load and blocked-rotor tests voltage, current and power measurements, and no-load test slip measurement, assuming simplified equivalent circuits generally admitted. Approximate values for rotor parameters may be reached from blocked rotor test measurements taking into account the approximate equivalent circuit of Fig.5.3

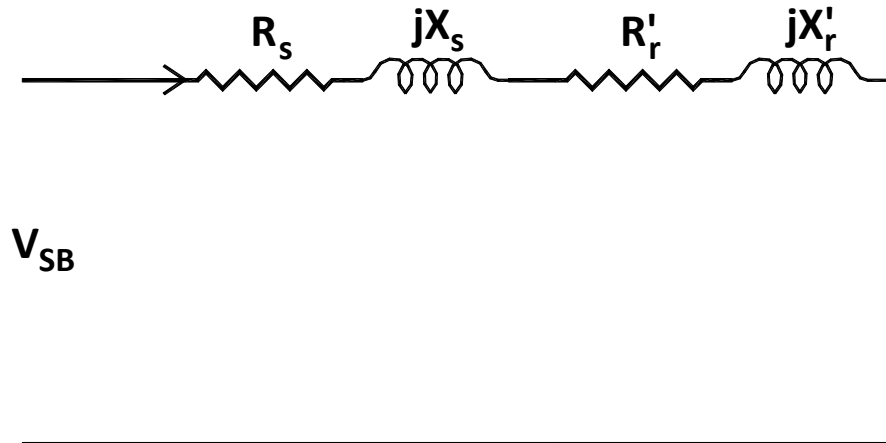


Fig. 5.3 Blocked rotor simplified equivalent circuit of an Induction Motor

The rotor parameter's approximate values will be found from

$$R_{01} = R_s + R_r = \frac{P_B}{I_{SB}^2}$$

$$R_r = \frac{P_B}{I_{SB}^2} - R_s \quad (5.39)$$

$$Z_T = \frac{V_{SB}}{I_{SB}} = \sqrt{(R_{01})^2 + (X_{01})^2}$$

$$X_r = \frac{f}{f_B} \frac{X_{01}}{(k_{12} + 1)} \quad (5.40)$$

Where f is rated frequency and f_B is frequency at which blocked rotor test is carried out.

A first guess for the magnetizing branch parameters may be reached from no-load test measurements and taking into account the approximate equivalent circuit of Fig. 5.4

The approximate Values for the magnetizing branch parameters (series equivalent) will be found from equations (5.41) and (5.42)

$$R_{FEs} = \frac{P_V}{I_{SV}^2} - R_s \quad (5.41)$$

$$X_{ms} = \frac{\sqrt{(V_{SV} * I_{SV})^2 - P_V^2}}{I_{SV}^2} - X_s \quad (5.42)$$

Where X_s is given by equation (5.29)

At last, we find a first guess for the magnetizing branch (parallel equivalent) parameters from following equations (5.43) and (5.44).

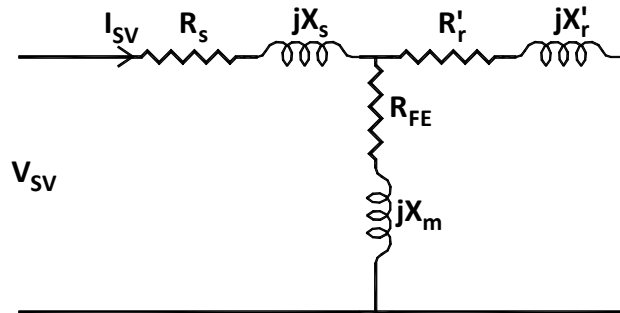


Fig. 5.4 No load simplified equivalent circuit of an Induction Motor

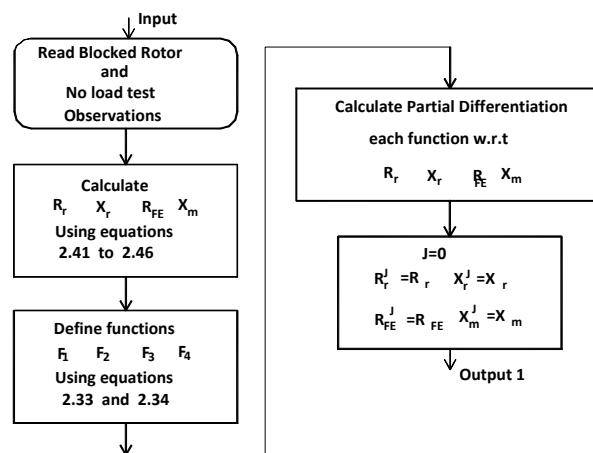
$$R_{FE} = \frac{R_{FEs}^2 + X_{ms}^2}{R_{FEs}} \quad (5.43)$$

$$X_m = \frac{R_{FEs}^2 + X_{ms}^2}{X_{ms}} \quad (5.44)$$

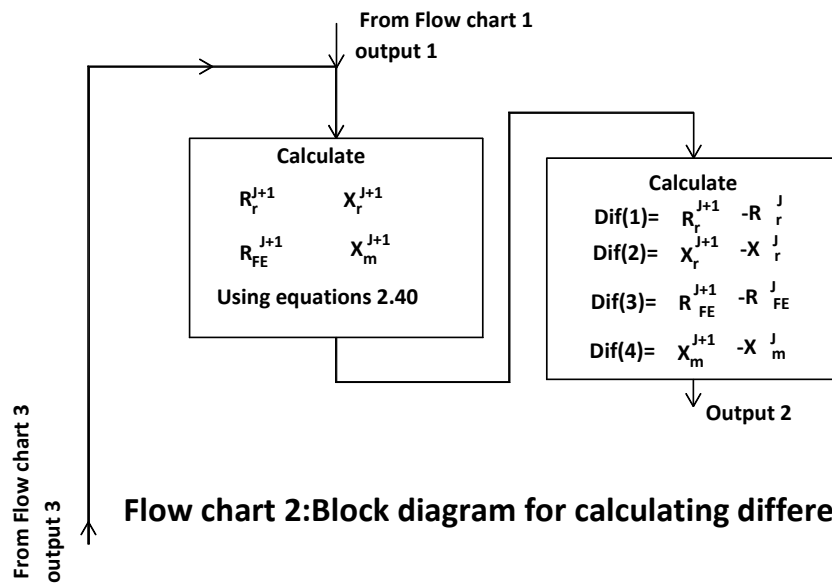
5.5.1.2 STOPPING CRITERIA

Due to the round character of an iterative process, it becomes still necessary to define a stopping criterion to impose when reached results are found to be adequate or when convergence is not achieved. Assuming that initial guesses for parameters are a good approximation to final values, the stopping criterion adopted was that all the absolute differences between the values of each parameter, in consecutive iterations, to be smaller than a fraction of the corresponding starting value. To prevent situations where convergence may not be achieved, the iterative process is also stopped after a given number of iterations, namely 10.

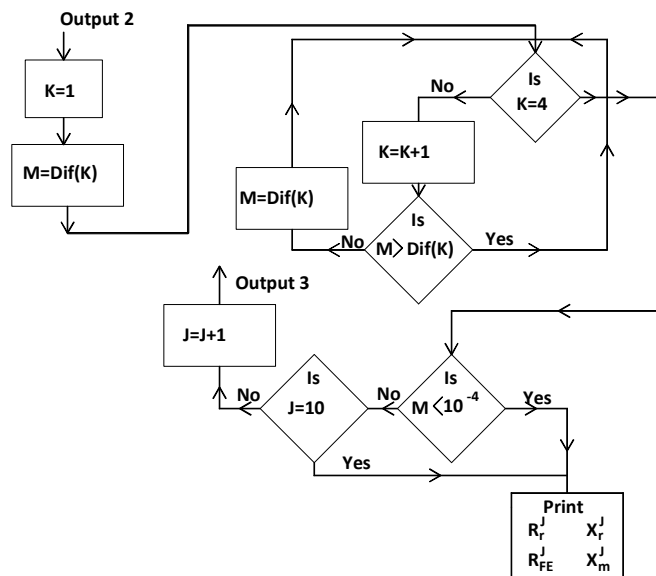
5.6 FLOW CHART FOR CALCULATION OF PARAMETERS.



Flow chart 1: Block diagram for calculating first iteration



Flow chart 2: Block diagram for calculating difference



Flow chart 3: Block diagram for printout of result

5.7 SENSITIVITY ANALYSIS

Taking into account the dependence on measurements whose accuracy, among others, is related with the quality of instrumentation, the developed algorithm was also applied to study the influence of measurement errors on the calculation of parameters.

To check the effectiveness of algorithm for variation in measurements on final value of parameters, the measurements with deviation are presented to algorithm.

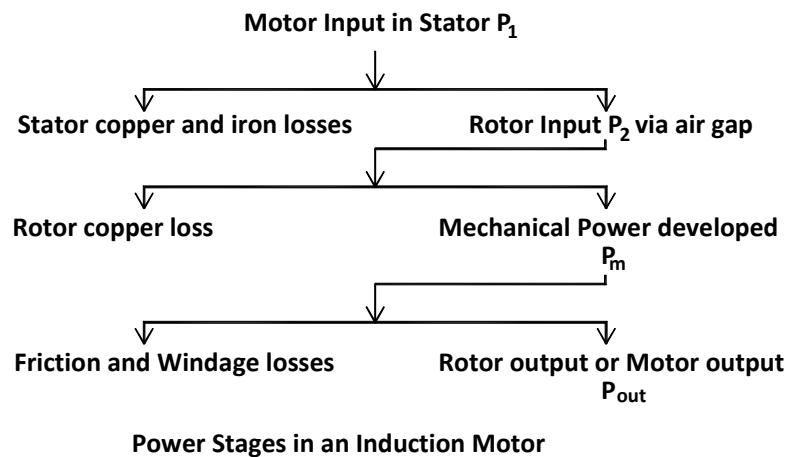
- Sensitivity analysis in terms are :

1. Sensitivity of Parameter to errors in current measurement in a Block-Rotor Test:
 - a) Magnetizing branch parameters; b) Rotor Parameters
2. Sensitivity of Parameter to errors in Voltage measurement in a No-Load Test:
 - a) Magnetizing branch parameters; b) Rotor Parameters

5.8 STEADY STATE PERFORMANCE OF INDUCTION MOTOR

Steady state performances of induction motor are found out algebraically as well as graphically.

Power stages in an induction motor are as below:



Performances are determined from following equations from equivalent circuit (Fig 2.1):

Stator input = Stator output + Stator losses

The stator output is transferred entirely inductively to the rotor circuit.

Obviously, Rotor input = Stator output

Rotor gross output = Rotor input – Rotor Cu losses

This Rotor output is converted into mechanical energy and gives rise to gross torque T_g .

Let N r.p.s. be the actual speed of the rotor and if T_g is an N-m, Then

$2\pi N * T_g =$ Rotor gross output in watts

$$R_L = R_r \left(\frac{1}{s} - 1 \right) \text{---(5.45)}$$

$$Z_r = \frac{R_r}{s} + jX_r \text{---(5.46)}$$

$$\frac{1}{Z_0} = \frac{1}{R_{FE}} + \frac{1}{jX_r} \text{---(5.47)}$$

$$\frac{1}{Z_{co}} = \frac{1}{Z_2} + \frac{1}{Z_0} \text{---(5.48)}$$

$$Z_{eq} = Z_{co} + Z_s \text{---(5.49)}$$

$$I_1 = V/Z_{eq} = I_0 + I_2 \text{---(5.50)}$$

$$I_2 = I_1 * \frac{Z_0}{Z_0 + Z_r} \text{---(5.51)}$$

$$P_{out} = 3I_2^2 R_L \text{---(5.52)}$$

$$T_g = P_{out}/\omega_m \text{---(5.53)}$$

$$\text{Rotor input} = T_g * 2\pi N_s \text{---(5.54)}$$

$$\text{Rotor cu loss} = T_g * 2\pi(N_s - N) \text{---(5.55)}$$

$$\phi = \left[\tan^{-1} \left\{ \frac{\text{Im}(Z_{eq})}{\text{Re}(Z_{eq})} \right\} \right] \text{---(5.56)}$$

$$\text{Power factor} = \cos \phi \text{---(5.57)}$$

$$\text{Power Input } P_{in} = 3VI_{eq} \cos \phi \text{---(5.58)}$$

$$\text{Efficiency} = \frac{P_{out}}{P_{in}} * 100 \text{---(5.59)}$$

5.9 MATLAB PROGRAMS FOR PREDICATING PERFORMANCE OF INDUCTION MOTOR AND TRANSIENT OVER VOLTAGE.

Matlab Programs for Predicating Performance of induction motor and Transient over Voltage are developed. The programs are as mentioned below in table 5.5,

Table 5.5 MATLAB Programs	
Program No.	Name of the Program
B1	This Program calculates Parameters of equivalent circuit of Induction motor.
B2	This Program calculates performance of Induction motor from equivalent circuit of the motor at any slip 's'.
B3	Program for Speed torque characteristic rated voltage and frequency.
B4	Program for Speed torque characteristic for variable voltage and rated frequency.
B5	Program for Speed torque characteristic for variable voltage and variable frequency i.e. constant V/f.
B6	Program for drawing Efficiency vs Output characteristic.
B7	Program is B6 but will draw Power factor vs Output and Stator current Vs Output. .
B8	Program is B6 but will draw Speed vs Output. For adjusting scale on Y-axis, dummy points C and D are inserted.
B9	Program is B6 but will draw Torque vs Output.
B10	Program for calculating voltage Transient.
A1	Simulation for No Load test and Load Test
A2	Simulation for Blocked rotor test
A3	Simulation for Voltage Transient

Chapter 6

Details of motors, Experimental setup and Voltage waveforms

6.1 INTRODUCTION

Five motors were tested. Out of these five four motors were design and manufactured under the supervision of the author whereas one motor was design and manufactured by other.

The four motors manufactured are having following details.

(1) First motor was design and manufactured for 415 V supply. The rating of this motor is as below: Frame 63, 3-phase, 415 V, 470 W, 1.3 A, 50 Hz, 2-Pole, Class F, Continuous duty Induction motor.

(2) Second motor was design and manufactured for 380 V supply. The rating of this motor is as below: Frame 63, 3-phase, 380 V, 470 W, 1.4 A, 50 Hz, 2-Pole, Class F, Continuous duty Induction motor.

Both above motors are now being used by ABB ltd. in their Isolator operating mechanism drive [72].

(3) Third motor was design and manufactured for 2- pole constructions. The rating of this motor is as below: Frame 71, 3-phase, 415 V, 300 W, 50 Hz, 2-Pole, Class F, Continuous duty Induction motor.

(4) Forth motor was design and manufactured for 4- pole constructions. The rating of this motor is as below: Frame 71, 3-phase, 415 V, 300 W, 50 Hz, 4-Pole, Class F, Continuous duty Induction motor.

Both above motors are now being used by Delmer Products ltd. in their magnetic polisher.

Fifth motor was having following rating: 3-phase, 380 V, 1250 W, 50 Hz, 4-Pole, Class F, Continuous duty Induction motor.

6.2 STAMPING

Motors were manufactured from CRNGO stamping of Grade 47A, having thickness 0.5 mm and maximum core loss of 6.98 W/Kg. at 1.5 tesla. The stampings were manufactured by Steel Authority of India Ltd., Rourkela Steel Plant, Rourkela- 769011 –Orissia.

[1],[2] The stamping size for first and second motor was as below:

Frame 63 (IS-1231)

Stator OD = 87 mm

Stator ID = 48 mm

Rotor OD = 47.5 mm

Rotor ID = 15 mm

Core Length = 70 mm

Stator slots/Rotor slots = 24/18

[3] The stamping size for third (two pole) motor was as below:

Frame 71 (IS-1231)

Stator OD = 105 mm

Stator ID = 58 mm

Rotor OD = 57.5 mm

Rotor ID = 20 mm

Core Length = 60 mm

Stator slots/Rotor slots = 24/18

[4] The stamping size for fourth (four pole) motor was as below:

Frame 71 (IS-1231)

Stator OD = 105 mm

Stator ID = 63 mm

Rotor OD = 62.5 mm

Rotor ID = 20 mm

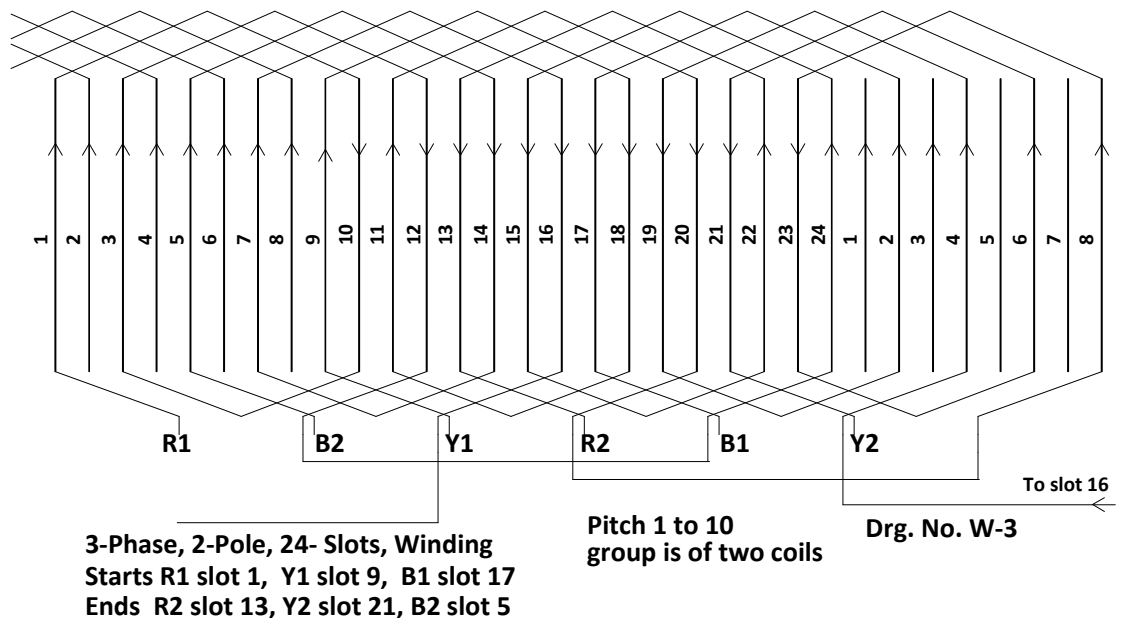
Core Length = 60 mm

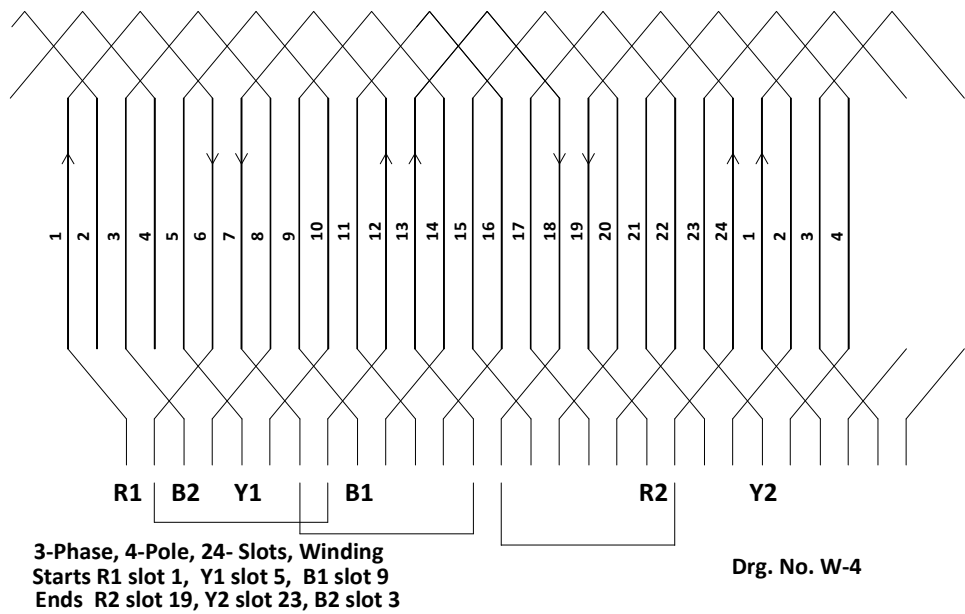
Stator slots/Rotor slots = 24/18

6.3 WINDING DETAIL

Stator of first and second motor was wound as per detail given in diagram W – 3. The number of turns per coil was 120 for motor number 3 and 110 for motor number 4. There were four coils in series per phase for all three phases. Two terminals per phase were taken out. The coils were made from dual coated hermetic grade super enameled copper wire of 27 swg. This wire is having fine covering of enamel. The diameter for 27 swg wire is 0.417 mm and with enamel covering diameter is 0.467 mm. The diameter for 28 swg wire is 0.376 mm and with enamel covering diameter is 0.425 mm.

Stator of third (2-pole) motor was wound as per detail given in diagram W – 3. The number of turns per coil was 130. There were four coils in series per phase for all three phases. The terminal at the end of each coil is taken out for the purpose of measuring voltage. Accordingly each phase winding is having five terminals as shown in figure 6.1. The coils were made from dual coated hermetic grade super enameled copper wire of 27 swg. This wire is having fine covering of enamel.





Stator of Fourth (4-pole) motor was wound as per detail given in diagram W – 4. The number of turns per coil was 130. There were four coils in series per phase for all three phases. The terminal at the end of each coil is taken out for the purpose of measuring voltage. Accordingly each phase winding is having five terminals as shown in figure 6.1. The coils were made from dual coated hermetic grade super enameled copper wire of 28 swg. This wire is having fine covering of enamel.

6.4 SLOT INSULATION

Polyester paper of 0.17 mm thickness was used as slot insulation and coil top insulation. There were only one coil side in slot hence coil side separating insulation was not required. Press phan paper of 0.13 mm thickness was used as phase separator on overhang of the coils.

6.5 TERMINAL INSULATION SLEEVE

To protect the winding from voltage surges and to enhance the insulation level near joints of enamel wire and terminal PVC wire, mica sleeve were used. Length of the sleeve was such that it can cover minimum three inch length of enamel wire and two inch length of PVC wire.

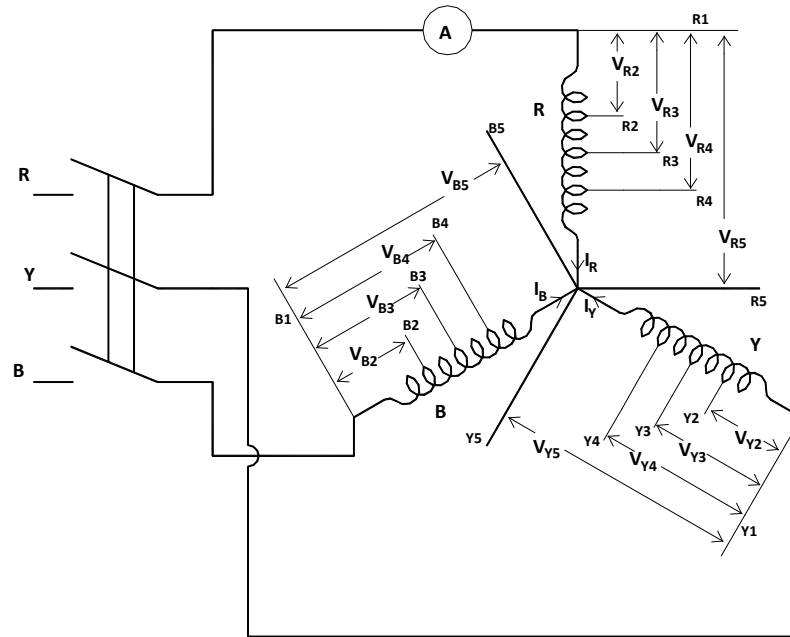


Fig. 6.1 Measurement of voltage waveform

6.6 VARNISHING

Varnish Elmo 65 E/R of Dr. back and co. was used. Elmo 65 E/R is an alkyd-phenolic resin based, baking impregnating varnish of temperature index 130 (Thermal Class B) The stator was pre heated in oven at 80⁰ C for 2 hours and then varnish was poured on the winding from one end. Pouring was stopped when varnish was reached to the second end. Now the winding was heated to 120⁰ C for four hrs. and then varnished was applied as per above procedure. Final curing was done at 120⁰ C for eight hrs.

6.7 TESTING OF MOTORS

6.7.1 MOTOR NO.1

Frame 63, 3-phase, 415 V, 470 W, 50 Hz, 2-Pole, Class F, Continuous duty Induction motor.

6.7.1.1 RESISTANCE MEASUREMENT:

Resistance of each phase was measured with Ohm meter of Agronic Electronics, Ghatkopar, Mumbai. Instrument Model No. is Agronic-65.

Table 6.1 Resistance of Frame 63, 3-phase, 415 V, 470 W, 1.3 A, 50 Hz, 2-Pole, I.M.				
Sr. No.	R-Phase	Y-Phase	B-Phase	Avg. DC

				Resistance
1	20.90 ohm	20.95 ohm	21.00 ohm	20.95 ohm

6.7.1.2 NO LOAD TEST:

Table 6.2 No Load test, Frame 63, 3-phase, 415 V, 470 W, 1.3 A, 50 Hz, 2-Pole, I.M.				
Sr. No.	Voltage(L-L) (V ₀) Volts	Line Current (I ₀) mA	Power(Total) (P ₀) Watts	Speed (N ₀) RPM
1	425	744.00	58.2	2980
2	415	640.00	50.0	2980
3	400	552.00	45.4	2980
4	380	488.00	38.2	2980
5	350	382.00	34.1	2970
6	320	328.00	30.9	2970
7	280	308.00	24.8	2966
8	200	252.00	21.8	2966
9	150	240.00	19.0	2966
10	100	200.00	17.0	2966

From curve between no load power and voltage it was estimated that friction and windage loss is 15 W.

6.7.1.3 BLOCKED ROTOR TEST

Table 6.3 Blocked Rotor test, Frame 63, 3-phase, 415 V, 470 W, 1.3 A 50 Hz, 2-Pole, I.M.			
Sr. No.	Voltage(L-L) (V _b) Volt	Line Current (I _b) Amp.	Power(Total) (P _b) Watts
1	200.0	1.30	165.0

6.7.1.4 EQUIVALENT CIRCUIT PARAMETERS

The equivalent circuit parameters calculated by Program B1 using results of above three test and resistance value corrected to 95⁰ C as mentioned in IEEE-112 for class B insulation are as below

Table 6.4 Equivalent Circuit Parameters Frame 63, 3-phase, 415 V, 470 W, 1.3 A 50 Hz, 2-Pole, I.M.					
R _s	X _s	R _{fe}	X _m	R _r	X _r
Ohm	Ohm	Ohm	Ohm	Ohm	Ohm
25.9025	41.3231	4258.64	376.6067	14.3353	41.3231

6.7.1.5 PERFORMANCE OF THE MOTOR FROM EQUIVALENT CIRCUIT

The performances of the motor using above parameters in MATLAB program B9 are as below.

Table 6.5 Performance of Frame 63, 3-phase, 415 V, 470 W, 1.3 A, 50 Hz, 2-Pole, I.M. obtained using MATLAB program B9							
Sr. No.	Output Power	Input Power	Input Current	PF	Speed	Torque	Efficiency
	(W)	(W)	(A)		(RPM)	(Nm)	(%)
1	197.82	265.20	0.7951	0.4821	2941	0.6422	74.59
2	290.94	372.90	0.8809	0.5888	2910	0.9546	78.02
3	371.36	472.47	1.0099	0.6508	2879	1.2319	78.60
4	390.66	497.51	1.0451	0.6622	2870	1.2967	78.52
5	448.75	576.47	1.1633	0.6893	2842	1.5077	77.84
6	469.99	606.92	1.2117	0.6968	2830	1.5857	77.43
7	531.47	702.46	1.3744	0.7110	2790	1.8192	75.65
8	580.38	791.47	1.5430	0.7135	2744	2.019	73.32

6.7.1. PERFORMANCE OF THE MOTOR FROM ACTUAL LOAD TEST

The motor was tested for different load. The loading set up is shown in Fig. 6.2 and 6.3 6.4. The reduction gear ratio was 30. The weight requires to be coupled with gear box shaft of ratio 30 for producing necessary torque at motor shaft is as below:

For ex T Nm at motor shaft corresponds to $T*30$ Nm at gear shaft $\equiv (T*30*1000)/9.81$ Kgmm or is equal to $(0.6*30*1000)/(9.81*52)$ Kg. wt at 104 mm pulley.

Table 6.6 The weight requires to be coupled with gear box shaft of ratio 30 for producing necessary torque at motor shaft.							
Torque at motor Shaft Nm	0.60	0.90	1.00	1.25	1.50	1.75	2.00
Approx. Weight required at GB shaft (Kg.) pulley dia. 104 mm	35.0	52.92	58.8	73.51	88.21	102.91	117.6



Fig. 6.2

Figure 6.2 Experimental setup for loading the motor.



Figure 6.3 Experimental setup for loading the motor.



Figure 6.4 Measuring instruments



Fig. 6.5

Figure 6.5 Dynamometer for loading the motor.



Fig.6.6

Figure 6.6 Dynamometer for loading the motor.

The motor was operated with above weight successfully. The distance to be travelled by loading trolley was 12 ft. With pulley diameter of 104 mm observations were to be noted in around 6.722 seconds. (i.e. Peripheral speed = $\pi * D * (N/60) = 3.14 * 104 * 3000/60 = 544.2$ mm/sec. and distance to be travelled $12 * 12 * 25.4 = 3657.6$ mm). As this time was very small, the observations are taken with dynamometer directly coupled with motor shaft.

Sr. No.	Voltage (Volts)	Current (A)	Input Power (Watts)	Motor Speed (RPM)	Weight At 150 mm (Kg)
1	415	0.95	322.20	2898	0.443
2	415	1.05	424.40	2884	0.655
3	415	1.15	520.60	2870	0.841
4	415	1.20	545.20	2868	0.884
5	415	1.30	626.00	2860	1.019
6	415	1.35	653.40	2856	1.068
7	415	1.50	745.20	2841	1.214
8	415	1.60	813.40	2830	1.330

Performances calculated from above observations are as below.

Sr. No.	Output Power (W)	Efficiency 1	Power Factor	Torque (Nm)
1	197.83	61.40	0.4718	0.6518
2	291.00	68.59	0.5623	0.9938
3	371.93	71.44	0.6297	1.2375
4	391.12	71.74	0.6320	1.3023
5	449.00	71.74	0.6699	1.4995
6	470.00	71.93	0.6733	1.5716
7	531.47	71.32	0.6911	1.7864
8	580.00	71.31	0.7072	1.9571

When the equivalent circuit parameters are presented to NR method algorithm discuss in chapter 5, following parameters are obtained.

Table 6.9 Equivalent Circuit Modified Parameters Frame 63, 3-phase, 415 V, 470 W, 1.3 A 50 Hz, 2-Pole, I.M.					
R_s	X_s	R_{fe}	X_m	R_r	X_r
Ohm	Ohm	Ohm	Ohm	Ohm	Ohm
25.90	41.695	4458.63	376.60	15.96	41.695

The performance of motor with modified parameters and taking in to account stray load loss as 1.85% as per IEEE 112 is being shown in table 6.10

Table 6.10 Performance of Frame 63, 3-phase, 415 V, 470 W, 1.3 A 50 Hz, 2-Pole, I.M. based on modified Parameters				
Sr. No.	Output Power	Efficiency	Power Factor	Torque
	(W)			(Nm)
1	197.95	78.72	0.4644	0.6437
2	291.00	80.86	0.5786	0.9573
3	371.37	80.25	0.6448	1.2366
4	390.79	79.98	0.6570	1.3056
5	448.74	78.78	0.6859	1.5163
6	470.03	78.18	0.6938	1.5958
7	531.39	75.86	0.7087	1.8350
8	580.00	72.95	0.7107	2.0433

6.7.2 MOTOR NO.2

Frame 63, 3-phase, 380 V, 470 W, 1.4 A, 50 Hz, 2-Pole, Class F, Continuous duty Induction motor.

6.7.2.1 RESISTANCE MEASUREMENT:

Table 6.11 Resistance of Frame 63, 3-phase, 380 V, 470 W, 1.4 A, 50 Hz, 2-Pole, I.M.				
Sr. No.	R-Phase	Y-Phase	B-Phase	Avg. DC Resistance
1	19.00 ohm	19.10 ohm	18.90 ohm	19.00 ohm

6.7.2.2 NO LOAD TEST:

Table 6.12 No Load test, Frame 63, 3-phase, 380 V, 470 W, 1.4 A, 50 Hz, 2-Pole, I.M.				
Sr. No.	Voltage(L-L) (V ₀) Volts	Line Current (I ₀) mA.	Power(Total) (P ₀) Watts	Speed (N ₀) RPM
1	415	692.00	62.2	2980
2	400	604.00	57.8	2980
3	380	625.00	52.2	2980
4	350	312.00	44.2	2980

From curve between no load power and voltage it was estimated that friction and windage loss is 15 W.

6.7.2.3 BLOCKED ROTOR TEST

Table 6.13 Blocked Rotor test, Frame 63, 3-phase, 380 V, 470 W, 1.4 A 50 Hz, 2-Pole, I.M.			
Sr. No.	Voltage(L-L) (V _b) Volt	Line Current (I _b) Amp.	Power(Total) (P _b) Watts
1	207.80	1.40	180.0

6.7.2.4 LOAD TEST

Table 6.14 Observations Table of Load Test of Frame 63, 3-phase, 380 V, 470 W, 1.4 A 50 Hz, 2-Pole, I.M.					
Sr. No.	Voltage (Volts)	Current (A)	Input Power (Watts)	Motor Speed (RPM)	Weight At 150 mm (Kg)
1	380	1.3	607.8	2816	0.993
2	380	1.35	662.2	2810	1.086
3	380	1.4	693.6	2800	1.134

Performance based on above test is as below.

Table 6.15 Performance of Frame 63, 3-phase, 380 V, 470 W, 1.4 A 50 Hz, 2-Pole, I.M. from Load test				
Sr. No.	Output Power	Efficiency	Power Factor	Torque
	(W)			(Nm)
1	430.89	70.89	0.7103	1.4612
2	470.24	71.01	0.7452	1.5980
3	489.28	70.54	0.7527	1.6687

6.7.2.5 EQUIVALENT CIRCUIT PARAMETERS

The equivalent circuit parameters calculated by Program B1 using results of above three test are as below

Table 6.16 Equivalent Circuit Parameters Frame 63, 3-phase, 380 V, 470 W, 1.4 A 50 Hz, 2-Pole, I.M.					
R_s	X_s	R_{fe}	X_m	R_r	X_r
Ohm	Ohm	Ohm	Ohm	Ohm	Ohm
23.4916	40.0205	3420.1264	353.8899	14.3574	40.0205

Motor performance from equivalent circuit is as below

Table 6.17 Performance of Frame 63, 3-phase, 380 V, 470 W, 1.4 A, 50 Hz, 2-Pole, I.M. obtained using MATLAB program B9							
Sr. No.	Output Power	Input Power	Input Current	PF	Speed	Torque	Efficiency
	(W)	(W)	(A)		(RPM)	(Nm)	(%)
1	430.82	568.00	1.2303	0.7014	2809	1.4647	75.84
2	470.15	630.62	1.3505	0.7095	2775	1.6174	74.55
3	489.15	663.82	1.4184	0.7110	2756	1.6946	73.68

When the equivalent circuit parameters are presented to NR method algorithm discuss in chapter 5, following parameters are obtained.

Table 6.18 Equivalent Circuit Modified Parameters Frame 63, 3-phase, 380 V, 470 W, 1.4 A 50 Hz, 2-Pole, I.M.					
R_s	X_s	R_{fe}	X_m	R_r	X_r

Ohm	Ohm	Ohm	Ohm	Ohm	Ohm
23.4916	43.1718	3580.74	442.01	15.9367	43.1718

The performance of motor with modified parameters and taking in to account stray load loss as 1.85% as per IEEE 112 is being shown in table

Table 6.19 Performance of Frame 63, 3-phase, 380 V, 470 W, 1.4 A 50 Hz, 2-Pole, I.M. based on modified Parameters				
Sr. No.	Output Power	Efficiency	Power Factor	Torque
	(W)			(Nm)
1	430.64	76.51	0.7410	1.4765
2	469.95	74.54	0.7415	1.6365
3	489.21	73.16	0.7381	1.7212

6.7.3 MOTOR NO.3

Frame 71, 3-phase, 415 V, 300 W, 50 Hz, 2-Pole, Class F, Continuous duty Induction motor.

6.7.3.1 RESISTANCE MEASUREMENT:

Table 6.20A				
Sr. No.	R-Phase ohm			
	R ₁ - R ₂	R ₁ - R ₃	R ₁ - R ₄	R ₁ -R ₅
1	6.161	12.322	18.502	24.642

Table 6.20B				
Sr. No.	Y-Phase Ohm			
	Y ₁ - Y ₂	Y ₁ - Y ₃	Y ₁ - Y ₄	Y ₁ -Y ₅
1	6.160	12.321	18.500	24.640

Table 6.20C				
Sr. No.	B-Phase ohm			
	B ₁ -B ₂	B ₁ - B ₃	B ₁ - B ₄	B ₁ -B ₅
1	6.162	12.323	18.503	24.644

6.7.4 MOTOR NO.4

Frame 71, 3-phase, 415 V, 300 W, 50 Hz, 4-Pole, Class F, Continuous duty Induction motor.

6.7.4.1 RESISTANCE MEASUREMENT:

Table 6.21A				
Sr. No.	R-Phase ohm			
	R ₁ - R ₂	R ₁ - R ₃	R ₁ - R ₄	R ₁ -R ₅
1	7.701	15.403	23.104	30.804

Table 6.21B				
Sr. No.	Y-Phase Ohm			
	Y ₁ - Y ₂	Y ₁ - Y ₃	Y ₁ - Y ₄	Y ₁ -Y ₅
1	7.702	15.404	23.106	30.806

Table 6.21C				
Sr. No.	B-Phase ohm			
	B ₁ -B ₂	B ₁ - B ₃	B ₁ - B ₄	B ₁ -B ₅
1	7.700	15.402	23.102	30.802

6.7.5 MOTOR NO.5

6.7.5.1 RESISTANCE MEASUREMENT:

Fifth motor (380V, 50 Hz, 1.2 KW, 4-Pole) was tested at ERDA

Stator resistance is obtained by DC test method. The value of resistance obtained is 5.568 Ω

6.7.5.2 NO LOAD TEST

Table No. 6.22	380 V, 50 Hz, 1.2 KW, 4-Pole IM
----------------	---------------------------------

	Voltage	Current	Power	PF	Speed
Practical	380	1.15	100	0.1321	1499
Simulation					
50 Hz	377.9	1.071	102.3	0.1459	1497.33
60 Hz	377.4	0.9061	101.7	0.1717	1799.2

6.7.5.3 BLOCKED ROTOR TEST

Table No. 6.23 380 V, 50 Hz, 1.2 KW, 4-Pole IM					
	Voltage	Current	Power	PF	Speed
Practical	99	2.8	230	0.479	0
Simulation					
50 Hz	98.57	2.847	240.7	0.4972	0
60 Hz	98.35	2.46	195.8	0.4672	0

Life of the motor means the period of time for which motor is available for doing specified work or is able to deliver the rated power starting from the time from where motor is put in to the service. Normally the life of the motor is decided by the healthiness of insulation system and bearing. This point is being discussed in chapter 2.

In this work stresses developed on winding insulation by the converter switching are investigated. For this purpose voltage wave forms at motor terminals and inside the winding are recorded. Experiments are being done on two pole and four pole winding as per details mentioned above are prepared. The photo graph of testing setup is shown in fig. 6.7 and 6.8

CRO of Yokogawa, Japan, Model No. DL 750 was used for the measurement purpose. Investigation was made for three different source of voltages (1) Sinusoidal utility 50 Hz supply (2) Filtered inverter supply taken from drive No. VDF007B43A of Delta (3). Unfiltered inverter supply taken from drive no. VFD004S43A of Delta. Experiments of wave forms measurement are being done on Motor No. 3 and 4. Around 600 waveforms are being recorded and investigated. The waveforms recorded are mentioned in table 6.24 and 6.25.

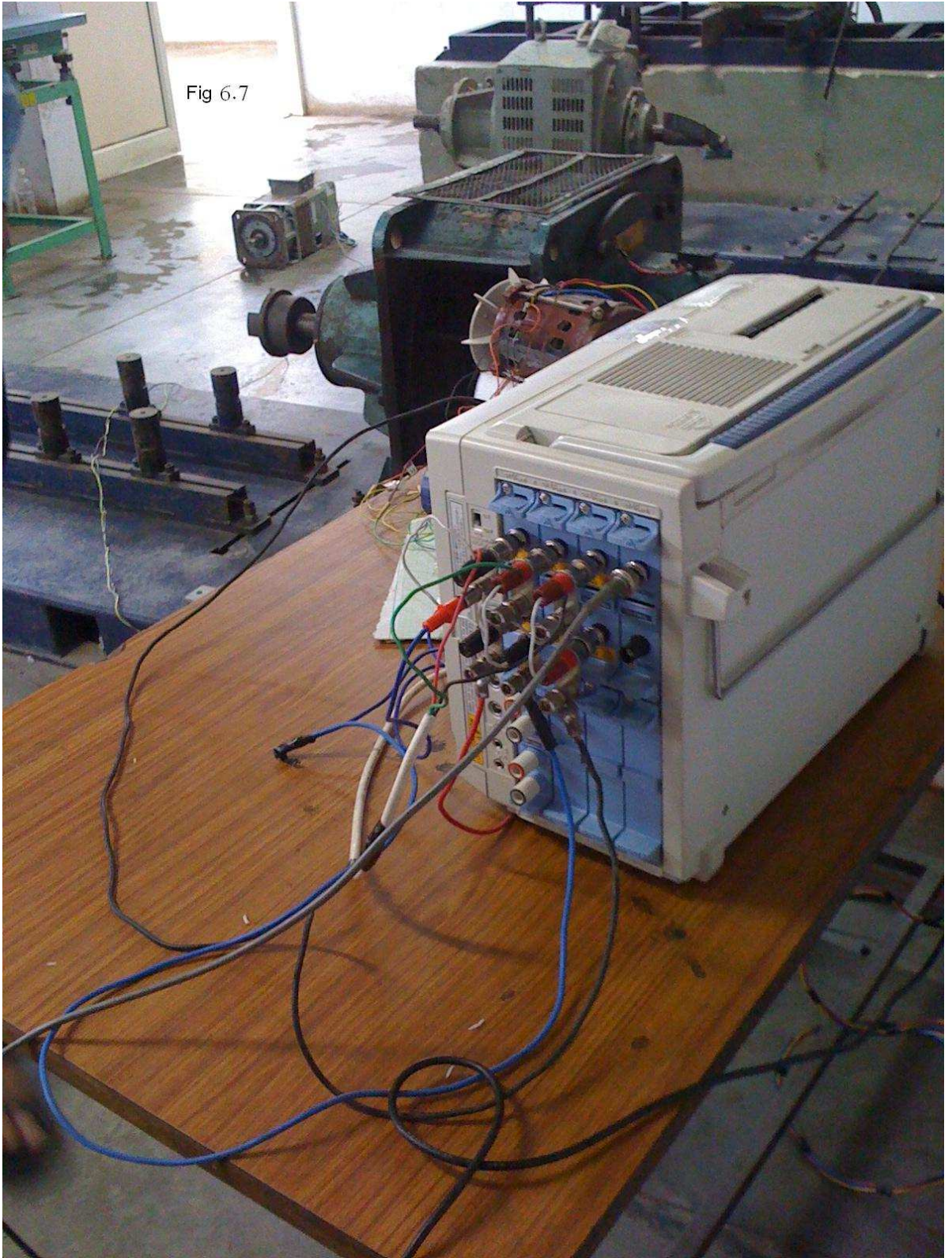


Figure 6.7 Waveform recording setup, ERDA

Fig. 6.8



Figure 6.8 Waveform recording setup, ERDA

Table 6.24 List of waveforms for 2 P windings		
Sr.No.	Waveform No	Waveform Description
1	KRK0040	Phase voltage and Voltage across first coil, and line current of 3-phase, 415 V, 250 W, 2-Pole Jewellery Polisher Motor on NO LOAD when supplied with sinusoidal supply-50 Hz.
2	KRK0041	Phase voltage and Voltage across second coil and line current of 3-phase, 415 V, 250 W, 2-Pole Jewellery Polisher Motor on NO LOAD when supplied with sinusoidal supply-50 Hz.
3	KRK0042	Phase voltage and Voltage across third coil of 3-phase, 415 V, 250 W, 2-Pole Jewellery Polisher Motor on NO LOAD when supplied with sinusoidal supply-50 Hz.
4	KRK0043	Phase voltage and Voltage across fourth coil of 3-phase, 415 V, 250 W, 2-Pole Jewellery Polisher Motor on NO LOAD when supplied with sinusoidal supply-50 Hz.
5	KRK0022	Phase voltage and Voltage across first coil of 3-phase, 415 V, 250 W, 2-Pole Jewellery Polisher Motor on NO LOAD when supplied with PWM inverter with frequency 25 Hz.
6	KRK0023	Phase voltage and Voltage across second coil of 3-phase, 415 V, 250 W, 2-Pole Jewellery Polisher Motor on NO LOAD when supplied with PWM inverter with frequency 25 Hz.
7	KRK0028	Phase voltage and Voltage across third coil of 3-phase, 415 V, 250 W, 2-Pole Jewellery Polisher Motor on NO LOAD when supplied with PWM inverter with frequency 25 Hz.
8	KRK0029	Phase voltage and Voltage across fourth coil of 3-phase, 415 V, 250 W, 2-Pole Jewellery Polisher Motor on NO LOAD when supplied with PWM inverter with frequency 25 Hz.
9	KRK0021	Phase voltage and Voltage across first coil of 3-phase, 415 V, 250 W, 2-Pole Jewellery Polisher Motor on NO LOAD when supplied with PWM inverter with frequency 40 Hz.
10	KRK0024	Phase voltage and Voltage across second coil of 3-phase, 415 V, 250 W, 2-Pole Jewellery Polisher Motor on NO LOAD when supplied with PWM inverter with frequency 40 Hz.
11	KRK0027	Phase voltage and Voltage across third coil of 3-phase, 415 V, 250 W, 2-Pole Jewellery Polisher Motor on NO LOAD when supplied with PWM inverter with frequency 40 Hz.
12	KRK0030	Phase voltage and Voltage across fourth coil of 3-phase, 415 V, 250 W, 2-Pole Jewellery Polisher Motor on NO

		LOAD when supplied with PWM inverter with frequency 40 Hz.
13	KRK0020	Phase voltage and Voltage across first coil of 3-phase, 415 V, 250 W, 2-Pole Jewellery Polisher Motor on NO LOAD when supplied with PWM inverter with frequency 50 Hz.
14	KRK0025	Phase voltage and Voltage across second coil of 3-phase, 415 V, 250 W, 2-Pole Jewellery Polisher Motor on NO LOAD when supplied with PWM inverter with frequency 50 Hz.
15	KRK0026	Phase voltage and Voltage across third coil of 3-phase, 415 V, 250 W, 2-Pole Jewellery Polisher Motor on NO LOAD when supplied with PWM inverter with frequency 50 Hz.
16	KRK0031	Phase voltage and Voltage across fourth coil of 3-phase, 415 V, 250 W, 2-Pole Jewellery Polisher Motor on NO LOAD when supplied with PWM inverter with frequency 50 Hz.
17	KRK0032	Phase voltage and Voltage across first coil of 3-phase, 415 V, 250 W, 2-Pole Jewellery Polisher Motor on NO LOAD when supplied with PWM inverter with frequency 60 Hz.
18	KRK0035	Phase voltage and Voltage across second coil of 3-phase, 415 V, 250 W, 2-Pole Jewellery Polisher Motor on NO LOAD when supplied with PWM inverter with frequency 60 Hz.
19	KRK0036	Phase voltage and Voltage across third coil of 3-phase, 415 V, 250 W, 2-Pole Jewellery Polisher Motor on NO LOAD when supplied with PWM inverter with frequency 60 Hz.
20	KRK0039	Phase voltage and Voltage across fourth coil of 3-phase, 415 V, 250 W, 2-Pole Jewellery Polisher Motor on NO LOAD when supplied with PWM inverter with frequency 60 Hz.
21	KRK0033	Phase voltage and Voltage across first coil of 3-phase, 415 V, 250 W, 2-Pole Jewellery Polisher Motor on NO LOAD when supplied with PWM inverter with frequency 70 Hz.
22	KRK0034	Phase voltage and Voltage across second coil of 3-phase, 415 V, 250 W, 2-Pole Jewellery Polisher Motor on NO LOAD when supplied with PWM inverter with frequency 70 Hz.
23	KRK0037	Phase voltage and Voltage across third coil of 3-phase, 415 V, 250 W, 2-Pole Jewellery Polisher Motor on NO LOAD when supplied with PWM inverter with frequency 70 Hz.
24	KRK0038	Phase voltage and Voltage across fourth coil of 3-phase,

		415 V, 250 W, 2-Pole Jewellery Polisher Motor on NO LOAD when supplied with PWM inverter with frequency 70 Hz.
25	KRK0106	R-Phase voltage and Voltage across all coils of 3-phase, 415 V, 250 W, 2-Pole Jewellery Polisher Motor when supplied with PWM inverter with frequency 20 Hz.
26	KRK0121	Y-Phase voltage and Voltage across all coils of 3-phase, 415 V, 250 W, 2-Pole Jewellery Polisher Motor when supplied with PWM inverter with frequency 20 Hz.
27	KRK0126	B-Phase voltage and Voltage across all coils of 3-phase, 415 V, 250 W, 2-Pole Jewellery Polisher Motor when supplied with PWM inverter with frequency 20 Hz.
28	KRK0107	R-Phase voltage and Voltage across all coils of 3-phase, 415 V, 250 W, 2-Pole Jewellery Polisher Motor when supplied with PWM inverter with frequency 30 Hz.
29	KRK0122	Y-Phase voltage and Voltage across all coils of 3-phase, 415 V, 250 W, 2-Pole Jewellery Polisher Motor when supplied with PWM inverter with frequency 30 Hz.
30	KRK0127	B-Phase voltage and Voltage across all coils of 3-phase, 415 V, 250 W, 2-Pole Jewellery Polisher Motor when supplied with PWM inverter with frequency 30 Hz.
31	KRK0108	R-Phase voltage and Voltage across first coil of 3-phase, 415 V, 250 W, 2-Pole Jewellery Polisher Motor when supplied with PWM inverter with frequency 40 Hz.
32	KRK0123	Y-Phase voltage and Voltage across all coils of 3-phase, 415 V, 250 W, 2-Pole Jewellery Polisher Motor when supplied with PWM inverter with frequency 40 Hz.
33	KRK0128	B-Phase voltage and Voltage across all coils of 3-phase, 415 V, 250 W, 2-Pole Jewellery Polisher Motor when supplied with PWM inverter with frequency 40 Hz.
34	KRK0109	R-Phase voltage and Voltage across first coil of 3-phase, 415 V, 250 W, 2-Pole Jewellery Polisher Motor when supplied with PWM inverter with frequency 50 Hz.
35	KRK0124	Y-Phase voltage and Voltage across all coils of 3-phase, 415 V, 250 W, 2-Pole Jewellery Polisher Motor when supplied with PWM inverter with frequency 50 Hz.
36	KRK0129	B-Phase voltage and Voltage across all coils of 3-phase, 415 V, 250 W, 2-Pole Jewellery Polisher Motor when supplied with PWM inverter with frequency 50 Hz.
37	KRK0110	R-Phase voltage and Voltage across first coil of 3-phase, 415 V, 250 W, 2-Pole Jewellery Polisher Motor when supplied with PWM inverter with frequency 60 Hz.
38	KRK0125	Y-Phase voltage and Voltage across all coils of 3-phase, 415 V, 250 W, 2-Pole Jewellery Polisher Motor when supplied with PWM inverter with frequency 60 Hz.
39	KRK0130	B-Phase voltage and Voltage across all coils of 3-phase, 415 V, 250 W, 2-Pole Jewellery Polisher Motor when

		supplied with PWM inverter with frequency 60 Hz.
--	--	--

Table 6.25 List of waveforms for 4 P windings		
Sr.No.	Waveform No	Waveform Description
1	KRK0004	Phase voltage and Voltage across first coil of 3-phase, 415 V, 250 W, 50 Hz, 4-Pole Jewellery Polisher Motor on NO LOAD when supplied with sinusoidal supply
2	KRK0005	Phase voltage and Voltage across second coil of 3-phase, 415 V, 250 W, 4-Pole Jewellery Polisher Motor on NO LOAD when supplied with sinusoidal supply-50 Hz.
3	KRK0006	Phase voltage and Voltage across third coil of 3-phase, 415 V, 250 W, 4-Pole Jewellery Polisher Motor on NO LOAD when supplied with sinusoidal supply-50 Hz.
4	KRK0007	Phase voltage and Voltage across fourth coil of 3-phase, 415 V, 250 W, 4-Pole Jewellery Polisher Motor on NO LOAD when supplied with sinusoidal supply-50 Hz.
5	KRK0017	Phase voltage and Voltage across first coil of 3-phase, 415 V, 250 W, 4-Pole Jewellery Polisher Motor on NO LOAD when supplied with PWM inverter with frequency 25 Hz.
6	KRK0016	Phase voltage and Voltage across second coil of 3-phase, 415 V, 250 W, 4-Pole Jewellery Polisher Motor on NO LOAD when supplied with PWM inverter with frequency 25 Hz.
7	KRK0011	Phase voltage and Voltage across third coil of 3-phase, 415 V, 250 W, 4-Pole Jewellery Polisher Motor on NO LOAD when supplied with PWM inverter with frequency 25 Hz.
8	KRK0010	Phase voltage and Voltage across fourth coil of 3-phase, 415 V, 250 W, 4-Pole Jewellery Polisher Motor on NO LOAD when supplied with PWM inverter with frequency 25 Hz.
9	KRK0018	Phase voltage and Voltage across first coil of 3-phase, 415 V, 250 W, 4-Pole Jewellery Polisher Motor on NO LOAD when supplied with PWM inverter with frequency 40 Hz.
10	KRK0015	Phase voltage and Voltage across second coil of 3-phase, 415 V, 250 W, 4-Pole Jewellery Polisher Motor on NO LOAD when supplied with PWM inverter with frequency 40 Hz.
11	KRK0012	Phase voltage and Voltage across third coil of 3-phase, 415 V, 250 W, 4-Pole Jewellery Polisher Motor on NO LOAD when supplied with PWM inverter with frequency 40 Hz.

12	KRK0009	Phase voltage and Voltage across fourth coil of 3-phase, 415 V, 250 W, 4-Pole Jewellery Polisher Motor on NO LOAD when supplied with PWM inverter with frequency 40 Hz.
13	KRK0019	Phase voltage and Voltage across first coil of 3-phase, 415 V, 250 W, 4-Pole Jewellery Polisher Motor on NO LOAD when supplied with PWM inverter with frequency 50 Hz.
14	KRK0014	Phase voltage and Voltage across second coil of 3-phase, 415 V, 250 W, 4-Pole Jewellery Polisher Motor on NO LOAD when supplied with PWM inverter with frequency 50 Hz.
15	KRK0013	Phase voltage and Voltage across third coil of 3-phase, 415 V, 250 W, 4-Pole Jewellery Polisher Motor on NO LOAD when supplied with PWM inverter with frequency 50 Hz.
16	KRK0008	Phase voltage and Voltage across fourth coil of 3-phase, 415 V, 250 W, 4-Pole Jewellery Polisher Motor on NO LOAD when supplied with PWM inverter with frequency 50 Hz.
17	KRK0136	R-Phase voltage and Voltage across all coils of 3-phase, 415 V, 250 W, 4-Pole Jewellery Polisher Motor when supplied with PWM inverter with frequency 20 Hz.
18	KRK0146	Y-Phase voltage and Voltage across all coils of 3-phase, 415 V, 250 W, 4-Pole Jewellery Polisher Motor when supplied with PWM inverter with frequency 20 Hz.
19	KRK0156	B-Phase voltage and Voltage across all coils of 3-phase, 415 V, 250 W, 4-Pole Jewellery Polisher Motor when supplied with PWM inverter with frequency 20 Hz.
20	KRK0137	R-Phase voltage and Voltage across all coils of 3-phase, 415 V, 250 W, 4-Pole Jewellery Polisher Motor when supplied with PWM inverter with frequency 30 Hz.
21	KRK0147	Y-Phase voltage and Voltage across all coils of 3-phase, 415 V, 250 W, 4-Pole Jewellery Polisher Motor when supplied with PWM inverter with frequency 30 Hz.
22	KRK0157	B-Phase voltage and Voltage across all coils of 3-phase, 415 V, 250 W, 4-Pole Jewellery Polisher Motor when supplied with PWM inverter with frequency 30 Hz.
23	KRK0138	R-Phase voltage and Voltage across first coil of 3-phase, 415 V, 250 W, 4-Pole Jewellery Polisher Motor when supplied with PWM inverter with frequency 40 Hz.
24	KRK0148	Y-Phase voltage and Voltage across all coils of 3-phase, 415 V, 250 W, 4-Pole Jewellery Polisher Motor when supplied with PWM inverter with frequency 40 Hz.
25	KRK0158	B-Phase voltage and Voltage across all coils of 3-phase, 415 V, 250 W, 4-Pole Jewellery Polisher Motor when supplied with PWM inverter with frequency 40 Hz.

26	KRK0139	R-Phase voltage and Voltage across first coil of 3-phase, 415 V, 250 W, 4-Pole Jewellery Polisher Motor when supplied with PWM inverter with frequency 50 Hz.
27	KRK0149	Y-Phase voltage and Voltage across all coils of 3-phase, 415 V, 250 W, 4-Pole Jewellery Polisher Motor when supplied with PWM inverter with frequency 50 Hz.
28	KRK0159	B-Phase voltage and Voltage across all coils of 3-phase, 415 V, 250 W, 4-Pole Jewellery Polisher Motor when supplied with PWM inverter with frequency 50 Hz.
29	KRK0160	R-Phase voltage and Voltage across first coil of 3-phase, 415 V, 250 W, 4-Pole Jewellery Polisher Motor when supplied with PWM inverter with frequency 60 Hz.
30	KRK0150	Y-Phase voltage and Voltage across all coils of 3-phase, 415 V, 250 W, 4-Pole Jewellery Polisher Motor when supplied with PWM inverter with frequency 60 Hz.
31	KRK0140	B-Phase voltage and Voltage across all coils of 3-phase, 415 V, 250 W, 4-Pole Jewellery Polisher Motor when supplied with PWM inverter with frequency 60 Hz.

Waveforms for 2-Pole winding No. KRK0040, No. KRK0106, No. KRK0107, No. KRK0108, No. KRK0109, No. KRK0110 and for 4-Pole winding No. KRK0004, No. KRK0138, No. KRK0139 are shown here below.

Wave form No. KRK0040

Phase voltage and Voltage across first coil, and line current of 3-phase, 415 V, 250 W, 2-Pole Jewellery Polisher Motor on NO LOAD when supplied with sinusoidal supply-50 Hz.

Fig. 0040A Normal View of wave forms

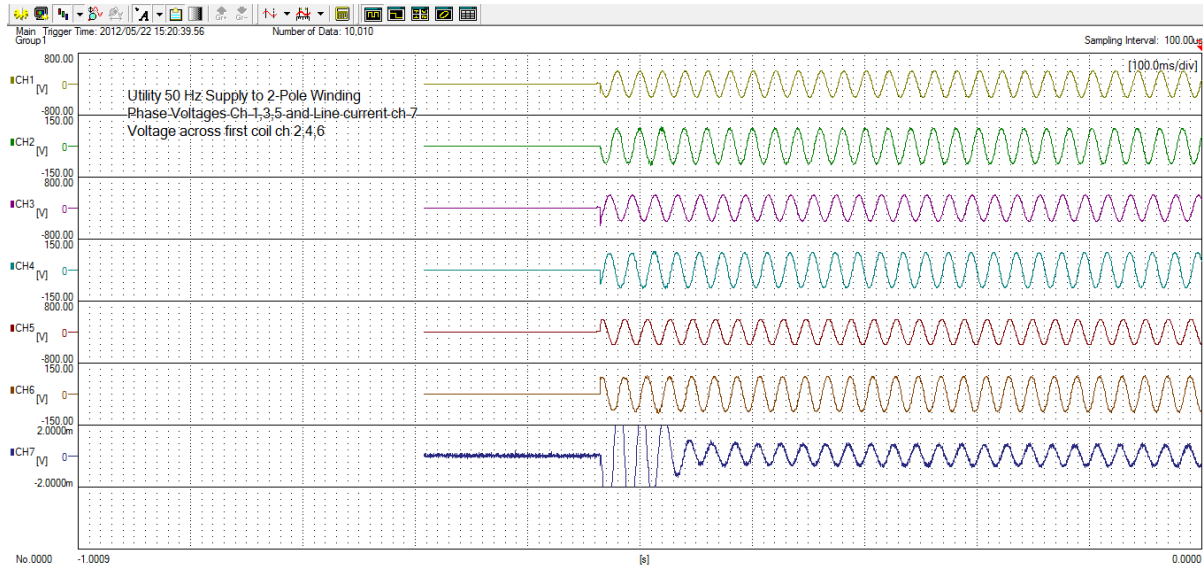
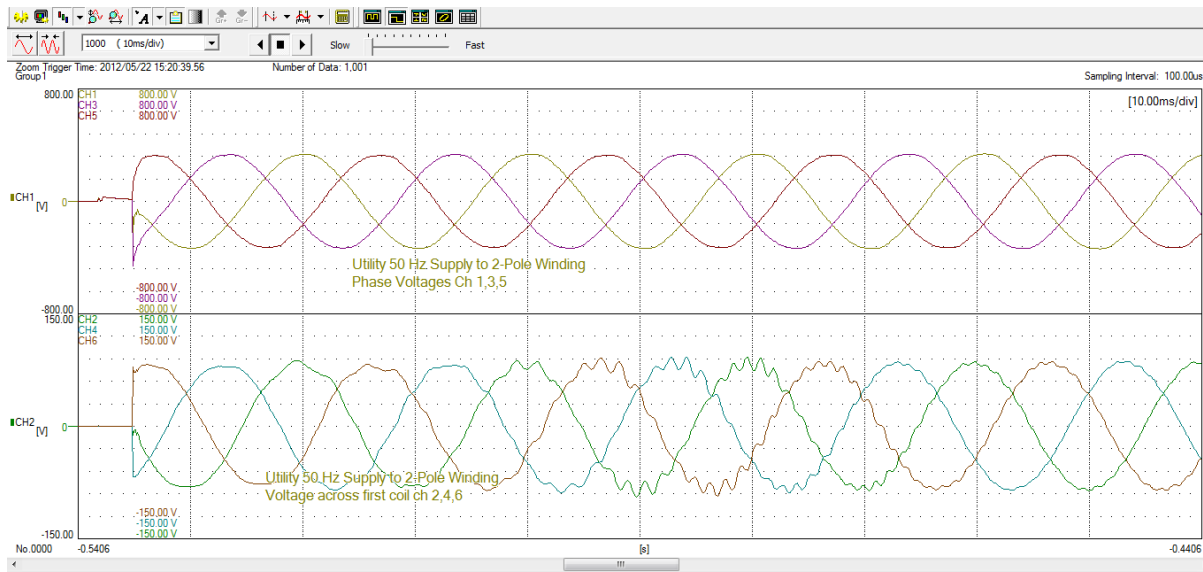


Fig. 0040B Enlarge View of wave forms



Wave form No. KRK0040

Fig. 0040C R-Phase

1

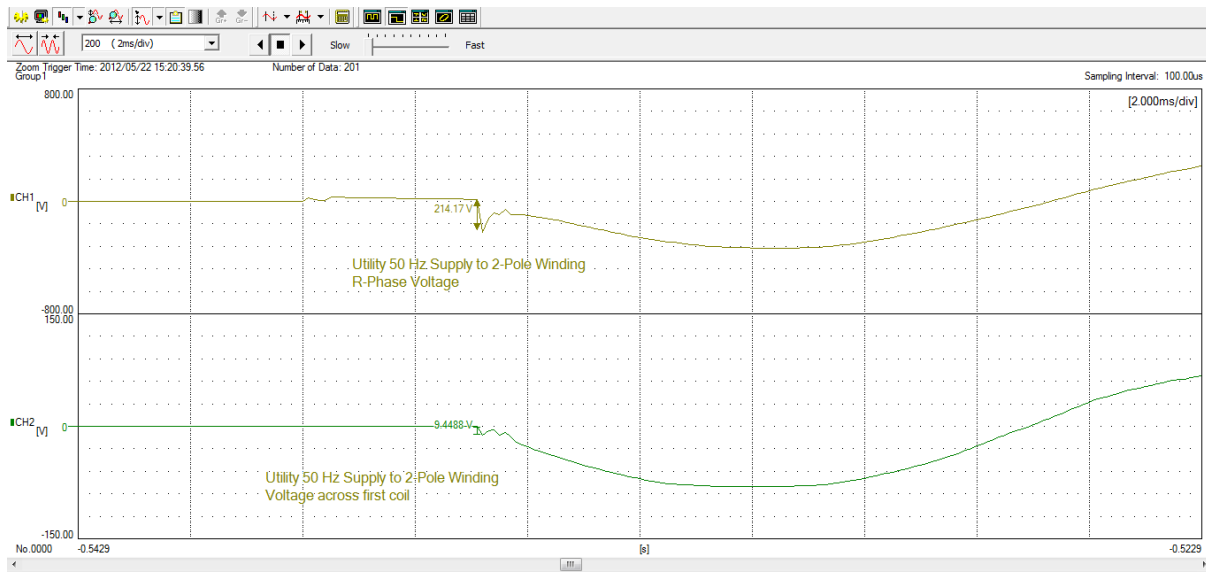
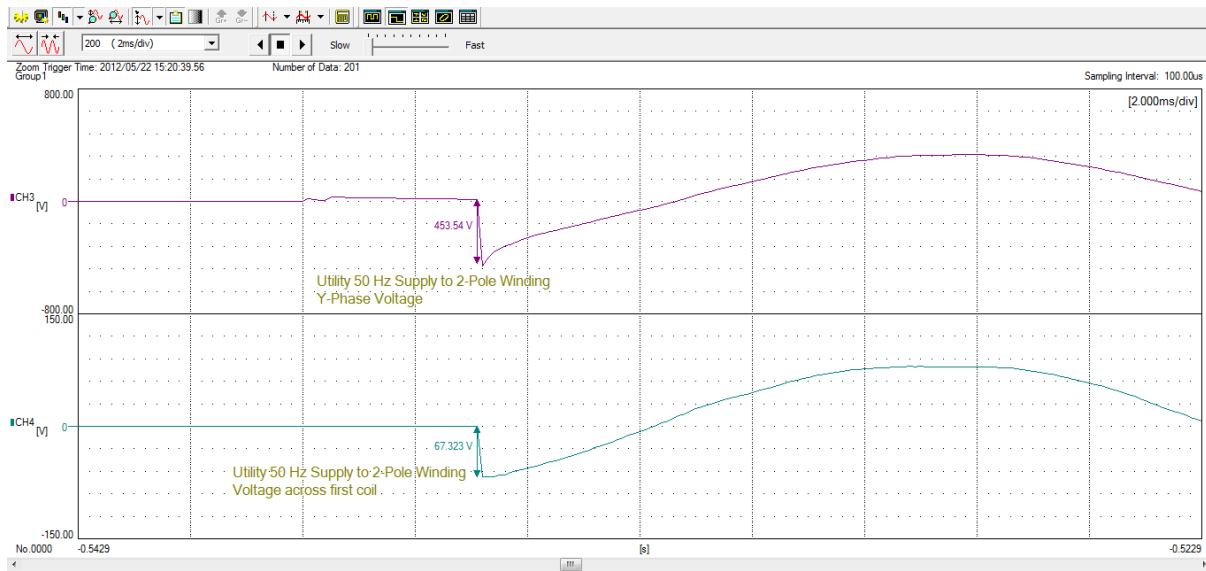
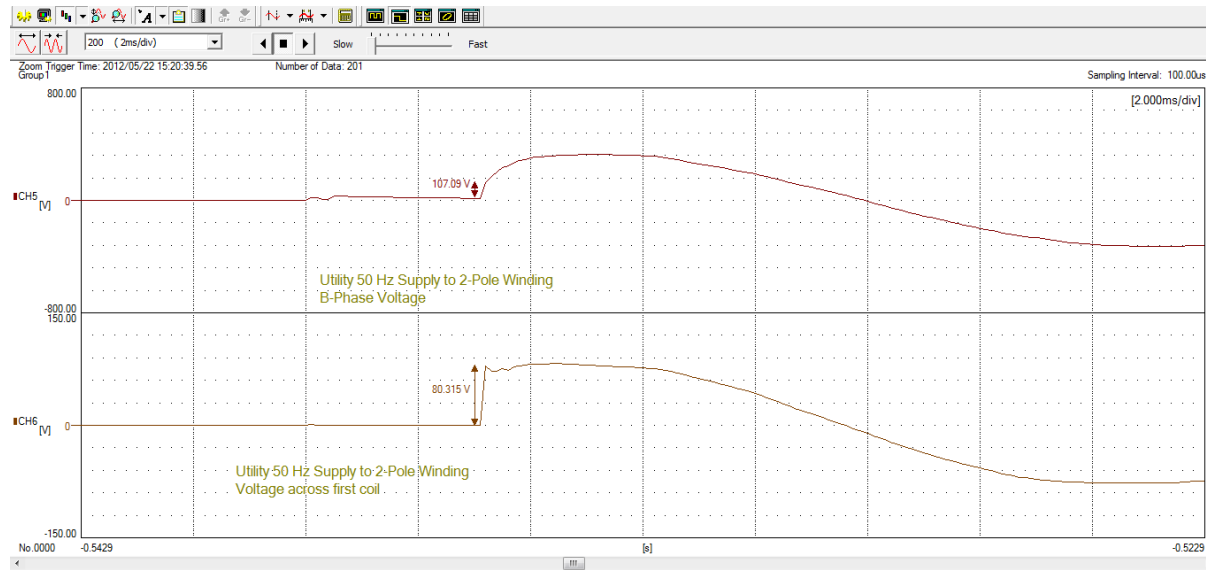


Fig. 0040D Y-Phase



Wave form No. KRK0040

Fig. 0040E B-Phase



Phase	Item	First Peak
R-Phase	Phase Voltage	214.17 V
	Voltage across coil	9.44 V
Y-Phase	Phase Voltage	453.54 V
	Voltage across coil	67.32 V
B-Phase	Phase Voltage	107.09 V
	Voltage across coil	80.31 V

Wave form No. KRK0106, Phase voltage and Voltage across all coils of 3-phase, 415 V, 250 W, 2-Pole Jewellery Polisher Motor when supplied with PWM inverter with frequency 20 Hz.

R-phase Voltage

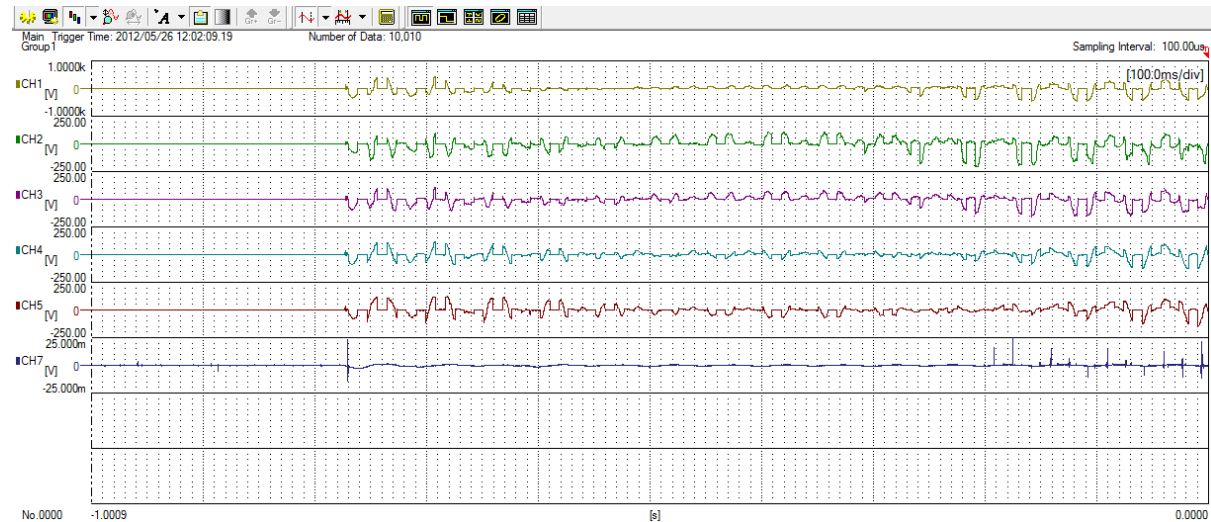


Diagram 1: Shows enlarge view of voltage wave forms across all four coils.

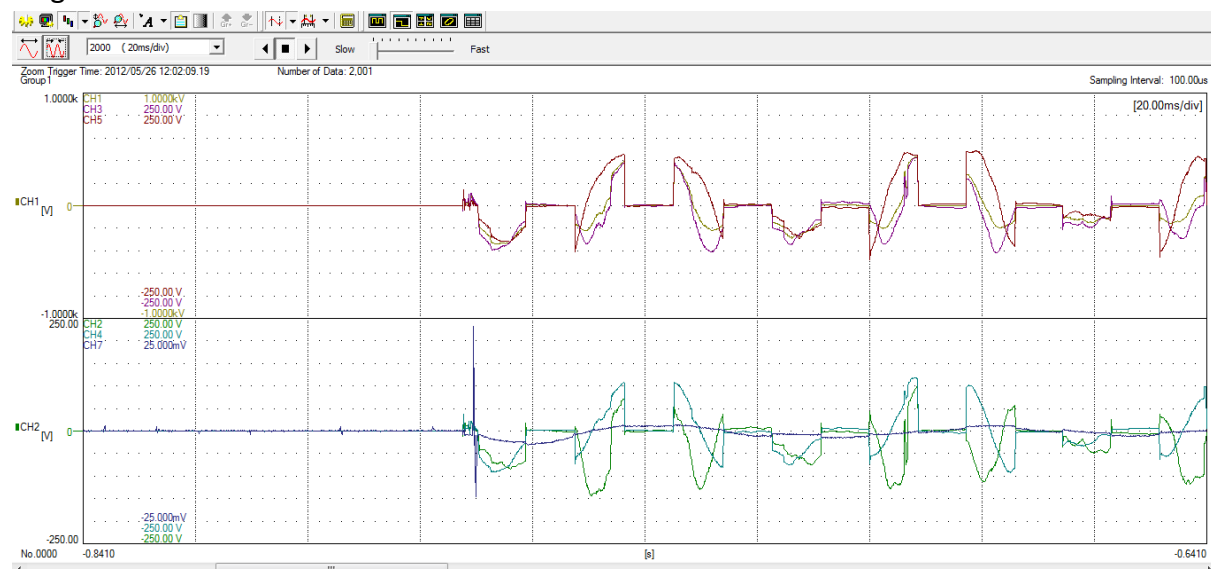
Diagram 2: Shows phase voltage wave form and voltage across first coil.

Diagram 3: Shows phase voltage wave form and voltage across second coil.

Diagram 4: Shows phase voltage wave form and voltage across third coil.

Diagram 5: Shows phase voltage wave form and voltage across fourth coil.

Diagram 1



Wave form No. KRK0106

Diagram 2

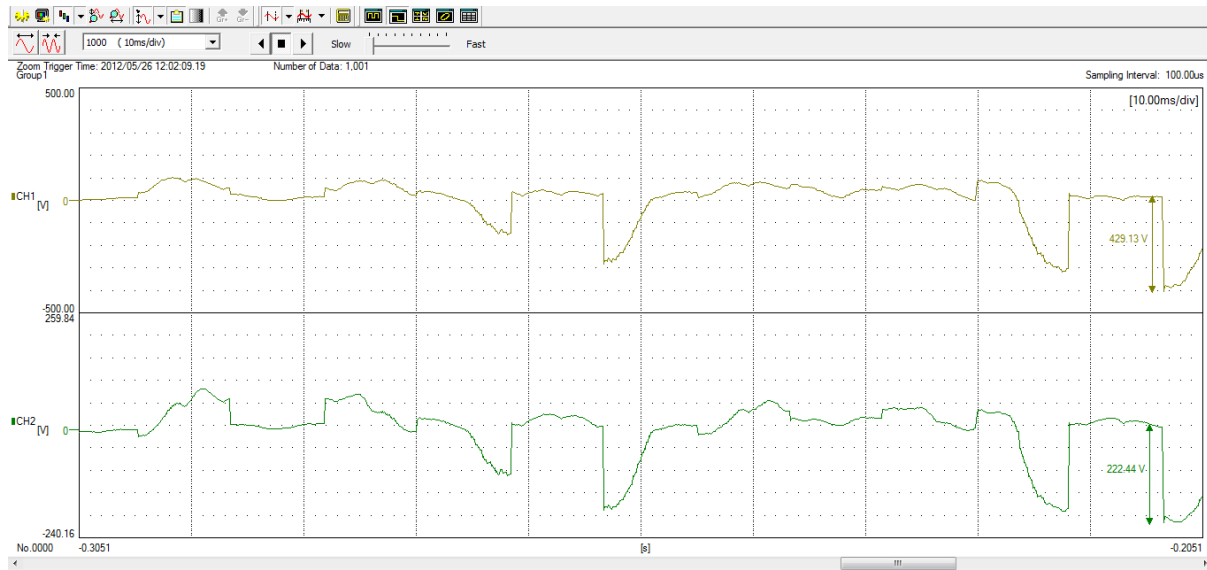
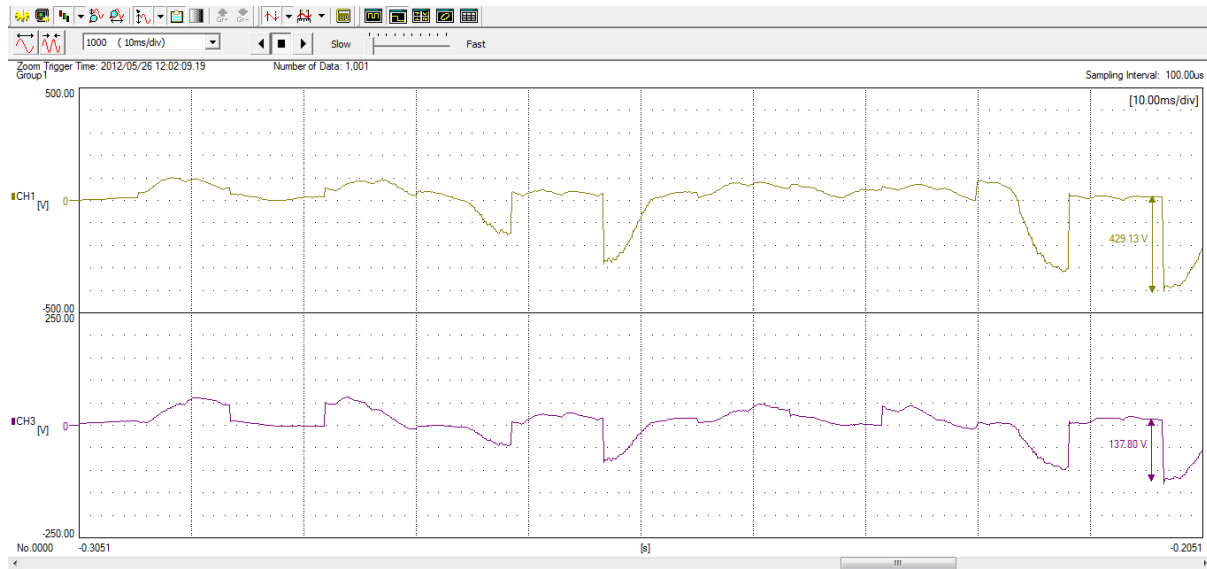


Diagram 3



Wave form No. KRK0106

Diagram 4

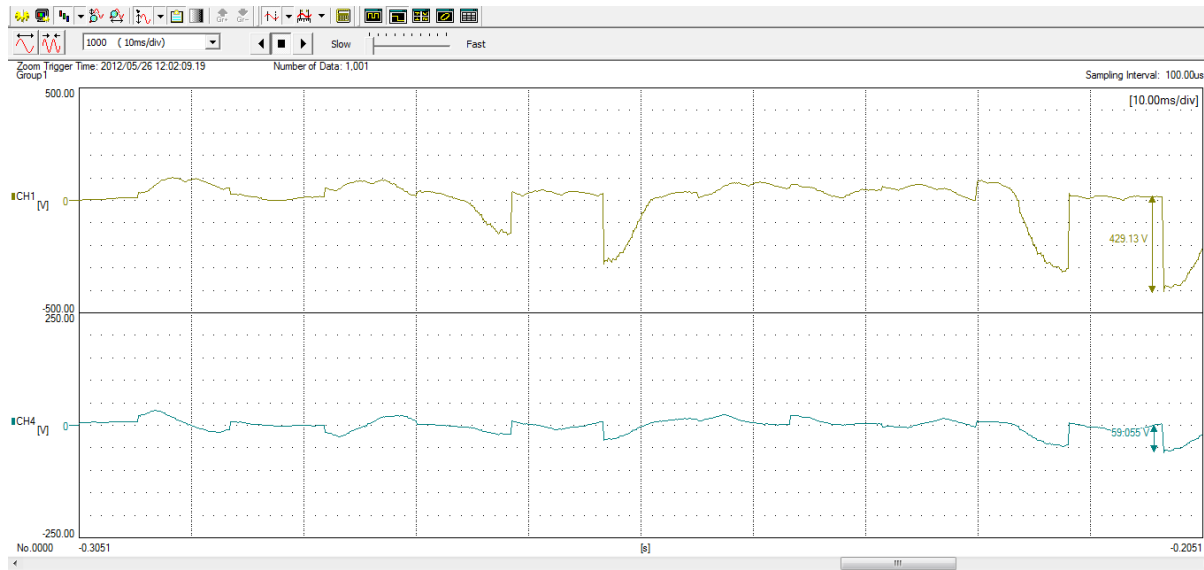
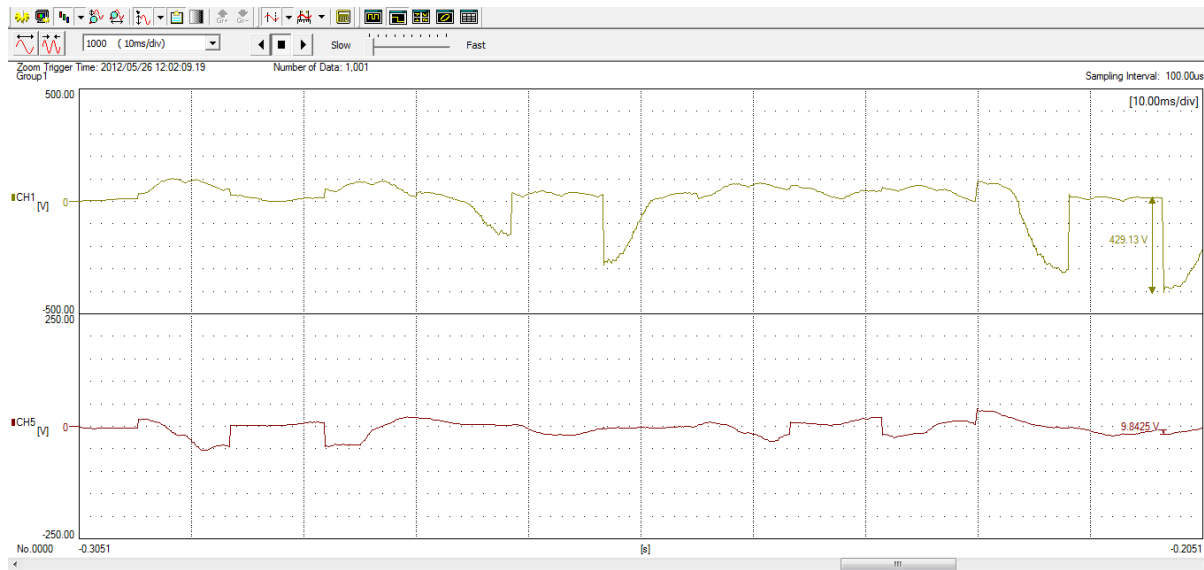


Diagram 5



Phase	Item	Voltage Variation
R-Phase	Phase Voltage V_{15}	429.43
	Voltage across first coil V_{12}	222.44
	Voltage across second coil V_{23}	137.80
	Voltage across third coil V_{34}	59.05
	Voltage across four coil V_{45}	9.84

Wave form No. KRK0107, Phase voltage and Voltage across all coils of 3-phase, 415 V, 250 W, 2-Pole Jewellery Polisher Motor when supplied with PWM inverter with frequency 30 Hz.

R-phase Voltage

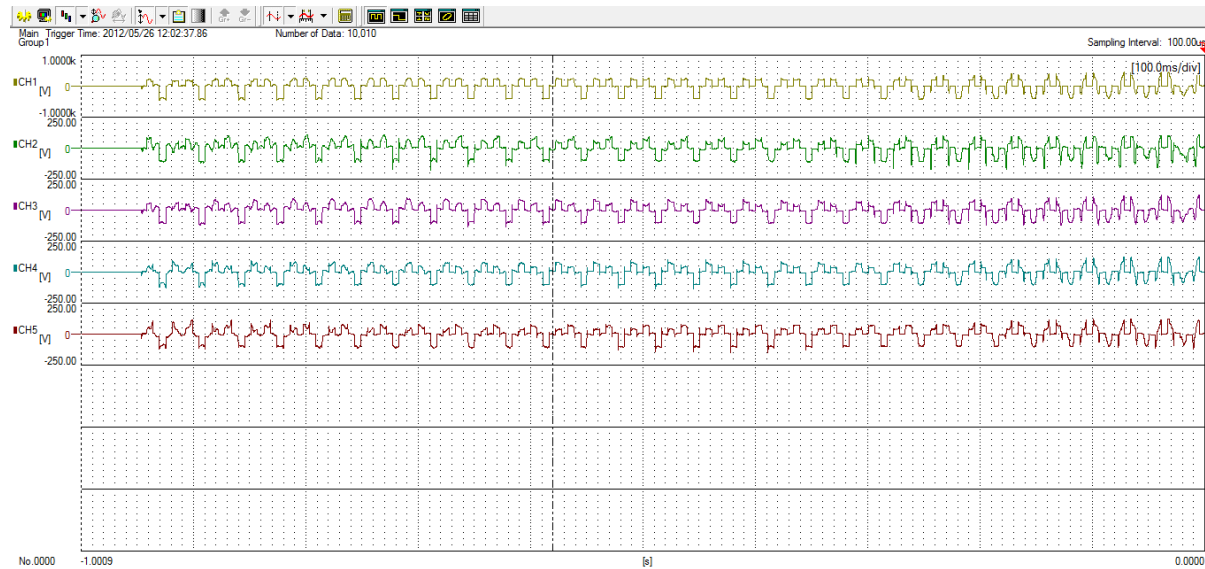


Diagram 1: Shows enlarge view of voltage wave forms across all four coils.

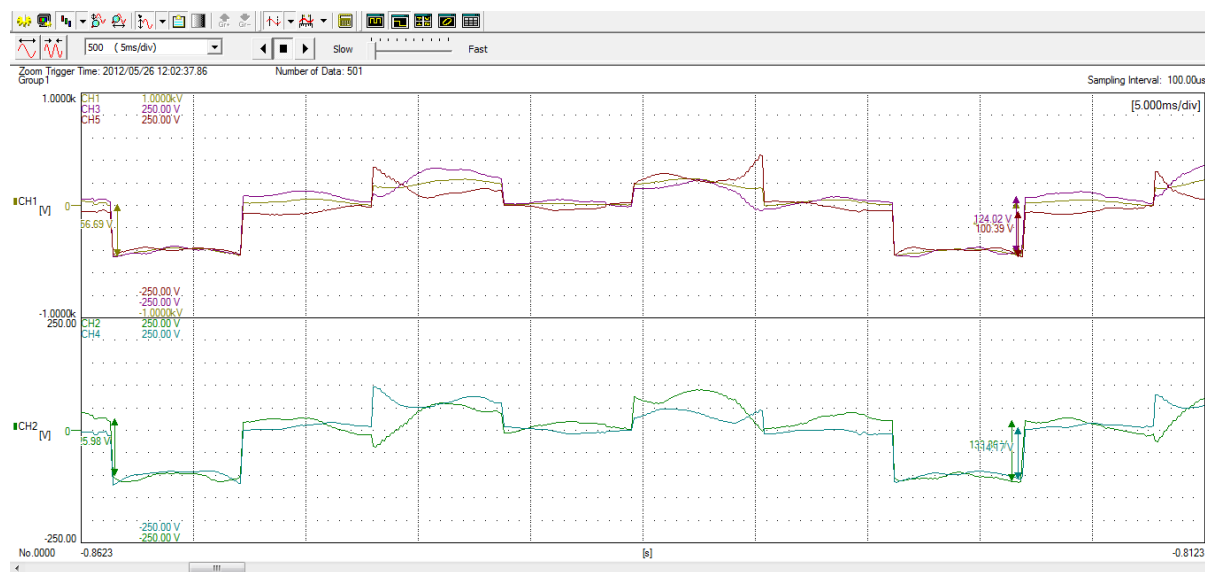
Diagram 2: Shows phase voltage wave form and voltage across first coil.

Diagram 3: Shows phase voltage wave form and voltage across second coil.

Diagram 4: Shows phase voltage wave form and voltage across third coil.

Diagram 5: Shows phase voltage wave form and voltage across fourth coil.

Diagram 1



Wave form No. KRK0107

Diagram 2

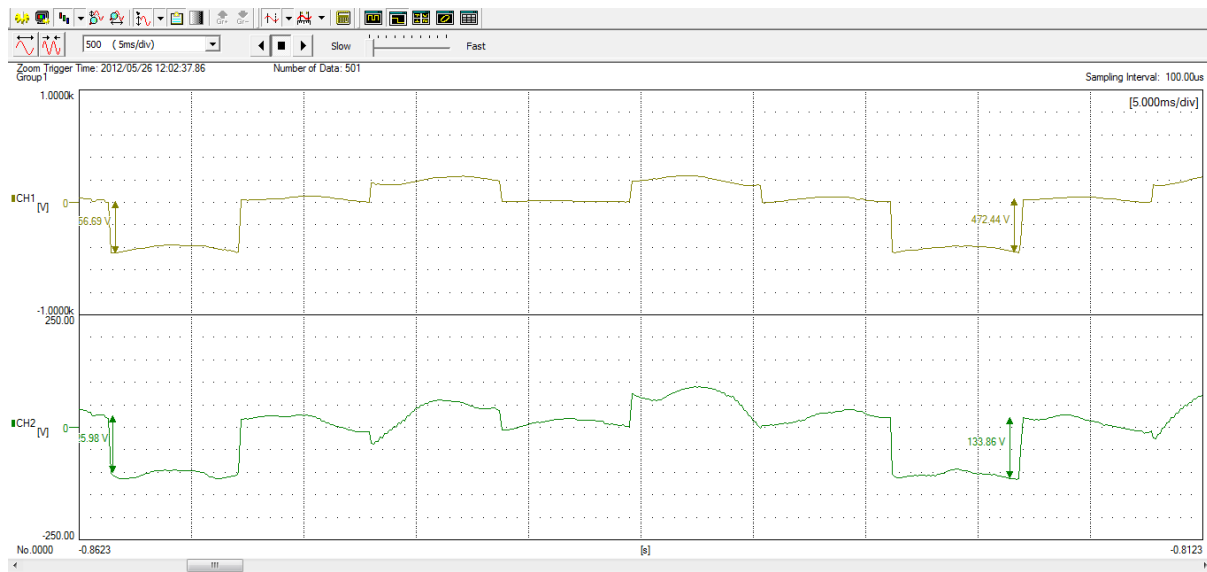
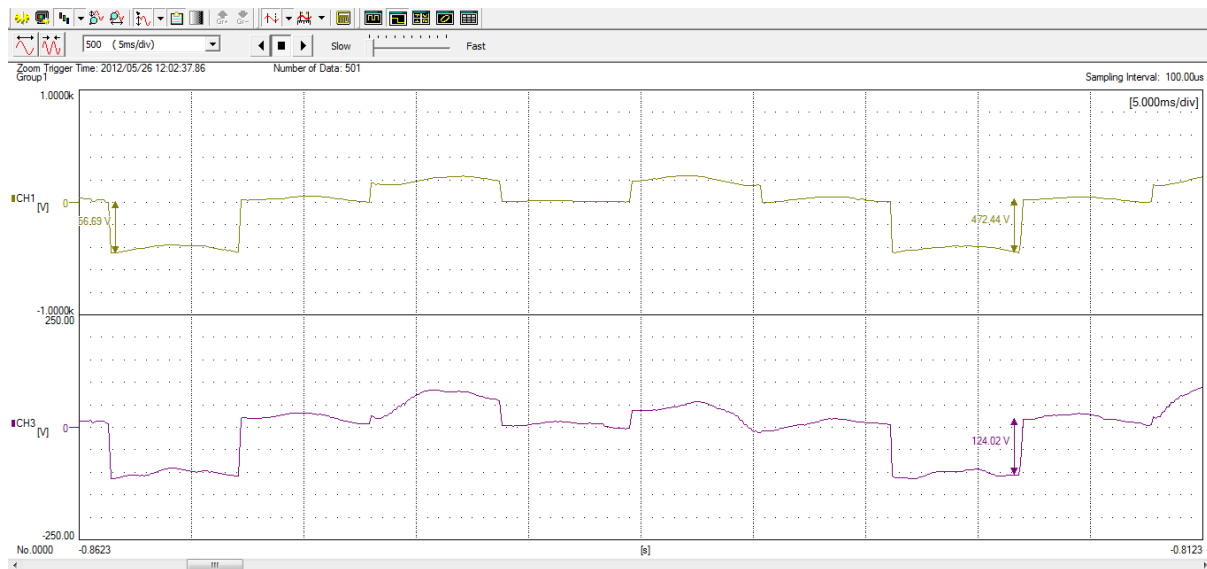


Diagram 3



Wave form No. KRK0107

Diagram 4

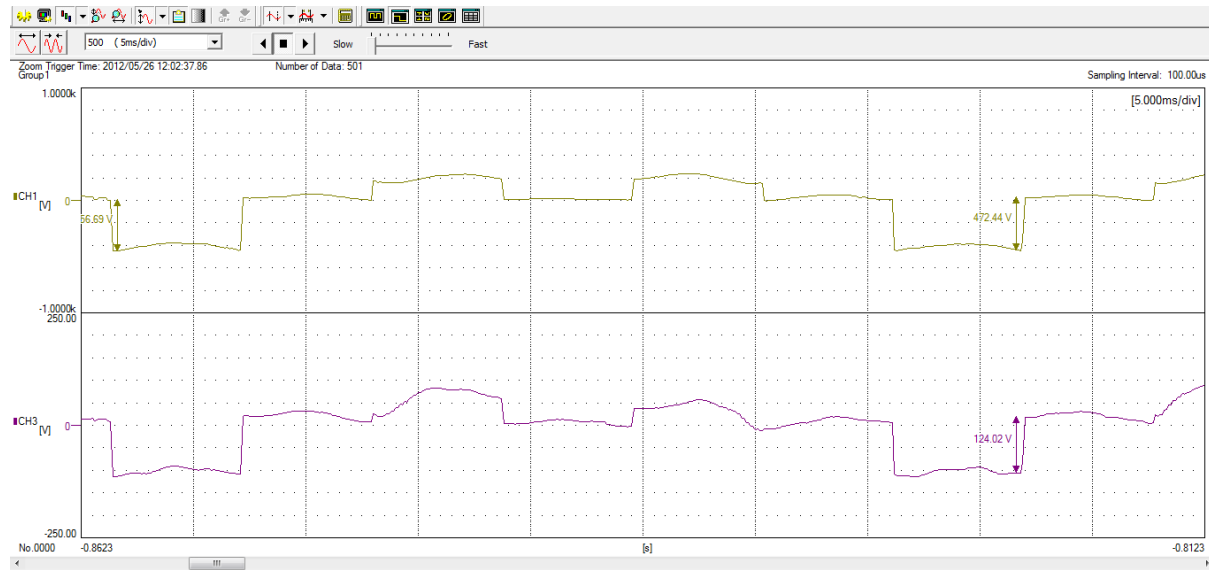
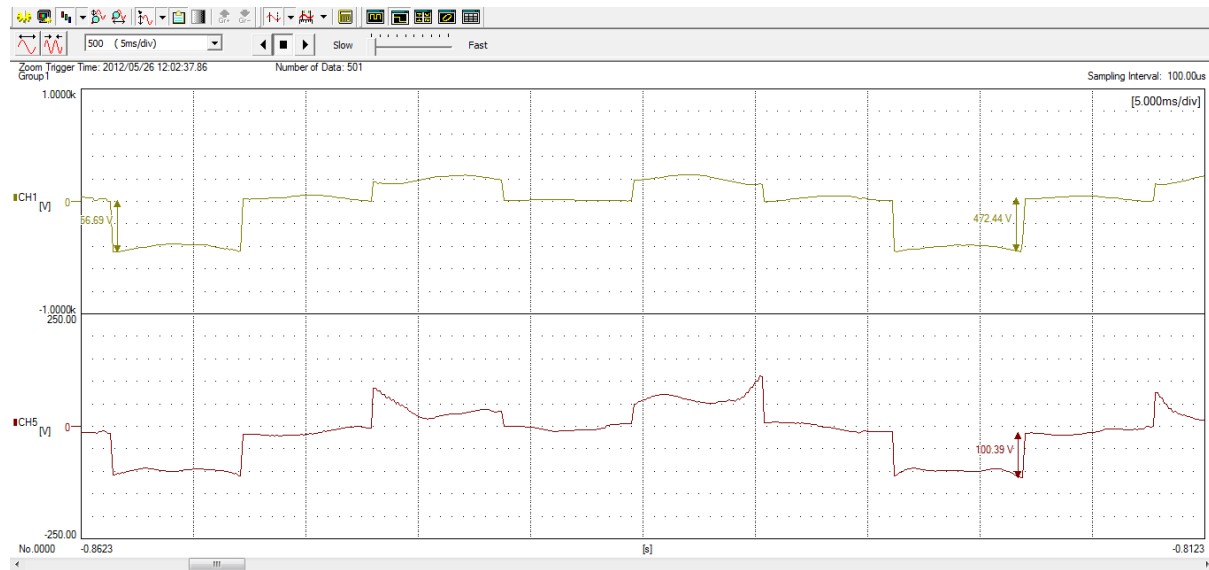


Diagram 5



Phase	Item	Voltage Variation
R-Phase	Phase Voltage V_{15}	472.44
	Voltage across first coil V_{12}	133.86
	Voltage across second coil V_{23}	124.02
	Voltage across third coil V_{34}	114.17
	Voltage across four coil V_{45}	100.39

Wave form No. KRK0108

Phase voltage and Voltage across all coil of 3-phase, 415 V, 250 W, 2-Pole Jewellery Polisher Motor when supplied with PWM inverter with frequency 40 Hz.

R-phase Voltage

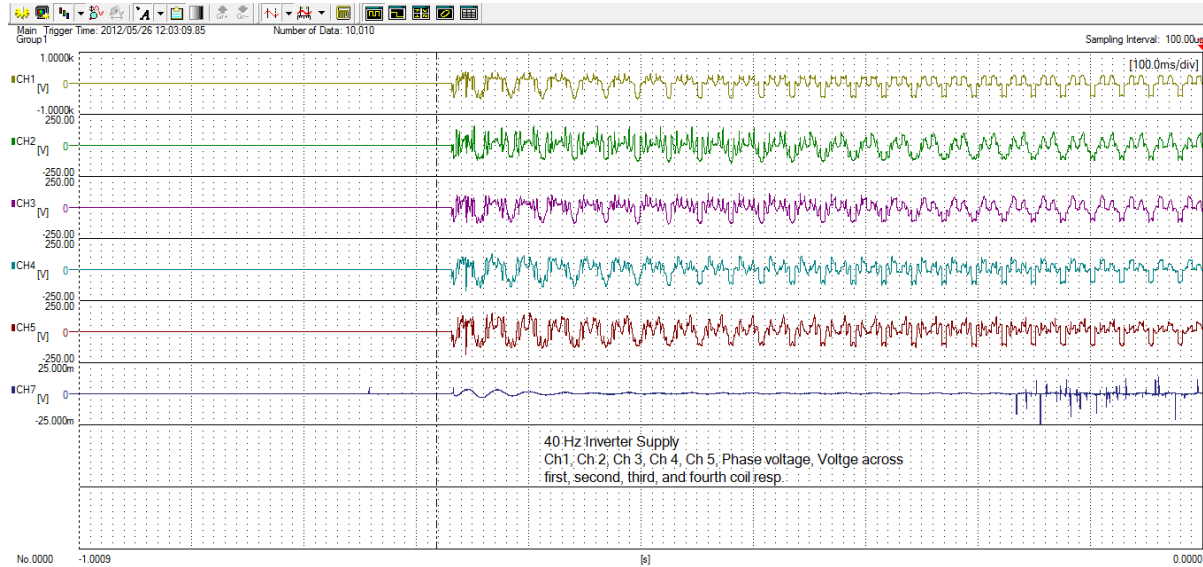


Diagram 1: Shows enlarge view of voltage wave forms across all four coils.

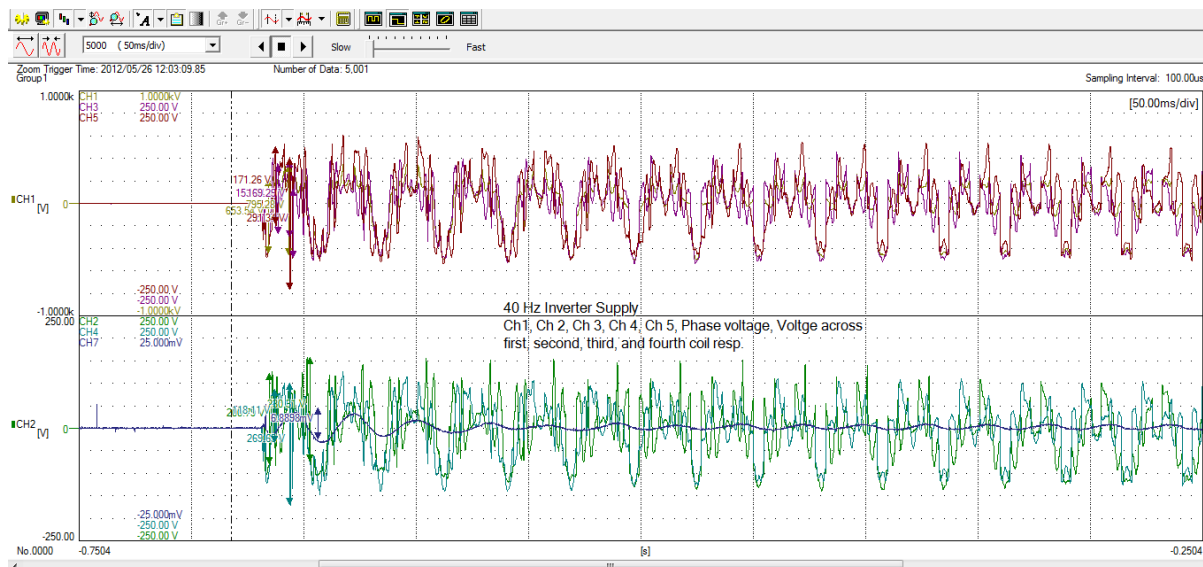
Diagram 2: Shows phase voltage wave form and voltage across first coil.

Diagram 3: Shows phase voltage wave form and voltage across second coil.

Diagram 4: Shows phase voltage wave form and voltage across third coil.

Diagram 5: Shows phase voltage wave form and voltage across fourth coil.

Diagram 1



Wave form No. KRK0108

Diagram 2

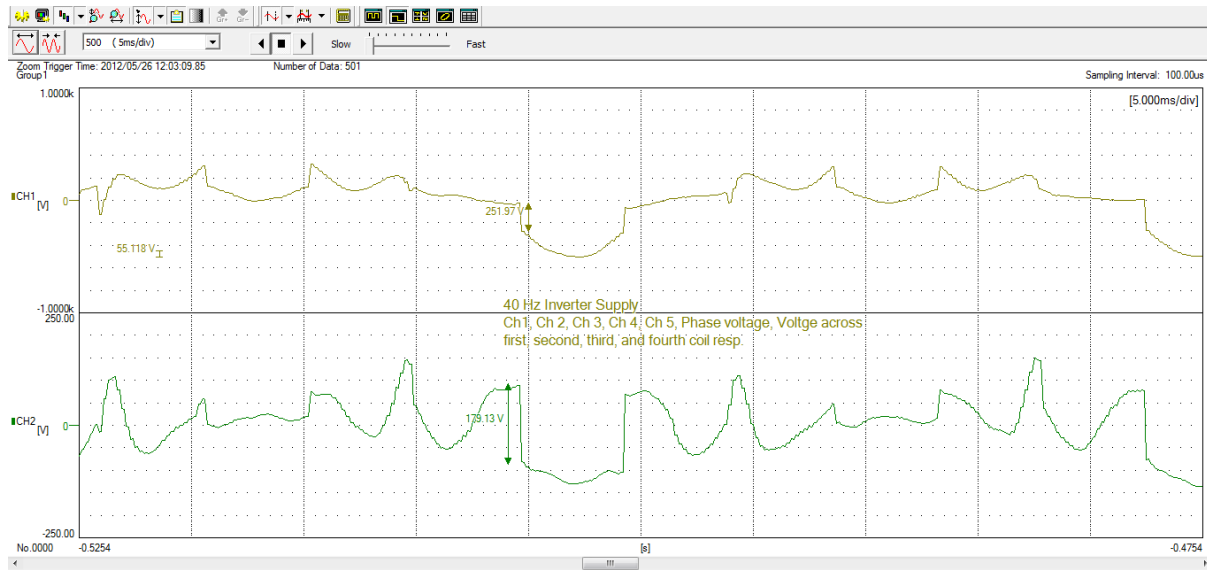
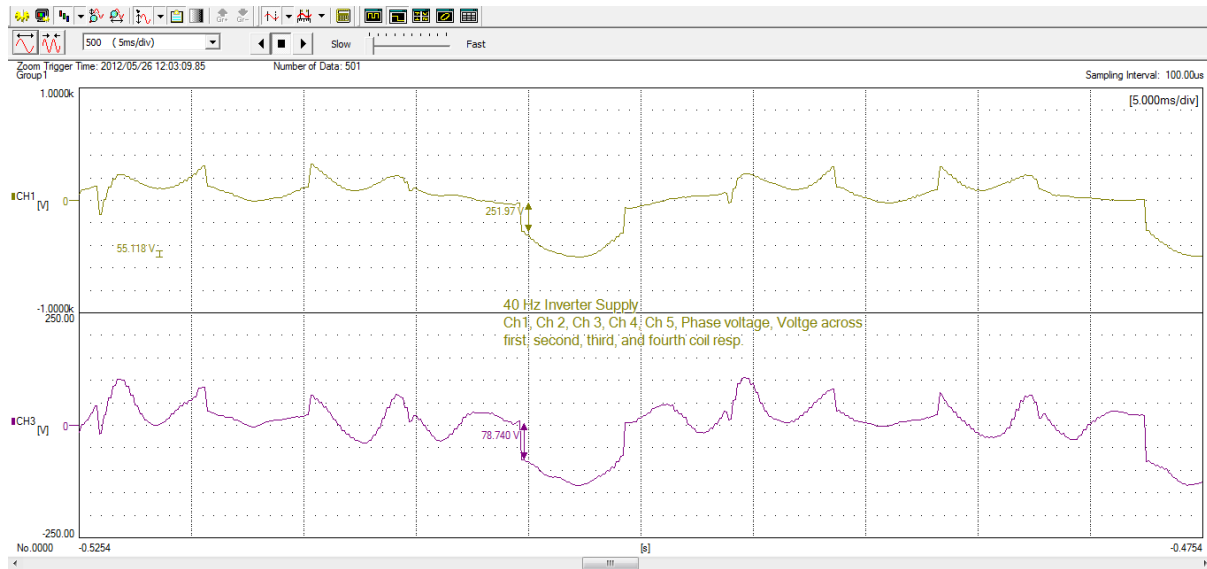


Diagram 3



Wave form No. KRK0108

Diagram 4

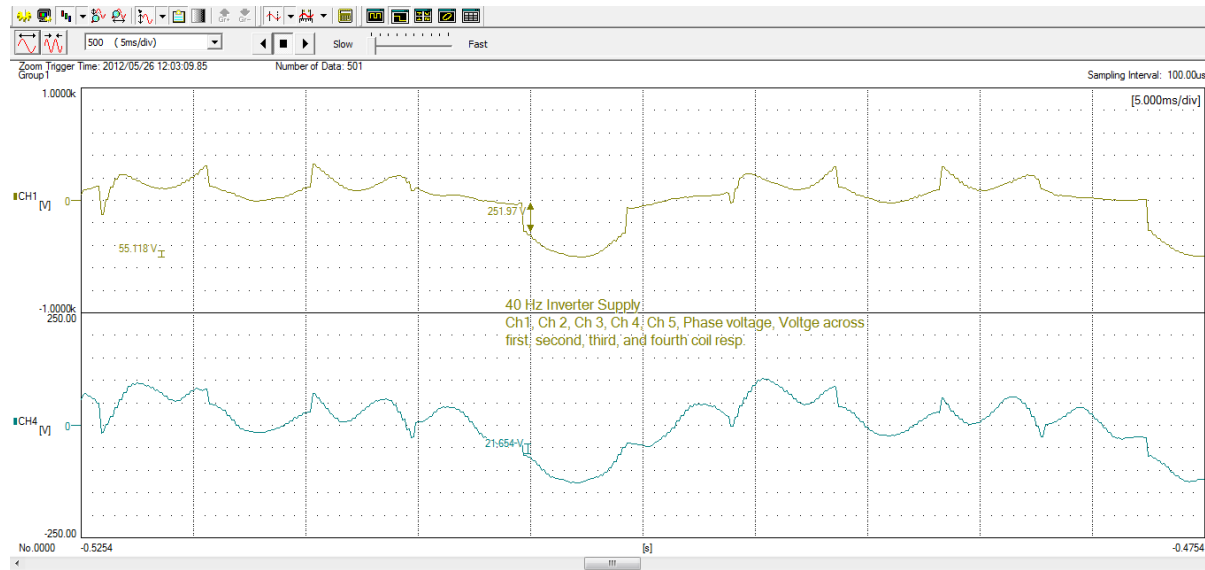
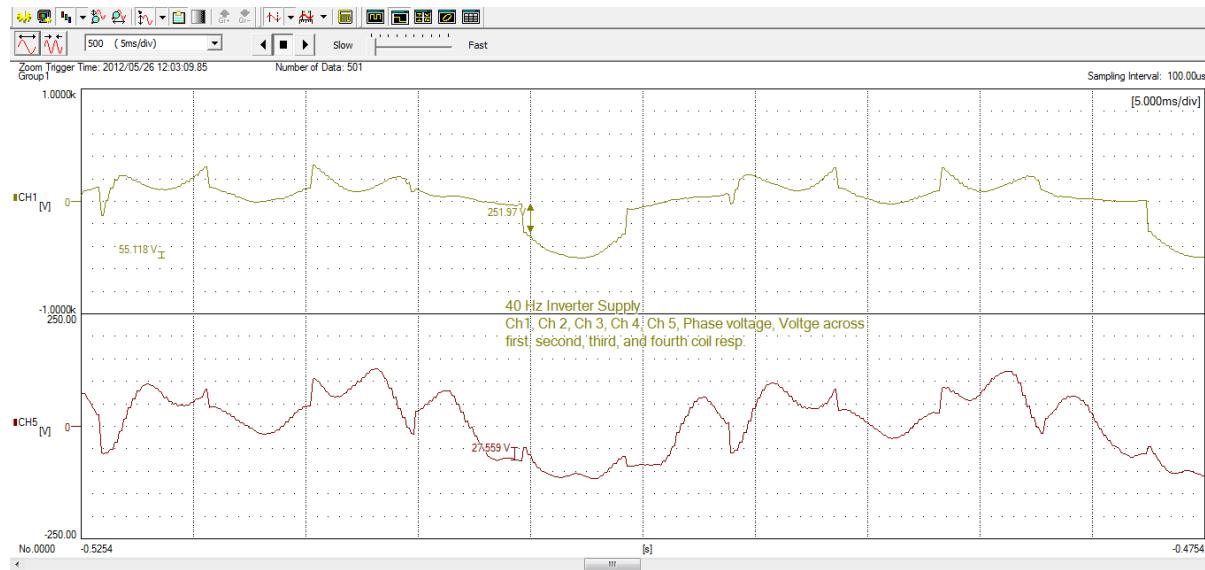


Diagram 5



Phase	Item	Voltage Variation
R-Phase	Phase Voltage V_{15}	251.97
	Voltage across first coil V_{12}	179.13
	Voltage across second coil V_{23}	78.74
	Voltage across third coil V_{34}	21.65
	Voltage across four coil V_{45}	-27.55

Wave form No. KRK0109

Phase voltage and Voltage across all coils of 3-phase, 415 V, 250 W, 2-Pole Jewellery Polisher Motor when supplied with PWM inverter with frequency 50 Hz.

R-phase Voltage

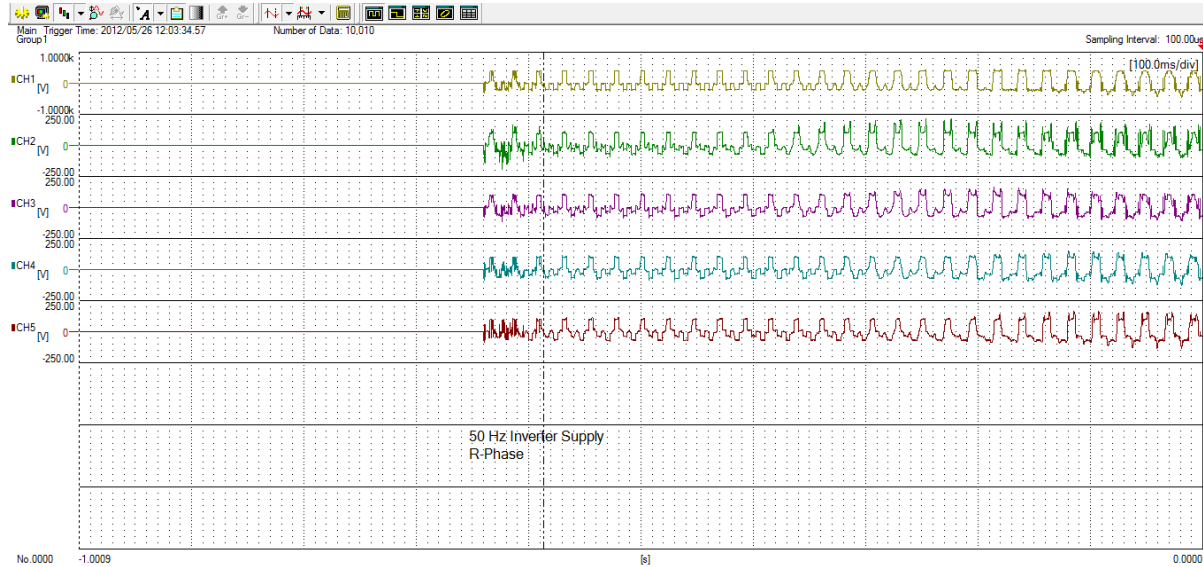


Diagram 1: Shows enlarge view of voltage wave forms across all four coils.

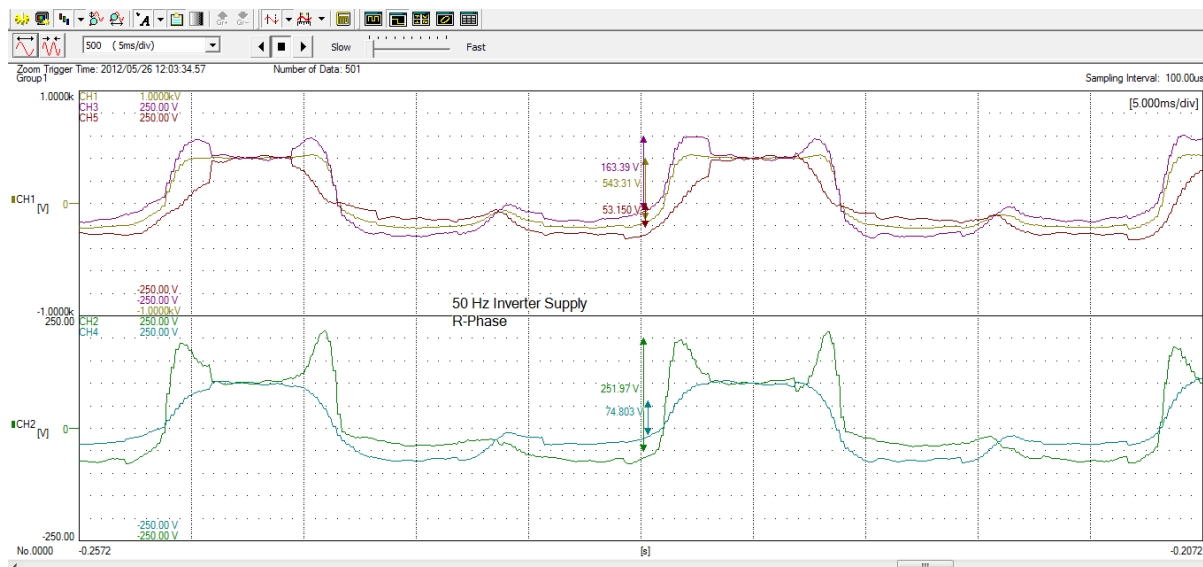
Diagram 2: Shows phase voltage wave form and voltage across first coil.

Diagram 3: Shows phase voltage wave form and voltage across second coil.

Diagram 4: Shows phase voltage wave form and voltage across third coil.

Diagram 5: Shows phase voltage wave form and voltage across fourth coil.

Diagram 1



Wave form No. KRK0109

Diagram 2



Diagram 3



Wave form No. KRK0109

Diagram 4

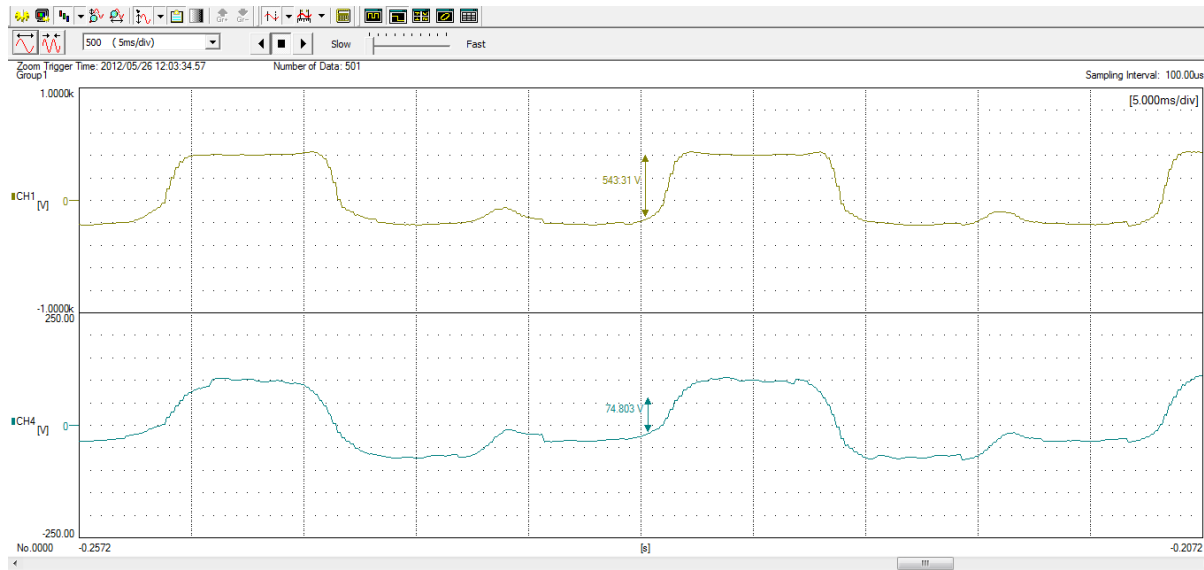
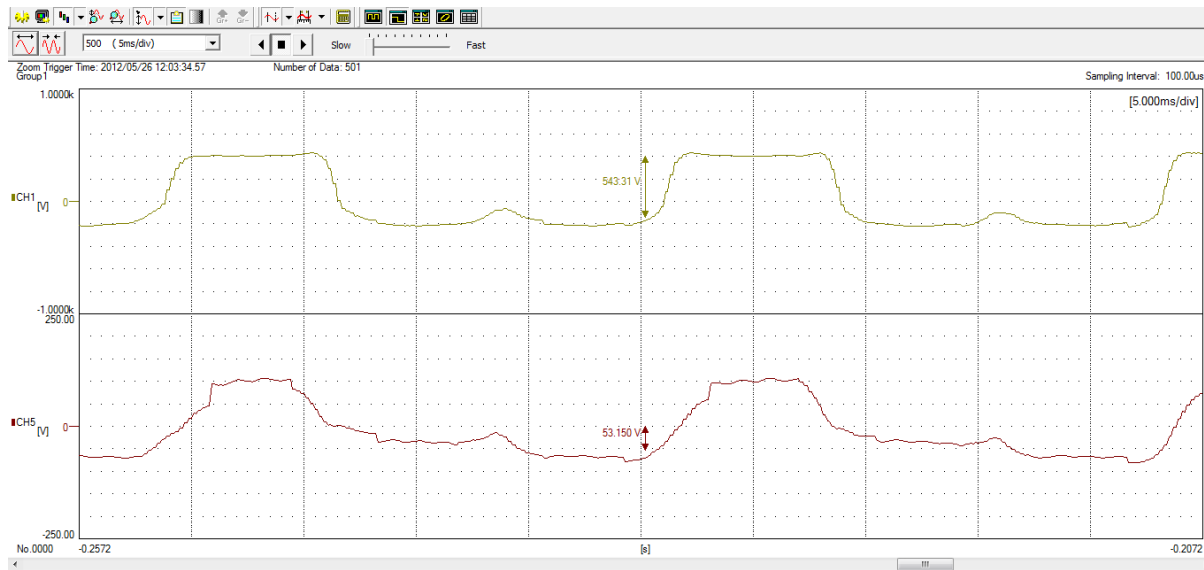


Diagram 5



Phase	Item	Voltage Variation
R-Phase	Phase Voltage V_{15}	543.31
	Voltage across first coil V_{12}	251.95
	Voltage across second coil V_{23}	163.39
	Voltage across third coil V_{34}	74.80
	Voltage across four coil V_{45}	53.15

Wave form No. KRK0110

Phase voltage and Voltage across all coils of 3-phase, 415 V, 250 W, 2-Pole Jewellery Polisher Motor when supplied with PWM inverter with frequency 60 Hz.

R-phase Voltage

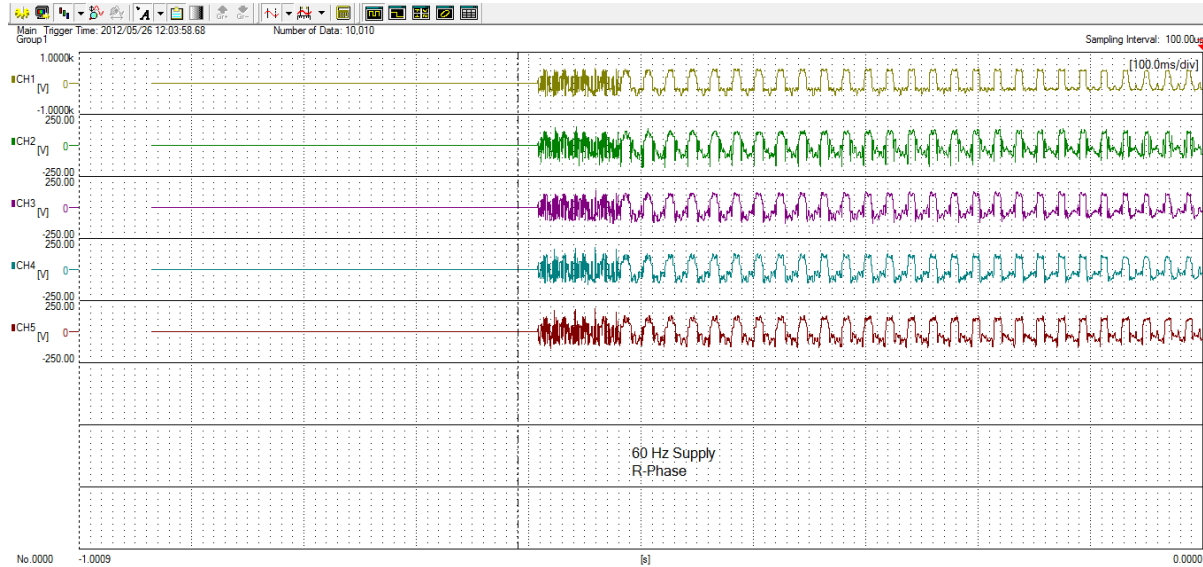


Diagram 1: Shows enlarge view of voltage wave forms across all four coils.

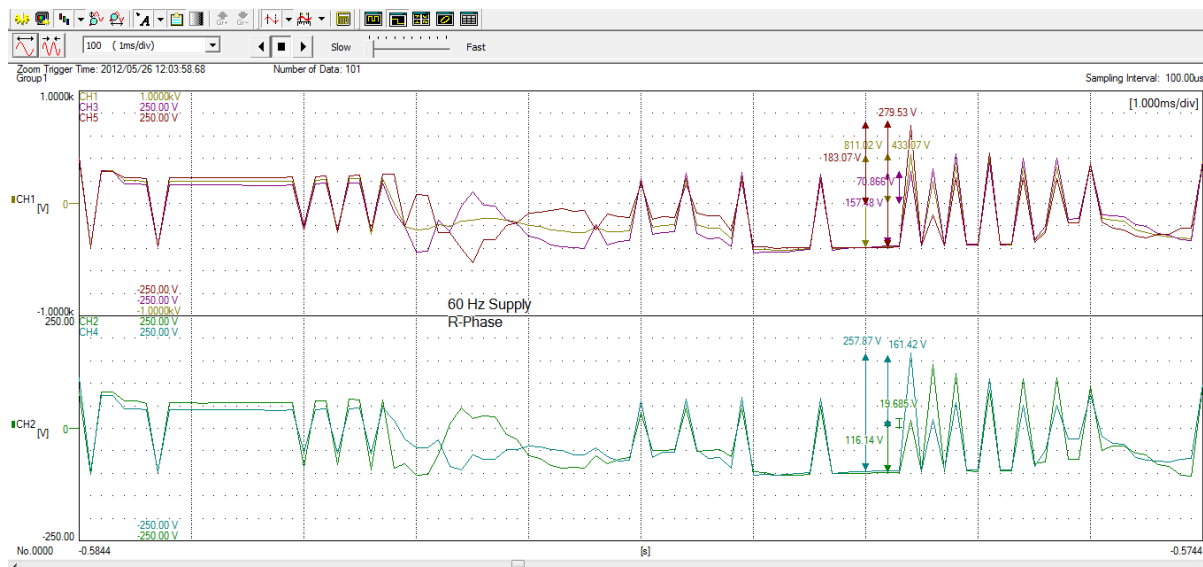
Diagram 2: Shows phase voltage wave form and voltage across first coil.

Diagram 3: Shows phase voltage wave form and voltage across second coil.

Diagram 4: Shows phase voltage wave form and voltage across third coil.

Diagram 5: Shows phase voltage wave form and voltage across fourth coil.

Diagram 1



Wave form No. KRK0110

Diagram 2

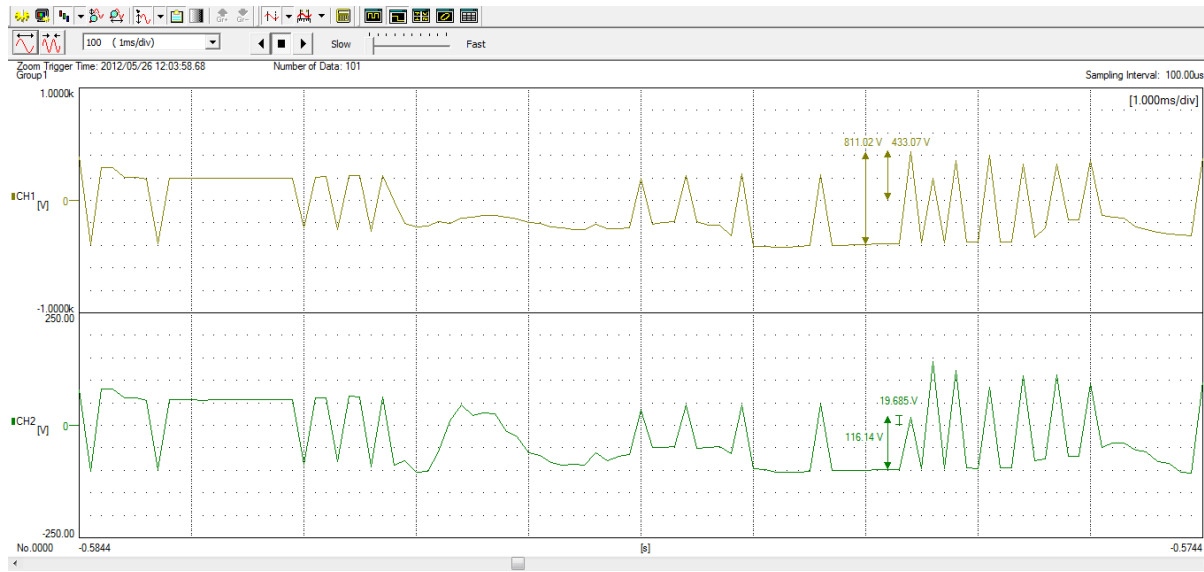
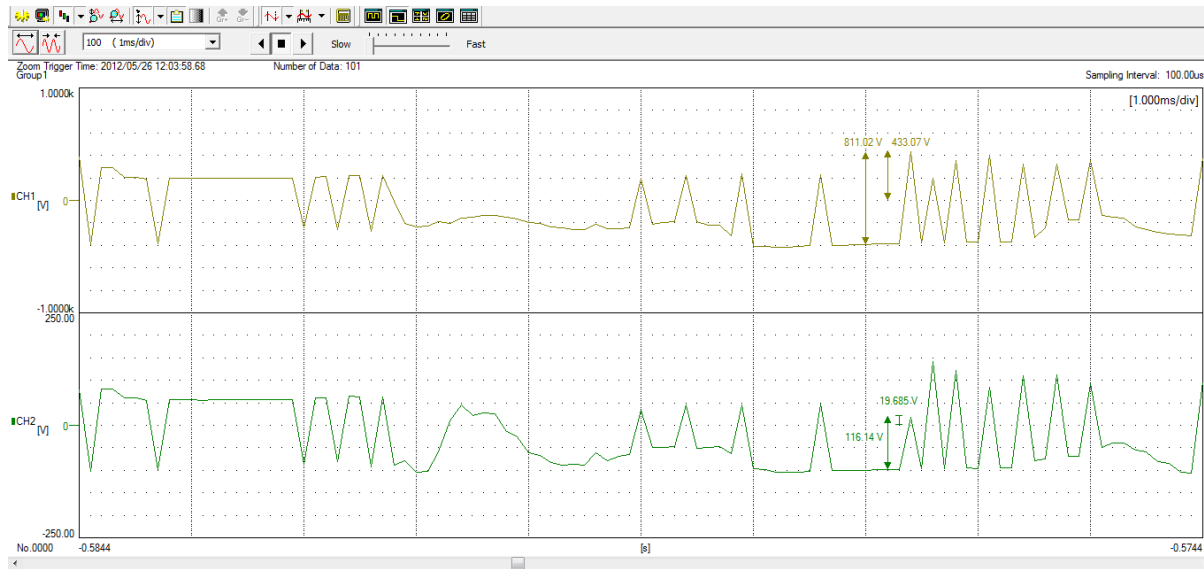


Diagram 3



Wave form No. KRK0110

Diagram 4

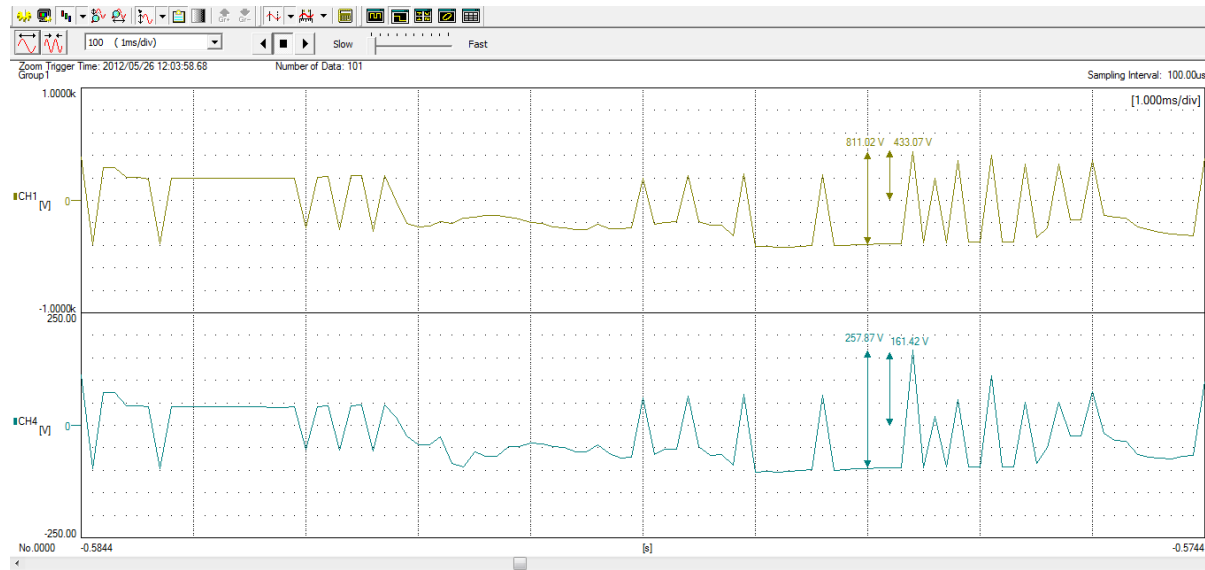
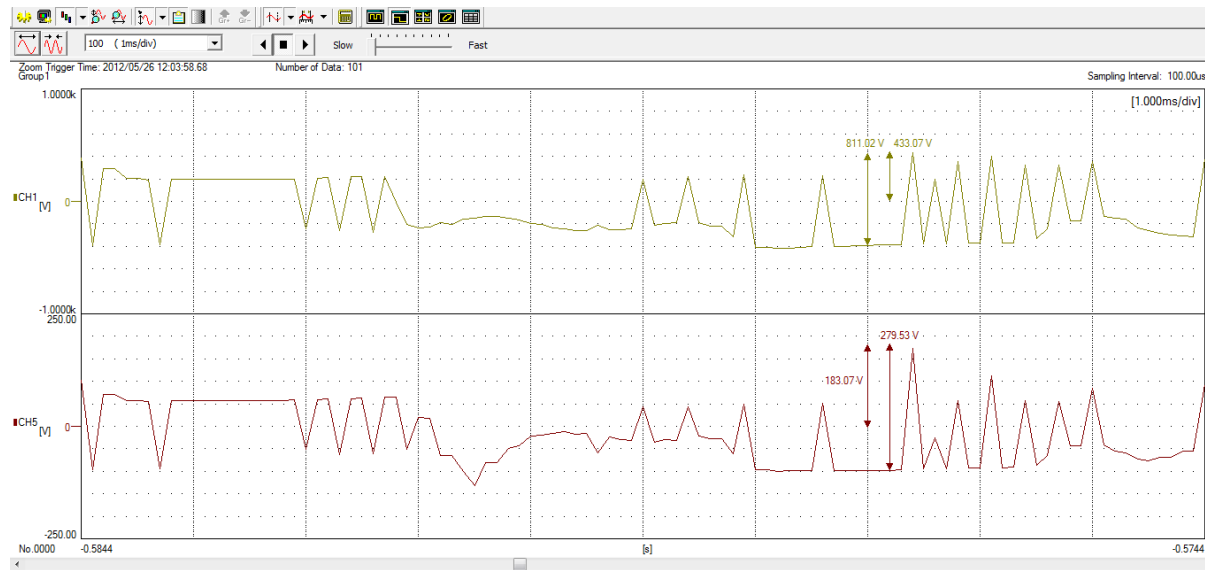


Diagram 5



Phase	Item	Change in 1 ms	Change in 0.5 ms
R-Phase	Phase Voltage V_{15}	811.02	433.07
	Voltage across first coil V_{12}	116.19	17.71
	Voltage across second coil V_{23}	157.48	70.86
	Voltage across third coil V_{34}	257.87	161.42
	Voltage across four coil V_{45}	279.53	183.07

Wave form No. KRK0004

Phase voltage and Voltage across first coil of 3-phase, 415 V, 250 W, 4-Pole Jewellery Polisher Motor on NO LOAD when supplied with sinusoidal supply- 50 Hz.

Fig. 0004A Normal View of wave forms

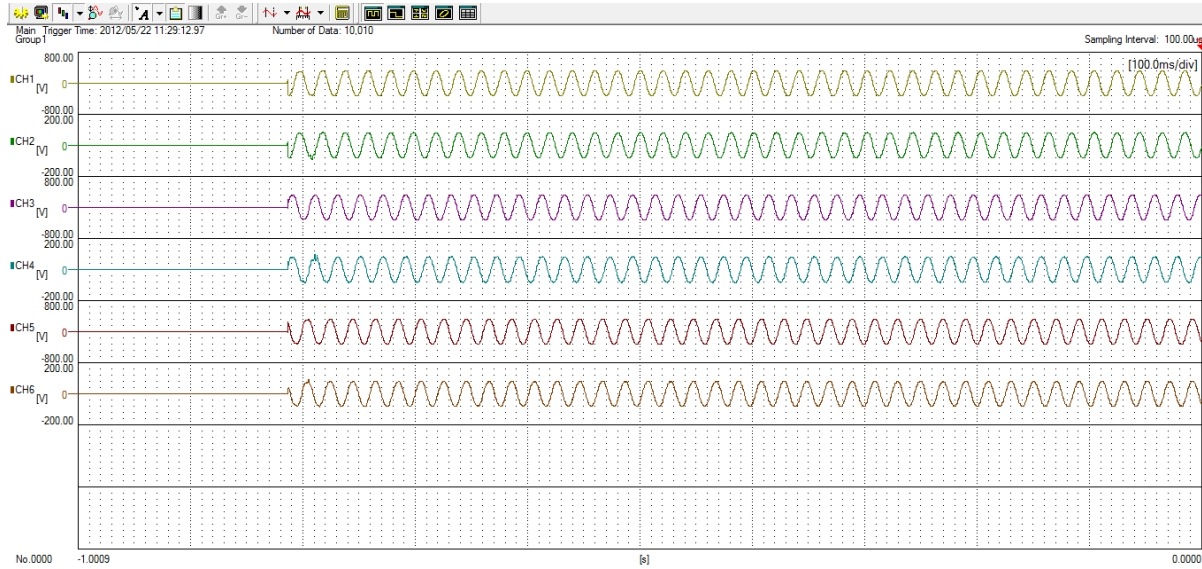
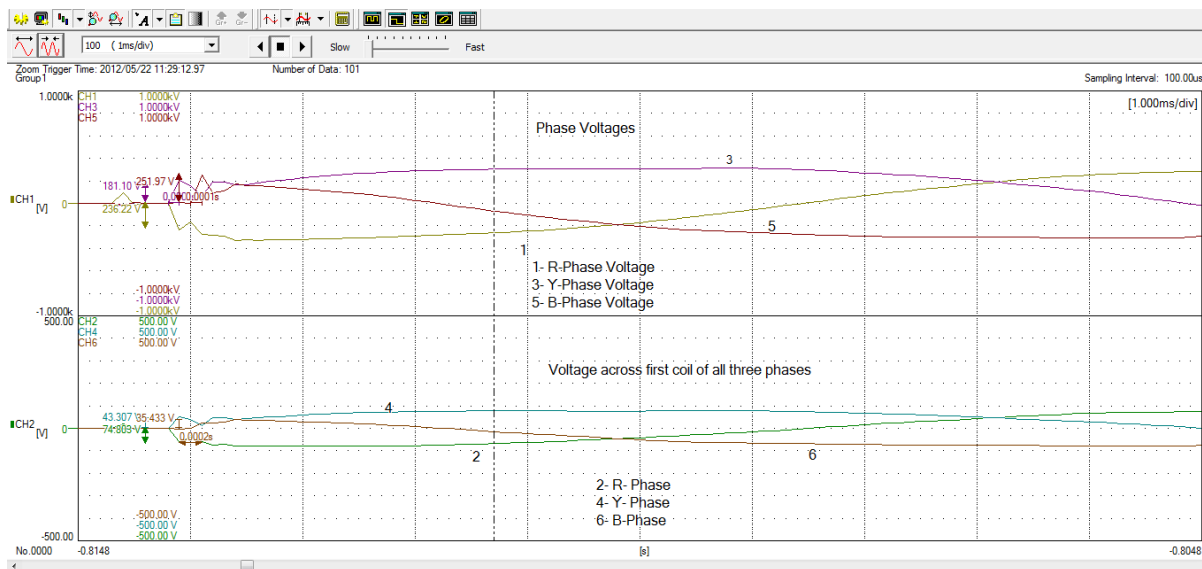


Fig. 0004B Enlarge View of wave forms



Wave form No. KRK0004

Fig. 0004C R-Phase

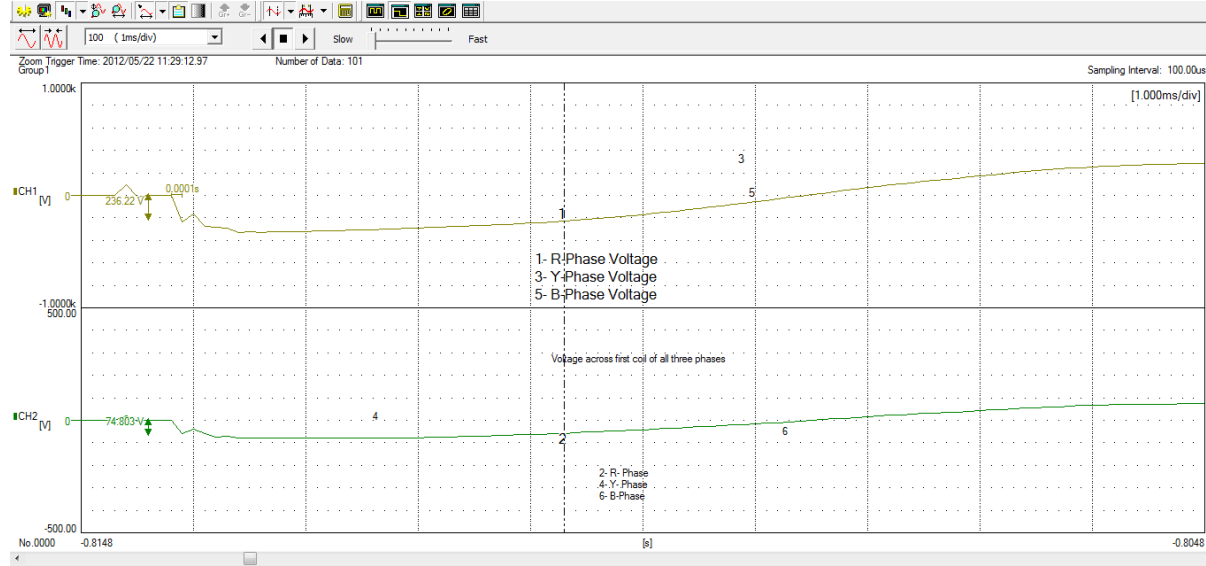
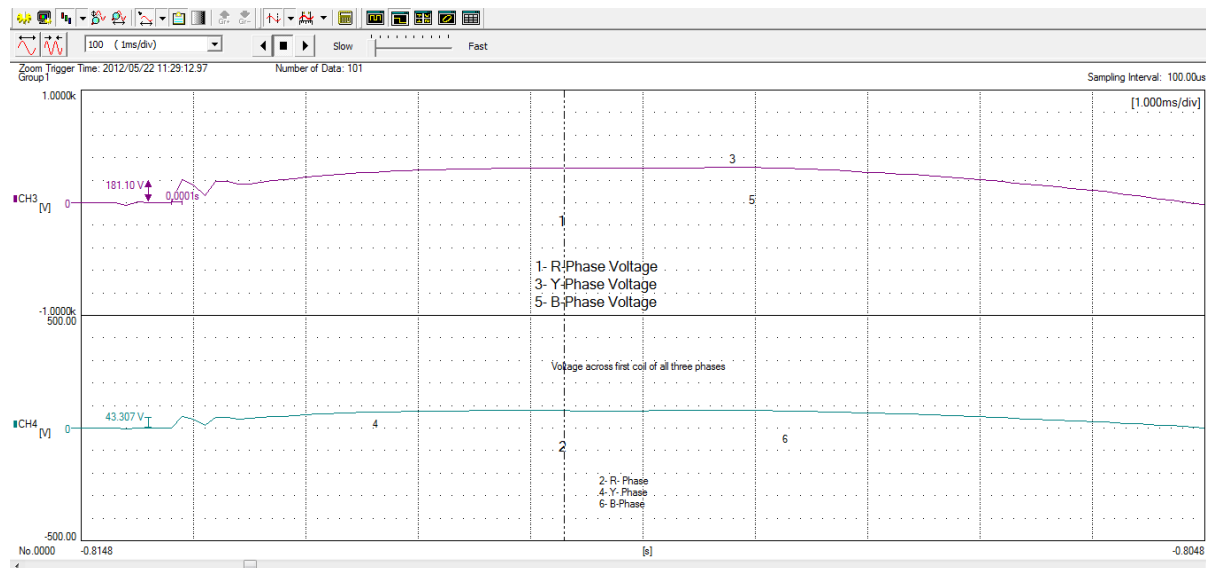
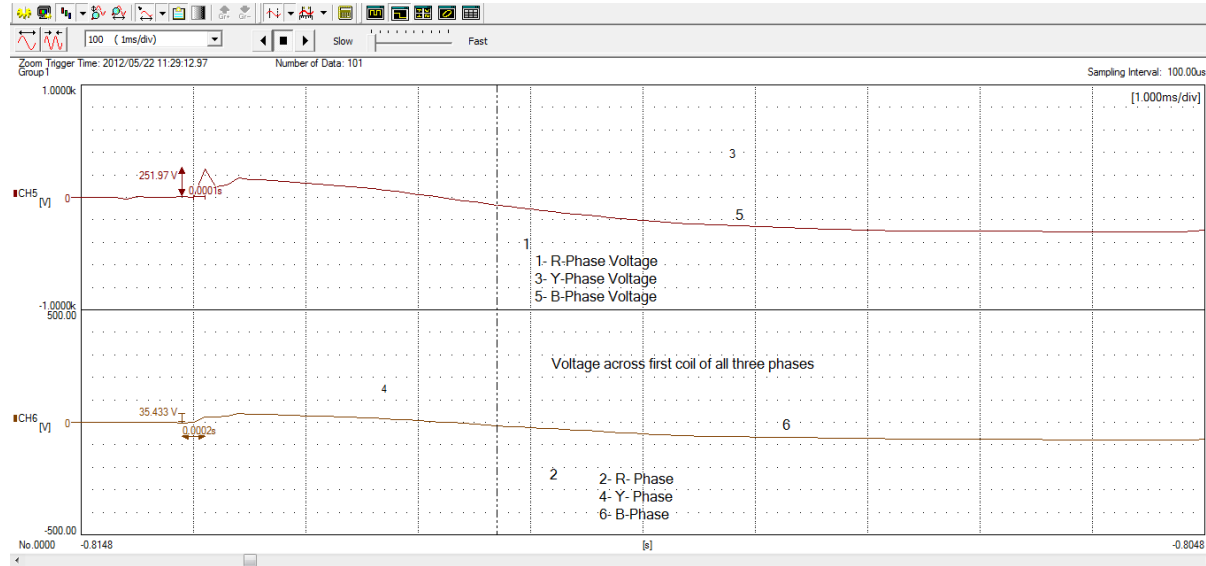


Fig. 0004D Y-Phase



Wave form No. KRK0004

Fig. 0004E B-Phase

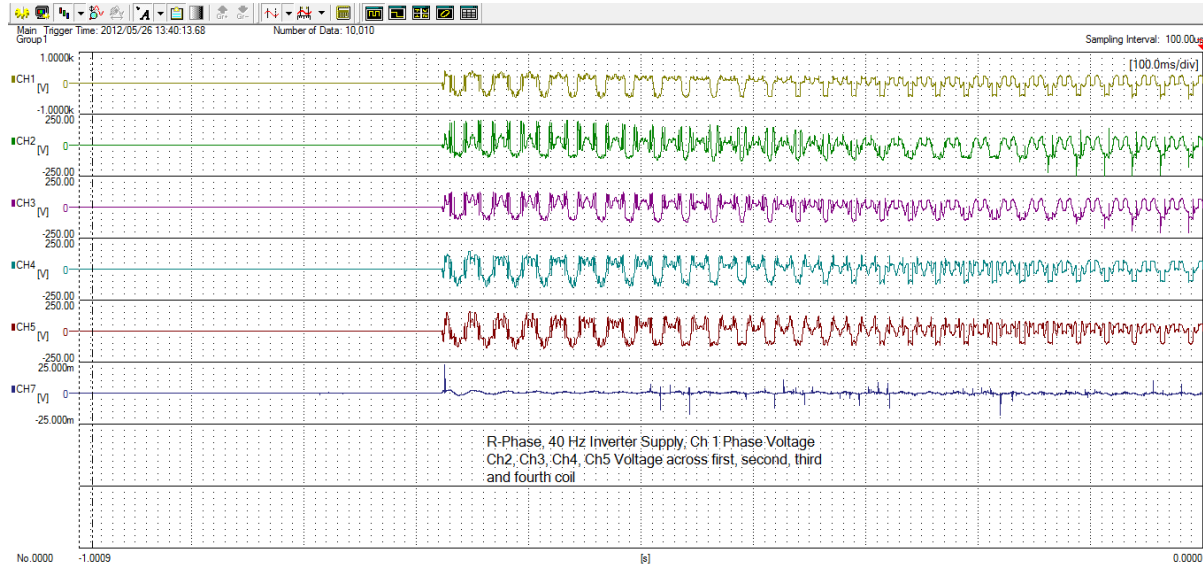


Phase	Item	First Peak
R-Phase	Phase Voltage	236.22 V
	Voltage across coil	74.803 V
Y-Phase	Phase Voltage	181.10 V
	Voltage across coil	43.307 V
B-Phase	Phase Voltage	251.97 V
	Voltage across coil	35.433 V

Wave form No. KRK0138

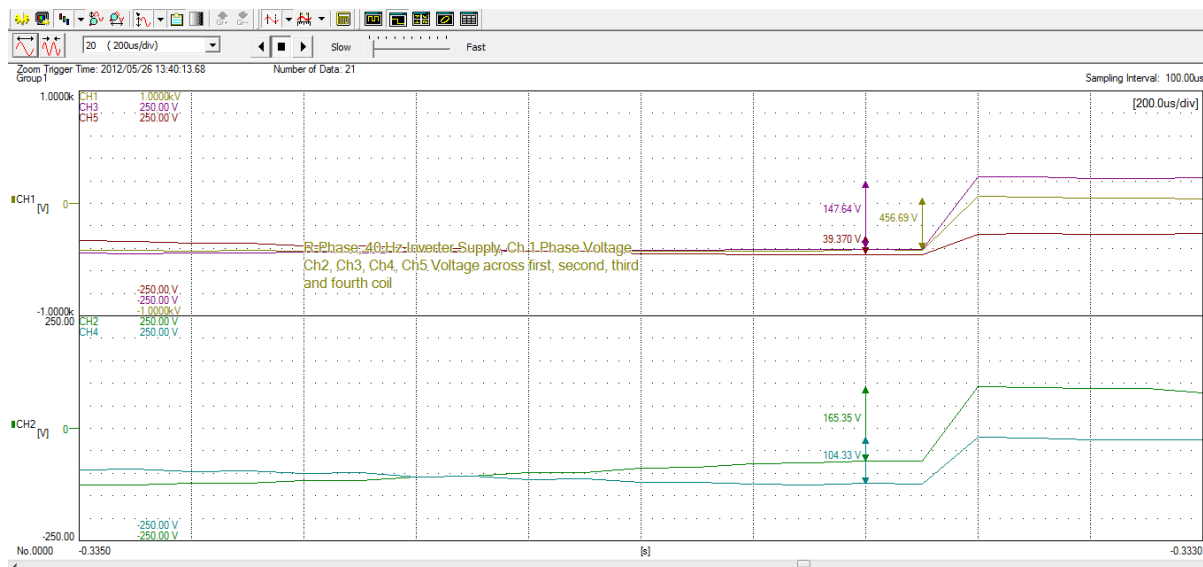
Phase voltage and Voltage across all coils of 3-phase, 415 V, 250 W, 4-Pole Jewellery Polisher Motor when supplied with PWM inverter with frequency 40 Hz.

R-phase Voltage



- Diagram 1: Shows enlarge view of voltage wave forms across all four coils.
- Diagram 2: Shows phase voltage wave form and voltage across first coil.
- Diagram 3: Shows phase voltage wave form and voltage across second coil.
- Diagram 4: Shows phase voltage wave form and voltage across third coil.
- Diagram 5: Shows phase voltage wave form and voltage across fourth coil.

Diagram 1



Wave form No. KRK0138

Diagram 2

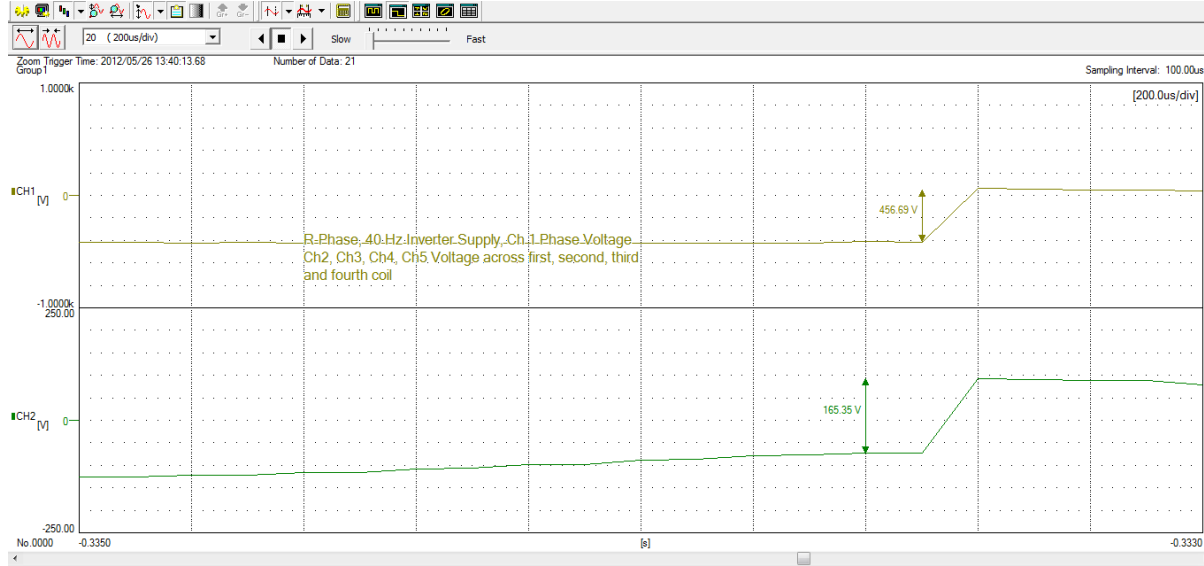
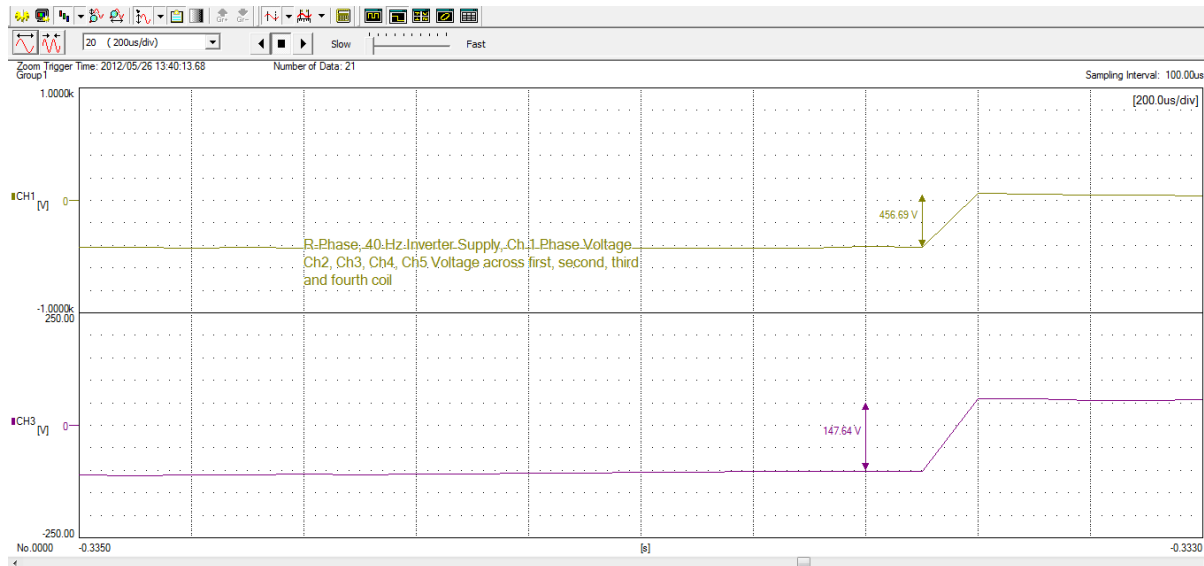


Diagram 3



Wave form No. KRK0138

Diagram 4

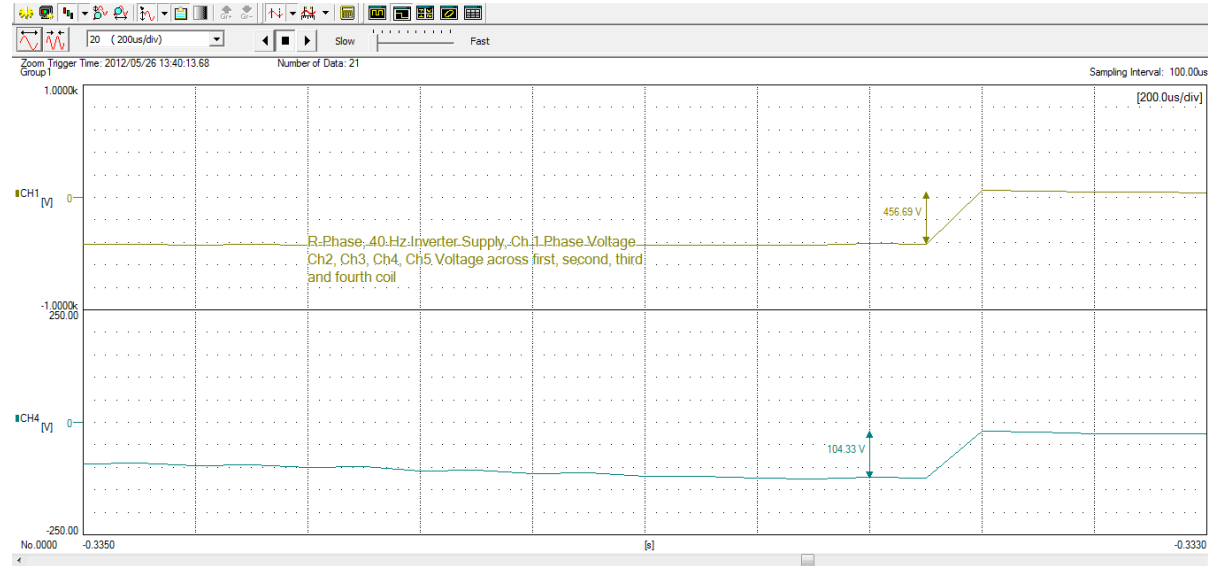
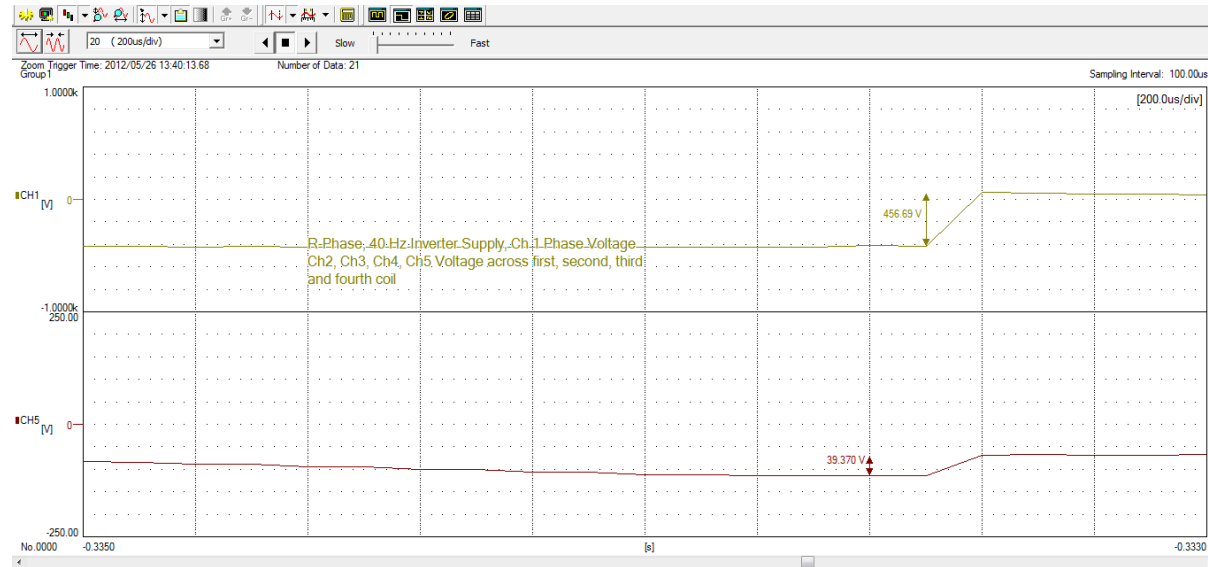


Diagram 5

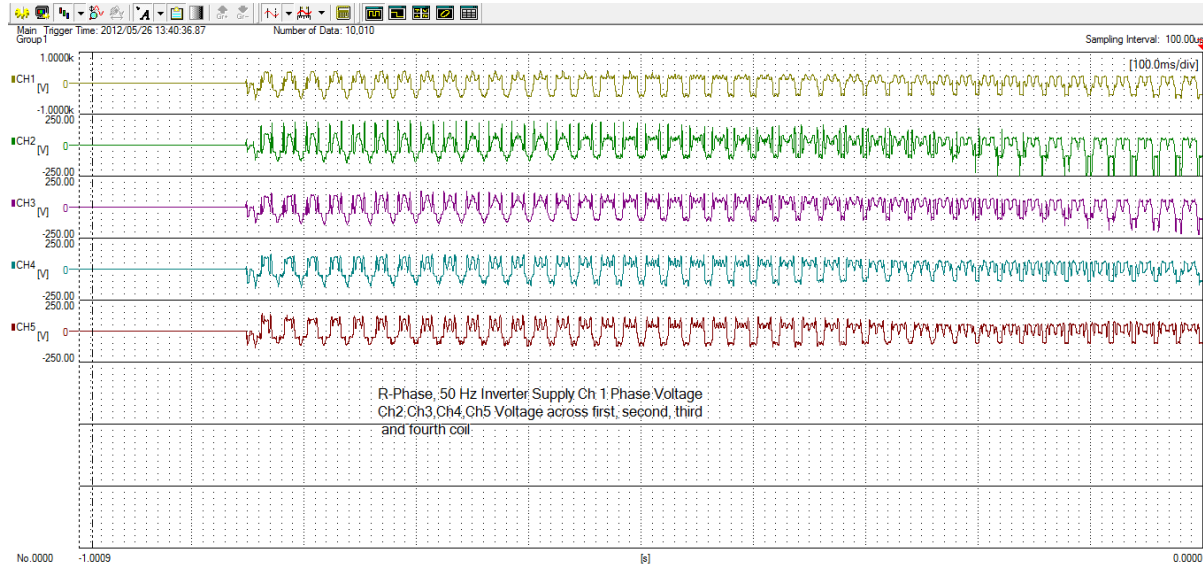


Phase	Item	Voltage Variation
R-Phase	Phase Voltage V_{15}	456.69 V
	Voltage across first coil V_{12}	165.35
	Voltage across second coil V_{23}	147.64
	Voltage across third coil V_{34}	104.33
	Voltage across four coil V_{45}	39.37

Wave form No. KRK0139

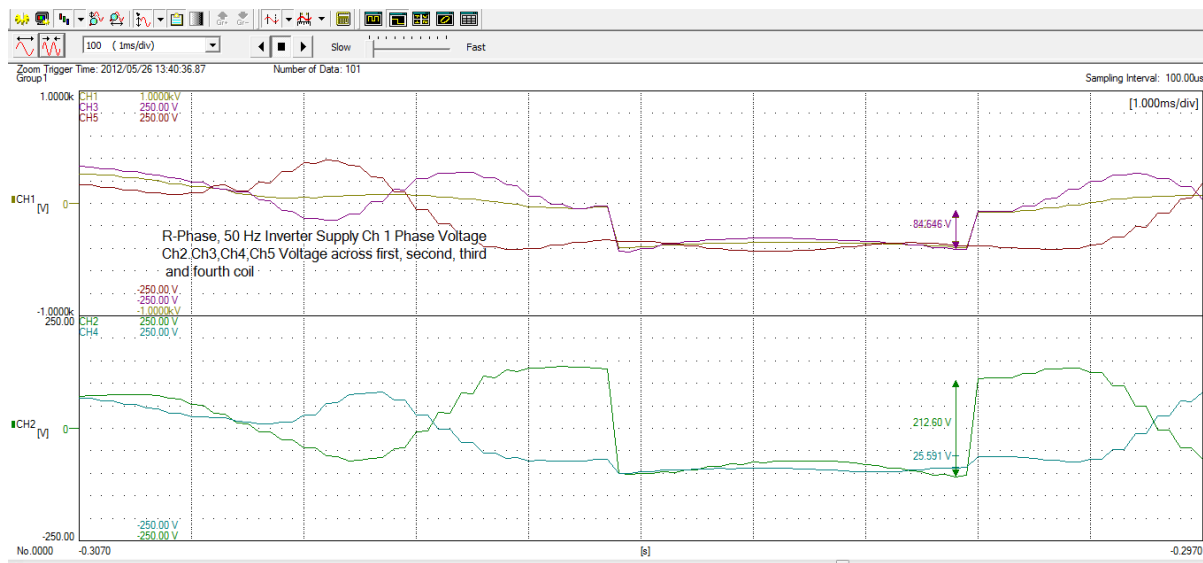
Phase voltage and Voltage across all coils of 3-phase, 415 V, 250 W, 4-Pole Jewellery Polisher Motor when supplied with PWM inverter with frequency 50 Hz.

R-phase Voltage



- Diagram 1: Shows enlarge view of voltage wave forms across all four coils.
- Diagram 2: Shows phase voltage wave form and voltage across first coil.
- Diagram 3: Shows phase voltage wave form and voltage across second coil.
- Diagram 4: Shows phase voltage wave form and voltage across third coil.
- Diagram 5: Shows phase voltage wave form and voltage across fourth coil.

Diagram 1



Wave form No. KRK0139

Diagram 2

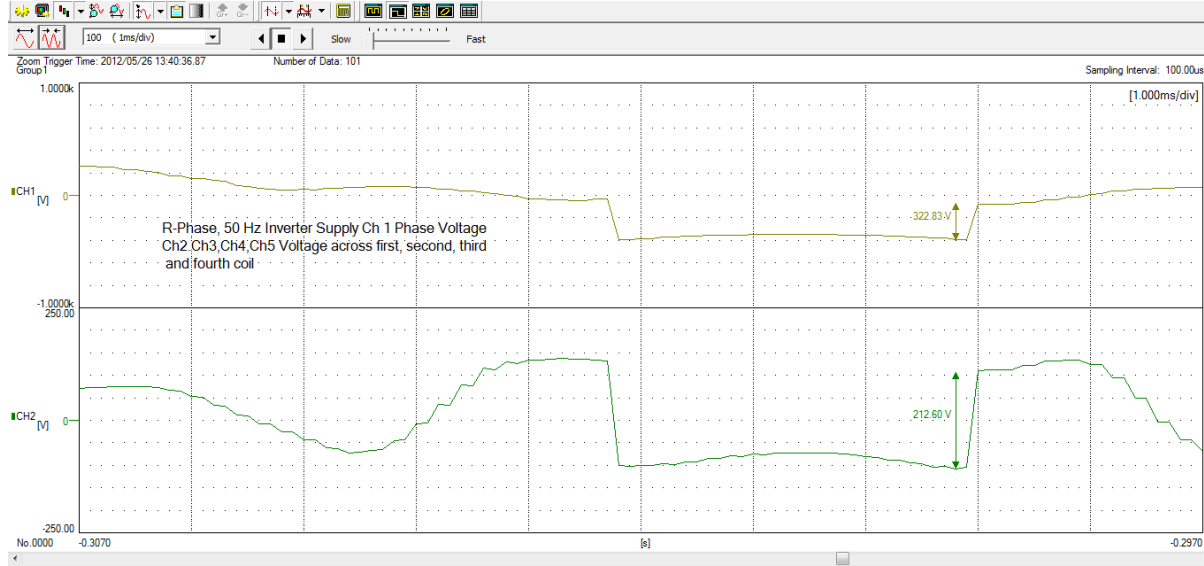
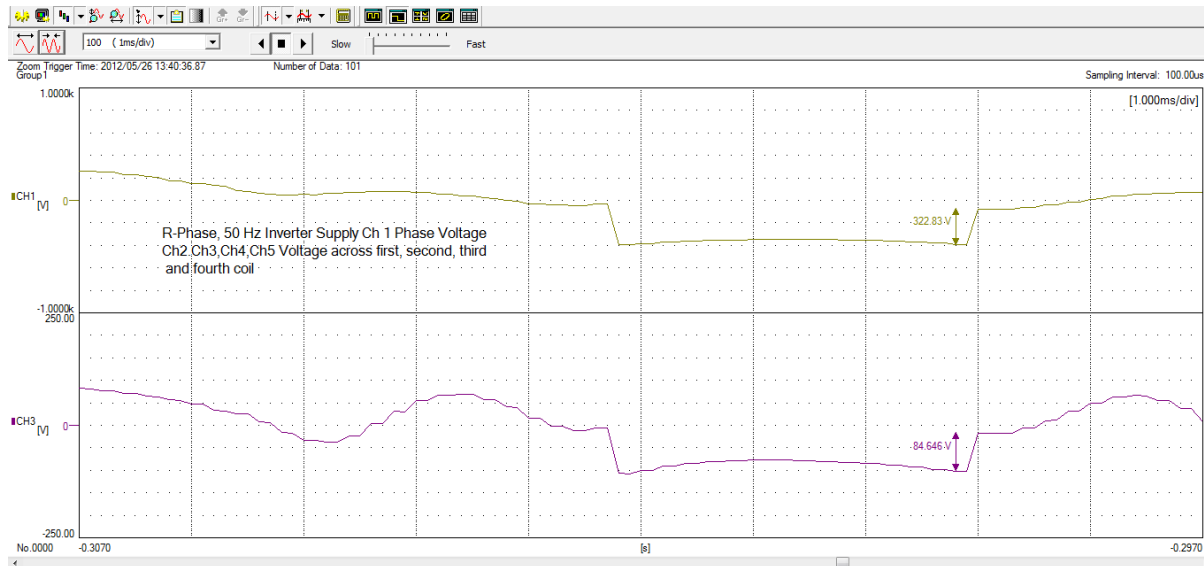


Diagram 3



Wave form No. KRK0139

Diagram 4

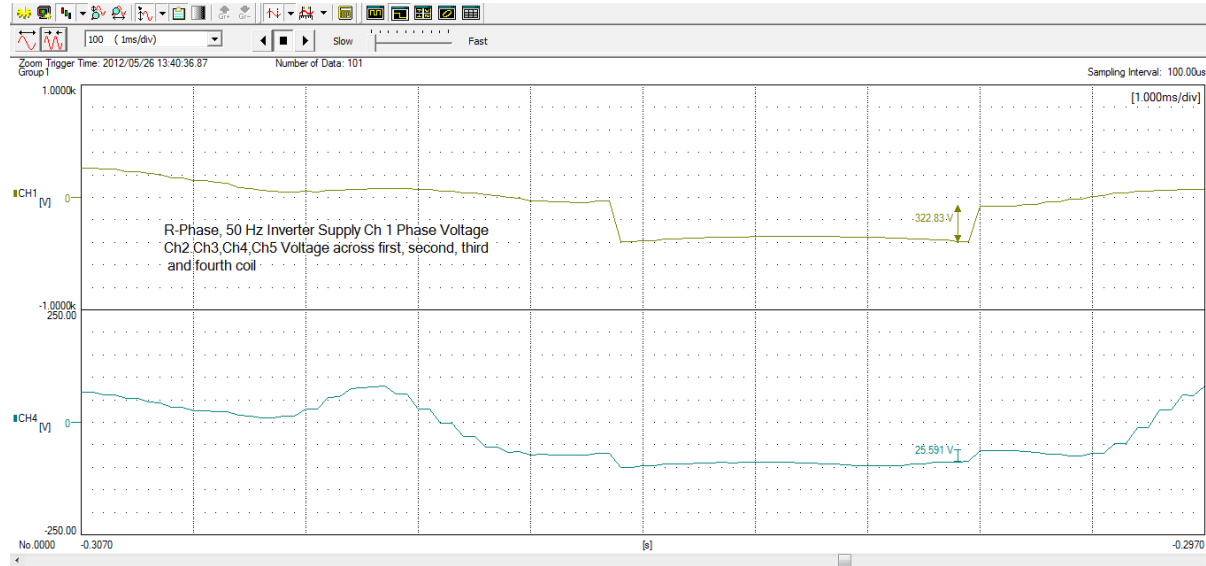
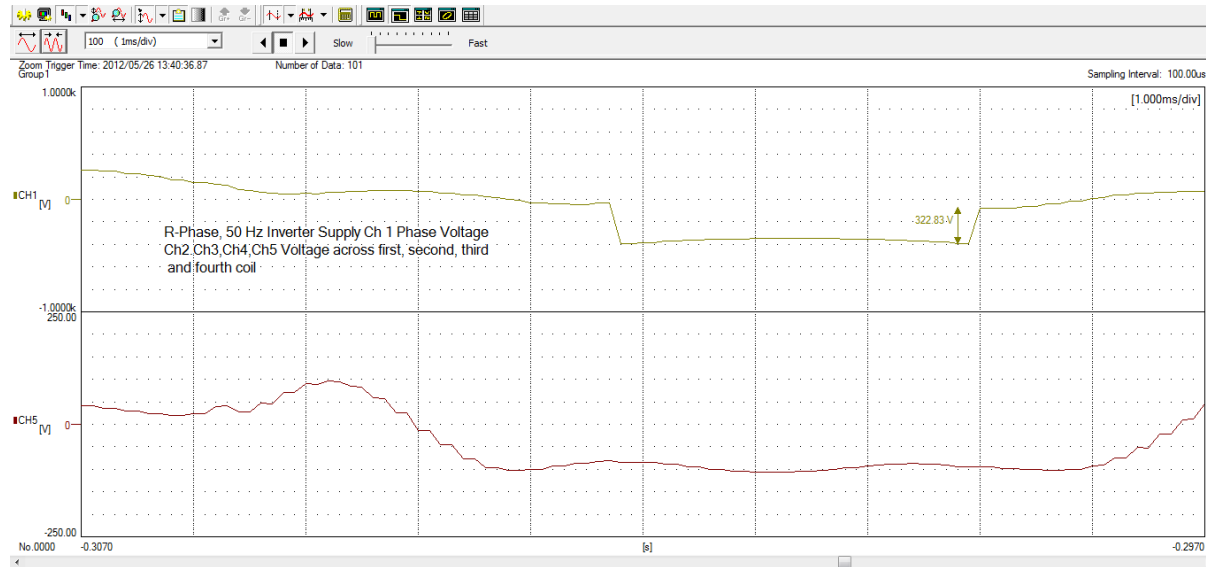


Diagram 5



Phase	Item	Voltage Variation
R-Phase	Phase Voltage V_{15}	322.83 V
	Voltage across first coil V_{12}	212.60
	Voltage across second coil V_{23}	84.64
	Voltage across third coil V_{34}	25.59
	Voltage across four coil V_{45}	0.0

Investigated waveforms are of coil voltages with respect to phase voltage and voltage of one coil with respect to voltage of second coil. When motor is operated on sinusoidal supply, then during switching period voltage across motor phase becomes equal to supply line voltage and the maximum voltage across any of the coil obtained is 80 V. Unexpected behaviour was observed in variation of coil voltage (harmonic voltage after few cycle from starting) with sinusoidal supply during starting, however this is not producing over voltages or high dv/dt . Voltage rise time when motor is supplied with converter is very small and is of the order of micro second. In some cases the peak voltage at motor terminals reaches to value which twice the value of dc link voltage. However for low voltage motor as peak is not reaches to large value coil manufactured with medium covering enamel wire and due care is taken to maintain the thickness around the conductor can withstand this voltages even though the variation of supply voltage is very peculiar particularly at low frequency.

The distribution of voltage during switching condition is not even among the coils of a winding and hence turns. The voltage drop in coils near terminal is more than that of in other coils. The measured voltage drop across first coil from terminal of winding of four coils in series is varying 30 to 56% of the phase voltage against 25% of the phase voltage. During the transition period voltage across first coil may be 70% of the total voltage. Comparison of wave forms for sinusoidal supply and inverter supply shows that distortions were very large with inverter supply which increases the losses and produces more stresses on the insulations.

Chapter 7

Discussion and Analysis of Experiment Results

7.1 COMPARISON OF PERFORMANCE

The performance obtained for Frame 63, 3-phase, 415 V, 470 W, 1.3 A, 50 Hz, 2-Pole, Induction Motor from actual load test, from equivalent circuit and from modified equivalent circuit is as shown in following table:

Sr. No.	Method	Output Power (W)	Power Factor	Torque (Nm)	Efficiency (%)
1	Actual Test	197.83	0.4718	0.6518	61.40
	Equiv. ckt	197.82	0.4821	0.6422	74.59
	Modified Par.	197.95	0.4644	0.6437	78.72
2	Actual Test	291.00	0.5623	0.9938	68.59
	Equiv. ckt	290.94	0.5888	0.6596	78.02
	Modified Par.	291.00	0.5786	0.9573	80.86
3	Actual Test	371.93	0.6297	1.2375	71.44
	Equiv. ckt	371.36	0.6508	1.2319	78.60
	Modified Par.	371.37	0.6448	1.2366	80.25
4	Actual Test	391.12	0.6320	1.3023	71.74
	Equiv. ckt	390.66	0.6622	1.2967	78.52
	Modified Par.	370.79	0.6570	1.3056	79.98
5	Actual Test	449.00	0.6699	1.4995	71.74
	Equiv. ckt	448.75	0.6893	1.5077	77.84
	Modified Par.	448.74	0.6859	1.5163	78.78
6	Actual Test	470.00	0.6733	1.5716	71.93
	Equiv. ckt	469.99	0.6968	1.5857	77.43
	Modified Par.	470.03	0.6938	1.5958	78.18
7	Actual Test	531.47	0.6911	1.7864	71.32
	Equiv. ckt	531.47	0.7110	1.8192	75.65

	Modified Par.	531.39	0.7087	1.8350	75.86
8	Actual Test	580.00	0.7072	1.9571	71.31
	Equiv. ckt	580.38	0.7135	2.019	73.32
	Modified Par.	580.00	0.7107	2.0433	72.95

Comparison of power factor obtained from equivalent circuit and modified equivalent circuit reveal that power factor calculated from modified equivalent circuit gives somewhat more nearer value to the actual value.

The torque obtained from modified equivalent circuit gives somewhat higher value than the value calculated from equivalent circuit however the deviation from actual value is very small.

The efficiency obtained from modified equivalent circuit gives higher value than the value calculated from equivalent circuit and obtained from actual test however the difference decreases as the load increases. The main advantage with modified parameters is this, it eliminates the calculation of friction and windage losses and hence running of motor at different voltages.

The relation between performance values obtained from modified equivalent circuit and actual test at full load are as below

$$PF_m = 1.00072 * PF_a \text{ ---(7.1)}$$

$$T_m = 1.01598 * T_a \text{ ---(7.2)}$$

$$Eff_m = 1.0869 * Eff_a \text{ ---(7.3)}$$

Where suffix 'm' stand for modified circuit parameters and 'a' stands for actual test.

The performance obtained for Frame 63, 3-phase, 380 V, 470 W, 1.4 A, 50 Hz, 2-Pole, Induction Motor from actual load test, from equivalent circuit and from modified equivalent circuit is as shown in following table:

Sr. No.	Method	Output Power (W)	Power Factor	Torque (Nm)	Efficiency (%)
1	Actual Test	430.89	0.7103	1.4612	70.89
	Equiv. ckt	430.82	0.7014	1.4647	75.84
	Modified Par.	430.64	0.7410	1.4765	75.51

2	Actual Test	470.24	0.7452	1.5980	71.01
	Equiv. ckt	470.15	0.7095	1.6174	74.55
	Modified Par.	469.95	0.7415	1.6365	74.54
3	Actual Test	489.28	0.7527	1.6687	70.54
	Equiv. ckt	489.15	0.7110	1.6946	73.68
	Modified Par.	489.21	0.7381	1.7212	73.16

The power factor at 90 % of full load (i.e. 430 W) obtained from modified circuit parameters is slightly higher than actual test but at full load it is almost same as actual. The power factor at 104 % of full load (i.e. 489 W) obtained from modified circuit parameters is lower than actual test but still gives better idea about the power factor. However it can be used to estimate the power factor without the knowledge of friction and windage loss.

The torque for the entire load range obtained from modified circuit parameters is slightly higher than actual test. Same is the case for efficiency.

The relation between performance values obtained from modified equivalent circuit and actual test at full load are as below

$$PF_m = 1.0049 * PF_a \text{ ---(7.4)}$$

$$T_m = 1.024 * T_a \text{ ---(7.5)}$$

$$Eff_m = 1.049 * Eff_a \text{ ---(7.6)}$$

7.2 MAXIMUM VOLTAGE TO WINDING

Numbers of wave forms are recorded for 2-Pole winding and 4-Pole winding. The motor operating voltage was 415 V (L-L). When motor is operated on sinusoidal supply, then during switching period voltage across motor phase becomes equal to supply line voltage and the maximum voltage across any of the coil obtained is 80 V. Unexpected behaviour was observed in variation of coil voltage (harmonic voltage after few cycle from starting) with sinusoidal supply during starting, however this is not producing over voltages or high dv/dt

When motor is operated on utility supply at 50 Hz, maximum voltage recorded during switching is 453.54 V (Wave form No. KRK040) and hence the ratio of voltage across the phase to L-L voltage is 1.09.

When motor was supplied with inverter supply at 25 Hz, the maximum voltage recorded across the phase is 1014.1 V with dc link voltage 466.14 V (Krk0023). The ratio of voltage across the phase to dc link voltage is 2.17 and the ratio of voltage across the phase to rated L-L voltage is 2.44.

When motor was supplied with inverter supply at 40 Hz, the maximum voltage recorded across the phase is 982.68 V with dc link voltage 478.74 V (Krk0030). The ratio of voltage across the phase to dc link voltage is 2.05 and the ratio of voltage across the phase to rated L-L voltage is 2.38.

When motor was supplied with inverter supply at 50 Hz, the maximum voltage recorded across the phase is 800 V with dc link voltage 466.14 V (Krk0023). The ratio of voltage across the phase to dc link voltage is 1.67 and the ratio of voltage across the phase to rated L-L voltage is 1.93.

When motor was supplied with inverter supply at 60 Hz, the maximum voltage recorded across the phase is 653.54 V with dc link voltage 590.55 V (Krk0035). The ratio of voltage across the phase to dc link voltage is 1.06 and the ratio of voltage across the phase to rated L-L voltage is 1.57.

When motor was supplied with inverter supply at 70 Hz, the maximum voltage recorded across the phase is 1133.9 V with dc link voltage 590.55 V (Krk0033). The ratio of voltage across the phase to dc link voltage is 1.92 and the ratio of voltage across the phase to rated L-L voltage is 2.73.

Voltage rise time when motor is supplied with converter is very small and is of the order of micro second. In some cases the peak voltage at motor terminals reaches to value which more than twice the value of dc link voltage and rated line to line voltage of the motor. However for low voltage motor as peak is not reaches to large value coil manufactured with medium covering enamel wire and due care is taken to maintain the thickness around the conductor can with stand this voltages even though the variation of supply voltage is very peculiar particularly at low frequency.

7.3 VARIATION OF PHASE VOLTAGE AND VARIATION OF VOLTAGE IN COIL NEAR TERMINALS

The variation of phase voltage and variation of voltage across coils are recorded for different frequencies. The distribution of voltage during switching condition is not even among the coils of a winding and hence turns.

The voltage drop in coils near terminal is more than that of in other coils. The measured voltage drop across first coil from terminal of winding of four coils in series is varying 30 to 56% of the phase voltage against 25% of the phase voltage. During the transition period voltage across first coil may be 70% of the total voltage. Comparison of wave forms for sinusoidal supply and inverter supply shows that distortions were very large with inverter supply which increases the losses and produces more stresses on the insulations. The results are shown in following tables.

Table 7.3	Item	Voltage Variation
R-Phase-30 Hz KRR0107	Phase Voltage V_{15}	472.44
	Voltage across first coil V_{12}	133.86
	Voltage across second coil V_{23}	124.02
	Voltage across third coil V_{34}	114.17
	Voltage across four coil V_{45}	100.39

Table 7.4	Item	Voltage Variation
Y-Phase-30 Hz KRR0122	Phase Voltage V_{15}	196.85
	Voltage across first coil V_{12}	104.33
	Voltage across second coil V_{23}	53.15
	Voltage across third coil V_{34}	17.71
	Voltage across four coil V_{45}	21.66

Table 7.5	Item	Voltage Variation
B-Phase, 30 Hz KRR0127	Phase Voltage V_{15}	440.94
	Voltage across first coil V_{12}	139.76
	Voltage across second coil V_{23}	118.11
	Voltage across third coil V_{34}	98.42
	Voltage across four coil V_{45}	78.74

Table 7.6	Item	Voltage Variation
R-Phase, 40 Hz KRR0108	Phase Voltage V_{15}	251.97
	Voltage across first coil V_{12}	179.13
	Voltage across second coil V_{23}	78.74
	Voltage across third coil V_{34}	21.65
	Voltage across four coil V_{45}	-27.55

Table 7.7	Item	Voltage Variation
Y-Phase, 40 Hz KRR0123	Phase Voltage V_{15}	338.58
	Voltage across first coil V_{12}	100.39
	Voltage across second coil V_{23}	82.67
	Voltage across third coil V_{34}	72.83
	Voltage across four coil V_{45}	82.67

Table 7.8	Item	Voltage variation
B-Phase 40 Hz K RK0128	Phase Voltage V_{15}	649.61
	Voltage across first coil V_{12}	116.14
	Voltage across second coil V_{23}	153.54
	Voltage across third coil V_{34}	175.20
	Voltage across four coil V_{45}	204.72

Table 7.9	Item	Voltage Variation
R-Phase 50 Hz K RK0109	Phase Voltage V_{15}	543.31
	Voltage across first coil V_{12}	251.95
	Voltage across second coil V_{23}	163.39
	Voltage across third coil V_{34}	74.80
	Voltage across four coil V_{45}	53.15

Table 7.10	Item	Voltage Variation
Y-Phase, 50 Hz K RK 0124	Phase Voltage V_{15}	314.96
	Voltage across first coil V_{12}	185.04
	Voltage across second coil V_{23}	90.55
	Voltage across third coil V_{34}	39.37
	Voltage across four coil V_{45}	0.0

Table 7.11	Item	Voltage Variation
B-Phase 50 HZ K RK0129	Phase Voltage V_{15}	393.70
	Voltage across first coil V_{12}	200.79
	Voltage across second coil V_{23}	122.05
	Voltage across third coil V_{34}	57.08
	Voltage across four coil V_{45}	13.70

Table 7.12	Item	Change in 1 ms	Change in 0.5 ms
R-Phase, 60 Hz K RK0110	Phase Voltage V_{15}	811.02	433.07
	Voltage across first coil V_{12}	116.19	17.71
	Voltage across second coil V_{23}	157.48	70.86
	Voltage across third coil V_{34}	257.87	161.42
	Voltage across four coil V_{45}	279.53	183.07

Table 7.13	Item	Change in 1 ms
Y-Phase, 60 Hz K RK0125	Phase Voltage V_{15}	480.31
	Voltage across first coil V_{12}	283.46
	Voltage across second coil V_{23}	169.29
	Voltage across third coil V_{34}	27.56
	Voltage across four coil V_{45}	-15.74

Table 7.14	Item	Change in 1 ms	Change in 0.5 ms
------------	------	----------------	------------------

B-Phase 60 Hz KRK0130	Phase Voltage V_{15}	889.76	480.31
	Voltage across first coil V_{12}	131.89	29.52
	Voltage across second coil V_{23}	185.04	78.74
	Voltage across third coil V_{34}	267.72	165.35
	Voltage across four coil V_{45}	305.12	198.82

During the experimentation no abnormal behavior of insulation was observed. This is due to the low system voltage, however if we select higher system voltage then we may come across partial discharges and premature insulation failure. Hence following precaution will help in avoiding the undesirable situation.

7.4 AVOIDING LIFE REDUCTION DUE TO PARTIAL DISCHARGES

The methods of avoiding reduced life in motors from partial discharges fall into two categories:

- A. Keep voltage at the motor below the starting voltage levels for partial discharge by:
- Using a very low system voltage (Like 230 Volts),
 - Using a longer rise time ASD,
 - Keeping cable lengths between motor and ASD very short,
 - Using filters between the motor and the ASD to either clip the voltage at a low value or increase the rise time of the voltage wave,
 - Using a form coil motor,
 - Using a special random wound motor construction

Or

- B. Design a special motor insulation that has adequate life in the presence of partial discharges.

7.4.1 USE A LOW VOLTAGE SYSTEM

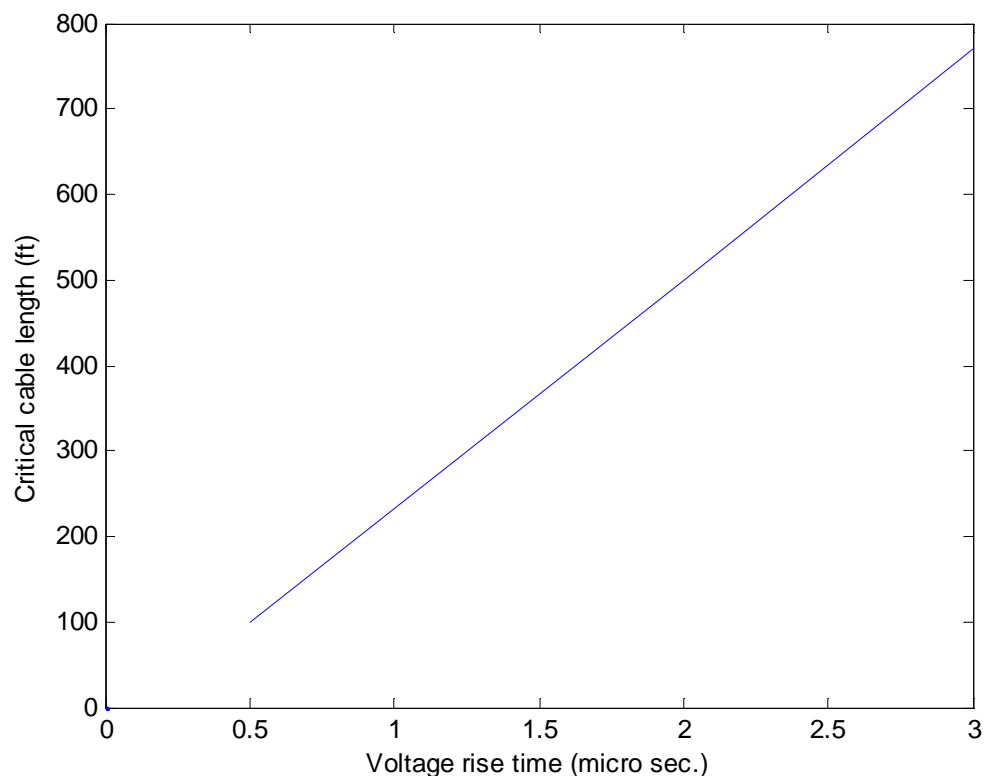
Utilizing 208 or 230 Volt systems is often not possible but should be considered if available

7.4.2 USING A LONGER RISE TIME ASD

While theoretically nice, these are not presently available, and for good reasons. The fast device turn-on times that result in the fast rise times allows higher ASD efficiencies, less effect on motor noise, and less effect on motor temperature rise. Because of these benefits, methods must be developed to achieve acceptable motor life in their presence.

7.4.3 KEEPING CABLE LENGTHS SHORT

Figure 7.1 shows [73] that “short” is defined by the rise time of the ASDs switches. With today’s ASDs having rise times measured in tenths of microseconds, critical cable length (the distance at which theoretical voltage doubling occurs) is happening at distances shorter than is used in most industrial applications. Where possible, shortening the cable length to less than critical length is desirable. Where not practical, one of the other alternatives must be used.



Critical cable length vs rise time

Fig.7.1

7.4.4 USING FILTERS

Several types of filters are commercially available to either increase rise times or to clip the voltage at a certain value with the same rise time [74]. There is great value in using these filters to minimize spare motors. Engineers are always interested in using standard motors on ASDs. The reasoning in this strategy is that somewhere between 10% and 20% of the motors in a typical plant today are used on ASDs, while the remaining 80% to 90% are used on utility power. If a special motor is used for ASD applications,

then either spares are required for both the standard and ASD motors of the same rating, or the extra cost of the ASD rating motors must be absorbed in all motors in the plant so that only one spare per rating is required. Using properly designed filters can allow standard motors to be used in these situations.

7.4.5 USING FORM COIL MOTORS

This solution is expensive and often not available in lower horsepower ratings. Certainly, though, when available and if affordable, it is a good solution. A motor built with an insulation system designed for medium-voltage supplies and applied on low voltage usually works well with today's low voltage IGBT ASDs.

7.4.6 USING MOTORS WITH A RANDOM WOUND SYSTEM

Several methods of making a random wound motor that will not experience partial discharges at the peak voltage seen on an ASD have been identified.

One method uses a wind in place coil insertion method instead of the more commonly used method of winding on an arbor (i.e. former) and then injecting into the stator slots. The theory behind this is that careful insertion can assure that the turn placement is more like a form coil winding where the first turn only touches the second turn and the second only touches the first and third, etc.

A second method is to use heavier builds of magnet wires. This method increases the voltage at which partial discharge starts. For a given slot size in the motor's stator, heavier insulation build causes higher slot fill that needs to be accommodated. Additionally, the starting voltage for partial discharge increases roughly by the square root of the insulation build thickness, so large build increases are required to obtain modest increases in the partial discharge starting voltage.

A third method is to use extra insulation within a phase in the motor-strategically placed to assure that no wire-to-wire voltages exist that would allow partial discharges. While adding extra labour and material, this method can be very effective.

A fourth method that has been identified is to use extra insulating sleeves on the turns closest to the line leads.

Chapter 8

Conclusion

8.1 PERFORMANCE OF THE MOTOR

This thesis dealt with the performance calculation of an induction motor with MATLAB programming and experiments on winding insulation and turns insulation and hence life for medium voltage motor. The performance is calculated using direct load test, equivalent circuit and modified equivalent circuit for two motors: (1) Frame 63, 3-phase, 415 V, 470 W, 1.3 A, 50 Hz, 2-Pole, Class F, Continuous duty Induction motor and (2) Frame 63, 3-phase, 380 V, 470 W, 1.4 A, 50 Hz, 2-Pole, Class F, Continuous duty Induction motor.

The modified equivalent circuit parameters method gives the performance values within acceptable limit and eliminates the evaluation of friction and windage loss. While calculating the efficiency of the motor stray load losses is taken as 1.85% of the output as mentioned in IEEE-112. Hence this method and MATLAB programs given in chapter can be used for calculating the performance of motor.

8.2 TURN INSULATION

The maximum voltage recorded during experimentation on 230 V (phase value) induction motor when operated with converter is 1133.9 V (KRRK0033) whereas the as per IS 4800 voltage with stand capability of enamel of 27 and 28 swg wire is 2800 V. This indicates that motor having phase voltage $567.95 \text{ V} \left(\frac{2800 \times 230}{1133.9} \right)$ can work on this converter safely.

However, turn insulation can fail for a number of reasons, not all of them within control. In general these could be design, quality, and site condition related:

- 1) The dielectric stress due to the surge exceeding the capacity of the turn insulation;
- 2) A much larger number of surges per unit time than was foreseen when the motor was specified and designed;
- 3) Insulation degradation over a time under the influence of normal dielectric and thermal stresses, moisture, vibration, and contaminations;

- 4) Turn insulation erosion due to corona if voids exist in locations next to the turn insulation, resulting in partial discharge; this is likely to happen at voltage greater than 6000 V and with voids larger than 0.05 mm in diameter;
- 5) Turn insulation erosion over time if due to high vibration, repeated start, and speed switching, the insulation work loose and relative movement becomes possible between individual turns in a coil;
- 6) Inadequate or absent routine and preventive maintenance of the motor;
- 7) A much more hostile surge environment than was originally envisioned.

Therefore, following points are to be considered while designing the inter-turn insulation.

1. Knowledge of the surge environment in which the motor is to operate is necessary in determining the surge capability requirements of the motor.
2. Although system studies can be made to determine the worst case surge that might impinge on the motor winding, the monitoring of surges at a number of sites on an industry-wide basis over a period of time is desirable to develop a better feel for surge requirements.
3. The surge capability specified for a motor should be based on application requirements, not simply on any particular standard. This is so because actual requirements might be the same, less, or greater than what the standards require.
4. Higher than necessary level of surge capability and specified dedicated turn insulation are not quite "free". Both the size (first cost) and the efficiency (operating expenses) are adversely affected. Dedicated surge protection equipment for the motor should be considered as a factor in the economic analysis for motor selection.
5. The application of dedicated turn insulation is no guarantee of freedom from failure. If the surge amplitude, rise time, and frequency of surges per unit time are higher than those specified, dedicated turn insulation can also fail.
6. In critical applications, irrespective of the level and type of turn insulation specified, the use of dedicated surge protection should be considered.
7. A large number of motors are functioning satisfactorily with a surge capability of 2 pu. It is not necessary to make a global switch to higher surge capability windings, since in many applications the surge environment is not very hostile.

8. A need exists for a standard definition for surges withstand capability of stator winding turn insulation. This definition should address not only the amplitude and rise times, but also the number of such surges that the insulation must be capable of withstanding.

8.3 EXTENSION OF WORK

For calculating the efficiency of the motor stray load losses is taken as 1.8 % of the output power as suggested in IEEE-112. This value of stray load losses gives somewhat higher efficiency than the actual hence further experimentation is required to fix the value of stray load losses.

In conclusion it is estimated that motor having 567.95 V (Phase value) can safely withstand the surges produced by the converter. So further experimentation can be done in this direction to confirm this.

References

- [1] W. Leonhard, "Control of Electrical Drives". Second edition, Springer Verlag, 1996
- [2] F. Corcoles, J. Pedra, M. Salichs, L. Sainz, " Analysis of the Induction Machine Parameters Identification", IEEE Transactions on Energy Conversion, Vol. 107 PP 183-190, June 2002.
- [3] A. Boglietti, P. Ferraris, M. Lazzari, F. Profumo, "Induction Motor Equivalent Circuit parameters Determination from Standard Tests Made with Inverter supply". Sixth international Conference on Electrical Machines and drives, Oxford. Conf. Publ. No. 376, PP 271-276,1993
- [4] A. T. dc Almeida, F Ferrira, J. Busch, P. Angers, "Comparative Analysis of IEEE 112-B and IEC 34-2 Efficiency testing standards Using Stray load losses in low voltage Three-Phase cage Induction Motors", IEEE Transactions on Industry Applications, Vol. 38 No.2, pp. 608-634, March/Apr. 2002.
- [5] A. Boglietti, A. Cavagnino, M. Lazzari, M. Pastorelli; Induction Motor efficiency Measurements in accordance of IEEE 112-B, IEC 34-2 and JEC 37 International Standards", Electric Machines and Drives Conference 2003-IEMDC03, IEEE International, Volume 3, pp 1599-1605, June2003.
- [6] A. Boglietti, A. Cavagnino, M. Lazzari, M. Pastorelli; International Standards for the Induction Motor Efficiency Evaluation; A Critical Analysis of the Stray- Load Loss Determination", IEEE Transactions on Industry Applications, Vol. 40 No.5, pp. 1294-1301, Sept.-Oct. 2004.
- [7] T. Kataoka, Y. Kandatsu, T. Akasaka, Measurement of Equivalent circuit Parameters of Inverter Fed Induction motor". IEEE Transactions on Magneti, Vol. Mag 23 No.5, pp. 3014-3016, Sept. 1987.
- [8] IEEE Std. 112-1996, " Standard Test Procedure for Polyphase Induction Motors and Generators". IEEE, September 1996.
- [9] Deqiang Zheng, Study on the life prediction of induction motors based on accelerated degradation testing method, "International conference on Reliability, Maintainability and safety (ICRMS), 2011, 9th International conference, PP 1101-1106
- [10] Naik, R. "Circuit model for shaft voltage prediction in induction motors fed by PWM-based AC drives", Industry Applications, IEEE Transactions on, Sept.-Oct. 2003, Volume 39, Issue 5, pp 1294-1299.

[11] Shaotang Chen, Thomas A. Lipo, " Modeling of motor bearing current in PWM Inverter drives. IEEE Transactions on Industry Applications, Volume 32, No. 6, November/December1996, pp 1365-1370.

[12] Jay M. Erdman, Russel J. Kerkman. "Effect of PWM Inverters on AC motor bearing currents and shaft voltages." IEEE Transactions on Industry Applications, Volume 32, No. 2, November/December1996, pp 250-259.

[13] Sidney Bell, Timothy J. Cookson, " Experience with variable-frequency drives and motor bearing reliability." IEEE Transactions on Industry Applications, Volume 32, No. 5, November/December1996, pp 1438-1446.

[14] Raymond ong and J.H. Dymond, " Shaft current in AC Induction machine- An online monitoring system and prediction rules." IEEE Transactions on Industry Applications, Volume 32, No. 4, November/December1996, pp 1189-1195.

[15] Ettore J. Bartolucci, "Cable design for PWM variable speed AC drives." IEEE Transactions on Industry Applications, Volume 37, No. 2, March/April 2001, pp 415-422.

[16] Raymond ong and J.H. Dymond, " Systematic Practical approach to the study of bearing damage in a large oil-ring lubricated Induction machine" IEEE Transactions on Industry Applications, Volume 36, No. 6, November/December2000, pp 1715-1724

[17] Austin H. Bonnett, "Root cause AC motor failure-Analysis with focus on shaft failure." IEEE Transactions on Industry Applications, Volume 36, No. 5, Septmber/October 2000, pp 1435-1448.

[18] Abdeldiebar, B. " Generalized predictive control: Application of the Induction Motor" Smart Manufacturing Application, 2008. ICSMA-2008, International Conference on, 9-11 April 2008, pp 526-529.

[19] F.M.H. Khater and D.W. Novotny, An equivalent circuit model for phase back voltage control of AC machines, IEEE Transactions on Industry Applic., vol. 22, no. 5, Sept./Oct., pp. 835-841

[20] T.A. Lipo, The analysis of induction motors with voltage control by symmetrically triggered thyristors, IEEE Trans. on Power Apparatus and Systems, vol. PAS-90, no. 2, March/April 1971, pp.515-525.

[21] B. Mokrytzki, The controlled slip static inverter drive, IEEE Trans. On Industry and General Applications, vol. IGA-4, May/June 1968, pp. 312-317.

- [22] K. Koga, R. Ueda and T. Sonoda, Achievement of high performances for general purpose inverter drive induction motor system, in Conf. Rec. IEEE IAS Annual Meeting, 1989, pp. 415-425.
- [23] F. Blaabjerg and J.K. Pedersen, Ideal PWM-VSI inverter using only one current sensor in the DC-link, in Conf. Rec. IEE 5th Power Electronics and Variable-Speed Drives Conf., 1994, pp. 458-464.
- [24] S.I. Moon and A. Keyhani, Estimation of induction machine parameters from standstill time-domain data, IEEE Trans. on Industry Applic, vol. 30, no. 6, 1994, pp. 1609-1615
- [25] J. Stephan, M. Bodson and J. Chaisson, Real-time estimation of the parameters and fluxes of induction motors, IEEE Trans. on Industry Applic., vol. 30, no. 3, 1994, pp. 746-758.
- [26] J.A. Capolino, Identification of induction machine parameters, in Conf. Rec. of the Int. Aegean Conf. on Electric Machines and Power Electronics, vol. 2, 1995, pp. 627-637.
- [27] Y. Kishimoto, S. Asaba, K. Nakata and S. Kawatsu, Control device for induction motor, U.S. Patent 5,231,339, July 27, 1993.
- [28] A. Munoz-Garcia, T.A. Lipo and D.W. Novotny, A new induction motor open-loop speed control capable of low frequency operation, IEEE Trans. on Industry Applications, vol. 34, no. 5, July/August, pp. 813-821.
- [29] D. Leggate and R. Kerkman, Pulse based time compensator for PWM voltage inverters, in Conf. Record of IEEE IECON, 1995, pp. 474-481.
- [30] J.W. Choi, S.I. Yong and S.K. Sul, Inverter output voltage synthesis using novel dead time compensation, IEEE Trans. on Industrial Applic., vol. 31, no. 5, 1995, pp. 1001-1008.
- [31] Y. Murai, T. Watanabe and H. Iwasaki, Waveform distortion and correction circuit for PWM inverters with switching lag-times, IEEE Trans. On Industrial Applic., vol. 23, no. 5, 1987, pp. 881-886.
- [32] T. Sukegawa, K. Kamiyama, T. Matsui, and T. Okuyama, Fully digital, vector controlled PWM-VSI fed AC drives with an inverter dead-time compensation strategy, in Conf. Rec. IEEE IAS Annual Mtg., 1988, pp. 463-469.
- [33] J.W. Choi, S.I. Yong and S.K. Sul, Inverter output voltage synthesis using novel dead time compensation, in Conf. Rec. IEEE IAS Annual Mtg., 1994, pp. 100-106.

[34] L. Manz, The motor designer's viewpoint of an adjustable speed drives specification' IEEE Industry Applications Magazine, Jan/Feb. 1995. P.16

[35] A. von Jouanne, P. Enjeti, W. Gray, The effect of long motor leads on PWM inverter fed AC motor drive systems, IEEE Applied Power Electronics conference, March 1995

[36] NEMA MG1,31.40.4.2

[37] NEMA MG1,30.02.2.9

[38] s. Mecker, Considerations in Derating Induction Motors for Applications on Variable Frequency Drives," 1992 IEEE pulp and paper conference. P.191

[39] L. Manz, "Motor insulation system quality for IGBT Drives" 1997 January/February , pp51 to 55

[40] Persson, E., Transient Effects in Application of PWM Inverters to Induction Motors, IEEE Transaction on Industry Applications, Vol. 28, 1992, No. 5, pp. 1095-1101.

[41] Kawkabani, B., Simond, J.J., Kehtari, F., Voltage Peaks of Low Voltage Induction Motors due to PWM Inverter Supply, in EPE'95, pp. 1465- 1469, Sevilla, Spain, 1995.

[42] Takahashi, T., Tetmeyer, M., Tsai, H., Lowery, T., Motor Lead Length Issues for IGBT PWM Drives, in Proceedings of IEEE Annual Pulp and Paper Conference, pp. 21- 27, 1995.

[43] Kerkman, R.J., Leggate, D., Skibinski, G., Interaction of Drive Modulation & Cable Parameters on AC Motor Transients, in Conference Record of IEEE Industry Applications Conference, 1996, pp. 143-152.

[44] Kerkman, R.J., Leggate, D., Schlegel, D., Skibinski, G., PWM Inverters and Their Influence on Motor Over-Voltage, in IEEE Annual Applied Power Electronics Conference and Exposition, 1997, pp. 103-113.

[45] von Jouanne, A., Enjeti, P. N., Design Considerations for an Inverter Output Filter to Mitigate Effects of Long Motor Leads in ASD Applications, IEEE Transactions on Industry Applications, Vol. 33, No. 5, September/October 1997, pp. 1138-1145.

[46] Doležal, I., Kramlík, J., Valouch, V., Parasitic Currents in PWM Voltage Inverter-Fed Asynchronous Motor Drives, in EPE'99, Lausanne, Switzerland, 1999.

- [47] Moreira, A. F., Lipo, T. A., Venkataramanan, G., Bernet, S., High Frequency Modeling for Cable and Induction Motor Over-voltage Studies in Long Cable Drives, in Conference Record of IEEE Industry Applications Conference, 2001, Chicago, USA, pp. 1787-1794.
- [48] Cacciato, M., Consoli, A., Finocchiaro, L., Testa, A., Modeling and HF Performance of Power Cables in Electrical Motor Drives, in EPE 2001, Graz, Austria, 2001.
- [49] Zden K. Peroutka, Motor insulation breakdowns due to operation of frequency converters. IEEE Power tech conference. June 23rd to 26th 2003, pp 128-136 Bologna, Italy.
- [50] Hoene, E., John, W., Reichl, H., Simulation of Conducted Electromagnetic Interference of Inverter-Fed Induction Motors, in EPE-99, Lausanne, Switzerland, 1999.
- [51] Skibinski, G., Kerkman, R. J., Leggate, D., Pankau, J., Schlegel, D., Reflected Wave Modeling Techniques for PWM AC Motor Drives, in IEEE Annual Applied Power Electronics Conference and Exposition, 1998, Vol. 2, pp. 1021-1029.
- [52] Dommel, H. W., Digital Computer Solution of Electromagnetic Transients in Single- and Multiphase Networks, IEEE Transactions on Power Apparatus and Systems, Vol. PAS-88, No. 4, April 1969, pp. 388-396.
- [53] Peroutka, Z., Overvoltage Phenomena in Systems with Distributed Parameters, Graduation Paper, Faculty of Electrical Engineering, University of West Bohemia, Plzeň, Czech Republic, 2000. (in Czech)
- [54] Benešová, Z., Mayer, D., Ulrych, B., Transient Phenomena in Three Phase Networks with Distributed Parameters, in Proceedings of SPETO'98 Conference, Gliwice, Poland, 1998, pp. 295-298.
- [55] High voltage test techniques; part 1: General Definitions and test requirements, IEC 60-1, 1989.
- [56] K.J. Cornick and T.R. Thomposon, " Steep-fronted switching voltage transients and their distribution in motor winding, Part 1 & 2 "Proc. Inst. Elect Eng. Vol. 29, Pt. B no.2 pp 45-63, Mar.1982
- [57] J. Acosta and K.J. Cornick, "Field investigation in to the factors governing the severity of pre-striking transient. IEEE Trans. Energy conversion, vol EC-2, no. 4 , PP 638-645 Dec. 1988.

- [58] E.P. Dick, B.K. Gupta, P.Pillai, A. Narang, and D.K. Shurma, "Practical calculation of switchingsurges at motor terminals IEEE Trans. Energy conversion, vol 3, no. 4, PP 864-872 Dec. 1988.
- [59]] E.P. Dick, B.K. Gupta, A. Narang, and D.K. Shurma, "Measurement and analysis of surge distribution in motor stator windings" IEEE Trans. Energy conversion, vol 4, no. 1, PP 126-134 March. 1989.
- [60] J.L. Guardado and K J Cornick, A computer model for calculating steep fronted surge distribution in machine winding," IEEE Trans. Energy conversion, vol 4, no. 1, PP 95-101 March. 1989.
- [61] M.T. Wright, S.J. Yang and K. McLeary, " The influence of coil and surge parameters on transient inrerturn distribution in stator windings," Proc. Inst. Elect. Eng. , vol 130, pt. B no. 4, PP 257-264 July. 1983.
- [62] J.L. Guardado and K J Cornick, "The effect of coil parameters on the distribution of steep fronted surges in machine windings," IEEE Trans. Energy conversion, vol 7, no. 3, PP 552-559 Sept. 1992.
- [63] IEEE guide for testing turn-to-turn insulation on form-wound stator coils for alternating current rotating machines: IEEE Standard 522-1992:
- [64] IEEE Trial-Use Recommended Practice for the Evaluation of the Impulse voltage Capability of the Insulation Systems for AC Electrical Machinery Employing Form wound Stator coils IEEE Standard 792-1987:
- [65] Motors and generators. NEMA MG1-1993. Draft International Standard 2 (co) 557.
- [66] Rotating Electrical machines, Part 15: Impulse Voltage withstand Levels of Rotating ac Machines with form-wound coils, IEC 34-15, 1990
- [67] Revision of IEC 34-15: 1990
- [68] H.A. Toliyat, G. Suresh, D.A. Rendussara, P.N. Enjeti, "Predicting the Transient Effects of PWM Voltage Waveform on the Stator Windings of Random Wound Induction Motors", IEEE APEC Conference Records, 1997, pp.135-141.
- [69] C.J. Melhorn, L. Tang, "Transient Effects of PWM Drives on Induction Motors", IEEE/ I&CPS Conference Records, May, 1995, pp.1-7
- [70] ATP Users' Manual, Section 23 on cable constants, BAP Publications.

[71] R. Kerkman, D. Legatte, G. Skibinski, "Interaction of the Drive Modulation and Cable Parameters on AC Motor Transient", IEEE IAS Conference Proceedings, 1996, PP143-152.

[72] Suresh J. Patel, Associate Prof., Electrical Engineering Department, MSU, Vadodara. Use of Motors in Switchgear Applications. National Conference on "Power Systems, Embedded Systems, Power Electronics, Communication, Control and Instrumentation", 9-11 January, 2012.

[73] S. Mecker, "Considerations in Derating Induction Motors for Applications on Variable Frequency Drives," 1992 IEEE pulp and paper conference. P.191

[74] R. Nelson, G. Skibinski, "Solution to motor Insulation Failure" Power Transmission Design, August 1995, p.43